11-6-2019 10:00 AM

Novel Night and Day Control of PV Solar Farm as STATCOM (PV-STATCOM) for Critical Induction Motor Stabilization and FIDVR Alleviation

Sibin Mohan, *The University of Western Ontario*

Supervisor: Varma, Rajiv K., *The University of Western Ontario*
A thesis submitted in partial fulfillment of the requirements for the Doctor of Philosophy degree in Electrical and Computer Engineering
© Sibin Mohan 2019

Abstract

Induction motors are globally used in several critical operations such as petrochemicals, mining, process control, etc., where their shutdown during faults causes significant financial loss. System faults can also lead to Fault Induced Delayed Voltage Recovery (FIDVR) causing service disruptions. Dynamic reactive power compensators such as SVC and STATCOM are conventionally employed to mitigate these issues, however, these are very expensive.

PV solar plants are growing at unprecedented rate globally and are likely to be installed near such critical motors. This thesis presents several novel applications of a patented technology of utilizing PV solar plants, both during night and day, as STATCOM, termed PV-STATCOM, for mitigating above issues at about 50 times lower cost than equivalent-size STATCOMs.

A reactive power modulation based PV-STATCOM control is developed to stabilize remotely located motor both during night and day in a realistic distribution feeder, even when reactive power support according to the pioneering German Grid code fails. This control was field demonstrated for first time in Canada (and perhaps in world) on the 10 kW PV solar system in the utility network of Bluewater Power, Sarnia, Ontario.

Another novel control strategy based on active and reactive power modulation of PV-STATCOM is developed. MATLAB/PSCAD simulation studies show that the proposed control can stabilize remotely located motor much faster and with reduced real power curtailment than conventional strategies.

A new real and reactive power control of PV-STATCOM is proposed to alleviate FIDVR. Electromagnetic Transients simulation studies on a realistic transmission network show that the proposed control on a 100 km remote solar farm can alleviate FIDVR and stabilize a cluster of motors for wide range of system parameters and operating conditions. PV-STATCOM can alleviate the need of local STATCOM for achieving the same objective.

Comprehensive sensitivity and stability analysis of single and two distribution level PV-STATCOMs are performed with: i) equivalent and detailed PV-STATCOM model, and ii) PV-

STATCOM control implemented at plant level and inverter level. The impact of modeling details, controller location and system parameters on controller interaction, are investigated.

Keywords

Summary for Lay Audience

This thesis deals with stability of induction motor (IMs), which constitute 80% of industrial and commercial motors as they are reliable, rugged and economical. Induction motors are highly sensitive to under-voltages. A large disturbance such as fault can lead to shutdown of IMs. This thesis addresses two issues associated with the shutdown of induction motors. The first issue is shutdown of critical induction motors. Induction motors are widely used in critical industries such as petrochemicals, mining, automotive, medicines, etc. Shutdown of these critical induction motors, even temporarily, can cause significant financial loss to the industries. For instance, shutdown of a critical motor for one-hour can cause $1 Million loss in a petrochemical industry in Ontario, Canada. The second problem is delayed voltage recovery after a fault due to stalling of large clusters of air-conditioning motors. This prolonged low voltage can lead to service disruption and reduced reliability of power system. Dynamic reactive power compensators, such as SVC and STATCOM, are conventionally employed to mitigate these issues but, these are very expensive. This provides motivation to find cheaper and alternative solutions.

One such alternative solution is use of new controls of PV solar plants. Due to the widespread growth of solar plants, they are quite likely to be installed near such critical motors. Application of existing voltage control strategies of PV solar plants are examined. It is observed that they are not sufficient to address above problems. Novel patented technology of utilizing PV solar plants, both during night and day, as STATCOM, termed PV-STATCOM is a promising technology to provide voltage support in a similar manner as conventional solutions. In this thesis, control strategies are developed for the application of PV-STATCOM for solving the above two issues.

The PV-STATCOM can address the above problems at a 50 times lower cost than conventional SVC/STATCOM solutions. This technology thus brings significant savings for utilities by reducing the need for expensive STATCOMs or SVCs, and opens new revenue making opportunities for solar plants for providing the above critical service.

Co-Authorship Statement

This thesis is based upon a patented technology of using PV solar farm as a dynamic reactive power compensator STATCOM termed, PV-STATCOM, developed by my supervisor Dr. Rajiv K Varma. I have used this technology for developing control strategies for utilizing PV solar farm for the applications of stabilizing remotely located induction motor and Fault Induced Dynamic Voltage Recovery (FIDVR) alleviation. No other student is involved in this research.

Chapter 4 presents the results of field demonstration of the PV-STATCOM technology. This field demonstration has two parts described in Sections 4.3 and 4.4.

In first field demonstration, presented in Sec. 4.3, the application of PV-STATCOM to provide dynamic reactive power support to stabilize induction motor connected at PV solar farm terminal is demonstrated. The results of this study are published in an IEEE Journal paper [1]. In this study, I did the field measurements and developed realistic simulation model of the Bluewater distribution feeder in PSCAD and performed all the time domain simulation studies. Based on these studies, I designed and purchased various equipment for the field demonstration. Further, I was involved in planning of experiments with the induction motor, setting up of the experimental setup and its troubleshooting. The PV-STATCOM control was developed by Ehsan Siavashi who is the second co-author in this paper, while I am the third co-author.

The second field demonstration presented in Sec. 4.4 is entirely my work.

1. R. K. Varma, E. M. Siavashi, **S. Mohan** and T. Vanderheide, "First in Canada, Night and Day Field Demonstration of a New Photovoltaic Solar Based Flexible AC Transmission System (FACTS) Device PV-STATCOM for Stabilizing Critical Induction Motor," in *IEEE Access*, vol. 7, pp. 149479-149492, 2019.

I dedicate this thesis to

my family

for their constant support and unconditional love.

Acknowledgments

This dissertation would not have been possible without the guidance and the help of several individuals who in one way or another contributed and extended their valuable assistance in the preparation and completion of this thesis. First and foremost, I express my sincere and deepest gratitude for my supervisor Dr. Rajiv K. Varma for accepting me into his group. During my tenure, he contributed to a rewarding graduate school experience by giving me intellectual freedom in my work, engaging me in new ideas, and demanding a high quality of work in all my endeavors. No words are adequate to express my gratefulness to him. I can only convey my warm regards to him.

I am sincerely thankful to my industry collaborator for NSERC IPS, Mr. Tim Vanderheide from Bluewater Power Distribution Corporation for his immense support towards my learning and completion of this research work. The opportunity to work inside the company helped me to acquire an expertise and familiarity of real issues related to power system. I am also grateful to Ms. Maureen Glaab for her support during my stay at Bluewater Power Distribution Corporation. I also take this opportunity to thank all the employees of Bluewater Power Distribution Corporation who provided all necessary information to complete this research work. Their technical supports and expertise made a valuable contribution towards my research work.

I would also like to thank Dr. Lyndon Brown, Dr. Mehrdad Kazerani, and Dr. Claudio Canizares of University of Waterloo for valuable and insightful courses they provided.

This research would have been impossible without the financial support of Bluewater Power Distribution Corporation, Natural Science and Engineering Research Council (NSERC) and Ontario Centres of Excellence. I would like to thank all these companies and organization for their valuable support.

I would like to thank Ken Strong, and Ron Struke of Electronic shop at Western University for the help they provided in developing the hardware for the demonstration at Bluewater Power Distribution Corporation, Sarnia. I would like to extend my sincere gratitude to Stephanie Tigert, and Michelle Wagler for all the administrative help. I thank all the wonderful staff of Electrical and Computer Engineering department for the help and guidance they provided during my PhD tenure.

I will forever be thankful to my master's research supervisor, Dr. S.A. Khaparde of IIT Bombay. He has been helpful in providing advice many times during my graduate school

Table of Contents

List of Tables

List of Figures

List of Symbols

V_t	Terminal Voltage of SVC or STATCOM
I_{cMAX}	Rated capacitive current of SVC or STATCOM
I_{LMAX}	Rated inductive current of SVC or STATCOM
P_{ref}	Active power reference
Q_{ref}	Reactive power reference
i_{cap}	Capacitive current required by the BDEW
L_g	Thevenin equivalent inductance of the high voltage network
R_g	Thevenin equivalent resistance of the high voltage network
P_L	Active power consumed by load
Q_L	Reactive power consumed by load
T_e	Electromagnetic torque of induction motor
T_m	Shaft mechanical torque of induction motor
J	combined rotor and load inertia coefficient
N_P	Number of solar panels connected in parallel
N_s	Number of solar panels connected in series
n_p	Number of solar cells connected in parallel in a solar panel
n_s	Number of solar cells connected in series in a solar panel
I_{PV}	Output current of PV Solar farm

V_{PV}	DC voltage across array of N_s solar panels connected in series
V_{dc}	DC link voltage of a VSI
v_{abc}	3 phase AC voltage
i_{abc}	Inverter output AC current
ω_{dc}	Cross over frequency of the DC link voltage controller
C_{dc}	DC link capacitor
L_f	Filter inductance
R_{f1}	ON resistance of IGBT and the resistance of L_f
C_f	Filter capacitance
R_{f2}	Resistance of the damping resistor connected in series with C_f
L_t	Inductance of the delta-star transformer used to connect the DG output to the distribution network
R_t	Resistance of the delta-star transformer used to connect the DG output to the distribution network
f_0	Nominal system frequency (60 Hz)
f_s	Switching frequency of VSI
f_r	Resonant frequency
V_{PCC}	PCC voltage
i_{inv}	VSI output current
V_{dc}	DC link Voltage

τ	Time constant of voltage measurement filter
v_f	Output of voltage measurement filter
V_{xd}	*d axis* voltage (x is used to denote appropriate quantity. For ex: inverter, grid etc.)
V_{xq}	*q axis* voltage (x is used to denote appropriate quantity. For ex: inverter, grid etc.)
I_{xd}	*d axis* current (x is used to denote appropriate quantity. For ex: inverter, grid etc.)
I_{xq}	*q axis* current (x is used to denote appropriate quantity. For ex: inverter, grid etc.)
I_{dref}	*d* axis current reference for VSI
I_{qref}	*q* axis current reference for VSI
θ	Grid voltage angle
ω_0	Synchronous frame frequency
m_d	*d* axis modulation index
m_d	*q* axis modulation index
pf	Power factor set point of VSI
n_{inv}	Number of inverters connected to a pad mounted transformer
V_m	Terminal voltage of critical induction motor.
P_{ramp}	Instantaneous value of active power ramp
i_{dlimit}	Limits of saturation block of I_{dref}

i_{qlimit}	Limits of saturation block of I_{qref}
I_{max}	Rated inverter current
P_{pre}	Pre -disturbance active power output of PV solar farm or solar inverter
P_{poi}	Active power output of PV solar farm
Q_{poi}	Reactive power output of PV solar farm
V_{poi}	Terminal voltage at POI
P_{pcc}	Active power output of a inverter in a solar farm
Q_{pcc}	Reactive power output of a inverter in a solar farm
V_{pcc}	Terminal voltage at PCC
$P_{available}$	maximum available active power
V_{m_thresh}	Threshold value of motor terminal voltage to trigger PV-STATCOM control
V_{TOVL}	Transient over voltage limit
V_{pre}	Pre disturbance motor terminal voltage
V_{pccref}	Utility's upper steady state voltage limit
P_{sens}	Sensitivity of voltage for active power output of PV solar farm
Q_{sens}	Sensitivity of voltage for reactive power output of PV solar farm
Q_{cmd}	Reactive power reference provided by Plant Level controller to Inverter Level controller

I_{VC}	Reactive current required by voltage controller to maintain V_{pcc} at V_{pccref}

List of Abbreviations

IM	Induction Motor
POI	Point of interconnection of PV solar farm (HV terminal of the substation transformer)
PCC	Point of Common Coupling of inverter in a solar farm (HV terminal of the $\Delta - Y$ pad mount transformer at the inverter unit)
FIDVR	Fault Induced Delayed Voltage Recovery
NERC	North American Electric Reliability Corporation
TIS	Transmission Issue Subcommittee of NERC
FACTS	Flexible Alternative Current Transmission Systems
SVC	Static Var Compensator
STATCOM	Static Synchronous Compensator
PV	Photovoltaic
VSI	Voltage Source Inverter
IGBT	Insulated Gate Bipolar Transistor
MPPT	Maximum Power point Tracking
LVRT	Low Voltage Ride Through
DG	Distributed generation
SPWM	Sinusoidal pulse width modulation

SVPWM	Space Vector pulse width modulation
PLL	Phase Locked Loop
WECC	Western Electricity Coordinating Council
TOV	Transient Over Voltage
GUI	Graphics User Interface
THD	Total Harmonic Distortion
PLC	PV Plant Level controller
ILC	Inverter Level Controller
UPF	Unity Power Factor
SCR	Short Circuit Ratio
HVRT	High Voltage Ride Through

List of Appendices

Chapter 1

1   Introduction

This thesis deals with stability of induction motor (IMs), which constitute 80% of industrial and commercial motors as they are reliable, rugged and economical. Induction motors are highly sensitive to under-voltages. A large disturbance such as fault can lead to shutdown of IMs. This thesis addresses two issues associated with the shutdown of induction motors. The first issue is shutdown of critical induction motors. Induction motors are widely used in critical industries such as petrochemicals, mining, automotive, medicines, etc. Shutdown of these critical induction motors, even temporarily, can cause significant financial loss to the industries. For instance, shutdown of a critical motor for one-hour can cause $1 Million loss in a petrochemical industry in Ontario, Canada. The second problem is delayed voltage recovery after a fault due to stalling of large clusters of air-conditioning motors. This prolonged low voltage can lead to service disruption and reduced reliability of power system. Dynamic reactive power compensators, such as SVC and STATCOM, are conventionally employed to mitigate these issues but, these are very expensive. This provides motivation to find cheaper and alternative solutions.

One such alternative solution is use of new controls of PV solar plants. Due to the widespread growth of solar plants, they are quite likely to be installed near such critical motors. Application of existing voltage control strategies of PV solar plants are examined. It is observed that they are not sufficient to address above problems. Novel patented technology of utilizing PV solar plants, both during night and day, as STATCOM, termed PV-STATCOM is a promising technology to provide voltage support in a similar manner as conventional solutions. In this thesis, control strategies are developed for the application of PV-STATCOM for solving the above two issues.

The PV-STATCOM can address the above problems at a 50 times lower cost than conventional SVC/STATCOM solutions. This technology thus brings significant savings for utilities by reducing the need for expensive STATCOMs or SVCs, and opens new revenue making opportunities for solar plants for providing the above critical service.

This chapter is organized as follow. The operating characteristic of induction motor, instability of critical motor and Fault Induced Delayed Voltage Recovery (FIDVR) are described in Sec. 1.1. The conventional solution for addressing instability of critical motor, and FIDVR are explained in Sec. 1.2 and Sec. 1.3, respectively. The growth of Photovoltaic (PV) solar plant and structure of a PV solar plant are described in Sec. 1.4 and Sec. 1.5, respectively. The existing control strategies of smart inverter control are discussed in Sec. 1.6. The PV-STATCOM technology is introduced in Sec. 1.7. The small signal modeling of PV solar plant for interaction analysis is discussed in Sec. 1.8. The knowledge gaps in available literature are discussed in Sec. 1.9. Finally, the scope and objectives of this thesis are presented in Sec. 1.10.

1.1 Stability of Induction Motors (IM)

Induction Motor (IMs) are widely used as they are reliable, rugged and economical. Single phase IMs are used for running small loads like residential fans and air conditioner (AC) units, whereas three phase induction motors constitute about 80% of all industrial motors.

1.1.1 Speed Torque Characteristics of an Induction Motor

The torque of an induction motor depends on its terminal voltage. The speed torque characteristics of an induction motor (IM) for various voltages V1, V2 and V3, where V1>V2>V3 is shown in Figure 1-1. The IM is assumed to be operating at rated voltage V1 by providing constant load torque. The operating point corresponding to steady state operation is shown as point A. If the voltage reduces to a lower value (V2) due to some disturbance, the IM speed reduces and the operating point changes to point B as shown in Figure 1-1. If the voltage reduces further to V3, the torque characteristics of the IM drops, and there is no operating point corresponding to the given load. It means, the IM is not able to generate the necessary electromagnetic torque at V3 to run the load. Thus, the IM speed drops and eventually it stalls.
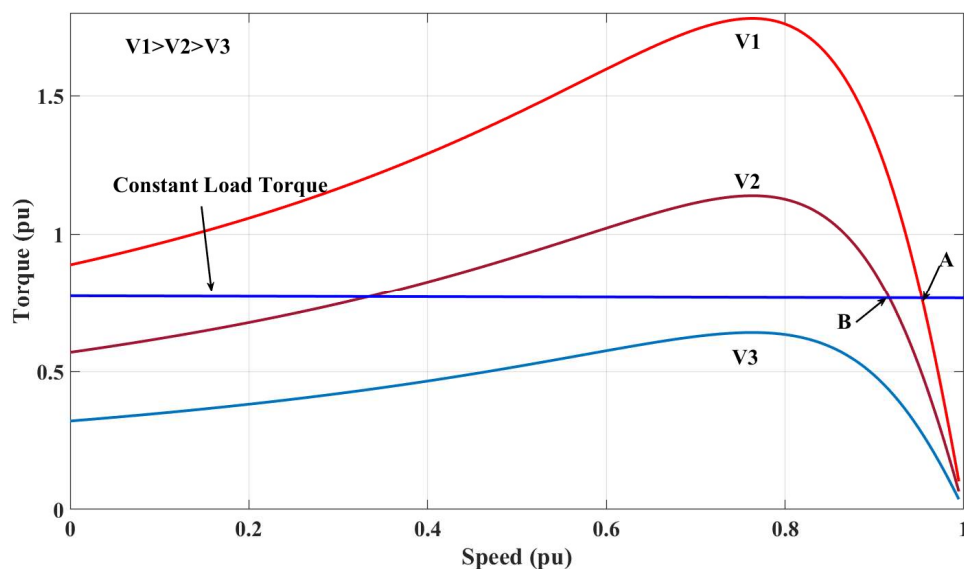
Figure 1-1. Torque - Speed characteristic of an IM

This figure shows that IMs are very sensitive to voltage; and having appropriate voltage at the terminal for IM is important for the motor to operate continuously, else it may stall.

1.1.2   Reactive Power Consumption of an IM

The reactive power consumption of an IM as a function of its terminal voltage is shown in Figure 1-2. When the IM is operating near rated voltage (1 pu), the reactive power reduces linearly with the drop in voltage. Once the voltage drops further to V_{stall}, the voltage at which IM stalls, the reactive power consumption increases sharply. If the voltage reduces further, the reactive power follows an almost linear characteristic with voltage.

This reactive power consumption of IM can have a severe impact on the voltage stability of the system. If the system voltage decreases to a voltage near to V_{stall}, the reactive power consumption of the IM increases to a high value, which causes further drop in the system voltage. This could eventually lead to system collapse or delayed voltage recovery.
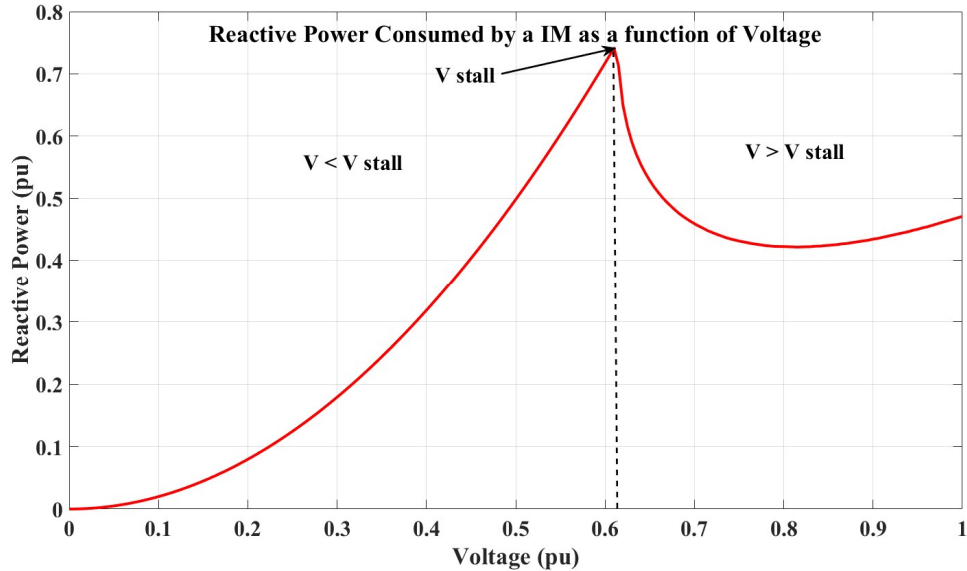
Figure 1-2. Reactive Power consumption of an IM as function of voltage

1.1.3   Behavior of an air conditioner during voltage disturbance

Air conditioner constitutes a major portion of the loads and stalling of these air conditioner loads could cause FIDVR issues. As this thesis deals with FIVDR, the behavior of air conditioner motors is described below.

The torque speed characteristic of an IM used for running an air conditioner (AC) load is shown in Figure 1-3. The air conditioner compressor load is modelled as two constant loads:

    (i)   Low load torque - this is the starting torque of the compressor.
    (ii)   High load torque – this is the normal running torque of the compressor [1].

When an air conditioner is turned on, the load torque is low, and IM quickly accelerates to operating point 'A'. As the compression increases, the load torque increases to High load torque and the operating point changes to point 'B', as shown in Figure 1-3. The running load torque of the compressor intersects the torque characteristics of the IM at points 'B' and 'C', which are greater than the starting torque of the IM.

If the motor voltage declines due to a fault and causes the motor to stop for a moment, the IM fails to restart after the fault is cleared, as the load torque is greater than

the starting torque of the IM. As shown in Figure 1-2, the stalled IM consumes a large reactive power and slows down the voltage recovery [1-3].
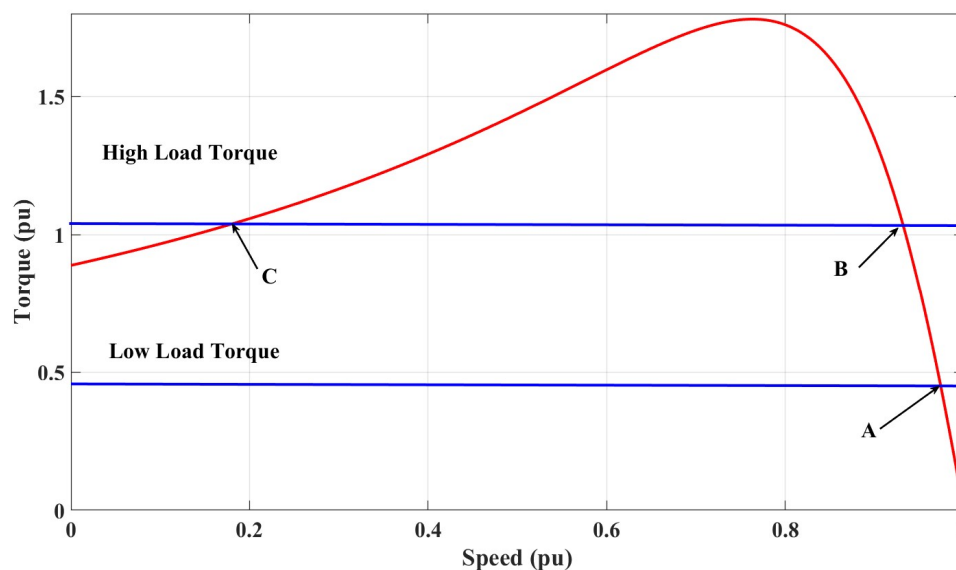
Figure 1-3. Torque Speed Curve of an air conditioner motor [1].

The air conditioner loads have two types of protection: (i) Thermal protection and (ii) Low voltage protection. Low voltage protection acts when the voltage is less than 40% of rated voltage. Usually, the stalled voltage will be greater than this cut off threshold and thus low voltage protection does not act during stalled operation. Thermal protection has an inverse time characteristic relay, which operates when the IM current increases. The thermal protection does not act instantaneously; it takes 3-15 seconds to act. So, the stalled air conditioner loads remain connected to the system till the thermal protection acts, consuming a large reactive power. This delays the recovery of voltage after a fault clearance, as described below.

1.1.4   Fault Induced Delayed Voltage Recovery (FIDVR)

Air conditioner loads constitute a major portion of the loads during summer [4]. A fault in the power system can lead to stalling of multiple air conditioner loads during this time. The stalled air conditioner loads will remain connected in the system for a while till the thermal protection of motors act and disconnect them from the system. While remaining connected to the system, the stalled air conditioner motors consume a large amount of

reactive power as shown in Figure 1-2, thus delaying the recovery of the system voltage. This phenomenon is called as Fault Induced Delayed Voltage Recovery (FIDVR). As the inertia constant of IMs used for operating air-conditioning loads are 0.1 - 0.5 sec [3], these motors will stall for even quickly cleared faults. It is reported that faults cleared in small as 3 cycles have caused FIDVR events [1]. This shows that with increasing penetration of low inertia air conditioner motors in the system, the probability of having voltage instability due to FIDVR is also increasing. Presently, FIDVR is one of the major voltage stability concerns faced by the utility.
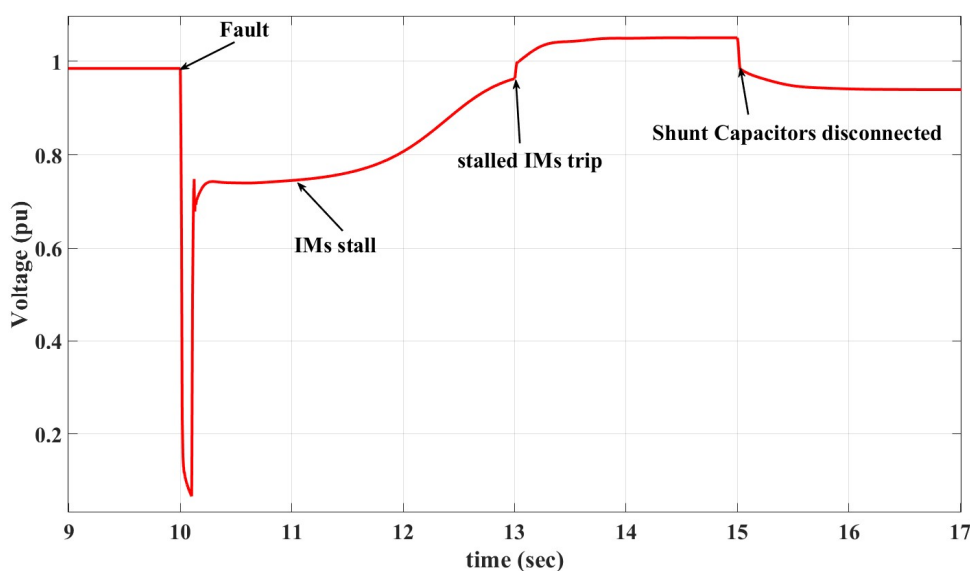
Figure 1-4. System Voltage for FIDVR [1]

According to Transmission Issue Subcommittee (TIS) of NERC, FIDVR is a low voltage event due to a fault, which typically takes more than two seconds for post fault steady state voltage recovery, and the initial recovery voltage after clearing of a fault is less than 90% of pre-contingency voltage [5]. The voltage for a typical FIDVR event is shown in Figure 1-4. A fault in the system causes the voltage to drop to almost zero at 10 sec. The fault is cleared in 6 cycles. The air conditioner motor loads fail to recover, and stall. The large reactive power consumption by the stalled air conditioner loads causes slowdown of recovery of the voltage as shown in Figure 1-4. After a delay, the thermal protection on the stalled motors act, and due to this the system voltage recovers and experiences an over voltage. Usually this over voltage is in the range of 8-15% and the delay for thermal

protection to act is 20-30 sec [1]. Due to the overvoltage, the shunt capacitors trip and causes a further reduction in voltage. If the disconnected AC loads try to reconnect during this low voltage, they can cause further decline in system voltage. The system controls typically bring the voltage to normal value after a further delay [1-3].

The delayed voltage recovery can cause large loss of loads and tripping of generators. Also, extended low voltages can affect lives of consumers and lifecycle of utility equipment [5]. FIDVR events are widely reported in literature. The FIDVR event in Union City, Metro Atlanta caused a tripping of 1900 MW load and seven small generating units [5]. A load of 445 MW was lost in Washington due to prolonged low voltage while 1700 MW load was lost in Toronto, Canada, due to FIDVR [3]. In Southern California Edison network alone, more than 50 events are reported, among which the largest event caused a load loss of 3500 MW [2]. The FIDVR event in Hassayampa, Arizona, caused a loss of 440 MW load and 2600 MW generation [2].

1.2 Mitigation of Instability of Motors in Industries by FACTS Devices

Shutdown of the industrial IMs, even for a short duration of few minutes, can result in significant economic loss to the industrial facilities as the entire batch of materials being transported/served by these motors may get damaged [6, 7]. In one petrochemical industry (name withheld for confidentiality) the loss caused by the shutdown of motors is estimated to be $ 1 Million for just one hour of the shutdown. Thus, industries employ various methods to ensure stable operation of these critical IMs during system disturbance.

Dynamic reactive power support is the most effective solution for preventing stalling of induction motor [8]. Shunt connected Flexible Alternative Current Transmission Systems (FACTS) devices like Static Var Compensator (SVC), and STATCOM are the mostly employed dynamic reactive power compensators [9, 10] for this purpose, due to their fast response (1-3 cycles). These FACTS devices are described below.

1.2.1   Static Var Compensator

Static Var Compensator (SVC) is a static reactive power compensation device. SVC consists of a thyristor controlled reactor (TCR) and thyristor switched capacitor (TSC) [9, 10]. The reactive power output of the SVC is controlled by varying the firing angle of TCR between 90° - 180°, and by turning TSC ON or OFF.

1.2.1.1   V-I characteristics of an SVC

The V-I control characteristics of an SVC is depicted in Figure 1-5. V-I characteristic of a SVC [10]. The characteristic can be divided into three parts [9, 10], as below:
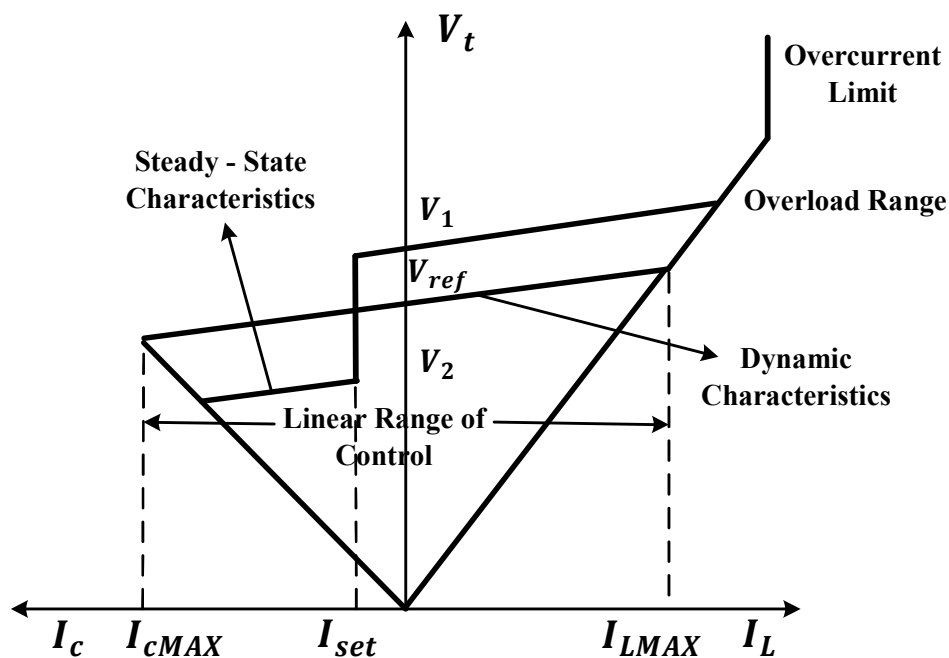
Figure 1-5. V-I characteristic of a SVC [10].

Linear Range of Control: The SVC current varies linearly with the SVC terminal Voltage (V_t) in this range. The SVC current is varied between rated capacitive current (I_{cMAX}) and rated inductive current (I_{LMAX}) in this range. The SVC current is controlled by varying the firing angle of TCR and by switching the TSCs.

Overload Range: In this range, the TCR acts as a fixed inductor, as it is operating at maximum conduction mode. In this case, the current increases linearly with the increase in voltage.

Overcurrent Limit: The maximum inductive current in overload range is limited to prevent excess thermal stress on the semiconductor switches.

The SVC can provide fast reactive power support, and they are employed in power system for providing voltage support [11-18], load compensation [19-23], power oscillation damping [24-27], providing reactive power to HVDC converter stations [28-30], etc.

The fast reactive power support by the SVC can help in preventing IM instability. The application of a Static Var Compensator (SVC) and its superior effectiveness compared to a breaker switched capacitor in preventing IM instability is described in [31]. The use of thyristor-based voltage regulators for stabilizing critical induction motors is presented in [32]. The improved performance of SVC over a thyristor-controlled tap changer for IM stabilization is discussed in [18].

The reactive power capability of SVC is limited at low voltage, as the reactive power of SVC varies in proportional with the square of the terminal voltage. Furthermore, it requires large footprint due to the size of large inductors and capacitors, as well as large filters that are required to mitigate the harmonics generated in SVC.

1.2.2 STATCOM

STATCOM is a Voltage Source Converter (VSC) [9, 10] based Flexible AC Transmission System (FACTS) device. The STATCOM is analogous to a synchronous condenser and is capable of generating three phase sinusoidal voltages with controllable amplitude and phase angle by switching of power electronic switches. The STATCOM is connected with the utility through a coupling reactance usually provided by the coupling transformer. Therefore, STATCOM can be represented as an ideal adjustable voltage source connected to a utility network. Like synchronous condenser, when STATCOM inverter output voltage is greater than utility voltage the STATCOM supplies reactive

power Q or leading current, and when inverter output voltage is less than the utility voltage it absorbs Q or provides lagging current. Therefore, the reactive power can be varied continuously from inductive to capacitive range by varying the magnitude of STATCOM terminal voltage.

1.2.2.1 V-I characteristics of a STATCOM

The V-I characteristics of a STATCOM is shown in Figure 1-6. V_t represents the AC system voltage at STATCOM terminal. I_{LMAX} and I_{cMAX} denote the rated inductive and capacitive current, respectively, of the STATCOM.
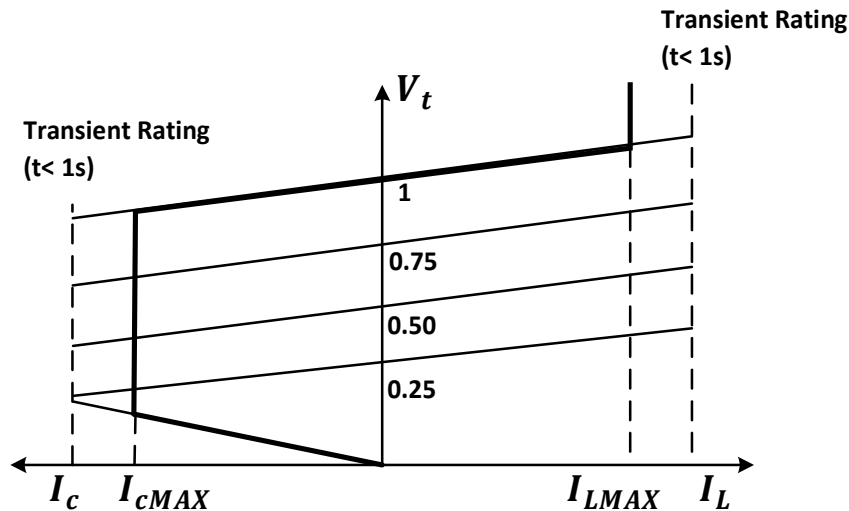
Figure 1-6. V-I characteristics of a STATCOM [10].

The STATCOM can provide any capacitive or inductive current between the rated capacitive or inductive current irrespective of the system voltage at its terminal. STATCOM can provide rated capacitive current even at a low system voltage (even as low as 0.15 pu). This is an added advantage of STATCOM compared to SVC. This rated capacitive current injection at a low system voltage is highly beneficial during voltage recovery after a severe disturbance.

STATCOM has a higher transient current rating. The transient capacitive current rating is decided by the maximum turn off capability of the switches and the transient inductive

current rating is determined by the maximum allowable junction temperature of the converter switches [10].

The STATCOM is faster device than a Static Var Compensator (SVC). Since the STATCOM controls reactive power flow through power electronics processing, it does not require any additional capacitor banks or reactors as an SVC. This results in a compact design, low noise and low magnetic impact. The only capacitor used is at the DC terminal of the STATCOM, which provides a constant voltage. As DC power does not have any reactive component and the voltage at the DC terminal is held constant, the DC link capacitor does not participate in any reactive power exchange. Since STATCOM does not inject any real power to the grid, the DC link provides an instantaneous power-circulating path to satisfy the power balance relation and thus the converter establishes a circulating reactive power exchange among the phases. However, in a practical STATCOM system there are real power losses in the semiconductor switches that are provided by the DC link capacitor. This reduces the DC link voltage over time. Thus, some real power must be absorbed from the AC system to charge the DC link capacitor and keep its voltage constant. This is accomplished by making the VSC terminal voltage lag the utility system voltage by an angle of θ. The magnitude of this angular difference depends on the amount of charge (real power absorption) that is needed to replenish the voltage drop in the DC link capacitor.

The fast reactive power support by a STATCOM can help in improving voltage stability [33-40], power oscillation damping and SSR mitigation [41-43], load compensation [44], and integration of distributed generators [45-48].

1.2.3 Applications of STATCOMs and SVCs to stabilize Industrial Induction Motors

Due to the fast reactive power support capability, STATCOMs and SVCs are used in industries to prevent IMs from stalling during voltage transients. Few of the installations by industries are listed here. Six 4.5 Mvar STATCOMs are installed in a gold mine in Matachewan, Ontario to provide dynamic reactive power support for motors fed over long cable lengths [49]. A 16.8Mvar STATCOM is connected in a petrochemical plant in Gulf coast, Texas, to prevent voltage instability during operation of large motors [49]. A

5 Mvar STATCOM is connected at Seattle Iron and Metal Corp. to provide dynamic support to critical Motors [50].

It is thus evident that dynamic reactive power compensation with SVC and STATCOM are effective and widely used solutions for stabilizing induction motor during grid disturbances. Despite their better performance, these devices are costly. The installation of STATCOMs and SVCs require a large investment and requires a large footprint.

1.3 Mitigation of FIDVR

Both customer level and system level solutions are employed to mitigate FIDVR.

1.3.1 Customer level Solutions

The most effective solutions in customer level are (i) Low Voltage Disconnection, and (ii) Fault Ride Through.

1.3.1.1 Low Voltage Disconnection

The air conditioner unit protection systems are modified to quickly disconnect at a voltage at which it will stall. This helps in fast voltage recovery, but at the cost of large load loss. The sudden tripping of the loads can cause over voltage in the system. The system controls should be modified to address this over voltage problem [1].

1.3.1.2 Fault Ride Through

The air conditioner units are modified to ride through the fault without stalling. This can be done by either oversizing the motor or increasing the inertia. By using an oversized motor, the air conditioner unit will be able to restart as the starting torque will be greater than the high load torque of the compressor. The motor with higher moment of inertia can store more kinetic energy and thus can aid in ride through without stalling. Again, these solutions are expensive, as they requires redesign of the IM [1].

1.3.2 System level solutions

The solutions used in system level to mitigate FIDVR are as follows:

1.3.2.1   Load Shedding

Disconnecting loads during a low voltage event can help in fast recovery of voltage [3]. A localized relay based load shedding scheme is discussed in [51]. A load shedding strategy using IM kinetic energy as the indictor is proposed in [52]. Another load shedding strategy based on IM slip and voltage is presented in [53]. These methods help in fast voltage recovery but have the disadvantage of large load disconnection.

1.3.2.2   Reactive power support

Fast reactive power support can reduce the number of occurrences of FIDVR and can also help in rapid recovery of voltage. The different strategies for optimal allocation and sizing of reactive power sources for FIDVR mitigation are discussed in [54-59].

Reactive power support is the most preferred method as it can help in fast voltage recovery with minimal load loss and it does not require modifications of the IM at customer level, which is a complicated process requiring a large financial and time commitment.

1.3.3   Installations of SVCs and STATCOMs for preventing FIDVR

Reactive power support is the most widely employed solution as it can minimize the adverse impacts of FIDVR, with minimal load loss. STATCOM and SVC are utilized to prevent FIDVR as they can provide fast reactive power as discussed before. A -100/ +300 Mvar SVC is installed in Indianapolis Power and Light system [60], while a ±260 Mvar SVC is installed in Georgia Transmission Corporation network for preventing FIDVR events [61]. An SVC rated 0-225 Mvar for 2 seconds, and 0 -112.5 Mvar capacitive for long term is employed in Massachusetts for fast voltage support [62]. A +200/ -100 Mvar SVC is installed in Western Region to prevent FIDVR [63], which helped in reduced dependence on the under voltage load shedding scheme to mitigate FIDVR. In Saudi Arabia, five SVCs of +600/ -60 Mvar capacity are installed at five 110 kV voltage buses to ensure voltage recovery within 1 s for all single phase faults affecting 380 kV and 110 kV system [64-68]. The size of SVC required for fast recovery (within 1 s) for two phase and three phase faults are extremely high and thus SVCs and therefore SVCs are limited for the fast recovery of voltage for only single phase faults in Saudi Arabia [64].

As discussed in section 1.2.3 that despite their benefits, both SVC and STATCOMs are quite expensive. For instance, a 3 Mvar STATCOM typically costs $ 5 Million, and a 200 Mvar STATCOM costs $ 50 Million.

The expensive conventional solutions motivate an investigation for cheaper and alternative solutions to address instability of critical motor and FIDVR mitigation. Photovoltaic (PV) Solar Systems can be a cheaper alternative solution, as due to their rapid growth worldwide, there is a high probability of having PV solar plant connected in a distribution network having critical motor and a transmission network experiencing FIDVR. In this thesis, novel controls of PV solar systems are developed to address the aforesaid issues. Hence, at first the Photovoltaic (PV) solar technology is described below.

1.4   Photovoltaic (PV) Solar Systems

With increasing concern over global warming, the use of renewable energy is growing at a rapid rate around the world [69]. In 2013, over 140 countries agreed to UN's framework convention on climate change to reduce carbon emission to combat global warming. This boosted the growth of renewable energy systems. Policies like priority dispatch from renewable energy sources, special feed in tariffs, quota obligations and energy tax exemptions has accelerated the growth of renewable energy sources.

PV solar plants are seeing an accelerated growth around the world in last decade with an average growth of 68% per year [70]. In 2017 the total global installed capacity of PV reached 398 GW [71]. It is predicted that global installation capacity of PV systems will reach 1100 GW by 2023 [72] and 4600 GW by 2050 [73].

A commitment was made by the Canadian Government under the Climate change plan for Canada to buy 20% of electricity from renewable energy sources [74]. This policy along with incentive programs, procurement through requests for proposals, standard offer and feed-in tariff programs, and legislated renewable portfolio standards accelerated the growth of wind and PV installations in Canada. Over the last ten years, wind power has grown thirty-fold to 12816 MW in 2018 [75], which is estimated to equal about 10 percent of total Canadian potential wind generation capacity. Similarly, solar photovoltaic (PV) has grown substantially, reaching 2913 MW in 2017 [76] from only 10 MW in 2002. The significant

growth started in 2009 with the installation of 62 MW of solar PV capacity and continued thereafter. A majority of these installations have been in Ontario [74].

Rapid integration of renewable energy is changing the structure of the traditional power systems. Some of the major problems caused due to the integration of renewable sources are variability of renewable energy sources, reverse power flows, system balancing, power quality, and energy management systems [77]. The design of over current protection becomes challenging due to low negative sequence current in renewables rich network. Further the traditional directional relays have to be redesigned due to reverse power flows.

1.5 Grid Connected PV plants

Photovoltaic solar plants are connected to grid at various voltage levels. Small scale residential PV systems (up to several kW) and commercial PV inverters (up to few MW) are connected to distribution networks. Large scale centralized PV plants (ranging up to 500+ MWs) are connected to the transmission system.

1.5.1   Small distributed PV plants

The structure of small scale residential inverters is shown in Figure 1-7. The PV power generated by the PV modules is fed into the DC bus of the inverter. Voltage Source Inverter (VSI) is an IGBT based converter which converts the DC voltage into a series of variable sinusoidal pulse width modulating signals using sinusoidal pulse width modulation technique [78-80]. An L-C-L filter is connected at the AC side of inverter to mitigate the harmonics generated by inverter [81-83]. The DC link capacitor voltage is controlled using Maximum Power point Tracking (MPPT) algorithm to extract maximum power from the PV panels [84-86].
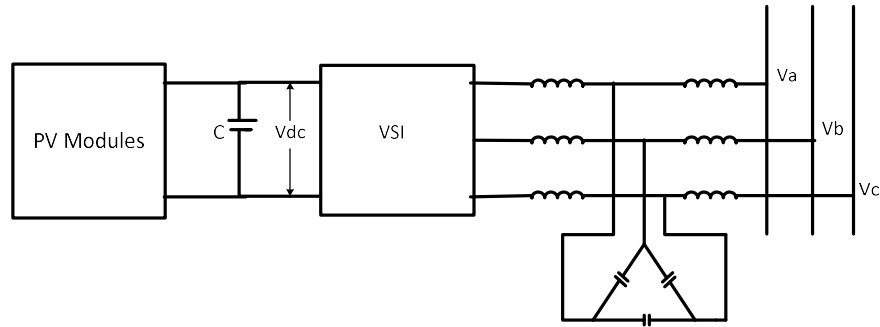
Figure 1-7. Structure of a distributed PV plant.

1.5.2 Large PV plant

Single line diagram of a large utility scale PV plant is shown in Figure 1-8. A large PV plant comprises multiple inverter units which are connected to the point of interconnection (POI) through medium voltage feeder cables [87, 88]. The individual inverters produce power according to the solar irradiance at their local solar panel array. The inverter unit consists of inverters and pad mount transformers. The pad mount transformers step up the inverter terminal voltage to the feeder voltage. The plant transformer steps up the feeder voltage to the transmission line voltage. Some plants have reactive power sources to provide reactive power support at the substation level.
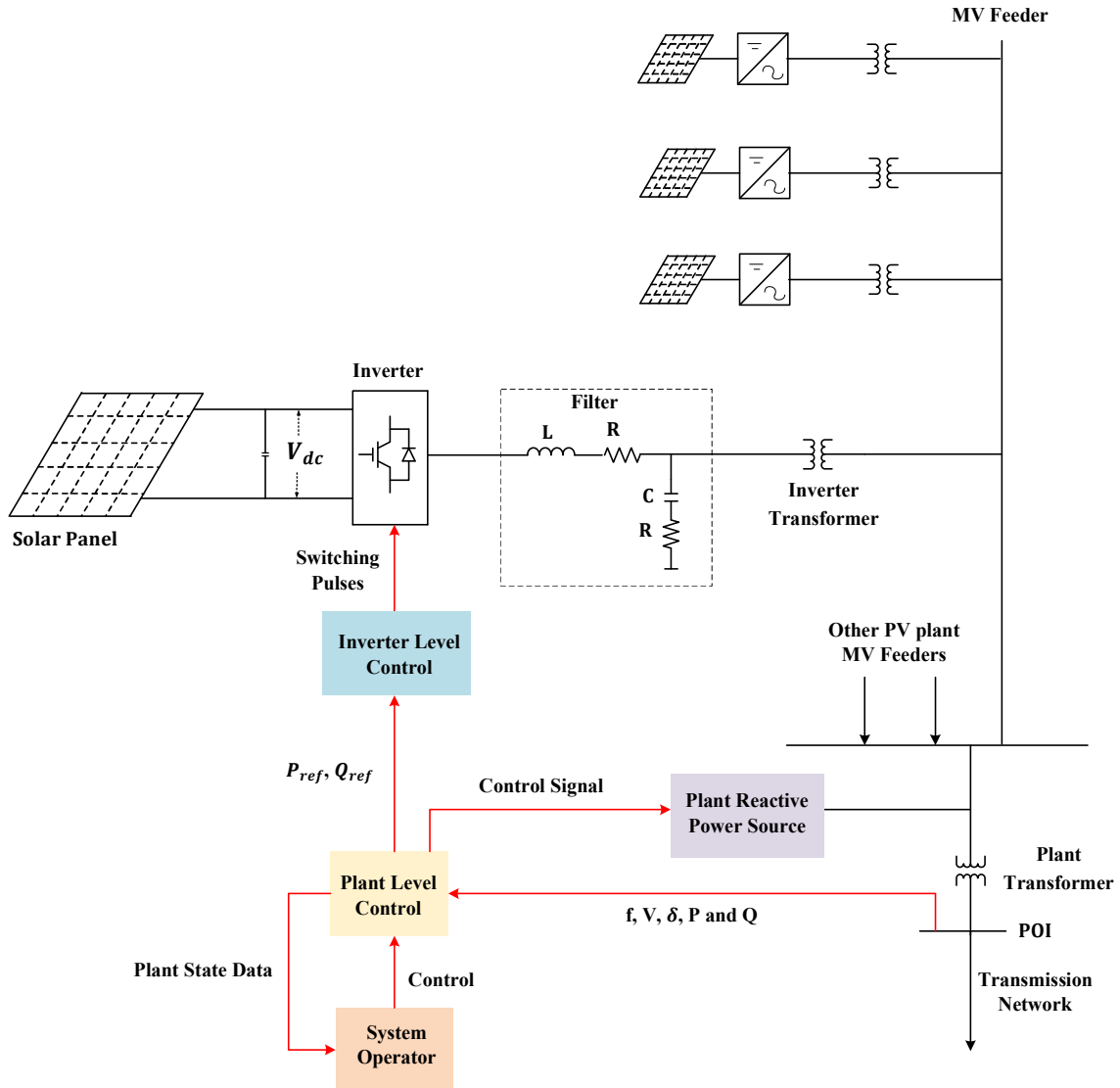
Figure 1-8. Structure of a large PV plant [87]

Large PV plants have two layers of control [87, 88], as described below.

1.5.2.1 Plant Level Controller

The operation of individual inverters in the plant is supervised by a plant level controller (PLC). It monitors the POI measurements and inverter outputs, and subsequently provides commands and power reference signals to the individual inverters. The PLC determines the active power reference (P_{ref}), and reactive power reference (Q_{ref}), based on system conditions, estimated solar irradiance and instructions from the system operator.

The PV plant perform various grid supporting functions viz. Automatic Governor Control (AGC), reactive power support etc., if requested by the system operator. The PLC provides instructions to individual inverter controllers through a dedicated communication channel. The closed loop time constant of a plant controller of large scale PV solar farm is approximately 100 ms [87, 88]. As the plant level controller is slow, grid supporting functions like Low Voltage Ride Through (LVRT) and dynamic reactive power support are done at the inverter level controller [87].

1.5.2.2   Inverter Level Controller

The inverter level control is same as the control system of distributed PV plant. The inverter level controller generates switching pulse for the voltage source inverter to produce the active and reactive power according to solar irradiance and command from the plant level controller.

1.6   Smart Inverters

A smart inverter provides control of real and reactive power both autonomously as well as in response to utility communicated signals [89]. This is contrast to legacy inverters which provide only real power generation. Smart inverters provide different grid support functions including: Volt/Var control, Volt/Watt control, Frequency/Watt control, primary frequency control, ramp rate control, High/Low Voltage Ride Through (H/L VRT) etc. [89], [88]. These Smart (or advanced) inverter functions are being incorporated in various standards for interconnecting distributed generation systems [90-92].

Smart inverter functions of PV inverter can improve the transient stability of the system [93, 94], reduce the adverse effects of PV integration and thus can increase the PV hosting capacity [95-97], improve voltage stability [94, 98-101], damp interarea oscillations [93] and provide frequency support [102].

1.6.1   Smart Inverter Functions for Voltage Control

Smart inverter can provide real and reactive power support to the system during both steady state and transient voltage disturbances. The steady state voltage supporting functions of smart inverter are Fixed Power Factor control, Volt-Var control, and Volt-

Watt Control. The smart inverter can provide dynamic reactive current injection during a disturbance to aid in fast recovery of system voltage.

1.6.1.1   Fixed Power Factor Control

In fixed (off-unity) power factor mode of operation, smart inverter provides reactive power to maintain the power factor of the inverter set by the operator [89].

Fixed power factor control can help in reducing the over voltage due to the large PV integration and can reduce the voltage fluctuation due to variability in PV power [103-108]. In this control strategy, the reactive power output of inverter depends on the real power production, and the amount of reactive power is also limited when the inverter is producing its rated active power.

1.6.1.2   Volt-Var Control

In Volt-Var control mode, the smart inverter produces reactive power according to the terminal voltage of the inverter. A typical Volt-Var curve for a smart inverter is shown in Figure 1-9. The smart inverter produces reactive power when the terminal voltage is beyond the acceptable limit. If the voltage is less than the lowest acceptable level (V_2), the inverter generates capacitive reactive power, till Q_1, which can be the maximum VAR rating of the inverter or the maximum VAR limit set by the operator. For a voltage lower than V_1, the inverter produces fixed capacitive reactive power Q_1. During Voltage swell, the inverter produces inductive reactive power till Q_2, which is the maximum inductive VAR rating of the inverter. For a voltage beyond V_4, the inverter produces fixed inductive reactive power. The Volt-Var characteristics of the inverter can be varied by varying the slope of the curve and the speed of response of inverter [89].

The Volt-Var control of smart inverter minimize the voltage fluctuation caused by the PV penetration [109-116] and also helps in increasing the hosting capacity [117, 118].
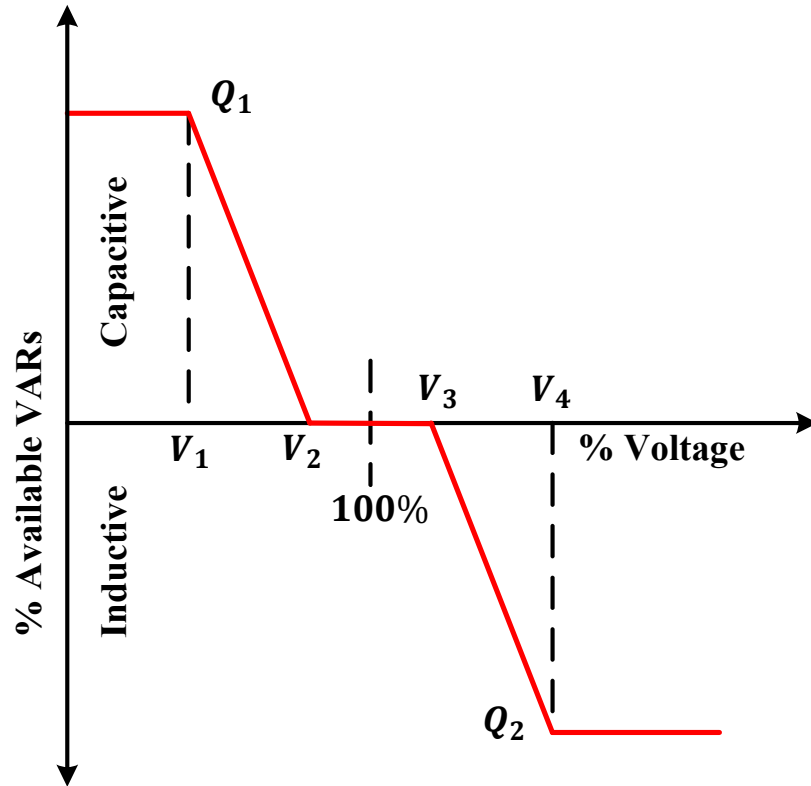
Figure 1-9. Typical Volt-Var Curve of a Smart Inverter [89]

1.6.1.3   Volt-Watt Control
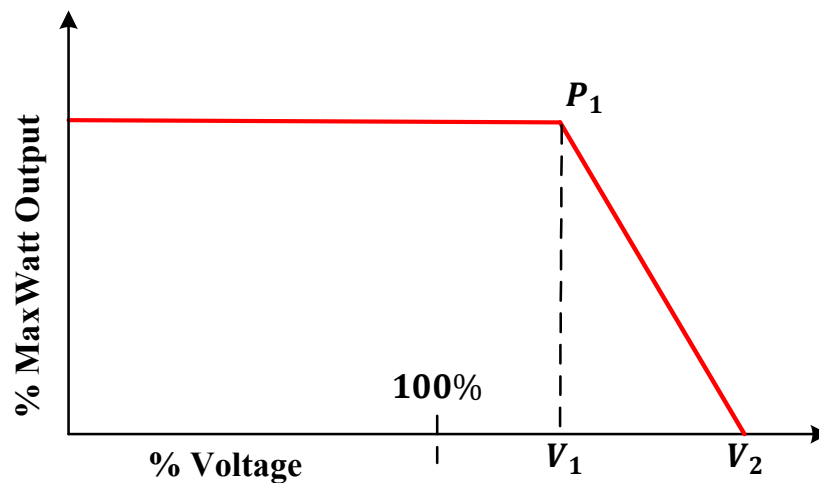
Figure 1-10. Typical Volt-Watt Curve of a Smart Inverter [89]

If high PV power production occurs during low load period, the utilities experience over voltage in the feeder. Volt-Watt control is defined to tackle this over voltage issue. A

typical Volt-Watt curve is shown in Figure 1-10. In Volt-Watt control mode, if the PV system experiences overvoltage beyond acceptable limit (V_1), the smart inverter curtails its active power according to the Volt -Watt curve. For a severe high voltage ($> V_2$), the smart inverter curtails its full active power production. The Volt-Watt function can reduce the overvoltage issue as discussed in [119-123].

1.6.1.4   Low/High Voltage Ride Through

Previously distributed generators (DGs) were required to trip during a voltage disturbance. With the increased penetration of DGs, the momentary tripping of DGs during a voltage transient reduces the reliability of electric supply. To improve the reliability of electric supply with high penetration of DGs, inverters are required to ride through the voltage disturbance for a specified time, after which they are allowed to disconnect from the grid. An example for a Low/High Voltage Ride Through requirement is shown in Figure 1-11. The ride through requirements are specified according to the inverter terminal voltage and duration for which the inverter is experiencing that low/high voltage. According to the VRT curve, the inverter is required to operate in either of the five modes during a Low/High Voltage event,

1. **Continuous Operation:** If the terminal voltage is within the normal operating voltage, the inverter should continue generating active power.

2. **Mandatory Operation:** In this mode, the inverter is required to remain connected by producing the maximum active power.

3. **Momentary Cessation:** The inverter can stop generating power but shall not trip.

4. **Shall Trip:** The inverter shall disconnect from the grid.

5. **May Ride Through or may Trip:** The inverter may remain connected or disconnected from the grid.

Voltage Ride Through (VRT) is required by the latest grid codes [90-92]. The VRT requirements of German Grid Code is shown in Figure 1-12 [91]. The requirements

according to California Rule 21 is shown in Figure 1-13 [92]. IEEE 1547-2018 [90] requires VRT requirement similar to California Rule 21.
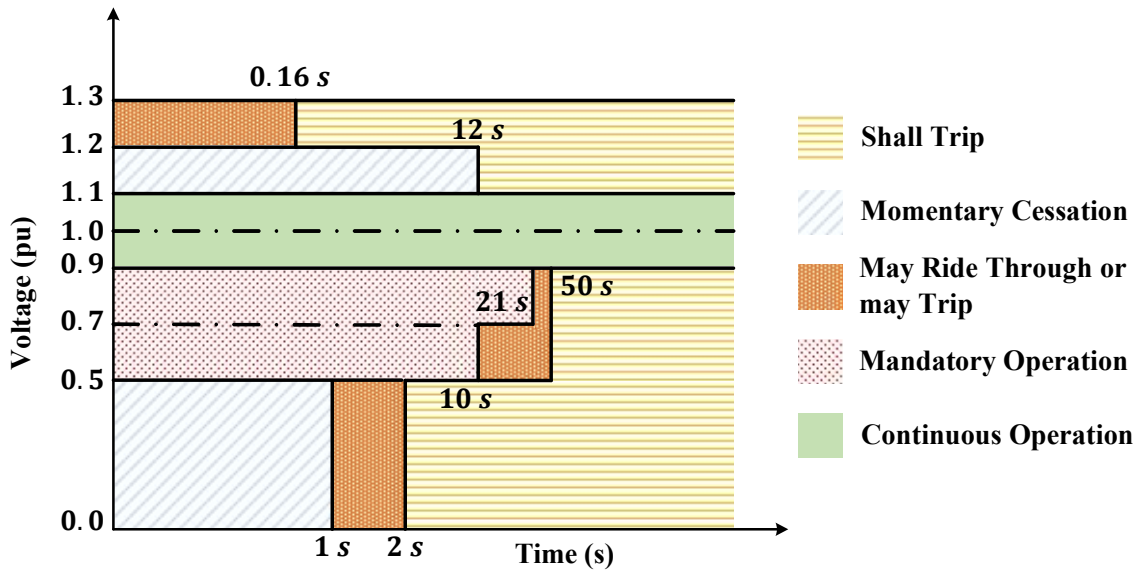
Figure 1-11. Typical VRT curve for a Smart Inverter [89]
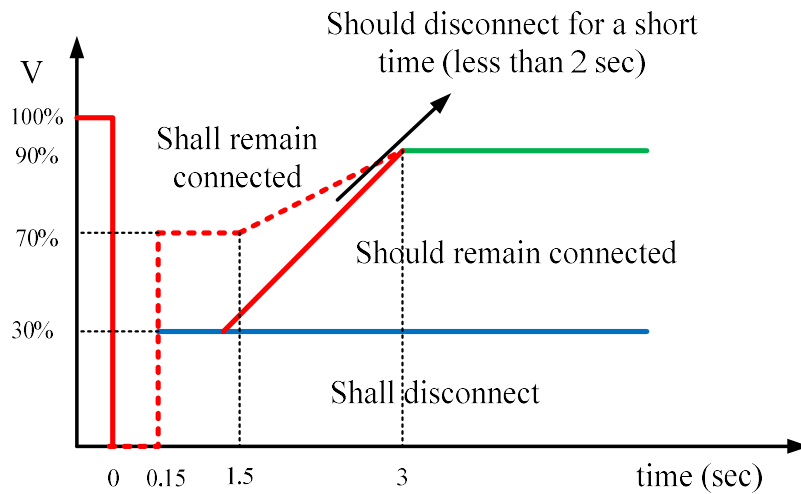
Figure 1-12. LVRT requirements according to BDEW [91].
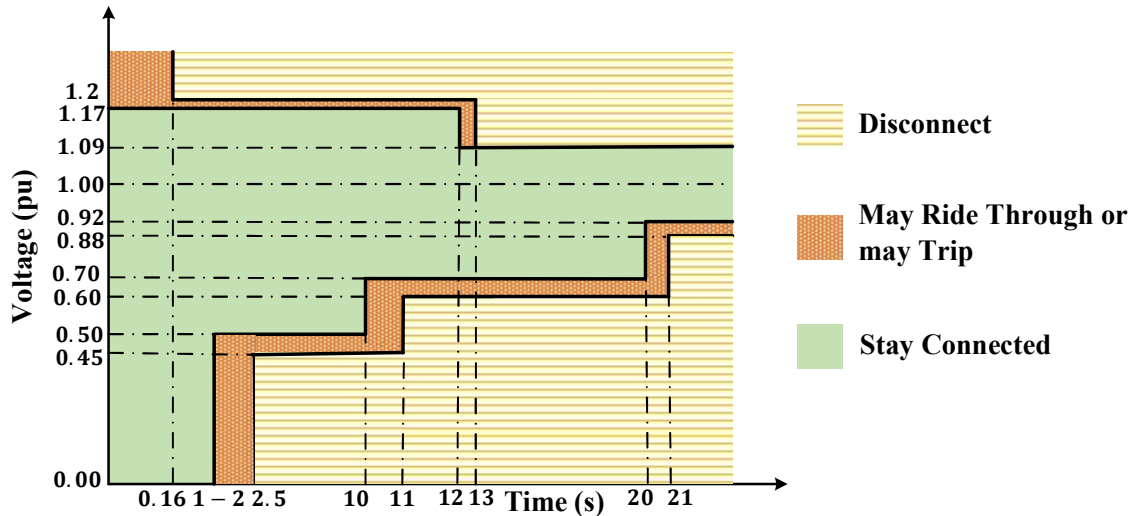
Figure 1-13. VRT requirements according to Rule 21 [92]

1.6.1.5   Dynamic Reactive Current Control

To improve short term voltage stability, smart inverters are required to inject reactive current during voltage ride through. An example for a dynamic reactive current injection requirement of a smart inverter is shown in Figure 1-14. During this control, the inverters are required to inject a capacitive reactive current during voltage sag, and inductive reactive current during a voltage swell. The amount of reactive current is calculated based on the instantaneous value and moving average value of the inverter terminal voltage. The percent of reactive current injection can be varied by varying the slope of the reactive current curve. For example, the German Grid Code (BDEW), the PV inverter needs to inject minimum 2% reactive current per 1% voltage drop below 0.9 pu. [91].

$$i_{cap} = \ 2 * \Delta V \qquad for\ V < 0.9\ pu \qquad\qquad (1.1)$$

i_{cap} = Capacitive current required by the BDEW

ΔV = Present Inverter terminal voltage – moving average voltage over one cycle

V = Present Inverter terminal voltage

The dynamic reactive current injection is optional in IEEE 1547 [90] and California Rule 21 [92].
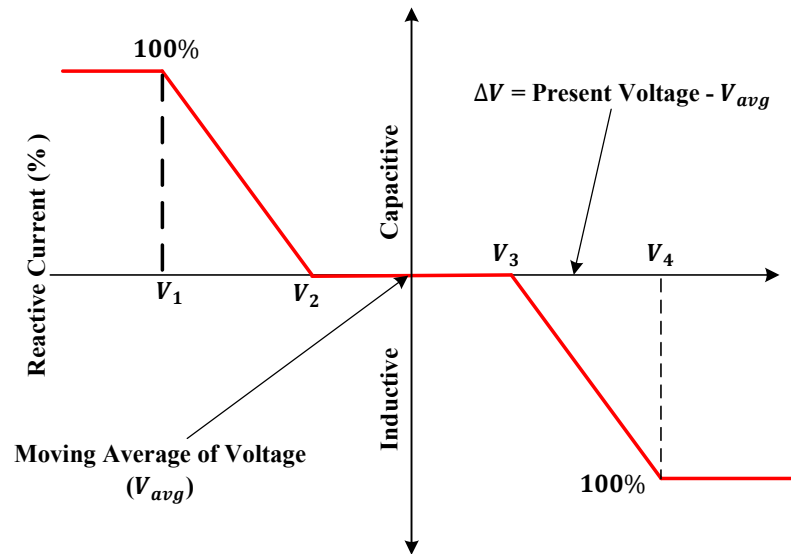
Figure 1-14. Typical Dynamic Reactive Power Support Function [89]

1.6.2 Applications of smart inverters to provide dynamic voltage support in distribution networks

Different dynamic voltage support strategies of PV inverters for voltage recovery during a disturbance in Low Voltage network are investigated in [124, 125]. It is shown that dynamic support from PV inverters can improve short term voltage stability. A control strategy for providing fixed amount of reactive power support to the grid during a disturbance is demonstrated in [126]. A model predictive based control of PV inverter for providing dynamic voltage support during a fault is presented in [127]. A dynamic voltage control strategy to provide reactive power support during High and Low Voltage Ride Through event is discussed in [128]. A control strategy utilizing the maximum current capacity of inverter to maximize the active current injection during a disturbance is presented in [125].

1.6.2.1   Active and Reactive Power control for dynamic voltage support

As the feeders have both resistance and inductance, the motor terminal voltage (V) is sensitive to change in both active and reactive power output of PV solar farm. Assume P_{sens} and Q_{sens} as the change in motor terminal voltage for unit change in active (P) and reactive power (Q) output of PV solar farm, respectively.

$$P_{sens} = \frac{\partial V}{\partial P} \tag{1.1}$$

$$Q_{sens} = \frac{\partial V}{\partial Q} \tag{1.2}$$

Thus, the change in voltage can be represented as,

$$\Delta V = \frac{\partial V}{\partial P}P + \frac{\partial V}{\partial Q}Q \tag{1.3}$$

In decoupled control of PV inverter,

$$P = \frac{3}{2}V_d i_d \tag{1.4}$$

$$Q = \frac{3}{2}V_d i_q \tag{1.5}$$

we can say,

$$P \propto i_d \text{ and } Q \propto i_q \tag{1.6}$$

The maximum change in motor terminal voltage can be found by solving following optimization problem [101, 125],

$$\text{Maximize, } \Delta V = \frac{\partial V}{\partial P}P + \frac{\partial V}{\partial Q}Q \tag{1.7}$$

Subject to,

$$\sqrt{i_d^2 + i_q^2} = I_{max}$$

<div align="right">(1.8)</div>

$$i_d, i_q \geq 0$$

From (1.7), it is evident that the maximum increase in voltage will occur if active and reactive power are injected according to the active and reactive power sensitivity.

1.6.3 Application of smart inverters to provide dynamic voltage support in transmission networks

Dynamic support from a large PV plant can help in fast recovery of voltage [100, 129, 130]. Dynamic reactive power support by large PV plant per BDEW German grid code [20] to improve short term voltage stability is presented in [100, 130]. Dynamic reactive current injection during LVRT is described but made optional in IEEE Standard 1547-2018 [90].

A combined real and reactive power control strategy of injecting real and reactive power in a constant 1:1 ratio is presented in [101]. However, the efficacy of the method presented in [101] is limited in transmission systems where X/R >> 1.

1.6.4 Field Demonstration of smart inverter functions

Field demonstrations of smart inverter functions for voltage control such as fixed (non-unity) power factor, volt-var and volt-watt, etc. have been performed by utilities [88, 131-134].

The fixed power factor operation of utility scale rooftop PV plants for mitigation of voltage related issues due to PV integration was demonstrated on a 2 MW PV system in California [131]. The effectiveness of fixed power factor smart PV inverter function in reducing voltage deviations was field-demonstrated on a distribution circuit near Porterville, California, for increasing hosting capacity of PV systems [132]. The results of field demonstration of smart inverters with volt-var control and power factor control for providing voltage support in San Diego Gas & Electric (SDG&E) distribution network were presented in [133]. A demonstration project was conducted in Puerto Rico on two utility-scale photovoltaic (PV) plants rated 20+ MW to demonstrate power smoothing,

frequency regulation services and power quality [134].The field demonstration results of smart inverter functionalities such as automatic governor control, power factor control, frequency droop control and voltage control done on a 300 MW PV power plant are presented in [88].

1.7 PV-STATCOM: a new smart inverter

A new smart inverter technology utilizing PV solar plants as a dynamic reactive power compensator STATCOM, termed PV-STATCOM is proposed in [135]. The different modes of operation of PV-STATCOM are described below.

1.7.1 Partial STATCOM Mode

In this mode, the PV system provides dynamic reactive power support using the PV inverter capacity remaining after real power generation. This mode gives priority to real power generation.

1.7.2 Full STATCOM Mode
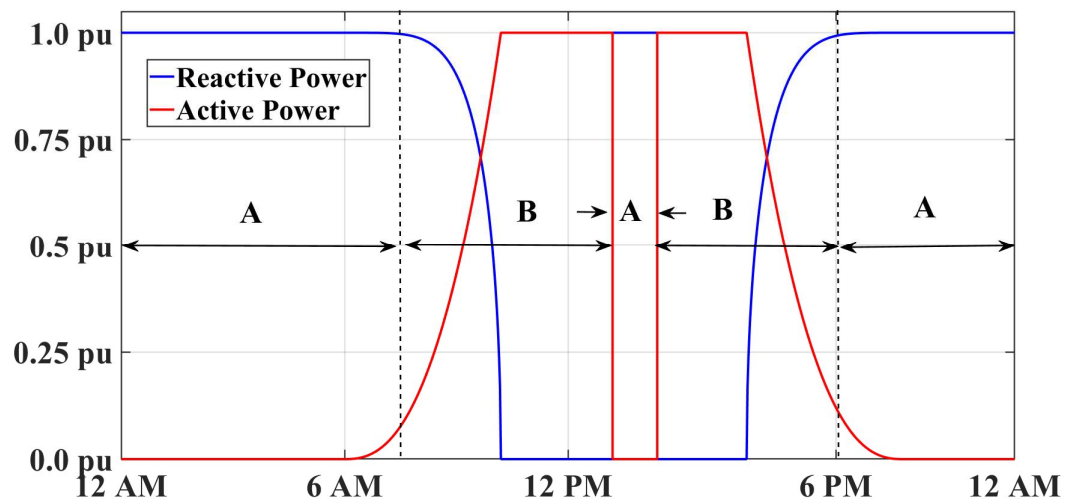
Figure 1-15. PV-STATCOM capability of PV inverter. Regions A illustrates Full STATCOM Mode (Variant 1) and Regions B depict Partial STATCOM mode.

In this mode, during any system disturbance in daytime the active power is curtailed for a short duration (typically less than a minute) and dynamic reactive power support is

provided to power system as a STATCOM. As soon as system stabilization need is fulfilled, the PV system returns to its predisturbance power generation level. This mode gives priority to reactive power exchange.

The Full-STATCOM mode has two variants. In Variant 1 the real power is curtailed to zero and entire inverter capacity is made available for providing reactive power exchange. If the need for reactive power is less than the entire inverter capacity, Variant 2 is used in which active power is curtailed (not to zero) but only by an amount which allows the needed reactive power to be exchanged with the power system. Variant 1 of Full STATCOM is completely available during nighttime. With the above two operating modes, the PV-STATCOM provides a 24/7 functionality as a STATCOM.

The applications of PV-STATCOM were presented for enhancing power transmission capacity [136], mitigation of sub synchronous resonance [137], and dynamic voltage control [138], etc. Initial studies on stabilization of an IM located at PV solar farm terminal using non-autonomous control of PV-STATCOM is presented in [139].

The PV-STATCOM technology can provide voltage recovery similar to STATCOM during both night and day time. Moreover, PV-STATCOM technology is about 50-100 times more economical than a STATCOM (and also SVC). This is because it requires the implementation of only certain additional controls on existing PV inverters and the already present electrical infrastructure (substation, transformers, breakers, buswork, etc) of the solar farm.

Due to the above said advantages, it is highly likely to operate neighboring PV plants as PV-STATCOMs. The neighboring PV-STATCOMs may interact adversely between them. The small signal analysis is done to study the interaction between multiple PV-STATCOMs as described below.

1.8 State Space Analysis of PV integration

State space analysis is performed to evaluate the small signal stability of power systems. Eigen values calculated from the state space model gives information on the stability of the system at that operating point. Participation factor analysis can be done to

find the factors affecting stability and can be used to design controllers for improving the stability of system.

1.8.1 Interaction between PV systems and other voltage regulating devices

The Smart Inverter control of PV systems can potentially have adverse interactions with traditional voltage regulating devices viz., switched capacitor, OLTC, etc. [140-146]. The participation of PV systems in voltage regulation increases the number of switching of these devices [140, 143-145]. Studies have shown that power factor operation of PV system has substantial impact on other voltage regulating devices [146]. The distributed PV inverters cause more severe impact than the centralized PV plant [145]. Adding a dead band in the voltage control range of PV inverters can reduce these adverse interactions [141]. Dividing power systems into different control zones and modifying the speed of operation of these devices according to distance between them can effectively reduce negative interactions and improve voltage profile [142].

1.8.2 Interaction between PV systems

Multiple PV units can also adversely interact with each other and reduce stability of the system. Interactions between multiple PV units are reported in micro grid [147], Low Voltage Distribution Network [148, 149], and Medium Voltage Distribution Network [150, 151].

In a microgrid, the converter interfaced loads acts as a negative load and can deteriorate the stability of the system [147]. If multiple PV units are taking part in Volt -Var control, the adverse interactions can be minimized by reducing the speed of response as reported in [151-154]. Studies in [155] have reported that increase in measurement delay reduces stability. A method based on dividing the system into different coherent groups and develop controller for each group assuming interactions with other groups as external disturbance is proposed in [156]. An output feedback minimax optimal control strategy is proposed to eliminate the negative interactions in [149]. Negative interactions are possible between Volt-Watt controller and Volt-Var controller, when the PV is operating near its

full capacity [157]. These interactions can be reduced by increasing the time constant of the voltage measurement filter only up to a limit [157].

1.9 Knowledge Gaps

The knowledge gaps existing in literature for the application of PV solar plant to address instability of critical motor and FIDVR are presented below. The knowledge gaps in demonstration of smart inverter technology and small signal analysis of interaction between multiple PV solar plants, are also presented.

1.9.1 Application of Smart Inverter function for stabilizing remotely located critical induction motor

Dynamic voltage support requirements of grid codes [90-92] and control strategies presented in literature [124-128] require PV systems to provide reactive current in proportional to the drop in its local bus voltage below prespecified limits. However, during system faults this function may not be adequate for stabilizing critical motors that are remotely located from the PV solar plants. This is because even if local voltage support is provided, the voltage at the remote motor terminal may not recover to sufficient levels to meet the extended reactive power needs of the IM. Moreover, Voltage Ride Through is neither defined nor expected from PV solar plants during nighttime [90].

Ref. [126-128] discusses the control strategies based on reactive power injection during a transient. But in a distribution network the $\frac{X}{R}$ ratio is low, and thus the impact of reactive power on system voltage is lower. So, the methods based on reactive power injection can be less effective in providing voltage support in distribution networks.

1.9.2 Application of Smart Inverter function for mitigation of FIDVR

Dynamic reactive power support using remaining inverter capacity presented in [158] is less effective during periods of high PV power generation. Fixed power factor operation of PV plant for providing voltage support discussed in [99] is less effective during a transient as the reactive power injected is limited by the active power output and set power factor reference of the PV.

Voltage Ride Through functions according to German grid code [91] and IEEE Standard

[90] are based on reactive power, and are not defined or prescribed during nighttime (when PV systems do not generate power). A VRT function based on combined modulation of real and reactive power can aid in fast recovery of system voltage than reactive power based control alone. Moreover, for effective voltage recovery the combined modulation of real and reactive power according to network X/R ratio should be investigated.

1.9.3 Field demonstration of smart inverter functions

In all the above utility demonstrations, voltage control based smart inverter functions had a response time of 1-3 seconds. The capability of PV solar plants to provide faster voltage support has not been tested in field so far. Furthermore, smart inverter functions have neither been defined nor demonstrated during nighttime. These aspects need to be researched and tested.

1.9.4 Application of PV-STATCOM for motor stabilization

The application of PV-STATCOM for providing dynamic voltage support for induction motors in distribution and transmission system is not explored in literature. Furthermore, this capability of a PV-STATCOM to provide dynamic voltage support for induction motor stabilization has not been tested in field so far.

1.9.5 Small Signal Analysis of multiple PV solar plants

The interactions between distributed small PV units operating according to grid code standards are studied in detail in [147-157, 159, 160]. The commercially available PV inverter has the maximum capacity up to 4 MW [161-163], and thus, utility scale PV plants connected to medium voltage distribution network have multiple inverters connected to the substation transformer using multiple pad mount transformers and collector system, thus having a structural difference with the distributed small PV inverter units. In literature, utility scale PV plants are modelled as a single equivalent unit for stability analysis [145, 164]. Due to the structural difference, the actual behavior of the PV plant could be different from the equivalent model and this needs to be investigated.

Small signal analysis of PV plants equipped with PV-STATCOM control has not been performed so far. The small signal analysis of PV plant equipped with PV-STATCOM

control has to be done to study the possible interactions between multiple inverters in the same plant and the interactions between adjacent plants, and to develop a guideline for the design of the PV-STATCOM systems before installation.

1.10 Scope and Objectives of Thesis

1.10.1 Scope of the Thesis

PV-STATCOM is a novel technology. It has a great potential to support the grid in several ways due to its ability to dynamically control both real and reactive power output. However, the application of PV-STATCOM for fast voltage support for stabilization of critical induction motors is not explored well in literature. Unstable operation of induction motors and FIDVR issues are one of the main causes of voltage instability in electrical network. Dynamic reactive power sources like SVC and STATCOM are conventionally utilized solutions for preventing motor instability. Due to the vast and increasing deployment of PV inverters, PV-STATCOM can be utilized as a low cost solution for supporting critical motors.

1.10.2 Objectives of the Thesis

The objective of this thesis is to explore novel applications of PV-STATCOM technology for stabilizing critical motors and obviating FIDVR in power systems.

To achieve this objective, the following tasks have been identified, which eventually lead to the different Chapters in this thesis:

- To develop a control strategy for dynamic reactive power control of PV-STATCOM for stabilizing a remotely located critical induction motor.

- To field demonstrate the application of PV-STATCOM for the stabilization of critical induction motor.

- To develop a comprehensive control strategy for combined real and reactive power control of PV-STATCOM for providing dynamic voltage support to a remotely located critical induction motor connected on the same distribution feeder.

- To demonstrate the capability of a PV-STATCOM to mitigate FIDVR in a transmission network.

- To perform the stability analysis of two utility scale PV plants connected to a medium voltage realistic feeder with PV-STATCOM control, and to develop design guidelines for the PV-STATCOM controller design considering the impact of interactions between PV plants and also the interactions between inverters in same PV plant.

1.11 Outline of Thesis

Chapter 2 presents the modeling of various components of a PV solar farm connected to the electrical network. The design strategies for the controller parameters are discussed in detail. The equivalent and detailed model of a large PV plant is also discussed. The overview of the proposed PV-STATCOM controller is presented.

Chapter 3 discusses the reactive power control of PV-STATCOM to stabilize remotely located critical IM. Detailed simulation studies are done on distribution network of Bluewater Power, Sarnia, Canada, to show the effectiveness of the proposed control. The effectiveness of the proposed control is further tested for variation of key system parameters on a realistic distribution network in Ontario, Canada, and the results are included. Simulation studies show that the proposed control can eliminate the need for installing STATCOMs, and it can ensure stable operation of critical IMs, even for the cases which the reactive power support from the PV systems according to the latest grid codes is inadequate for motor stabilization.

Chapter 4 presents results of first time field validation of the proposed control on distribution network of Bluewater Power Corporation Sarnia, Canada. The capability of PV-STATCOM technology for both day and night time are tested. It is shown that PV-STATCOM technology can ensure stable operation of remotely located IM 24/7. The performance of this technology is further compared with the German Grid Code requirements. The impact of weak communication link on the performance of PV-STATCOM technology is also tested.

Chapter 5 presents a comprehensive control strategy for combined real and reactive power control of PV-STATCOM for providing dynamic voltage support to a remotely located critical induction motor connected on the same distribution feeder. Extensive simulation studies are done on a medium sized PV plant connected to a distribution feeder in Ontario, Canada. The studies confirm that the proposed control can ensure stable operation of critical IM in systems with various X/R ratios, and even for cases where other smart inverter control strategies fail. Simulation studies are further done using detailed PV plant model to compare the implementation of proposed control on Plant Level or Inverter Level. Small signal studies are done to find the impact of PV plant parameters and system parameters on the stability of a medium sized PV plant equipped with the proposed control.

Chapter 6 presents a control strategy for PV-STATCOM, for FIDVR alleviation. The proposed control involves dynamic modulation of both reactive and real power during day, and of reactive power during night. Eigenvalue analysis is done to study the sensitivity of proposed controller performance to various power system and PV plant parameters. Extensive PSCAD simulation studies of FIDVR are performed in a realistic power transmission system with large-scale PV plant and comprehensive IM loads. It is shown that the proposed PV-STATCOM control: (i) mitigates FIDVR even if solar farm is located more than 100 km from motor loads, (ii) is more effective than reactive power support required by German Grid Code, (iii) is equally effective as a STATCOM connected locally at motor loads, and iv) stabilizes motors at night which is beyond Grid Code requirements.

Chapter 7 presents the results of stability analysis of two utility scale PV plants connected to a medium voltage realistic feeder with PV-STATCOM control. The studies are done for (i) PV-STATCOM control done at plant level, and (ii) PV-STATCOM control done at inverter level. Studies are done to compare the application of equivalent model and detailed model of PV plants for stability analysis. Further studies are done to test the sensitivity of proposed controller performance to X/R ratio of the feeder, system strength, PV plant active power output, PV plant delay, speed of response of voltage controllers and distance between the PV plants.

Chapter 8 presents the conclusions and the main contributions of this thesis. Future research work with the PV-STATCOM controller is also proposed.

Chapter 2

2 Modeling of Grid Connected PV System

2.1 Introduction

This chapter presents the detailed modeling of different components of a PV solar farm connected to power distribution grid. The modeling of different distribution grid components is presented first, while the modeling of a PV system components and controller is described later. The design strategy for various controller components is further discussed. The model of a large PV plant is also presented. Then the structure of the PV-STATCOM controller is explained.

2.2 Radial Distribution System

The single line diagram of a typical radial distribution system is shown in Figure 2-1. A distribution system consists of substation connected to the transformer, distribution feeders and loads. The modeling of various components of the distribution system is discussed in detail in this section.
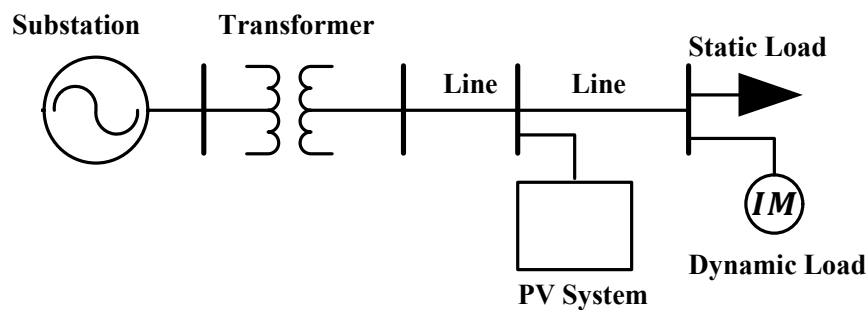
Figure 2-1. Single Line Diagram of a distribution system

2.2.1 Substation System

The radial distribution systems are fed by high voltage transmission system. For the distribution system studies, the high voltage system is modelled as a voltage source behind Thevenin equivalent impedance as shown in Figure 2-2. The source voltage is V_g. The

Thevenin equivalent resistance and inductance of the high voltage network is represented as L_g and R_g, respectively. The dynamics of substation is represented by (2.2).
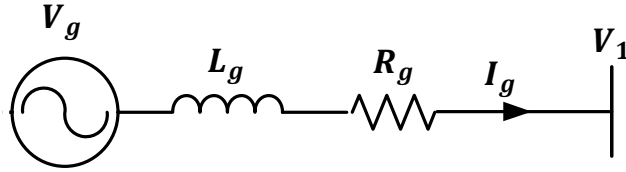
Figure 2-2. Substation Model

$$L_g \frac{dI_g}{dt} = V_g - R_g I_g - V_1 \tag{2.2}$$

2.2.2   Distribution Line Model

The distribution line is represented by a lumped π equivalent model as illustrated in Figure 2-3. V_S and V_R are, respectively, the sending end and receiving end positive sequence voltages. The sending end and receiving end currents are denoted by I_S and I_R, respectively. The series parameters R and L denote the lumped resistance and inductance of the equivalent π model and are given by (2.3) and (2.4), respectively. The shunt parameters are conductance and susceptance. The conductance of distribution lines is very small, and they are usually neglected. The lumped susceptance of the distribution line, C is given by (2.5).

$$R = r * l \tag{2.3}$$

$$L = \frac{x * l}{2 * \pi * f} \tag{2.4}$$

$$C = \frac{y * l}{2 * \pi * f} \tag{2.5}$$

where, r, x and y are respectively the resistance, inductive reactance and susceptance per unit length of the distribution line. l and f are the length of line and frequency of the system, respectively.
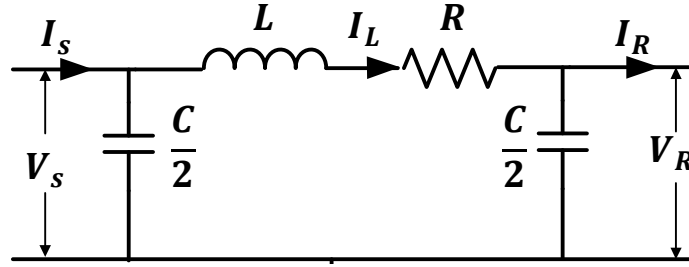
Figure 2-3. Distribution Line Model

The dynamics of the distribution line can be represented by (2.6).

$$L\frac{dI_L}{dt} = V_S - RI_L - V_R$$

$$\frac{C}{2}\frac{dV_S}{dt} = I_S - I_L \qquad\qquad (2.6)$$

$$\frac{C}{2}\frac{dV_R}{dt} = I_L - I_R$$

2.2.3   Transformer

Transformers are widely used in distribution system for transformation of voltage and to provide isolation. Usually, the transmission voltage is transformed to medium voltage at the substation for feeding distribution lines. Transformers are further used in distribution network to step down the voltage to feed low voltage loads. The distributed generators (DGs) are connected to the distribution network through a transformer, which provides an electrical isolation between the DG and distribution network and transform the DG output voltage to the distribution network rated voltage.

A two winding transformer is represented by its equivalent shunt and series parameters as shown in Figure 2-4. The series resistance and reactance represent the copper loss and leakage reactance of the windings, respectively. The leakage reactance of primary and secondary coils are L_P and L_S respectively. The copper loss in primary and secondary coil are modelled as R_P and R_S respectively. The core loss (R_C) and magnetizing reactance (L_M) of the transformer is modelled as shunt parameters. The shunt impedance of the transformer

is very high, and usually neglected while modeling transformer for power system steady state studies. Thus, a transformer is modelled as series resistance R and reactance L as shown in Figure 2-5, for steady state analysis. The resistance R and reactance L are the equivalent resistance and reactance of primary and secondary coil. The voltage transformation ratio of the transformer is denoted as n. The differential equation governing the transformer dynamics is given by (2.7).
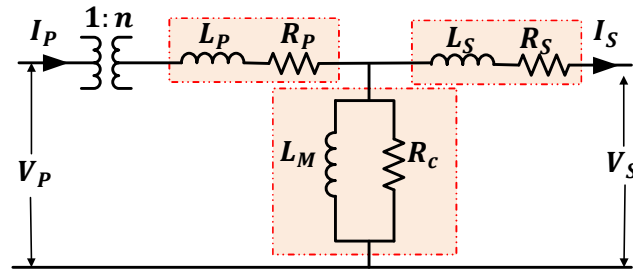
Figure 2-4. Model of a Transformer

$$L\frac{dI_S}{dt} = n * V_P - RI_S - V_S \tag{2.7}$$
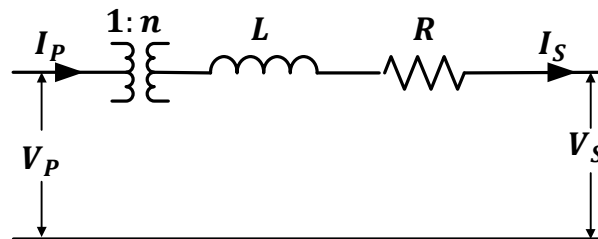
Figure 2-5. Simplified Model of transformer

2.2.4   Load Model

The loads can be classified into static loads, dynamic loads and power electronic based loads based on their power consumption characteristics. The power consumption of the load is dependent on voltage and frequency. Dynamic loads such as induction motor loads are highly dependent on system voltage and require detailed modeling for voltage stability studies. The other loads are represented as voltage dependent loads in this thesis.

2.2.4.1 Static loads

Static loads are modelled as voltage dependent load as given in (2.8).

$$P_L = P_0 \left(\frac{V}{V_0}\right)^{a1}$$

$$Q_L = Q_0 \left(\frac{V}{V_0}\right)^{a2}$$

(2.8)

where, P_L and Q_L are the active and reactive power consumed by load at a voltage V. P_0 and Q_0 are the active and reactive power consumed by load at rated voltage V_0, respectively. The factors $a1$ and $a2$ are dependent on the load types. Typical values of $a1$ and $a2$ used in North America are 0.72, and 1.27, respectively [100].

2.2.4.2 Induction Motor loads

The working principle of induction motor (IM) is electromagnetic induction. So, the IM can be modelled similar to a transformer. Since the frequency of operation of stator and rotor are different, the equivalent model can be represented in stationary reference frame, rotor reference frame or a synchronously rotating frame. In this thesis, the IM is modelled in stationary reference frame.

The equivalent circuit of an IM is illustrated in Figure 2-6. L_s and R_s denotes the stator inductance and resistance respectively. L_M is the magnetizing inductance of IM. L_R and R_R represent the rotor inductance and resistance transformed to stationary frame respectively. The IM load is represented by $\frac{1-s}{s} R_R$, where s is the slip of IM.
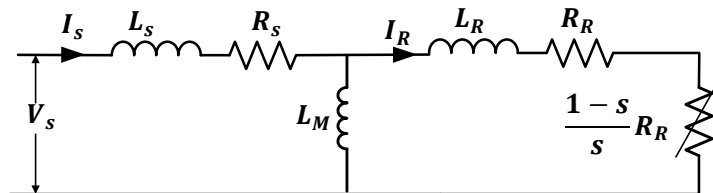
Figure 2-6. Model of Induction Motor load

The IM stator and rotor dynamics are modelled by using flux linkages as the variables. The stator and rotor flux linkages are given by (2.9) and (2.10) respectively. The electromagnetic torque (T_e) of the IM is represented by (2.11). The electro mechanical equation of the IM is given by (2.12).

$$\frac{\partial \Psi_{ds}}{\partial t} = -I_{ds} * R_S + V_{sd} + \psi_{qs} * \omega_g$$

$$\frac{\partial \Psi_{qs}}{\partial t} = -I_{qs} * R_S + V_{sq} - \psi_{ds} * \omega_g$$

(2.9)

$$\frac{\partial \Psi_{dr}}{\partial t} = -I_{dr} * R_R + \psi_{qr} * (\omega_g - \omega_r)$$

(2.10)

$$\frac{\partial \Psi_{qr}}{\partial t} = -I_{qr} * R_R - \psi_{dr} * (\omega_g - \omega_r)$$

$$T_e = \left(\left(\Psi_{ds} * I_{qs} \right) - \left(\Psi_{qs} * I_{ds} \right) \right) * \left(\frac{3}{2} \right) * \left(\frac{P}{2} \right) \qquad (2.11)$$

$$\frac{\partial \omega_r}{\partial x} = \frac{P}{2 * J} * (T_e - T_m) \qquad (2.12)$$

The relation between fluxes and currents are given by (2.13).

$$\begin{bmatrix} \Psi_{ds} \\ \Psi_{dr} \end{bmatrix} = \begin{bmatrix} L_{SS} & L_M \\ L_M & L_{RR} \end{bmatrix} \begin{bmatrix} I_{ds} \\ I_{dr} \end{bmatrix}$$

(2.13)

$$\begin{bmatrix} \Psi_{qs} \\ \Psi_{qr} \end{bmatrix} = \begin{bmatrix} L_{SS} & L_M \\ L_M & L_{RR} \end{bmatrix} \begin{bmatrix} I_{qs} \\ I_{qr} \end{bmatrix}$$

where, L_{SS} and L_{RR} are given by (2.14).

$$L_{SS} = L_S + L_M$$

(2.14)

$$L_{RR} = L_R + L_M$$

where,

I_{ds} and I_{qs} are the stator d and q axis current.

I_{dr} and I_{qr} are the rotor d and q axis current.

V_{ds} and V_{qs} are the stator d and q axis voltage.

Ψ_{ds} and Ψ_{qs} are the stator d and q axis fluxes.

Ψ_{dr} and Ψ_{qr} are the rotor d and q axis fluxes.

ω_g is the stator frequency

P is the number of poles

ω_r is the rotor frequency

T_e and T_m are the electromagnetic and shaft mechanical torque respectively.

J is the combined rotor and load inertia coefficient.

L_{SS} is the total stator inductance.

L_{RR} is the total stator inductance.

2.3 Model of PV System

The PV system converts solar power to electrical power and feed into the electrical grid. The PV system consist of solar panels, inverter, filter and coupling transformer. The schematic of a grid connected PV system is shown in Figure 2-7. Point of Common Coupling (PCC) is defined as the point where the PV plant is connected to the electrical grid. The Electrical Point of Connection (EPC) is defined as the point where, the inverter is connected to the rest of the PV plant [89]. EPC is considered as the low voltage terminal of the coupling transformer in this thesis.
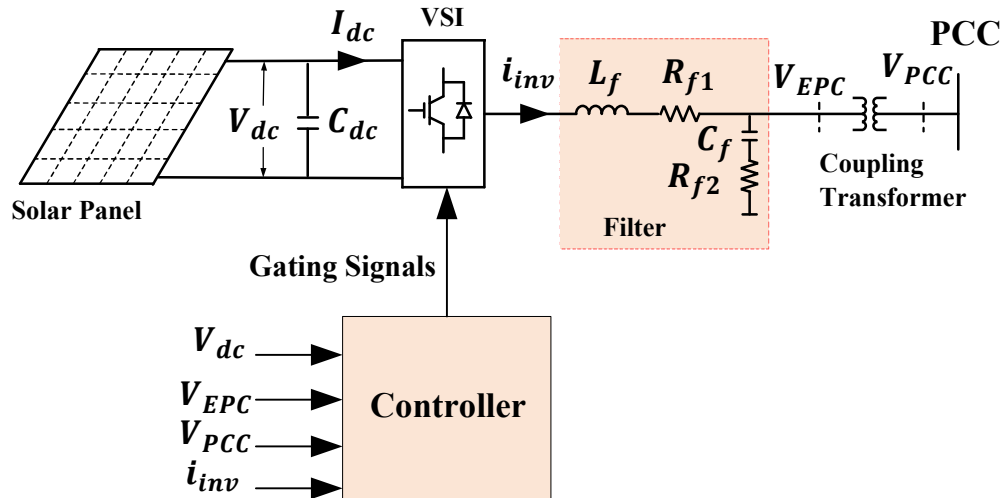
Figure 2-7. Single Line Diagram of a Grid Connected PV System.

2.3.1   Solar Panels

The solar cells generate electric current, when solar irradiance falls on them. The power output of a solar cell is very small, so multiple solar cells are connected in series-parallel configuration in a solar panel. The rating of typical solar panels currently available on market are 200 -350 watts. Thus, in a large solar farm, multiple panels are connected in series and parallel combination to extract maximum power.
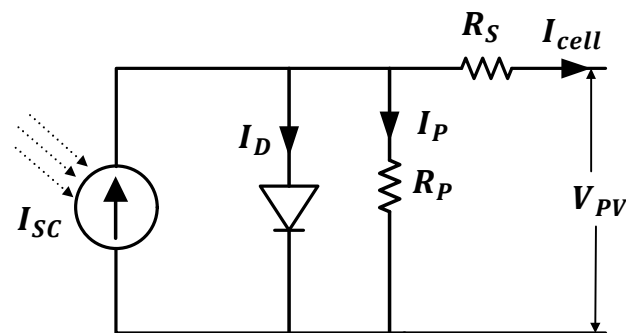
Figure 2-8. Equivalent Circuit of a Solar Cell

The equivalent circuit of a solar cell is shown in Figure 2-8 [165]. The equivalent circuit consist of current source, anti-parallel diode, and a series and parallel resistance. The I_{sc} is the current generated by the solar cell, when it is exposed to sunlight. I_D is the current flowing through the anti-parallel diode. R_P and R_s are the shunt and series resistance of

the solar cell, respectively. I_P is the current flowing through the shunt resistance R_P. V_{cell} is the voltage across the solar cell. The solar cell output current I_{cell} is given by (2.15).

$$I_{cell} = I_{sc} - I_D - I_P \qquad (2.15)$$

The current generated by the solar cell is dependent on the irradiance and temperature as shown in (2.16).

$$I_{sc} = I_{sc0} \left(\frac{G}{G_0}\right)[1 + \alpha(T - T_0)] \qquad (2.16)$$

where, I_{sc0} is the current by solar cell at Standard Reference Condition (SRC), G is the radiance, T is the temperature, G_0 and T_0 are the radiance and temperature at SRC, and α is the temperature coefficient of the solar cell current. G_0 and T_0 are 1000W/m² and 298 K respectively.

The diode current I_D is given by (2.17).

$$I_D = I_0 \left[\exp\left(\frac{qV_{cell} + I_{cell}R_s}{nkT}\right) - 1\right] \qquad (2.17)$$

where, I_0 is the diode saturation current, q is the electronic charge ($q = 1.602 * 10^{-19}C$), k is the Boltzmann constant ($k = 1.3806503 * 10^{-23}J/K$), n is the ideality factor of the diode, and T is the temperature of the cell.

The current flowing through the shunt resistance, I_P is given by (2.18).

$$I_P = \frac{V_{cell} + I_{cell} * R_s}{R_p} \qquad (2.18)$$

For a solar panel having n_s and n_P cells connected in series and parallel respectively, the output current (I_{panel}) and voltage (V_{panel}) are given by (2.19).

$$I_{panel} = n_P * I_{cell}$$

$$V_{panel} = n_s * V_{cell} \qquad (2.19)$$

For a solar farm consist of N_P solar panels connected in parallel and N_s solar panels connected in series, the output current (I_{PV}) and voltage (V_{PV}) are given by (2.20).

$$I_{PV} = N_P * I_{panel}$$

$$(2.20)$$

$$V_{PV} = N_s * V_{panel}$$

The variation of a PV panel output power with respect to change in the panel voltage is depicted in Figure 2-9. The panel voltage corresponding to maximum power (P_{MPPT}) is represented as V_{MPPT}. Several algorithms are available in literature to detect V_{MPPT} [85, 166, 167].
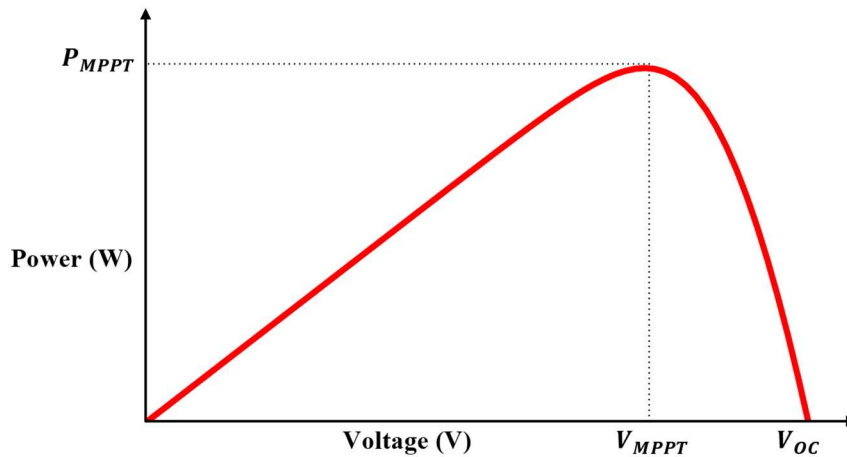
Figure 2-9. Power-Voltage Curve of a Solar Panel.

2.3.2 Inverter

The energy generated by the solar panel is transferred to electrical grid through a *dc- ac* converter. A two level voltage source inverter (VSI) is used in this thesis for feeding solar power to the grid. It consists of six insulated gate bipolar transistor (IGBT) switches and a capacitor on the dc side. Two IGBTs are connected in each leg of the inverter, which generates one phase of the AC voltage. The IGBTs are controlled by different modulation techniques like Sinusoidal pulse width modulation (SPWM), third harmonic pulse width modulation, Space Vector pulse width modulation (SVPWM) etc. [168]. The switching signals are generated in a complimentary manner for switches in the same leg to prevent

short circuiting of the leg. SPWM is employed in this thesis as it is easy to implement and is widely used. Due to the switching, the AC side voltage has a fundamental frequency component, and high frequency components which must be attenuated by a low pass filter. The harmonic component can be reduced by increasing the switching frequency, but switching losses increases with higher switching frequency. Thus, switching frequency is selected such that the harmonics generated are within stipulated limits and switching losses are also not high. The selection of DC link voltage for a two level VSI with SPWM is guided by (2.21).

$$V_{dc} \geq 2 * \sqrt{\frac{2}{3}} V_{LL} \qquad (2.21)$$

where, V_{dc} is the DC bus voltage and V_{LL} is the fundamental frequency component of line - line voltage at the AC terminal of the inverter.

Depending on the objective of the study, VSI can be modelled in detail by a switching model or as an average model. In switching model, VSI is modelled with detailed switching model of the power electronic switches. This model can provide detailed information on the harmonic spectrum of the VSI output voltage. But for fast simulation studies, the equivalent average model of VSI can be used. In this model, no switching strategy is used, and the AC side voltage is approximated as per their switching cycle moving average value. The disadvantages of average model are that it does not contain information on the harmonic spectrum of VSI output. Moreover, the model is valid only for one-third of switching frequency if the VSI operates in linear modulation region [169]. For an average model, the relation between DC link voltage and AC side voltage of a VSI is given by (2.22).

Since, the equivalent average model of a VSI, given in (2.22), captures all the dynamics of the inverter at the modulating frequency (60 Hz), the average model is used for analytical studies and switching model is used for time domain simulation studies in this thesis.

$$v_{abc} = m \frac{V_{dc}}{2} \qquad (2.22)$$

where, v_{abc} is the AC terminal voltage, V_{dc} is the dc link voltage and m is the modulation index.

The dynamics of the dc link capacitor is modelled by (2.23),

$$C\frac{dV_{dc}}{dt} = I_{PV} - I_{dc} \tag{2.23}$$

C is the capacitance of the dc link capacitor, and dc current I_{dc} is given by (2.24).

$$I_{dc} = \frac{3}{4}mi_{abc} \tag{2.24}$$

i_{abc} is the inverter output AC current.

2.3.2.1 Design of DC link Capacitor

The stability of DC link voltage controller depends on the DC link capacitor value (C_{dc}), minimum DC link voltage (V_{dcmin}), and the cross over frequency of the DC link voltage controller (ω_{dc}) [170]. C_{dc} is designed using (2.25) to ensure that any stability issue is alleviated [170]. A safety factor of 25% is added to the value of C_{dc} designed using 2.25.

$$C_{dc} \geq \frac{I_{sc}}{V_{dcmin}\omega_{dc}} \tag{2.25}$$

2.3.3 Filter and Interconnection Transformer

The harmonics in the VSI output has to be limited within the limits imposed by the standards [168]. Filters are employed at VSI terminal to attenuate the harmonics generated by the VSI switching [171]. Filters of various degrees of complexities are available in literature. Low pass LC and LCL are widely employed due to simplicity and low cost [168, 172]. In this thesis, an LC filter is used to limit the total harmonic distortion (THD) of the inverter output current within 5%.

A transformer is used to transform the DG output voltage level to the distribution system voltage. In North America, the utility networks operate with a solidly grounded neutral and the PV systems have DC side grounded. Thus, a galvanic isolation is required between the

DC side and the distribution system [173, 174]. Usually a delta-star transformer is employed for this purpose. Apart from providing galvanic isolation and voltage transformation, the delta configuration at DG side, and star at distribution network terminal further help in confining the zero sequence harmonics generated by the DG at DG side itself [169].

The equivalent circuit of an LCL filter is shown in Figure 2-10. L_f is the filter inductance, which is connected at the inverter terminal. The resistance R_{f1} represents the ON resistance of IGBT and the resistance of L_f. C_f is the filter capacitance, and R_{f2} is the resistance of the damping resistor. L_t and R_t are the inductance and resistance of the delta-star transformer used to connect the DG output to the distribution network.
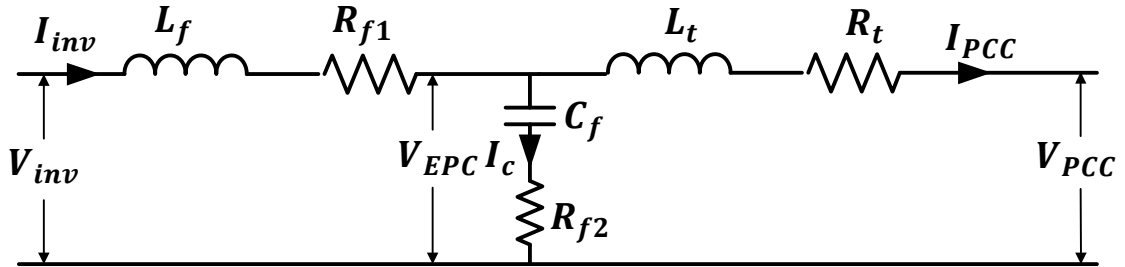
Figure 2-10. Model of an LCL filter

The filter is designed based on the following criteria,

The value of the inductance L_f is designed such that the inverter current ripple is within 10 -15% [82, 83, 171], and is given by (2.26).

$$L_f = \frac{V_{dc}}{8 * \Delta i_{max} * f_s}$$

(2.26)

where, V_{dc} is the DC link voltage, Δi_{max} is the maximum allowed ripple current, and f_s is the switching frequency.

The voltage drop across L_f should not exceed 0.3 pu in inverter base. Otherwise, if the voltage drop across L_f is higher, a large DC voltage is required to provide specific AC

voltage. Typically, a value between 0.1 - 0.25 pu, is selected for L_f to reduce the cost and size of reactor [169].

The capacitance C_f is chosen such that the reactive power consumed by the filter capacitor C_f is less than the 5% of the VSI rated capacity [171]. The C_f is designed by (2.27).

$$C_f = \frac{x * S_n}{\omega * V_{LL}} \tag{2.27}$$

where, x is the amount of reactive power consumed by the capacitor C_f (should be less than 0.05 pu), S_n is the rated capacity of VSI, ω is the nominal angular frequency and V_{LL} is the rated line-line voltage at VSI terminal.

The resonant frequency of the designed filter should satisfy (2.28). The resonant frequency is computed using (2.29).

$$10 f_0 \ < \ f_r \ < 0.5\, f_s \tag{2.28}$$

where f_0 is the nominal system frequency, f_r is the resonant frequency of the filter and f_s is the switching frequency of VSI.

$$f_r = \frac{1}{2\pi} \sqrt{\frac{L_t + L_f}{L_f C_f L_t}} \tag{2.29}$$

The damping resistance R_{f2} is designed such that there is enough damping at the resonant frequency. The resistance R_{f2} is designed according to (2.30) [175].

$$R_{f2} = \frac{1}{3 * 2 * \pi * f_r * C_f} \tag{2.30}$$

The dynamics of the filter is governed by (2.31).

$$L_f \frac{dI_{inv}}{dt} = V_{inv} - R_{f1} I_{inv} - V_{EPC} \tag{2.31}$$

$$C_f \frac{dV_{EPC}}{dt} = I_{inv} - I_{PCC} - R_{f1}(I_{inv} - I_{PCC})$$

$$L_t \frac{dI_{PCC}}{dt} = V_{EPC} - R_t I_{PCC} - V_{PCC}$$

where, V_{inv} and I_{inv} are the VSI AC terminal voltage and current. V_{EPC} is the voltage at Electrical Point of Connection (EPC). V_{PCC} and I_{PCC} are the voltage and current at the point of common coupling (PCC).

2.4 Control System for a Smart Inverter
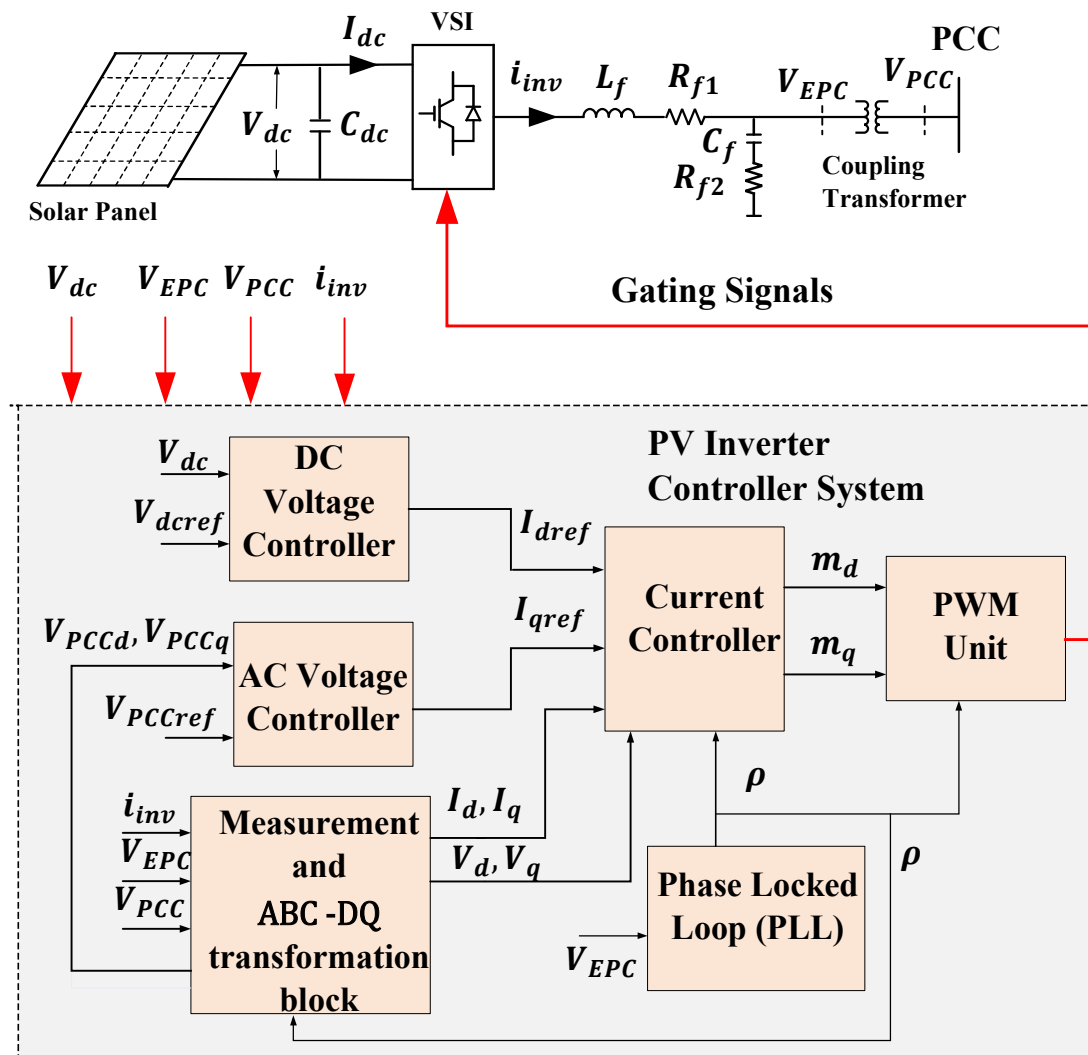
Figure 2-11. A typical PV Inverter Controller

A smart inverter provides multiple functions of real and reactive power support to aid in healthy operation of the power system. The support functions can be provided autonomously by monitoring system conditions or according to the instruction from the system operator. The schematic of the control system for a smart inverter is shown in Figure 2-11. The control system consists of (i) measurement system, (ii) Phase Locked Loop (PLL), (iii) *abc- dq* transformation, (iv) current controller, (v) DC voltage controller, and (vi) PCC voltage controller. The functions and design of these controller blocks are described in following subsections.

2.4.1   Measurement System

The smart inverter measures the VSI output current (i_{inv}), DC link Voltage (V_{dc}), Electrical Point of Coupling Voltage (V_{EPC}), PCC voltage (V_{PCC}), Active Power (P_{PPC}), and Reactive Power (Q_{PPC}) injected into the grid for operating the VSI according to a desired control strategy. Due to the switching of VSI, these quantities will have fundamental quantities and switching side band harmonics. A measurement filter is employed to attenuate the side band harmonics from the measured signal. The measurement system however incurs delays due to signal processing, computation and communication of the measured signal to the controller. Thus, the time constant τ of the measurement filter is incorporated to represent the delays incurred in measurement process. The measurement filter is modelled as a time delay for analytical studies as given in (2.32).

$$v_f = \frac{1}{1 + s\tau} v \tag{2.32}$$

where, v is the input to measurement filter, v_f is the filtered component, and τ is the time constant of filter.

2.4.2   *abc- dq* transformation
 The AC system voltages and currents are sinusoidally varying at system frequency ω, which requires a resonant controller to compensate the components corresponding to system frequency. To achieve satisfactory operation, the controller needs to be of higher order, and bandwidth should be larger than the frequency of the reference, which increases the complexity of controller. In *dq* rotating reference frame, the three phase signals are

transformed to a reference frame, which is rotating at ω. As the reference frame and signals are rotating at same speed, the signals appear to be dc in dq frame[176]. Thus, simple Proportional Integral (PI) compensators can be used, as the signals are dc in nature. It can ensure zero steady state error due to the infinite DC gain of a PI controller.

The three phase signals can be transformed to dq frame by using Parks transformation as shown in (2.33) [176].
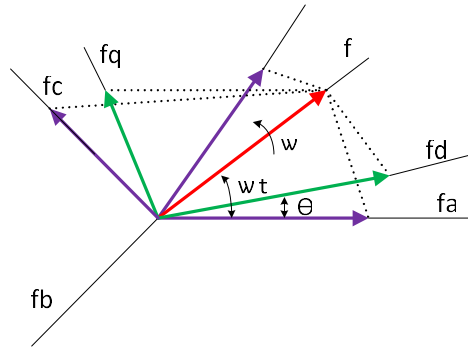
Figure 2-12. Vector representation of three phase signal in stationary (abc) and rotating (dq) reference frame.

$$\begin{bmatrix} f_d \\ f_q \\ f_0 \end{bmatrix} = \frac{2}{3} \begin{bmatrix} \cos(\omega t) & \cos(\omega t - 120) & \cos(\omega t + 120) \\ -\sin(\omega t) & -\sin(\omega t - 120) & -\sin(\omega t + 120) \\ \frac{1}{\sqrt{2}} & \frac{1}{\sqrt{2}} & \frac{1}{\sqrt{2}} \end{bmatrix} \begin{bmatrix} f_a \\ f_b \\ f_c \end{bmatrix} \tag{2.33}$$

The transformation is done such that the resultant voltage and current vector remains same in both reference frames.

The instantaneous power in synchronous frame is

$$P = v_a i_a + v_b i_b + v_c i_c \tag{2.34}$$

The active and reactive power in dq frame is given by (2.35)

$$P = \frac{3}{2}(V_d I_d + V_q I_q)$$

(2.35)

$$Q = \frac{3}{2}(V_d I_q - V_q I_d)$$

It can be noted from (2.35), that the active and reactive power are coupled in dq frame also. If the q axis component of voltage (V_q) is made zero, the active and reactive power becomes decoupled, and the active power and reactive power becomes proportional to I_d and I_q respectively as given in (2.36) [176].

$$P = \frac{3}{2}(V_d I_d)$$

(2.36)

$$Q = \frac{3}{2}(V_d I_q)$$

This decoupled control of active and reactive power control is used in this thesis.

2.4.3   Phase Locked Loop (PLL)

The grid voltage angle (θ) is required for transforming the signals from abc frame to dq frame. A phase locked loop (PLL) is employed to extract the voltage angle. The schematic of a PLL is shown in Figure 2-13. The voltage at electrical point of coupling (V_{EPC}) is transformed into V_d and V_q. The dq frame rotational angle (ρ) is controlled by the compensator $H(s)$, such that V_q is made zero. This condition is achieved when $\rho = \theta$. To limit deviation of the PLL frequency from the network frequency, and to prevent integrator wind up, the compensator output is limited by a saturation block. The voltage controlled oscillator (VCO) is a resettable integrator, whose output is reset to zero whenever it reaches 2π.
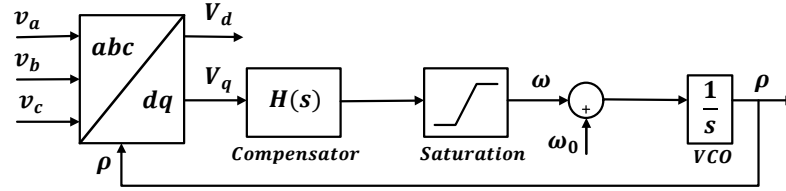
Figure 2-13. PLL Model

2.4.3.1 Design of PLL Compensator $H(s)$

In order to ensure no steady state error, $H(s)$ should contain at least one pole at $s = 0$ [172]. The degree of unbalance or harmonics in the grid voltage should be considered while designing PLL, as they can influence the performance of PLL. Second harmonic component is present in unbalanced voltage, and this can be avoided if $H(s)$ is modelled with a low pass characteristic. But it will reduce the closed loop bandwidth of the PLL. Including two complex conjugate poles at $s = \pm j2\omega_0$ can eliminate the second harmonic component. The other higher order harmonics can be removed by adding two real poles $s = -2\omega_0$ [172]. $H(s)$ is further modified to meet the required gain margin and phase margin. Lead or lead-lag compensator is added to $H(s)$ to achieve the needed phase margin.

2.4.4 Current Controller

The active and reactive power is decoupled in dq axis, and they can be independently controlled by controlling d axis current (i_d) and q axis current (i_q) as shown in (2.36). The active and reactive power controllers generate d axis current reference (i_{dref}) and q axis current reference (i_{qref}) according to the active and reactive power to be injected to the grid. The current controller ensures that the VSI currents i_d and i_q track the references i_{dref} and i_{qref} in a fast manner.

The model of VSI in dq frame is given by (2.37),

$$L_f \frac{di_d}{dt} = V_{dinv} - R_{f1}i_d + \frac{\omega_0}{L_f}i_q - V_d \qquad (2.37)$$

$$L_f \frac{di_q}{dt} = V_{qinv} - R_{f1}i_q + \frac{\omega_0}{L_f}i_q - V_q$$

where, inverter terminal voltage V_{dinv} and V_{qinv} are given by,

$$V_{dinv} = m_d \frac{V_{dc}}{2}$$

$$V_{dinv} = m_q \frac{V_{dc}}{2}$$

(2.38)

m_d and m_q are the dq axis modulation indices generated by the current controller, L_f is the filter inductance, ω_0 is the synchronous frame frequency, V_{dc} is the DC link voltage, and R_{f1} is the sum of ON resistance of IGBT and filter resistance.

As i_d and i_q are coupled in (2.37), the modulation indices m_d and m_q are computed using (2.39).

$$m_d = \frac{2}{V_{dc}}\left(u_d - L_f \omega_0 i_q + V_d\right)$$

$$m_q = \frac{2}{V_{dc}}\left(u_q + L_f \omega_0 i_d + V_q\right)$$

(2.39)

u_d and u_q are new control inputs. By substituting (2.39), and (2.38) in (2.37), the VSI model becomes (2.40),

$$L_f \frac{di_d}{dt} = -R_{f1}i_d + u_d$$

$$L_f \frac{di_q}{dt} = -R_{f1}i_q + u_q$$

(2.40)

Thus the i_d and i_q dynamics become decoupled and they can be controlled independently. The d axis compensator processes $i_{dref} - i_d$ and generates u_d. Similarly, q axis

compensator processes $i_{qref} - i_q$ and generates u_q. Thus, the current controller computes m_d and m_q using (2.39).

The schematic of a current controller is shown in Figure 2-14. The saturation block is employed in current controller to protect the VSI from instantaneous over current and network faults [169].
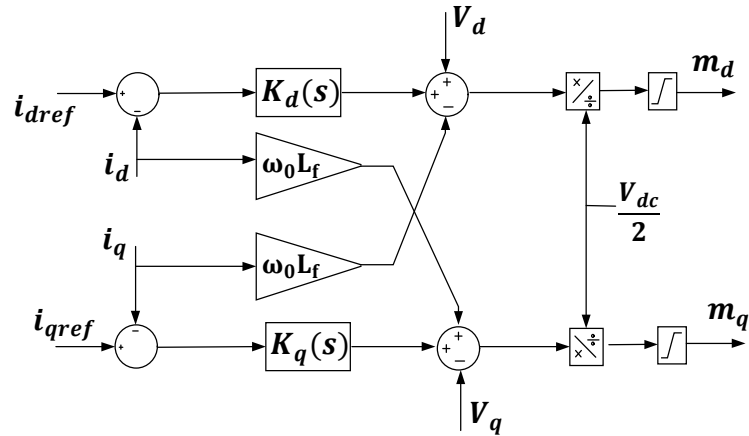
Figure 2-14. Block Diagram of Current Controller

2.4.4.1 Design of Current Controller

The simplified block diagram of the current controlled inverter is depicted in Figure 2-15. A proportional integral (PI) controller is employed to control *d axis* current i_d and *q axis* current i_q at the references i_{dref} and i_{qref}. The PI controller parameters K_p and K_i are designed based on the required closed loop phase margin and gain margin of the simplified current controller, shown in Figure 2-15. The controller is designed so that the closed loop bandwidth is at least 10 times smaller than the switching frequency of VSI [172].
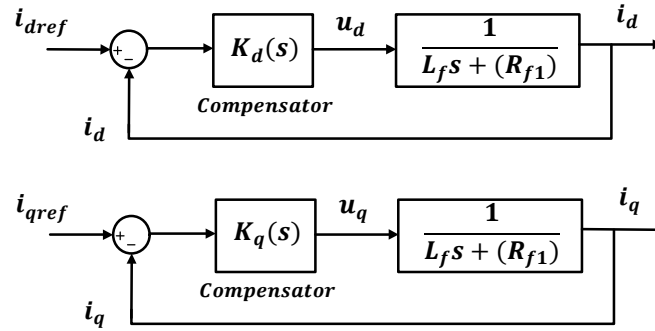
Figure 2-15. Simplified diagram of the current controlled inverter.

2.4.5   DC link Voltage Controller

The PV panel power output depends upon the DC voltage across the PV panel terminals as shown in Figure 2-9. The objective of DC link voltage controller is to maintain the DC link voltage (V_{dc}) at the reference voltage (V_{dcef}) to extract the corresponding power from the solar panels.

The power balance equation across the DC link capacitor is defined by (2.41),

$$\frac{C}{2}\frac{dV_{dc}^2}{dt} \cong P_{PV} - P_{VSI} \tag{2.41}$$

Where, P_{PV} is the power generated by the solar panel, P_{VSI} is the power fed by the VSI to grid, C is the capacitance of the DC link capacitor.

The control of DC link voltage ensures that power balance is met and the generated power from solar panel is fed to grid through VSI. The DC link controller generates the real axis current reference (i_{dref}) for the current controller, such that the DC voltage is maintained at the reference and the maximum active power is transferred to the grid. The structure of a DC link voltage controller is shown in Figure 2-16. Usually, the MPPT controller determines the V_{dcef}, which corresponds to the maximum power point operation of the solar panels.
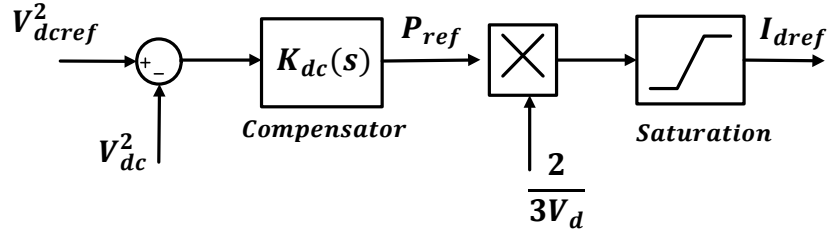
Figure 2-16. Block diagram of DC link voltage controller.

2.4.5.1   Design of DC link Voltage Controller

V_{dc}^2 is controlled as it gives a linear relationship with P_{VSI}. The DC link voltage controller tries to minimize the error $(V_{dcref}^2 - V_{dc}^2)$. The DC link voltage controller consists of a PI controller, and a lead compensator to ensure the required phase margin. The closed loop DC controller has minimum phase, when VSI is feeding power to the DC terminal. But, in a PV system without energy storage, the minimum phase occurs when the active power output of solar panel is zero. So, the controller is designed for this operating point to ensure that the designed controller can ensure minimum phase margin for all the operating conditions [172].

2.4.6   PCC voltage controller

The smart inverter can provide reactive power support to the system. Various reactive power control strategies are employed to provide reactive power support, viz., (i) dynamic current in proportional to drop in PCC voltage (V_{pcc}) during transients, (ii) constant power factor operation or (iii) by regulating V_{pcc} at the reference value [89].

The dynamic current support is provided by setting i_{qref} according to the dynamic reactive current curve given in Figure 1-14. For power factor control, the i_{qref} is calculated using (2.42).

$$i_{qref} = \tan(\cos^{-1}(pf)) * i_{dref} \tag{2.42}$$

Where, pf is the power factor set point.

For regulating V_{pcc} at the reference (V_{pccref}), PCC voltage control is employed. The schematic of a PCC voltage controller is shown in Figure 2-17. The reactive power output of the VSI is controlled to regulate the PCC voltage. The compensator generates i_{qref} for the current controller such that the error ($V_{pccref} - V_{pcc}$) is minimized.

V_{pcc} is the PCC voltage calculated by the controller in dq frame using (2.43).

$$V_{pcc} = \sqrt{V_{pccd}^2 + V_{pccq}^2} \tag{2.43}$$

Where, V_{pccd} and V_{pccq} are the d and q axis components of PCC voltage computed by the abc-dq transformation block.
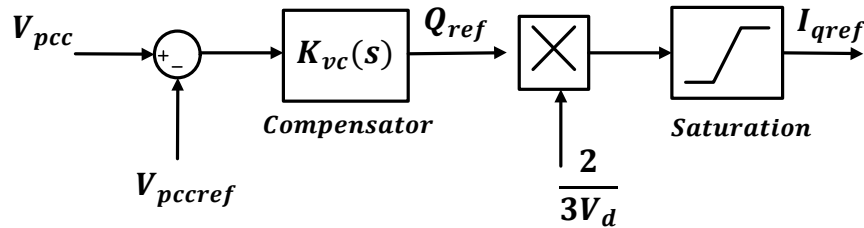
Figure 2-17. Block Diagram of PCC Voltage Controller.

2.4.6.1 Design of PCC Voltage Controller

A proportional controller or proportional integral (PI) controller is used for PCC voltage controller. The controller parameters are selected such that the bandwidth of the PCC voltage controller is at least three times lower than the bandwidth of the q axis current controller [172].

2.4.7 PWM Unit

The PWM unit generates the switching pulses for IGBT switches of VSI. Sinusoidal PWM modulation technique is used to generate the switching pulses [168]. The modulation indices (m_d and m_q) generated by the current controller is projected to the abc frame using the voltage angle information from the PLL, to generate the modulation signal. A triangular wave of 10 kHz is used as the carrier wave.

2.5   Model of Large PV Plant

The single line diagram of a large PV plant is shown in Figure 1-8. As discussed in Sec. 1.5.2, a large PV plant is spread across a large geographic area having multiple inverters, solar panels and pad mount transformers, connected to the substation transformer through collector cables [87, 88].

2.5.1   Detailed Model of inverter units in a Large PV plant

For studying the dynamics within the PV plant, each inverter unit is modelled in detail. The PV array, DC link capacitor, inverter, and pad mount transformer of each individual inverter unit in the PV plant is modeled in detail as explained in Sec. 2.3.

2.5.1.1   Collector System

The inverters in the PV plant are connected to the substation transformer through collector cables. The collector cables are modelled by their equivalent π models. The equivalent π model of a collector cable is similar to the model of distribution line discussed in Sec. 2.2.2.

2.5.2   Equivalent model of inverter units in a Large PV plant

The modeling of the complete PV plant is tedious and complex task. An equivalent positive sequence model for a transmission connected large PV plant is developed by the Western Electricity Coordinating Council (WECC) [87], which can give an average response of the inverters in the plant. The equivalent model can capture the dynamics of a large PV plant, but not the dynamics within the plant itself [87]. The developed model can be used for studying the response of the plant for balanced faults external to the PV plant. This model can be used for analyzing electrical phenomenon in 0-10 Hz frequency range. The model performs accurately in a transmission system with SCR greater than two [87].
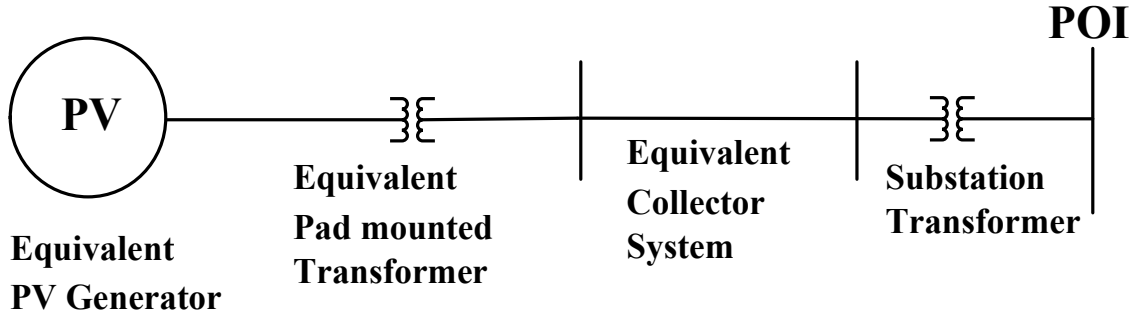
Figure 2-18. Equivalent Model of a large PV plant.

2.5.2.1 Equivalent Generator Model

In the average model, the dynamics in the DC side (PV arrays, inverter DC link and DC link voltage controller) are neglected [87]. Thus, in this thesis, the equivalent model is modelled as the average model of the VSI as given in Sec. 2.22, with constant dc link voltage.

The equivalent pad mounted transformer is modelled as discussed in Sec. 2.2.3. The equivalent impedance is calculated from PV plant data as explained in [177].

$$Z_{eq} = \frac{Z}{n_{inv}} \tag{2.44}$$

where,

Z = impedance of a single pad mount transformer.

n_{inv} = number of inverters connected to a pad mounted transformer.

2.5.2.2 Equivalent Collector System

The cable impedances vary as the inverters are spread across a large geographical area. In the equivalent model, the cable dynamics are represented by an equivalent collector system. A method to calculate parameters of equivalent model is discussed in [177]. The π model representation of the equivalent collector system is used in the simulation system. The equivalent collector system π model is similar to the model of distribution line discussed in Sec. 2.2.2.

The series impedance of the equivalent collector system is calculated using (2.45).

$$Z_{eq} = \frac{\sum_{m=1}^{n} m^2 Z_m}{n^2} \qquad (2.45)$$

where,

n = number of inverters.

m = running index

Z_m = impedance of a branch.

The shunt impedance of the equivalent collector system is calculated using (2.46)

$$B_{tot} = \sum_{m=1}^{n} B_i \qquad (2.46)$$

n = number of branches.

m = index

B_i = susceptance of a branch.

Detailed or equivalent model of the inverter units are selected based on the study objectives. To study the average response of the PV plant, the equivalent model is sufficient. However, to study interactions between the inverter units in a plant, or the dynamics within the plant, the detailed model of the PV plant is required.

2.5.3   Plant Level Controller

The plant level controller provides control instructions to the individual inverter level controllers to regulate active and reactive power outputs of the plant. The functions of plant level controller are discussed in detail in Sec. 1.5.2.1. The plant level controllers are slower, having time constant between $0.15 - 5$ sec [87].

2.5.4 Inverter Level Controller

The inverter level controller generates the switching signals to the inverter to provide active and reactive power according to the active (P_{pref}) and reactive power (Q_{pref}) references provided by the plant level controller.

The controller structure of an inverter level controller is similar to the controller for distributed PV discussed in Sec. 2.4. Since in equivalent model, the DC side dynamics are neglected, the DC voltage controller is eliminated, and the real current reference (i_{dref}) is generated from P_{pref} using (2.47).

$$i_{dref} = \frac{2P_{pref}}{3V_{EPCd}} \qquad (2.47)$$

In detailed model, the real current reference (i_{dref}) is provided by the DC link voltage controller to operate the PV panels at MPPT, as discussed in Sec. 2.4.4

Apart from PCC voltage control, fixed power factor operation and dynamic reactive power discussed in Sec. 2.4.6, the inverter can provide reactive power according to Q_{pref} provided by the plant level controller. The reactive current reference (i_{qref}) is calculated from Q_{pref} using (2.48).

$$i_{qref} = \frac{2Q_{pref}}{3V_{EPCd}} \qquad (2.48)$$

2.6 Structure of PV-STATCOM Controller

The proposed PV-STATCOM controller is designed with an objective of providing fast voltage support to the system during a transient to ensure fast voltage recovery with minimal active power curtailment. The schematic of a PV plant with proposed PV-STATCOM controller is shown in Figure 2-19. During a transient, the PV-STATCOM controller disables the conventional control of PV inverter and provides real (i_{dref}) and reactive current reference (i_{qref}) to the current controller. In large PV plant, the proposed controller is embedded in inverter level controller to provide fast support. The PV-

STATCOM controller consist of a mode selector, active power controller and reactive power controller.

A general overview of the different components of the PV-STATCOM controller is presented in this subsection. In Chapter 3 and 5, PV-STATCOM controller is developed for a distribution system to provide fast support to critical induction motor. In Chapter 6, a PV-STATCOM controller to mitigate FIDVR in transmission system is proposed. The detailed structure of the proposed controllers for distribution and transmission system are provided in the corresponding chapters.

2.6.1 Mode Selector

Proposed PV-STATCOM controller modulates the active and reactive power based on the system need in case of a system disturbance/fault, to ensure fast recovery. The operation of the controller can be classified into different modes according to the control objective, which are discussed in later chapters. The Mode Selector Block continuously monitors the system variables and decides the mode of operation.

2.6.2 Active Power Controller

The active power controller generates active power reference for the various modes of operation of the proposed controller.

2.6.3 Reactive Power Controller

The reactive power reference for the various modes of operation is generated by the reactive power controller.
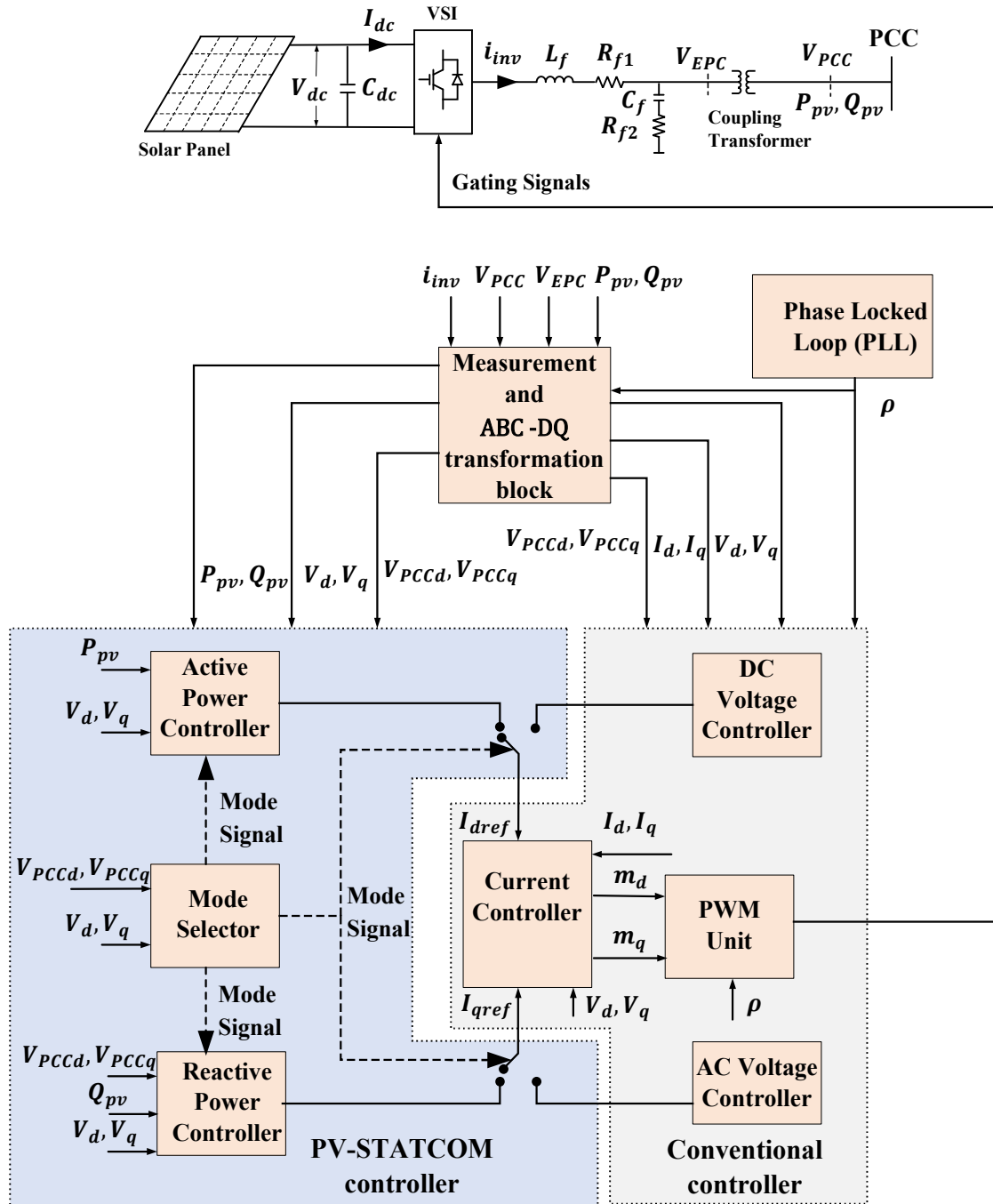
Figure 2-19. A PV plant with proposed PV-STATCOM controller

2.7   Conclusion

The detailed modeling of various components of a PV solar farm connected to an electrical network is presented. The modeling of various controller blocks of a PV inverter controller is presented along with the design strategies for each controller block. Modeling of a large

PV plant used for simulation studies is presented. The overview of the proposed PV-STATCOM controller structure is also described.

Chapter 3

3 PV-STATCOM Control for Stabilizing a Remote Critical Induction Motor

3.1 Introduction

This chapter presents a novel night and day autonomous control of PV solar farm as STATCOM, termed PV-STATCOM, for preventing instability of critical induction motors (IMs) whose shutdown during faults, even temporarily, can cause significant financial loss to industrial facilities. At the occurrence of a network fault that can likely destabilize the critical IM, the solar farm disables its real power production temporarily (typically for few seconds), transforms into a STATCOM and provides dynamic voltage support to prevent motor instability. Once satisfactory voltage conditions are created for stable operation of IM, the solar farm autonomously returns to its pre-disturbance real power production level. The proposed control using entire PV inverter capacity provides enhanced voltage control up to utility Temporary Overvoltage limits. The effectiyess of PV-STATCOM control is investigated for ensuring stable operation of critical IM: i) even if located 15-20 km away, ii) with very large delay in communication of motor terminal voltage to PV farm, and iii) for wide-ranging system parameters and operating conditions. The performance of remote PV-STATCOM in providing similar motor stabilization as a locally connected STATCOM is studied. Furthermore, it is shown that the solar farm with PV-STATCOM capability is able to stabilize IM while implementation of dynamic current injection capability on solar farm as specified in grid codes is unable to do so.

The proposed PV-STATCOM control for motor stabilization is simulated in MATLAB Simulink for the 10 kW PV solar farm located at Bluewater Power Distribution Corporation Sarnia, ON, Canada. Subsequent studies are performed on a realistic feeder in Canada to show the effectiveness of proposed PV-STATCOM control strategy for variation of key system parameters viz., (i) system strength, (ii) distance between the PV solar farm and the critical induction motor, (iii) $\frac{X}{R}$ ratio, and (iv) depth of voltage sag. Further studies are performed to show the effectiveness of the proposed controller to stabilize a combination of multiple industrial motors.

3.2   Study System

Two study systems are utilized in this chapter for performing different studies, as described below.

3.2.1   Study System 1

MATLAB Simulink based simulation studies are performed for the 10 kW PV solar farm located at Bluewater Power Distribution Corp., Sarnia, ON, Canada. The single line diagram of the test system is presented in Figure 3-1. The study system consists of a PV array rated at 10 kW, 280 V, and 49 A. The PV power is fed into the distribution system using an existing three-phase inverter rated at 10 kVA, 600 V, and 9.6 A, which is connected to the Bluewater distribution network. A 5 hp IM M_1 is considered as the critical motor for this study.
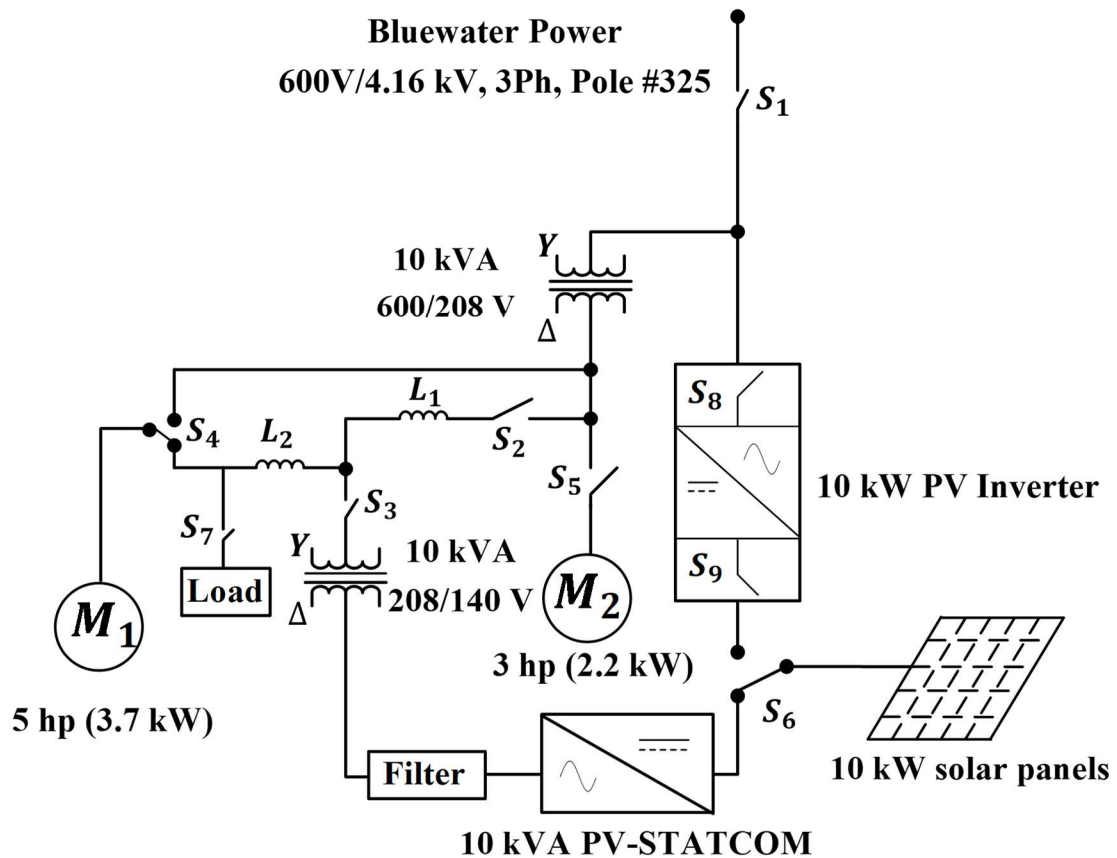
Figure 3-1. Single Line Diagram of study system 1.

Although the critical motor is physically located at the site of the solar farm, its effective distance from the solar farm is varied by using a variable inductor L_2 which is inserted through switch S_4. The delay in communication of motor terminal voltage signal to the solar farm is implemented in software. The overall delay represents: i) the communication delay between motor terminal and PV-STATCOM, and ii) the communication delay between master control and individual inverter controllers in an actual PV solar farm. The latency for fiber optic cable is $3.34\ \mu s/km$ [178] and the communication delay incurred in a PV solar farm plant control is approximately 100 ms [88]. Thus, the delay in the study system with a distance of about 15.6 km between the IM and the PV solar farm is 100.05 ms and is approximated as 100ms.

A large system disturbance is created by turning on a large inductive load of 10 kvar at the motor terminal using switch S_7. The inductor L_1 is used to vary the short circuit ratio of the system. A 3 hp motor M_2 is used for the maximum power point tracking of the PV panels.

3.2.2   Study System 2

PSCAD/EMTDC simulation studies are also conducted on a realistic 45 km long 27.6 kV feeder in Ontario, Canada [179] to investigate the impact of key system parameters on the performance of the proposed PV-STATCOM controller. The single line diagram of the study system 2 is shown in Figure 3-2. The transformer T_1 is rated 115 kV/27.6 kV, 32 MVA with 5% impedance. The distribution lines are represented by their equivalent π models. Resistances R_{TL1}, R_{TL} , R_{TL3} and inductances L_{TL} , L_{TL2}, L_{TL} denote the resistance and inductance of distribution lines between Bus 2 and Bus 3, Bus 3 and Bus 4, and Bus 4 and Bus 5, respectively. A 6-MW PV solar farm is connected to the feeder at bus 3 which is 25 km away from the IM loads. A total load of 5.3 MVA at 0.9 power factor is connected at feeder end. For simulation studies, 50% of loads are modelled as IM loads and other 50% as voltage dependent static loads. The IM loads are rated at 4 kV [180] and are connected through a transformer rated 27.6kV/4 kV and 5% impedance.

The inductor L_f, capacitor C_f, and inductance of $\Delta - Y$ transformer constitutes the LCL filter. R_{f1} and R_{f2} represents the resistance of inductor and capacitor respectively. To

provide 24/7 PV-STATCOM operation, modifications are made in the PV inverter system. In a PV inverter system, the dc link capacitor is charged from the PV solar panel, during start up. But at night, the PV panel is idle, and therefore a charging circuit is added for nighttime dc link capacitor charging. This is accomplished by keeping switch S_2 on and S_1 off. Once the capacitor voltage reaches the peak of ac phase voltage, switch S_1 is turned on, and S_2 is turned off. The PV inverter thus become ready to function as a STATCOM at night.

The voltage at motor terminal is denoted as V_m, which is measured and communicated (through a fiber optic cable) to the PV-STATCOM controller incurring a delay in the process. The overall delay represents: i) the communication delay between motor terminal and PV-STATCOM, and ii) the communication delay between master control and individual inverter controllers in an actual PV solar farm. The latency for fiber optic cable is $3.34\,\mu s/km$ [178] and the communication delay incurred in a PV solar farm plant control is approximately 100 ms [88]. Thus, the delay in the study system with a distance of about 25 km between the IM and the PV solar farm is 100.08 ms and is approximated as 100ms.
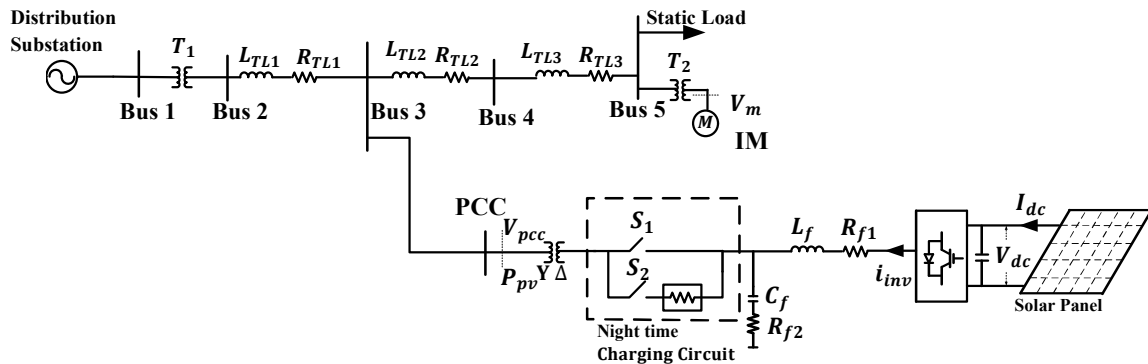
Figure 3-2. Single Line Diagram of the study system 2.

3.3   Study System with PV-STATCOM Control

The PV inverter (as PV-STATCOM) is connected to the PCC bus in both Study Systems 1 and 2. Figure 3-3 (a) illustrates the PV inverter connected to study system 2 at PCC bus. Figure 3-3 (b) and (c) depict the conventional PV inverter controller and the proposed PV-

STATCOM controller, respectively, used in studies relating to both Study System 1 and Study System 2.

Figure 3-3 (b) shows the structure of a conventional PV inverter control used in studies for both Study Systems 1 and 2. It consists of dc link voltage controller and power factor controller, inner current controller and PLL, as discussed in Sec. 2.4.
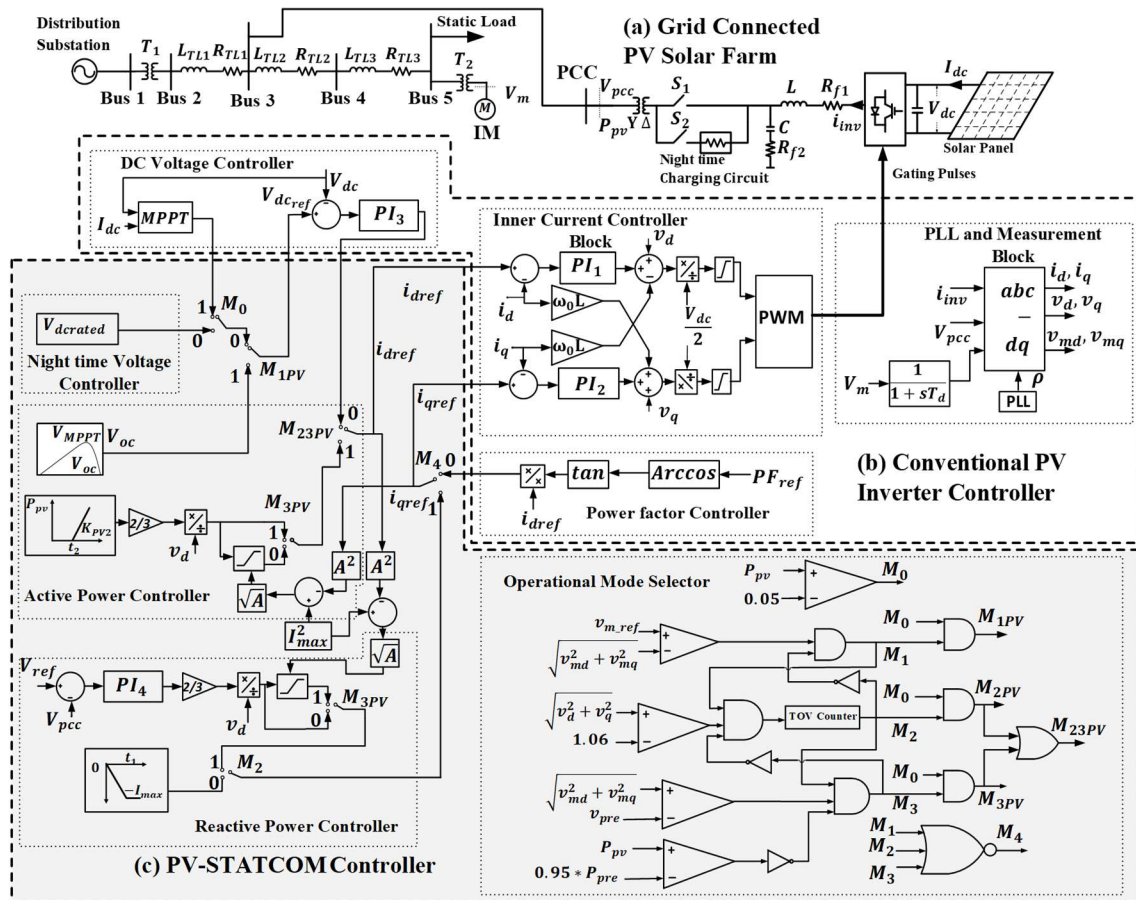
Figure 3-3. Single Line Diagram of a PV system connected to Study System 2 with the architecture of the proposed PV-STATCOM controller.

3.3.1   PV-STATCOM Controller

The proposed PV-STATCOM controller is illustrated in Figure 3-3 (c). It consists of: i) Operation Mode selector, ii) Active Power Controller, iii) Reactive Power Controller, and iv) Night time Voltage Controller. During a system disturbance, the PV-STATCOM controller generates the reference signals for real current (i_{dref}) and reactive current

(i_{qref}) for the inner current controller based on V_{pcc} and V_m, to ensure fast recovery of the critical IM.

The functioning of different blocks of the proposed PV-STATCOM controller is described below.

3.3.1.1   Operation Mode Selector

The proposed PV-STATCOM control functions in four modes of operation described below. These modes are decided by the Operation Mode Selector block based on V_{pcc}, V_m, and active power output of PV solar farm (P_{pv}).

The Operation Mode Selector periodically compares P_{pv} with a small value (selected as 0.05 pu) to determine if PV-STATCOM operation is being performed during day (P_{pv} >0.05 pu) or night (P_{pv} <0.05 pu), setting flag M_0 to 1 or 0, respectively.

The operation of the controller during various modes are discussed below.

3.3.1.1.1   Mode 1 (represented by flag M₁ and M₁PV)

This is Variant 1 of the Full-STATCOM mode. If V_m goes below a predetermined threshold value V_{m_ref} (considered to be 0.8 pu for this study), Mode 1 operation is selected by setting M_1=1, and correspondingly M_{1PV} = 1 during day time.

During night time operation, the flag M_{1PV} is disabled to 0, and V_{dc} is set to $V_{dcrated}$, which is set at double of V_{pcc} to ensure the proper operation of SPWM modulated inverter during night time [31]. During daytime, M_{1PV} is enabled and active power is curtailed to zero by the active power controller. The full inverter capacity is utilized for injecting reactive power to the system by setting i_{qref} = −1. The controller continues Mode 1 operation till V_{pcc} does not exceed the TOV limit specified by the grid operator (V_{TOV_L}). According to the transient overvoltage curve [90], an overvoltage between 1.06 pu and 1.3 pu is permitted for a maximum period of 166 msec. The proposed PV-STATCOM control strategy utilizes this extra room for reactive power support for stabilization of the critical

motor. Flag M_1 is kept enabled for 150 msec (slightly less than 166 msec), since the V_{pcc} exceeds 1.06 pu.

3.3.1.1.2   Mode 2 (represented by flag M₂ and M₂PV)

This is Variant 2 of the Full-STATCOM mode. In this mode, flag M_2 is enabled and maximum reactive power is injected into the grid with the objective of maintaining V_{pcc} at its steady state voltage limit of 1.06 pu. During day time flag M_{2PV} is enabled and active power is ramped to the pre-disturbance level (P_{pre}) by using the remaining inverter capacity. The dc voltage controller is disabled and the i_{dref} is calculated by the power ramp function in active power controller using (3-1).

$$i_{dref} = \frac{2P_{ramp}}{3v_d}$$

(3-1)

P_{ramp} is the instantaneous value of active power ramp. The i_{dref} calculated using (3-1) is passed through the saturation block to limit it to within the available inverter capacity. The limits of saturation block (i_{dlimit}) are calculated using (3-2).

$$i_{dlimit} = \pm \sqrt{I_{max}^2 - i_{qref}^2}$$

(3-2)

where, I_{max} is the rated inverter current.

During night time, $M_0 = 0$. Hence, M_{2P} (and M_{3P}) get disabled and consequently $M_{23PV}=0$. DC voltage controller then regulates V_{dc} to $V_{dcrated}$. The inverter operates in this mode until V_m reaches an acceptable limit (i.e. prefault voltage v_{pre}).

3.3.1.1.3   Mode 3 (represented by flag M₃PV)

This is the Partial-STATCOM mode, and it is enabled during day time while ramping active power to pre – disturbance P_{PV} (P_{pre}). Once V_m reaches its pre-fault voltage, Mode 3 operation is enabled by setting $M_{3PV} = 1$, and subsequently $M_{23PV} = 1$. The active power is ramped to the maximum value according to available solar irradiance using active power controller.

The dc voltage controller is disabled, and i_{dref} is calculated by the power ramp function in active power controller using (3-1). The remaining inverter capacity is simultaneously used for dynamic reactive power support to maintain V_{pcc} at 1.06 pu. The i_{qref} generated by PCC voltage controller is limited by the saturation block using (3-3), to ensure the maximum current rating of inverter is not violated.

$$i_{qlimit} = \pm \sqrt{I_{max}^2 - i_{dref}^2}$$ (3-3)

The Mode 3 operation is continued till P_{PV} reaches the maximum available power. One practical way of checking is that P_{PV} is at least 0.95 times pre – disturbance P_{PV} (P_{pre}).

The PCC voltage control during Mode 3 allows a fast ramp rate for active power without violating PCC voltage limit. This is a novel feature of the proposed control and allows to ramp-up much fast than the rates specified in grid codes such as [90].

3.3.1.1.4   Mode 4 (represented by flag M4)

In this mode, during day time, the PV system generates the maximum available active power at the power factor specified by the system operator. During night time, it regulates V_{dc} at $V_{dcrated}$ and remains on standby for Full STATCOM operation.

3.3.1.2   Active Power Controller

The Active Power Controller block generates i_{dref} for the proposed control strategy. This block consists of a dc voltage reference generator and active power ramp up functions. During Mode 1 operation, the V_{dcref} is set at open circuit voltage of PV panels (V_{oc}) by the dc voltage reference generator to curtail the active power generation. Active power ramp up function generates i_{dref} during Mode 2 and 3.

3.3.1.3   Reactive Power Controller

The Reactive Power Controller block determines i_{qref} for the various modes of operation of proposed PV-STATCOM control. It consists of PCC voltage controller and a reactive current reference generator. During Mode 1, the reactive current reference generator

increases the current $i_{qref} = -1$ in time t_1, to utilize the full inverter capacity to provide reactive support. In Mode 2 and 3, the PCC voltage controller controls the V_{pcc}.

3.3.1.4   Night time Voltage Controller

During night time, this block masks the operation of Active Power Controller block. It maintains V_{dc} at $V_{dcrated}$, and operates PV inverter as a STATCOM at night, as needed.

3.4   Simulation Stuies on study system 1

The effectiveness of the proposed PV-STATCOM controller in stabilizing the 5 hp motor is first studied using MATLAB Simulink software. The results are presented below.

3.4.1   Performance of the proposed PV-STATCOM controller

Two cases are shown in Figure 3-4. The solid lines show the performance of the IM and the PV solar farm with PV-STATCOM controller (stable motor operation), and dashed lines show the operation without PV-STATCOM control (unstable motor operation). Figure 3-4 (a)-(h) depict the PCC rms voltage (V_{pcc}) and motor terminal rms voltage (V_m), reactive and active power output of the inverter, IM speed, IM torque, i_q, i_d, V_{dc}, and converter terminal voltage, respectively.

t < 1.25 s. V_{pcc} and V_m are 1.05 and 1.02 pu, respectively. The PV inverter is operating in Mode 4 by injecting the maximum available active power at unity power factor. The induction motor is providing 0.75 pu load torque at 2% slip.

t = 1.25 s. A large disturbance is created at the motor terminal by connecting a 10 kvar inductive load. This causes V_m to drop below 0.8 pu. The active power injected by PV solar farm reduces slightly due to the drop in V_{pcc}. The motor speed starts to reduce, and the motor torque become oscillatory due to the voltage reduction.

t = 1.35 s. A 100 ms communication delay is considered between the voltage measurement at motor terminal and its receipt at the PV solar farm. Due to this delay, the controller detects the drop in V_m at t=1.35 s, and switches to Mode 1 operation. The active power is curtailed, and the full inverter capacity is used to inject reactive power. Due to
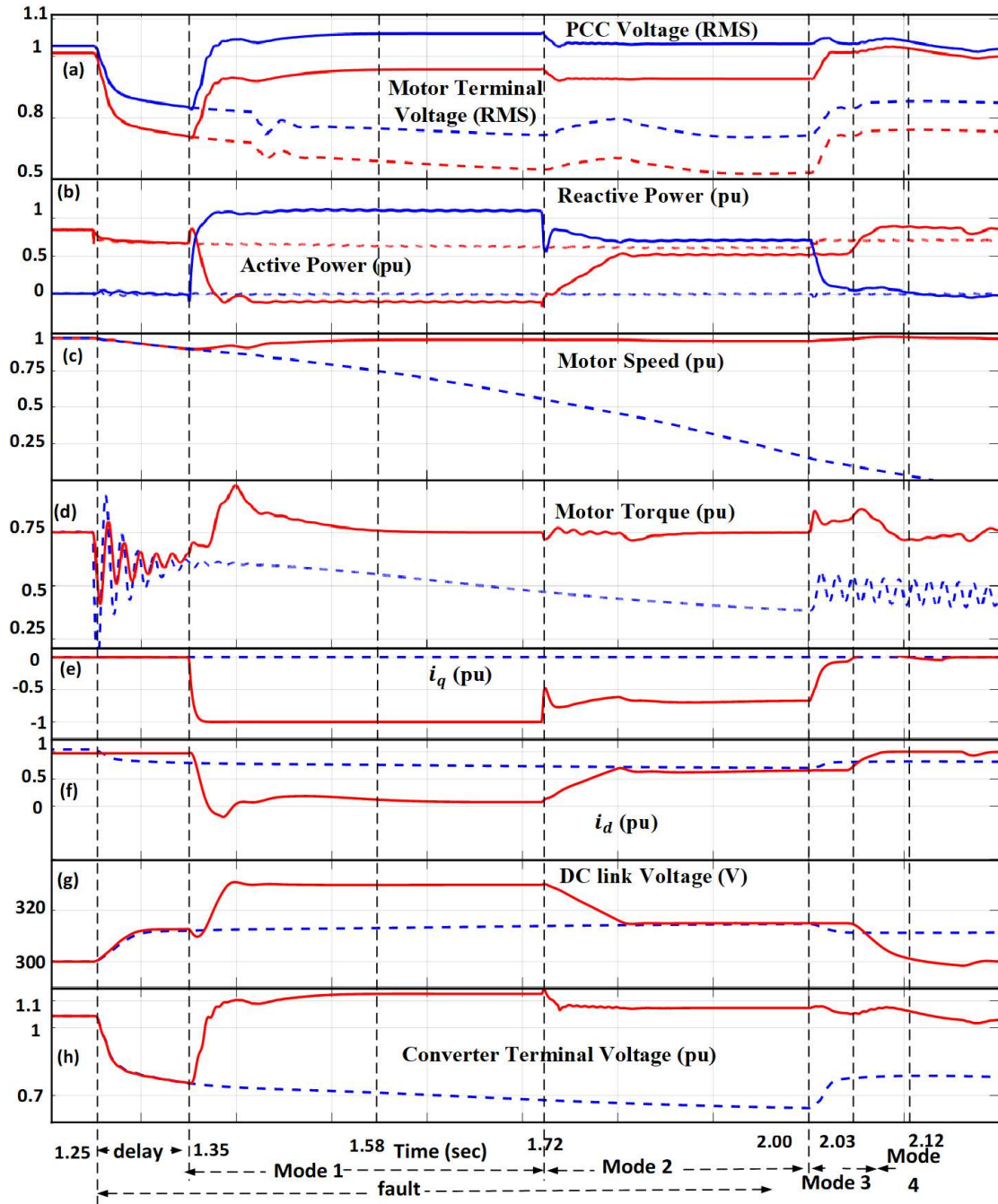
Figure 3-4. Response of the IM and PV-STATCOM

this fast-reactive current injection, the motor speed starts to recover, and it rapidly restores steady state torque.

Without PV-STATCOM control, the PV system continues operating at unity power factor (UPF). The voltages at PCC and motor terminal decrease. The motor torque declines and the motor eventually stall.

t = 1.58 s. V_{pcc} crosses the steady state limit of 1.06 pu at 1.58 s. In order to provide maximum reactive power support, the inverter continues to operate in Mode 1 without violating the TOV limit V_{TOV_L} over the maximum allowable duration (166 ms) of overvoltage (between 1.06 pu and 1.3 pu) per IEEE Std. 1547-2018 [90].

t = 1.72 s. The inverter switches to Mode 2 operation. In this mode, V_{pcc} is regulated at 1.06 pu. During this period, the PV-STATCOM injects 0.8 pu reactive power for maintaining the PCC voltage and 0.6 pu active power is generated utilizing the remaining inverter capacity. The IM is able to provide steady state torque at an acceptable slip of 6%, even though V_m has reduced to 0.9 pu.

t = 2 s. The large load is disconnected. This causes motor voltage V_m to ramp up.

t = 2.03 s. The motor terminal voltage reaches the pre-fault voltage level and the PV-STATCOM switches to Mode 3 operation. The active power is ramped up to the maximum available power in about 1.5 cycles without causing any oscillations in the PCC voltage on V_{pcc}.

t = 2.12 s. The controller switches to Mode 4 and the inverter starts operating at unity power factor (UPF).

This study shows that the proposed PV-STATCOM control can stabilize the IM, which would have stalled otherwise.

3.4.2 Advantage of utilizing voltage control up to TOV limit

The performance of the PV-STATCOM controller for stabilizing the IM utilizing the TOV limit and without it are now compared for a large disturbance at motor terminal. The results are illustrated in Figure 3-5. For this study, a 15 kVA PV solar farm is considered and the distance between the PV solar farm and the IM is increased to 20 km. Figure 3-5

(a)-(f) depict V_{pcc}, V_m, reactive power of the PV-STATCOM, IM speed, IM torque, and converter terminal voltage respectively.

A large load is connected at 1.25 s. The PV starts Mode 1 operation at 1.35 s. V_{pcc} violates the steady state limit of 1.06 pu. If the TOV limit is not utilized, the controller switches to Mode 2 operation by enabling PCC voltage control at 1.06 pu. On the other hand, if TOV limit is utilized, the controller continues Mode 1 till 1.52 s, and then switches to Mode 2 operation. The large load is disconnected at 1.75 s.

For the controller not utilizing the TOV limit, the motor become unstable and continues consuming a large reactive power beyond 1.75 s. Due to this large reactive power consumption, V_m fails to reach its pre-fault level. The motor speed reduces further, and it fails to provide the load torque.
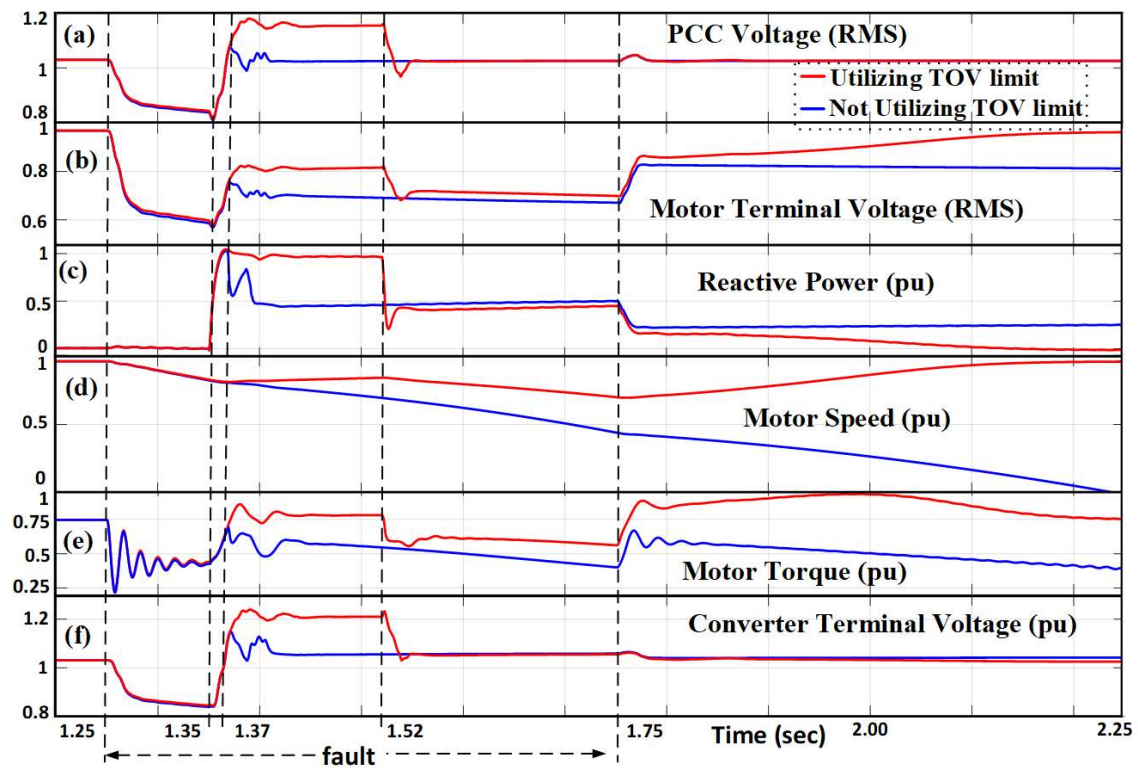
Figure 3-5. Comparison of the performance of the PV-STATCOM controller utilizing TOV limit and not utilizing TOV limit for stabilizing a remote IM.

For the controller utilizing the TOV limit, V_m increases and reaches its pre-fault voltage at 2.25 s. The controller switches to Mode 3 operation at 2.25 s and ramps up the active power. The motor accelerates to normal speed of 2.25% slip and starts delivering its pre-fault torque.

This study demonstrates that the enhanced reactive power support utilizing the TOV limit ensures stable operation of a critical motor even for a severe disturbance, whereas control without this extended support could fail.

3.4.2.1 Importance of monitoring the motor voltage:

In Figure 3-5, it is further observed that when V_{pcc} reaches the pre-fault voltage at 1.36 s, the motor terminal voltage is only 0.8 pu. Therefore, a controller based on control of PCC voltage only will discontinue voltage support at 1.36 s and will fail to stabilize IM. This study thus shows that for effective stabilization of remotely located IMs, the controller must be based on both the motor terminal voltage and PCC voltage.

3.4.3 Comparison of STATCOM and PV-STATCOM operation

The effectiveness of the proposed PV-STATCOM controller for stabilizing a remotely located IM is now compared with a STATCOM of same capacity located at the motor terminal itself. The response of the 5 hp IM during a large disturbance with: (a) with a 10 kvar STATCOM located at motor terminal and (b) 10 kVA PV-STATCOM located 15.6 km away from the motor terminal with 100 msec delay are depicted in Figure 3-6.

The STATCOM for this study is modelled according to [9]. Figure 3-6 (a)-(d) represent the motor terminal voltage V_m, STATCOM or PV-STATCOM reactive power output, IM speed, and IM torque, respectively.

A large load of 10 kvar is connected at IM terminal at t=1.25 s. The STATCOM located at IM terminal starts injecting reactive power immediately to support V_m, and continues providing the support till V_m recovers. The response of the remote PV-STATCOM controller is same as the response in Sec. 3.4.1.
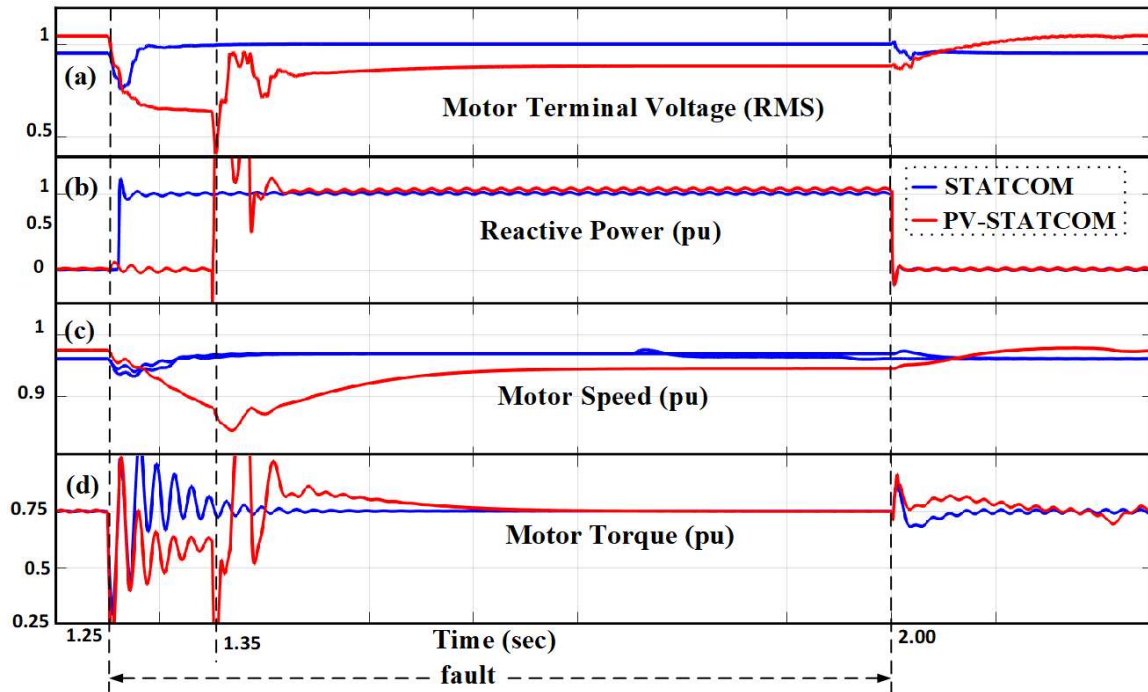
Figure 3-6. Comparison of a remotely located PV-STATCOM and locally located STATCOM for stabilizing an IM for a large disturbance at the motor terminal.

This study shows even if the PV-STATCOM is located 15.6 km away from the critical motor, it can still stabilize the motor during a large disturbance in a similar manner as a STATCOM located at the motor terminal.

3.5   Simulation Studies on study system 2

The PV-STATCOM performance is now investigated on Study System 2 comprising a realistic 27.6 kV utility distribution feeder in Ontario, Canada. Simulation studies are conducted with PSCAD/EMTDC software. The PV-STATCOM performance over a wide range of key system parameters/conditions is evaluated in terms of Critical Clearing time (CCT) which is defined as the maximum fault duration for a three phase fault at Bus 1 for which the IM will not stall. The system parameters considered are (i) system strength, (ii) distance between the PV solar farm and the critical induction motor, (iii) $\frac{X}{R}$ ratio, and (iv) depth of voltage sag. The results of these simulation studies are presented in this section.

The pre fault Bus 1 voltage and IM terminal voltage are maintained at 1.03 pu and 1.01 pu, respectively, for all the studies.

3.5.1   Impact of system strength

The short circuit ratio (SCR) of the feeder at Bus 3 is 3.0. Simulation studies are conducted for SCR of 1.5, 3, and 6. The impact of SCR is examined by: (i) calculating the critical clearing time, (ii) plotting the response of the PV-STATCOM controller for the same fault with various system strengths.

The response of PV-STATCOM controller for a three phase fault at Bus 1 for various SCR is shown in Figure 3-7. Figure 3-7 (a)-(f) depict the motor terminal voltage, motor speed, active power output of PV-STATCOM, reactive power output of PV-STATCOM, PCC voltage and converter terminal voltage, respectively.
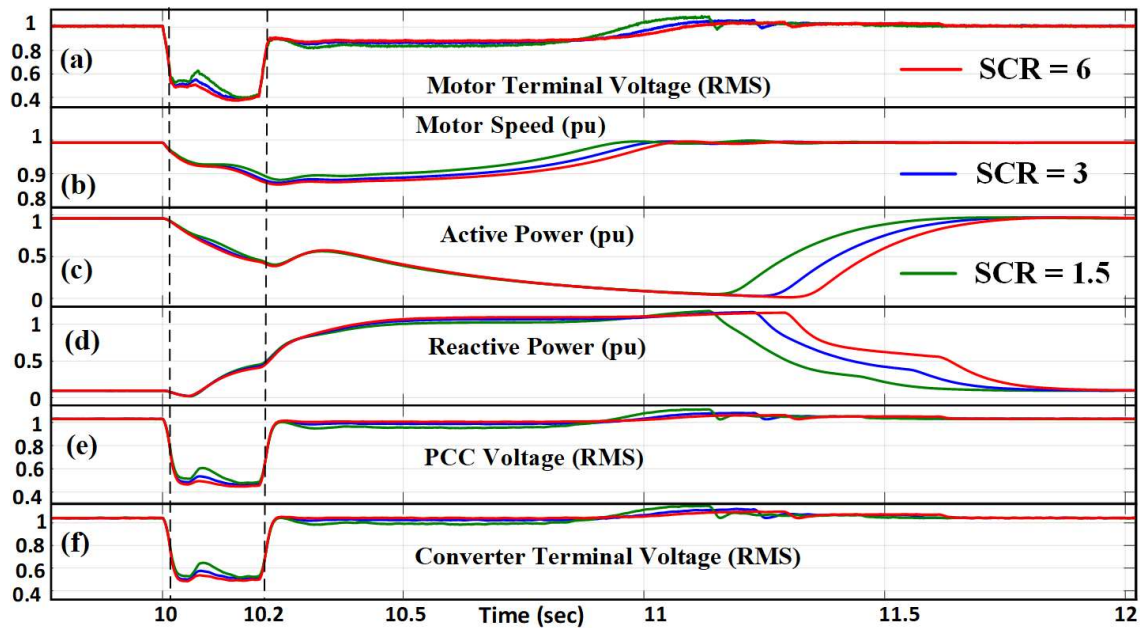
Figure 3-7. The response of PV-STATCOM controller for a three-phase fault at bus 1, for various SCRs at PCC.

$t = 10\,s$. A three-phase fault is applied at Bus 1 for 200 msec. The Bus 1 voltage becomes 0.2 pu during fault. The motor terminal voltage drops down to 0.37 pu, 0.39 pu and 0.42 pu for systems with SCR of 6, 3, and 1.5, respectively. The PCC voltage reduces to 0.48,

0.53 and 0.54 pu, respectively. The IM speed declines in all the three cases. The communication delay is considered to be 100 ms, and hence the reactive current reaches 1 pu at 10.1 s.

t = 10.2 s. The fault is cleared. Due to fault clearance, the PCC and motor terminal voltages increase.

t = 11.14 s. The TOV limit is violated at t = 11.14 s, 11.23 s and 11.29 s for systems with SCR = 1.5, 3 and 6, respectively. Therefore, the controller switches to Mode 2 operation at t = 11.14 s, 11.23 s and 11.29 s for systems with SCR = 1.5, 3 and 6, respectively.

t = 11.16 s. The controller enables Mode 3 operation at t = 11.16 s, 11.23 s and 11.32 s, respectively, for systems with SCR = 1.5, 3 and 6, as the motor terminal voltage reaches the pre fault voltage.

t = 11.6 s. The controller changes the mode of operation to Mode 4 at t = 11.6 s, 11.73 s, and 11.81 s, respectively, for systems with SCR = 1.5, 3 and 6, as the active power is ramped to the maximum available power.

The critical clearing time for various system strengths are obtained and listed in Table 3.1.

Table 3.1: Critical clearing time for various system strengths.

Sl. No	Short Circuit Ratio (SCR) at Bus 3	Critical clearing time (ms)
1	1.5	212
2	3	207
3	6	200

From Figure 3-7, and Table 3.1, it can be seen that PV-STATCOM is able to stabilize the IMs for various system strengths. It is further observed that the proposed controller provides fast response in a weak system.

3.5.2   Impact of $\frac{X}{R}$ ratio

The $\frac{X}{R}$ ratio of the considered feeder is 2.47. The simulation studies are conducted for $\frac{X}{R}$ ratio of 1, 2.47, and 5, and the results are shown in Figure 3-8. The impact of SCR is examined by (i) calculating the critical clearing time, and (ii) plotting the response of the PV-STATCOM controller for the same fault, with various $\frac{X}{R}$ ratios.
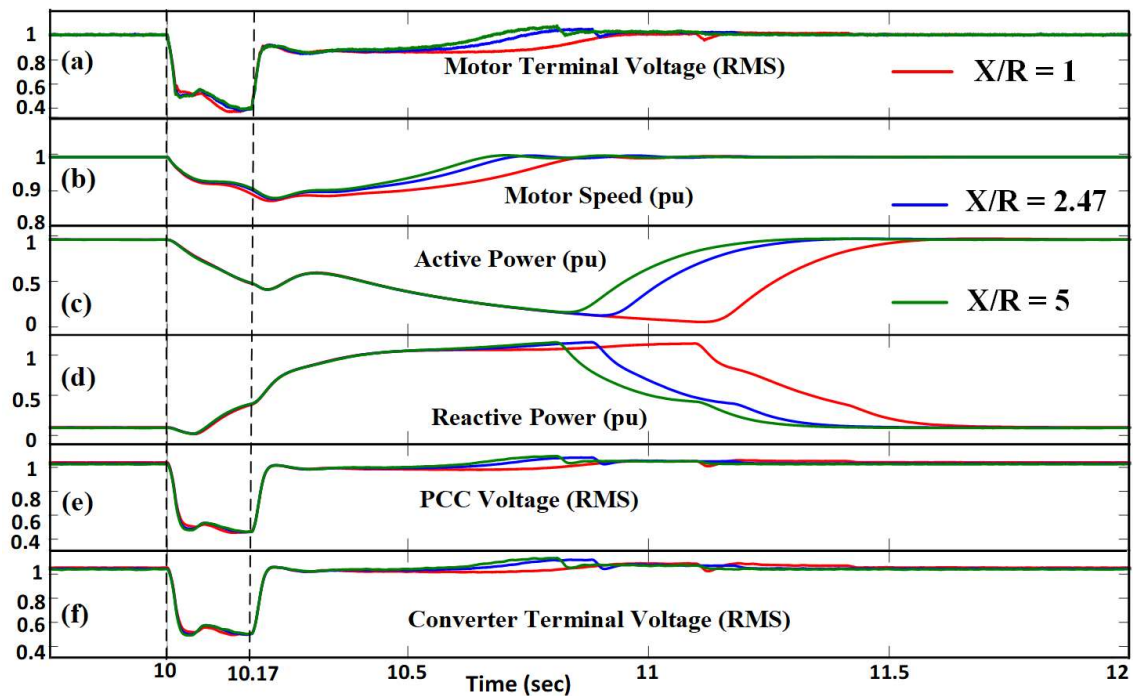
Figure 3-8. The response of PV-STATCOM controller for a three phase fault at bus 1, for various X/R ratios.

Figure 3-8 (a)-(f) illustrate the motor terminal voltage, motor speed, active power output of PV-STATCOM, reactive power output of PV-STATCOM, PCC voltage and converter terminal voltage, respectively. The operational characteristic of the PV-STATCOM and IM are similar to the behavior explained in Sec. 3.4.1 and 3.5.1.

The critical clearing time for various $\frac{X}{R}$ ratios are given in Table 3.2.

Table 3.2. Critical clearing time for various X/R ratios.

Sl. No	$\frac{X}{R}$ ratios	Critical clearing time (ms)
1	1	175
2	2.47	207
3	5	215

The PV-STATCOM controller can successfully stabilize the IMs for various $\frac{X}{R}$ ratios considered as shown in Figure 3-8. The controller is however, more effective in a reactive network, as given in Table 3.2.

3.5.3   Impact of distance between PV solar farm and the IM

Studies are conducted for distances of 40 km, 20 km and 5 km between the PV solar farm and IMs. The response of PV-STATCOM for a three phase fault at bus 1 is plotted for various distances in Figure 3-9. The critical clearing time is calculated and presented in Table 3.3. The operational characteristic of the PV-STATCOM and IM are similar to the behavior explained in Sec. 3.4.1 and Sec. 3.5.1.

Figure 3-9 (a)-(f) depict the motor terminal voltage, motor speed, active power output of PV-STATCOM, reactive power output of PV-STATCOM, PCC voltage and converter terminal voltage, respectively.
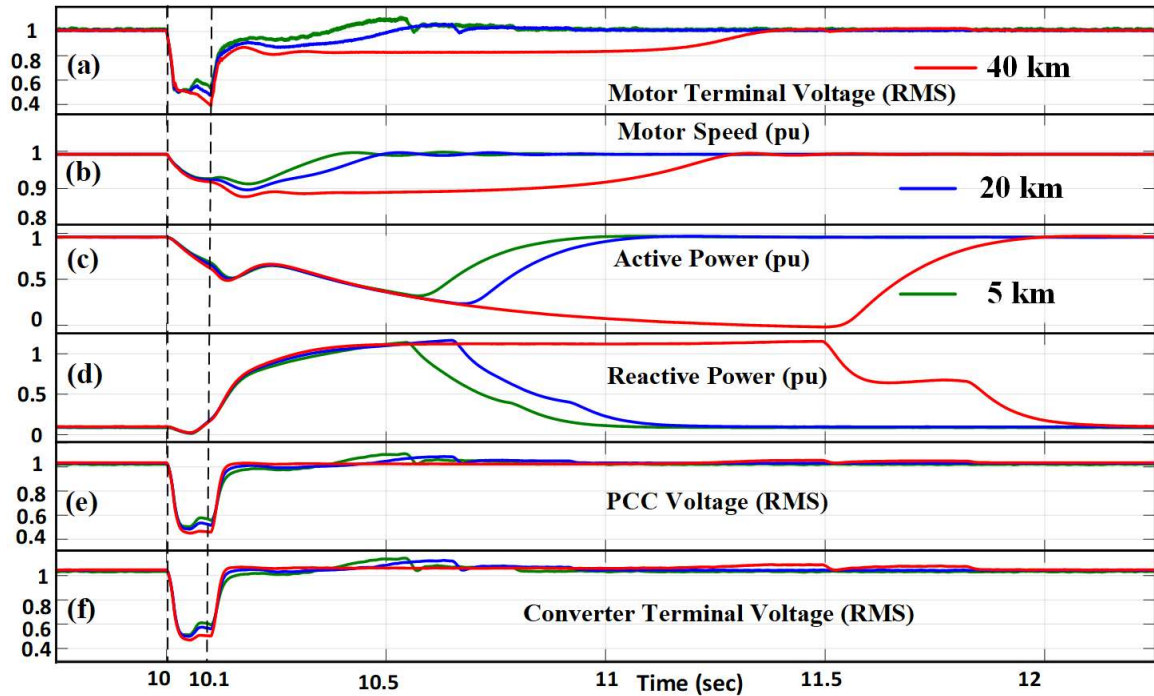
Figure 3-9. The response of PV-STATCOM controller for a three phase fault at bus 1, for various distance between PV solar farm and IM.

Table 3.3. Critical clearing time for various distance between PV solar farm and IM.

Sl. No	Distance between PV solar farm and IM (km)	Critical clearing time (ms)
1	40	100
2	20	207
3	5	250

The PV-STATCOM controller can successfully stabilize the critical IM for wide ranging distances between them as shown in Table 3.3. However, the fastest stabilization is achieved for short distances.

3.5.4   Impact of voltage sag

The performance of PV-STATCOM controller for various voltage sag depths are evaluated by conducting studies for 100%, 75%, 50% and 25% voltage sags at bus 1. The critical clearing time is given in Table 3.4 and the response of the PV-STATCOM for a three-phase fault at bus 1 is plotted in Figure 3-10 for various voltage sag depths. The operational characteristic of the PV-STATCOM and IM are similar to the behavior explained in Sec. 3.4.1 and Sec. 3.5.1.
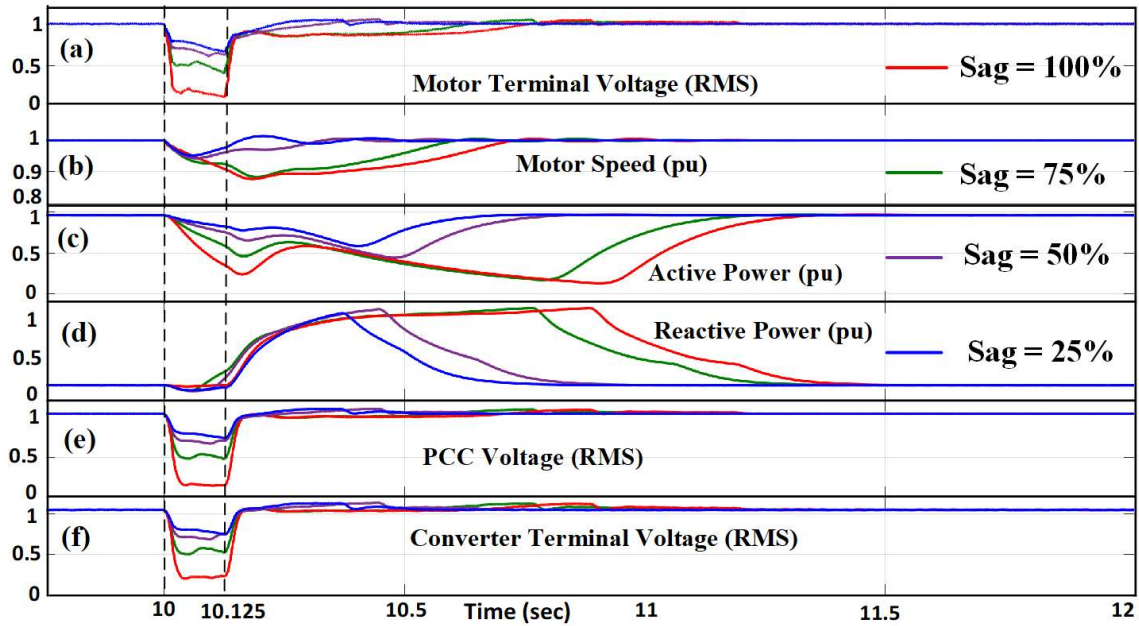
Figure 3-10. The response of PV-STATCOM controller for a three-phase fault at bus 1, for various voltage sag depths.

Table 3.4. Critical clearing time for various voltage sag depths.

Sl. No	Depth of Voltage Sag at Bus 1 (%)	Critical clearing time (ms)
1	100	125
2	75	209
3	50	750

	25	4500

The PV-STATCOM controller is successful in stabilizing the IM for a wide range of voltage sags, although the response is slower for larger voltage sags, as expected.

The studies in this section demonstrate the effectiveness of the proposed PV-STATCOM controller in stabilizing the critical IM in a realistic distribution feeder for wide ranging values of key system parameters. The critical clearing time is seen to decrease with: i) increasing distance, ii) decreasing X/R ratio, iii) increasing system strength (SCR), and iv) increasing voltage sag depth. Despite these wide variations in key system parameters, the proposed PV-STATCOM successfully stabilizes the motor.

3.5.5 Performance of the PV-STATCOM controller with multiple Induction motors.

The capability of the proposed PV-STATCOM controller for stabilizing a combination of multiple IM loads is now demonstrated in Study System 2. Three different IM loads are considered, to examine the performance of PV-STATCOM. The IM loads considered are (i) 1.25 MVA large industrial motor (Motor A), (ii) 0.7 MVA weighted aggregate of residential and industrial motors (Motor B), and (iii) 0.7 MVA small industrial motors (Motor C). The motor loads are modelled as per [100, 181].

Figure 3-11 (a)-(f) illustrate the motor terminal voltage, speeds of different motors, active power output of PV-STATCOM, reactive power output of PV-STATCOM, PCC voltage and converter terminal voltage, respectively.
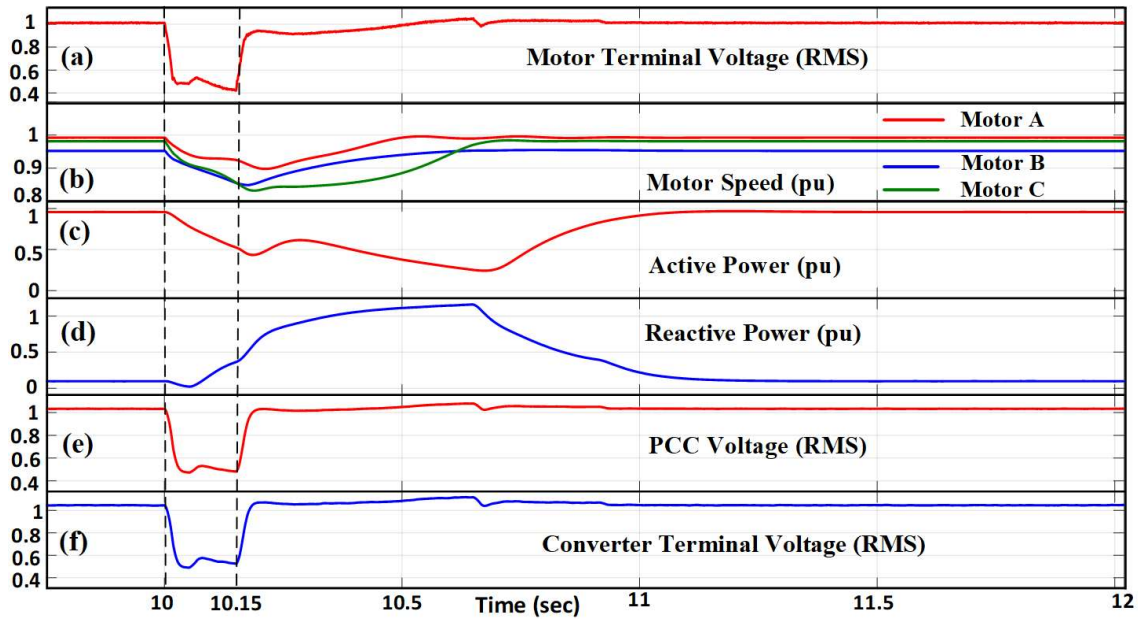
Figure 3-11. Response of PV-STATCOM for a three phase fault at bus 1, with multiple IMs connected.

t = 10 s. A three-phase fault is applied at Bus 1 for 150 ms. The Bus 1 voltage becomes 0.2 pu during fault. The motor terminal reduces to 0. 41 pu and the PCC voltage decreases to 0.48 pu. The speed all the three IMs decline. Motor C experiences the highest drop in speed, as it has the lowest inertia. Since the communication delay is 100 ms, the reactive current reaches 1 pu at 10.1 s.

t = 10.15 s. The fault is cleared. Due to the fault clearance, the PCC and motor terminal voltages increase. All the motors start accelerating, however, motor C has the lowest acceleration due to its low inertia.

t = 10.63 s. The TOV limit is violated at t = 10.63 s, at which time the controller switches to Mode 2 operation.

t = 10.65 s. The controller enables the Mode 3 operation at t = 10.65 s.

t = 11.2 s. The controller changes the mode of operation to Mode 4 at t = 11.2 s, as the active power is ramped to the maximum available power.

This study demonstrates that the PV-STATCOM is successful in stabilizing a group of different industrial and residential induction motors having different inertias.

3.6 Conclusion

This chapter presents a novel reactive power control of PV-STATCOM, for stabilizing remotely located critical induction motors during system disturbances. The proposed control provides: i) a novel enhanced voltage support to the extent of the acceptable Temporary Over Voltage (TOV) limit of the utility, and ii) a new power ramp-up control while keeping the dynamic voltage control function activated. The effectiveness of the proposed control is demonstrated through detailed simulation studies using MATLAB Simulink software, on a 10 kW PV solar system in the network of Bluewater Power Distribution Corporation, Sarnia, in Canada. It is shown that the PV-STATCOM control on a solar farm:

1) can stabilize a critical induction motor located as far as 15.6 km, away.

2) is equally effective as a STATCOM connected at motor terminals.

3) is able to ensure stable operation of critical induction motor, even for the cases which the reactive power support from PV systems required under German Grid Code [91] fails to do so.

Further studies on a realistic 27.6 kV distribution feeder in Ontario showed that a PV solar farm as PV-STATCOM can stabilize a critical IM, even if located 20 km away, for a wide range of system conditions viz. (i) system strength, (ii) X/R ratio of the feeder, (iii) distance between PV plant and IM, and (iv) depth of voltage sag.

Chapter 4

4 Night and Day Field Demonstration of PV-STATCOM Technology for Stabilizing Critical Induction Motor

4.1 Introduction

This chapter presents the first in Canada (and perhaps first in the world) utility demonstration of a novel nighttime and daytime technology of utilizing PV solar farm as a dynamic reactive power compensator (STATCOM) and named PV-STATCOM. The field demonstration was performed on a 10 kW PV solar farm installed in the utility network of Bluewater Power Distribution Corporation, in Sarnia, Ontario. It is demonstrated that the solar farm autonomously transforms into a STATCOM and ensures stable operation of a critical induction motor on a 24/7 basis during a large disturbance which would otherwise destabilize the motor. The PV-STATCOM is further demonstrated to be a new smart inverter which operates much fast than a conventional smart inverter and also during nighttime, which present-day smart inverters do not. Two field demonstrations are performed. The first field demonstration is for the case when the critical motor is located at the PV system bus, and the second field demonstration is for the case when the critical motor is located at a site remote from the PV solar system.

4.2 Study System

The field demonstration of PV-STATCOM technology was conducted on the 10-kW grid-connected PV solar farm located on Confederation Street in the utility system of Bluewater Power Distribution Corporation, Sarnia, Ontario, Canada. The single line diagram of the study system and the photographs of the demonstration site are shown in Figure 4-1, and Figure 4-2 respectively. The PV solar farm is connected to Pole 325 using switch S_1. Pole 325 in turn is connected through a 150kVA 600V/4.16kV transformer to the 4.16 kV distribution feeder 14F1 of Bluewater Power distribution system, although not shown in Figure 4-1. The voltage and current of the PV panels are 280V and 35.7A, respectively, for Maximum Power Point (MPP) operation. Solar power is fed to the grid using a commercial utility inverter rated 10kW, 600 V AC and 475V DC, operating at unity power factor. Switches S_8 and S_9 are used to isolate the existing PV inverter from the

circuit. A 3-hp induction motor M_2 is used to operate the tracking system of the PV panels. This motor is connected to the 208V terminal of transformer T_1 (Bus 1) using switch S_5.

The utility inverter is controlled by its propriety control provided by the manufacturer and is not amenable to any modifications. For this reason, a separate three-phase two-level 10 kVA inverter controlled as PV-STATCOM is used for the field demonstration. This 10 kVA PV-STATCOM inverter includes six insulated gate bipolar transistors, gate drives and protection circuit. The PV-STATCOM controller is designed in MATLAB/Simulink software and implemented on the dSPACE controller board. Current and voltage sensors are installed at the PV-STATCOM inverter and the load. The sensor signals are sent to dSPACE controller board (DS1103) through ADC channels. The PV-STATCOM controller is implemented on the dSPACE controller board which generates appropriate firing pulses for the IGBT gates of the PV-STATCOM inverter based on the selected control objectives and operation mode. The Pulse Width Modulation (PWM) pulses generated from the dSPACE board are applied to the PV-STATCOM inverter interface panel through appropriate level shifter circuits. A graphics user interface (GUI) is designed in Control Desk software to provide a control environment to supervise the PV-STATCOM system operation. A Yokogawa power analyzer (DL850E) is used to capture the various signal waveforms.

The PV-STATCOM inverter and the utility PV inverter are connected to the solar panels using a double-pole double-throw switch S_6. An LCL filter is used at the inverter terminal to filter out the switching harmonics and to maintain the THD of the inverter output within 5% [168]. The filter inductance and capacitance are designed to be 1 mH and 300 μF, respectively. As the MPPT voltage of PV panel is 280 V, a 140-208/208V intermediate transformer T_2 with 5% impedance is employed to connect the PV-STATCOM inverter to the utility transformer T_1.

In this field demonstration, the 10 kVA PV-STATCOM is used to stabilize a 5 hp induction motor M_1 during a major system disturbance. This large system disturbance is initiated by the switching of a 10 kvar inductive load. In this demonstration, a variable line inductor L_1 rated 5.1 mH in combination with the system short circuit reactance L_S at Pole

#325 is used to vary the effective short circuit inductance of the grid, L_g, as seen by the PV-STATCOM. Switch S_2 is used to isolate the PV-STATCOM and load from the grid.

For nighttime operation of PV-STATCOM, the PV panels are disconnected from PV-STATCOM inverter using switch S_6.
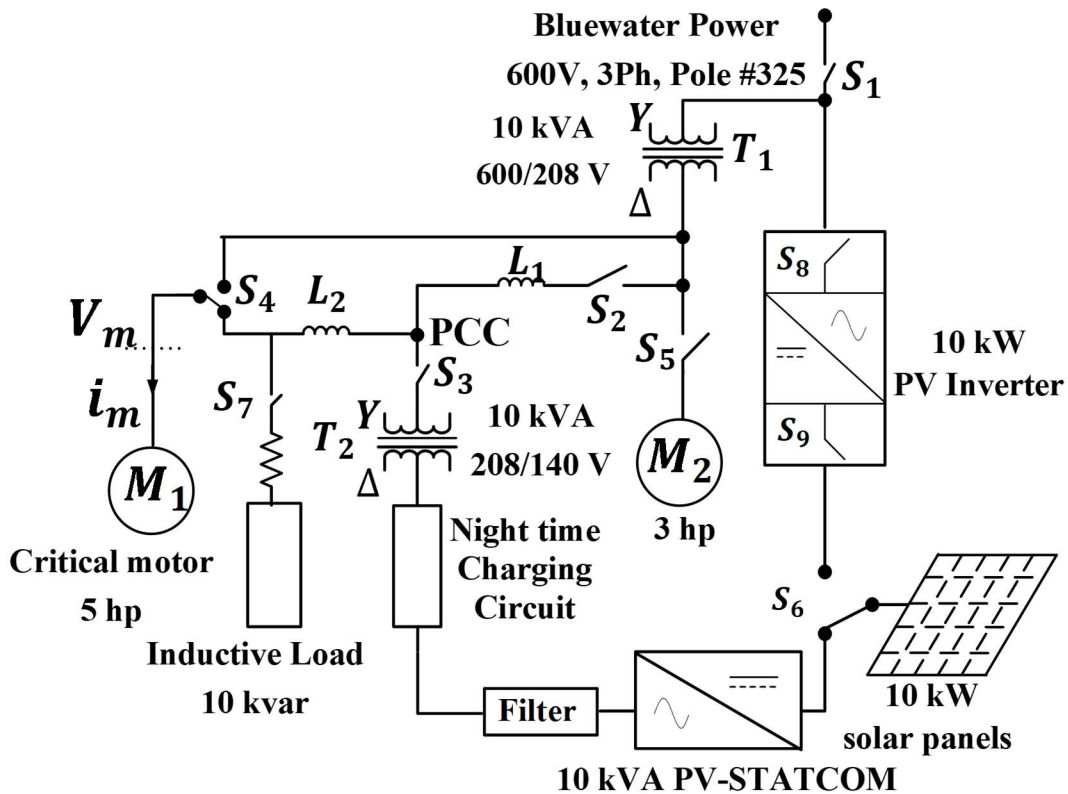
Figure 4-1. Single Line Diagram of the study system.

For demonstrating the capability of PV-STATCOM to stabilize a remotely located critical motor, the effective distance between the motor and the solar farm is varied by using a variable inductor L_2 which is inserted through switch S_4. The delay in communication of motor terminal voltage signal to the solar farm is implemented in software. The overall delay represents: i) the communication delay between motor terminal and PV-STATCOM, and ii) the communication delay between master control and individual inverter controllers in an actual PV solar farm. The latency for fiber optic cable is $3.34\ \mu s/km$ [178] and the communication delay incurred in a PV solar farm plant control is approximately 100 ms [88]. Thus, the delay in the study system with a distance

of about 15.6 km between the IM and the PV solar farm is 100.05 ms and is approximated as 100ms.

Figure 4-2. Field demonstration site at Bluewater Power, Sarnia, Canada.

The PV-STATCOM controller is discussed in detail in Sec. 3.3.1

4.3 First Field Demonstration: Application of PV-STATCOM for stabilizing locally connected Induction Motor

This section presents the results for the first field demonstration of utilizing the PV solar farm as PV-STATCOM for stabilizing a locally located critical induction motor during nighttime and daytime.

4.3.1 Response of Conventional Inverter for Large Disturbance During Night Time

Studies are now performed during nighttime. The response of the PV solar farm and the induction motor for the switching of 10 kvar inductor at PCC during night time without PV-STATCOM controller is shown in Figure 4-3.
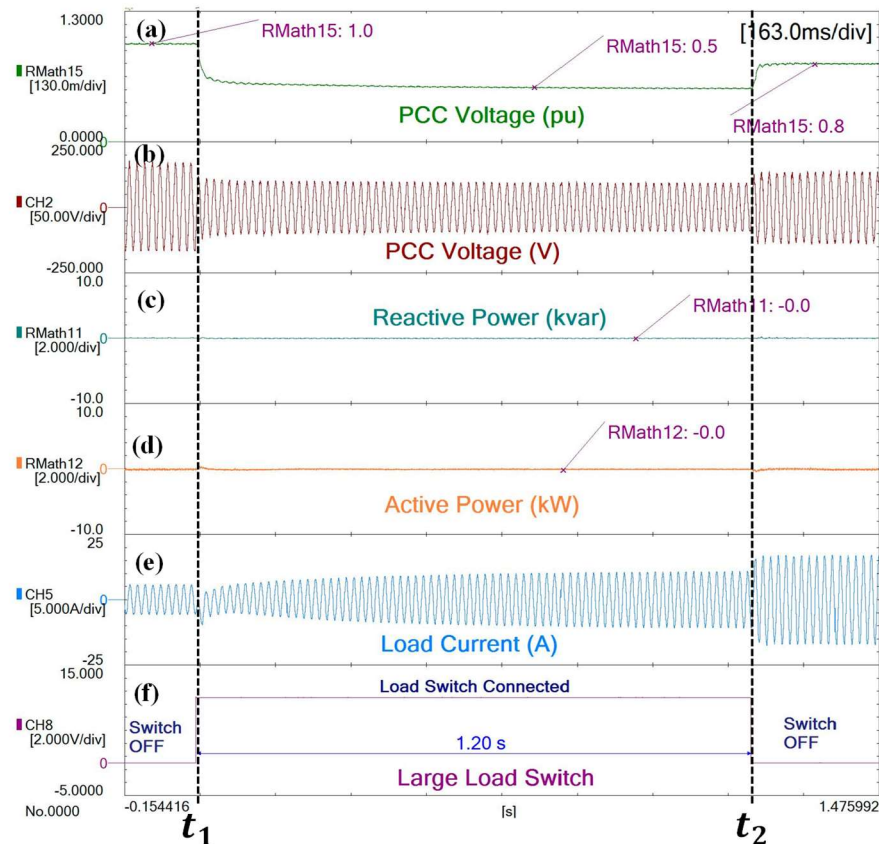
Figure 4-3. Response of the conventional PV inverter for large load switching during night time.

Figure 4-3 (a) - (f) illustrate the PCC rms voltage (pu), PCC instantaneous voltage (V), Reactive power output of the inverter (kvar), Active power output of the inverter (kW), Motor current (A) and status of the large load switch, respectively.

t < t_1: The inverter is idle as the solar power is zero. The motor is operating at steady state by providing the required load torque, by drawing power from the grid.

t = t_1: A large disturbance is created by connecting 10 kvar inductor to the PCC. Due to this large load switching, the PCC voltage drops to 0.5 pu. Due to this large voltage drop, the motor starts consuming a high amount of reactive power and the motor current increases to 12 A.

t = t_2: The large load is disconnected, due to which the voltage starts recovering but only up to 0.8 pu. Since no reactive power support is available the motor consumes a larger current of 16 A and eventually stalls.

This study demonstrates that the induction motor will become unstable and stall during a large disturbance at night when no reactive power support is available.

4.3.2   Response of PV-STATCOM for Large Disturbance During Night Time

Studies are conducted during nighttime with the PV-STATCOM control activated. The PV-STATCOM inverter and induction motor response for the large load switching at PCC during night time with PV-STATCOM controller is shown in Figure 4-4.

Figure 4-4 (a) - (g) illustrate the PCC rms voltage (pu), PCC instantaneous voltage (V), Reactive power output of the PV-STATCOM inverter (kvar), Active power output of the PV-STATCOM (kW), PV-STATCOM inverter current (i_{pv}) (A), Motor current (A) and status of the large load switch, respectively.

t < t_1: The system is operating in steady state with a PCC voltage of 1 pu. The PV-STATCOM is idle. The motor is providing the load torque by consuming 8 A from the grid.

t = t_1: The large load is connected and as a consequence the bus voltage drops to 0.65 pu. The PV-STATCOM detects the drop in the voltage and switches to Full STATCOM operation. In this mode, the full inverter capacity is utilized for injecting reactive power. The PV-STATCOM inverter injects 9.4 kvar reactive power. The speed of response for the controller is seen to be 1.4 cycle. This fast reactive power injection is able to bring the PCC voltage to 0.99 pu and thus prevent the motor from stalling.
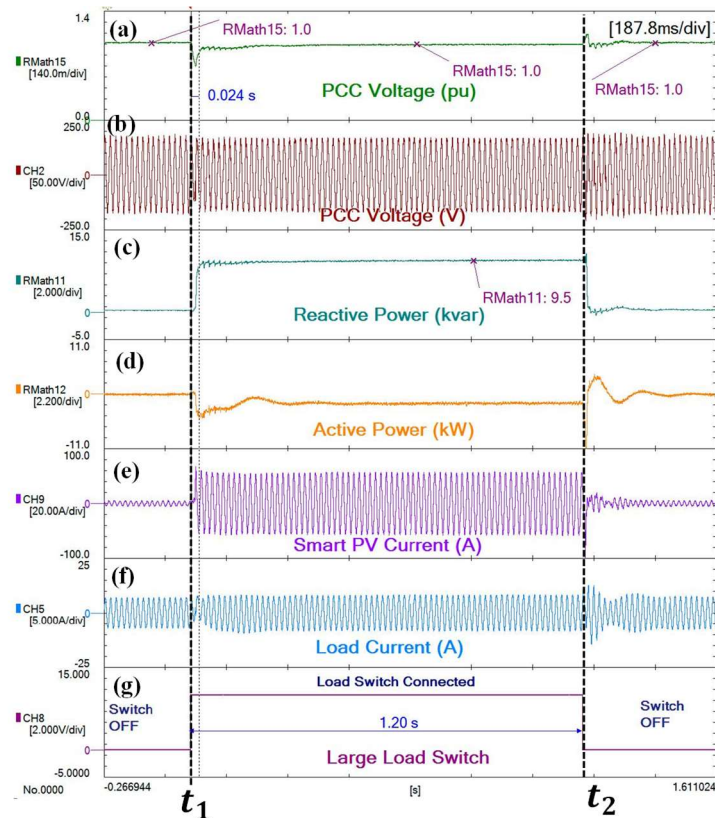
Figure 4-4. Response of the PV-STATCOM for large load switching during night time.

t = t_2: The large load is disconnected at t=t2. The controller detects it and ceases reactive power injection. The motor continues to operate in a stable manner with its pre-disturbance current level of 8 A.

This study demonstrates that the fast reactive power support by the PV solar farm with the proposed PV-STATCOM control can prevent the motor instability during large disturbance at night time, when conventional PV solar plants are usually dormant.

4.4 Second Field Demonstration: Application of PV-STATCOM for stabilizing remotely located Induction Motor

The effectiveness of the proposed PV-STATCOM controller in stabilizing a remotely located 5 hp critical IM is now field-demonstrated on a 10 kW PV solar farm in the utility network of Bluewater Power Distribution Corporation. Three studies are reported: i) solar

farm operation with reactive power support according to the German Grid Code (BDEW) [91], ii) solar farm control as PV-STATCOM with varying (and very large) communication delay, iii) PV-STATCOM operation at night. The superiority of the PV-STATCOM control is thus demonstrated.

4.4.1   PV solar farm operation according to German Grid Code

At first, the impact of reactive current injection by the PV solar farm while following the existing grid codes in motor stabilization is investigated. The German Grid Code (BDEW) [91] requires the PV inverter to inject reactive power to support the grid during transients. This dynamic reactive current support is presently optional in IEEE 1547-2018 [90], and in California Rule 21 [92]. According to BDEW [91], the PV inverter needs to inject a minimum of two percent reactive current per one percent voltage drop for voltage below 0.9 pu. The performance of dynamic reactive current injection by the smart PV inverter according to BDEW code in stabilizing the remotely located induction motor is tested and the results are shown in Figure 4-5. The distance between the PV solar farm and the motor terminal is kept at 15.6 km and the delay between voltage measuring unit at motor terminal and PV system is considered to be 100 ms.

Figure 4-5 (a)-(h) shows the motor terminal phase voltage, motor terminal RMS voltage, active and reactive power output of the PV solar system, motor current, i_d and i_{dref}, i_q and i_{qref} of PV solar system, and DC link voltage, respectively.

The zoomed images of transients during initiation of disturbance (t=0 s) and transients during termination of disturbance (t=2 s) is shown in Figure 4-6 and Figure 4-7, respectively.
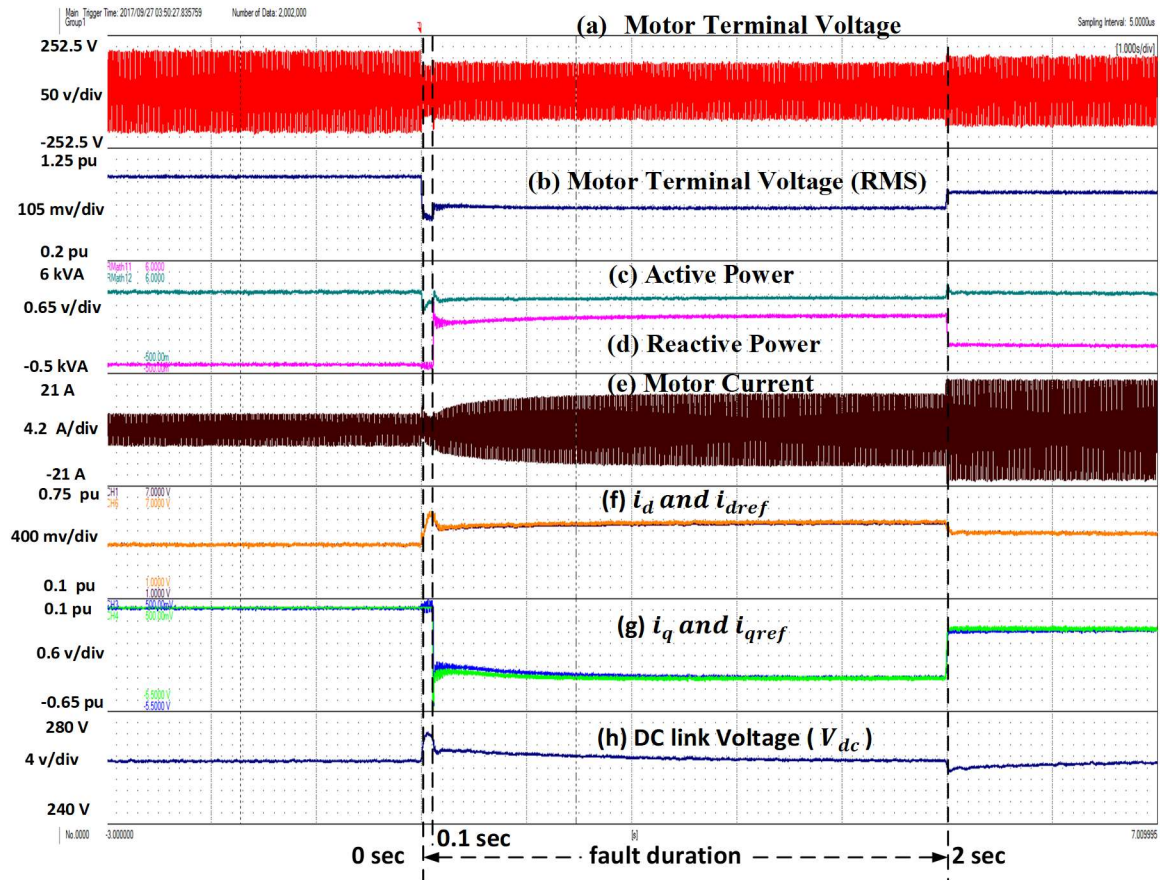
Figure 4-5. Response of the IM and the PV solar system operating according to German Grid Code for a large disturbance at motor terminal.

t < 0 s. The motor terminal voltage is 1.02 pu. The motor is operating in steady state and consuming 8A.

The PV solar farm is operating at unity power factor and injecting 4.8 kW.

t= 0 s. A large disturbance is applied at the motor terminal by connecting a 10 kvar inductive load. This causes the motor terminal voltage to drop from 1 pu to 0.58 pu as shown in Figure 4-5 (b). The PV system rides through the fault and injects the maximum available active power as illustrated in Figure 4-5 (c). The PV active power reduces slightly due to the drop in the terminal voltage. The reactive power output of PV inverter is zero as seen in Figure 4-5 (c) and Figure 4-5 (f). Due to the reduction in voltage, the motor starts consuming a large current of 12 A.
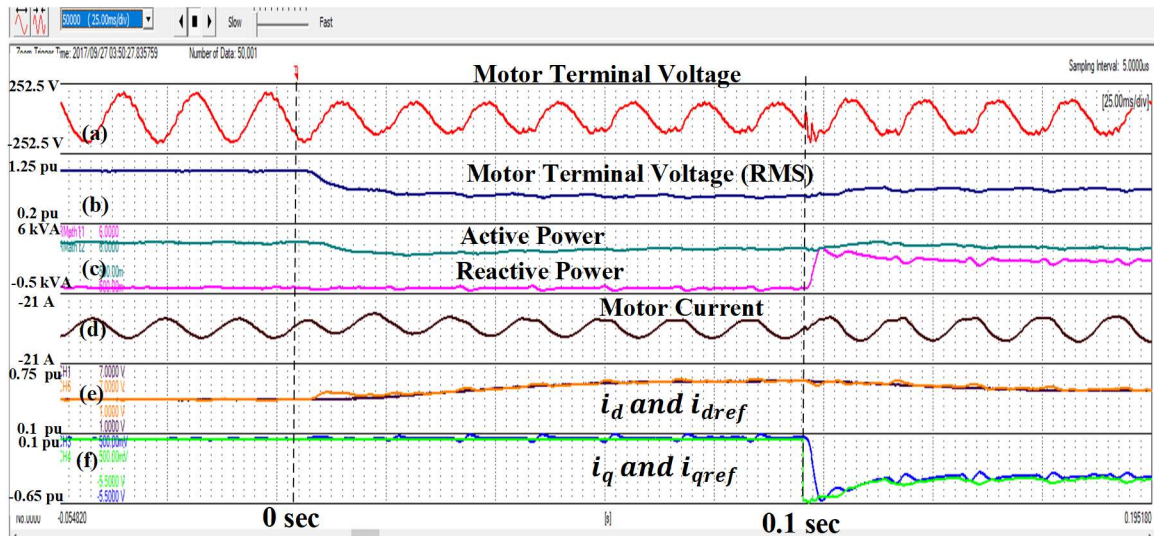
Figure 4-6. Zoomed response of the IM and the PV solar system operating according to the dynamic reactive current injection of German Grid Code for a large disturbance at motor terminal at initiation of disturbance (t = 0 s).

t = 0.1 s. Since the motor terminal voltage has reduced to 0.58 pu, the inverter injects 0.64 pu reactive current (according to BDEW code) as depicted negatively in Figure 4-5 (f). This causes the voltage to increase rapidly up to 0.69 pu. At this time, the inverter modifies the reactive current injection to 0.62 pu (per BDEW code), as seen in Figure 4-6 (f). The inverter active power remains almost constant during this interval as the total apparent power of the inverter is within the maximum kVA rating of the inverter. The motor consumes a large current of 16 A during this period.

t = 2 s. The large load is disconnected at t = 2 s. The motor terminal voltage increases but only up to 0.82 pu (due to increased motor current). The PV inverter injects 0.16 pu reactive current as the voltage is below 0.9 pu (per BDEW code). The motor consumes a larger reactive current of about 20 A and eventually stalls.
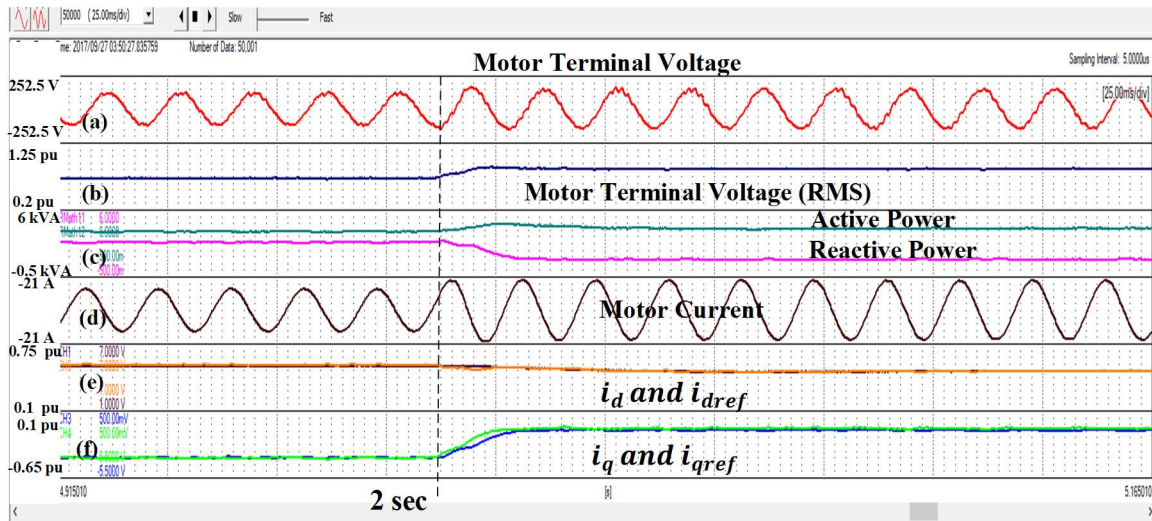
Figure 4-7. Zoomed response of the IM and the PV solar system operating according to the dynamic reactive current injection of German Grid Code for a large disturbance at motor terminal at termination of disturbance (t = 2 s).

This field test further demonstrates that reactive current injection by PV inverter according to German grid code requirement is not adequate to stabilize a remotely located induction motor during a large disturbance. In contrast, the PV-STATCOM successfully stabilizes the remotely located motor under the same conditions, as shown below.

4.4.2   Impact of Communication delay on PV-STATCOM Performance

In this field test, the impact of communication delay on PV-STATCOM's capability to stabilize the remotely located motor is investigated. While the distance between the PV solar system and the motor is kept at 15.6 km, the communication delay is varied from 100 ms up to 850 ms. This implies a sluggish communication link or increased delays within a solar plant. The performance of the PV-STATCOM controller for a communication delay of 750 ms, which is almost 7.5 times the normal delay for a PV solar farm located 15.6 km away from the motor is shown in Figure 4-8.

Figure 4-8 (a)-(h) illustrate the motor terminal voltage, motor terminal RMS voltage, reactive and active power output of PV-STATCOM, motor current, i_d and i_{dref}, i_q and i_{qref} of PV-STATCOM, and DC link voltage, respectively.
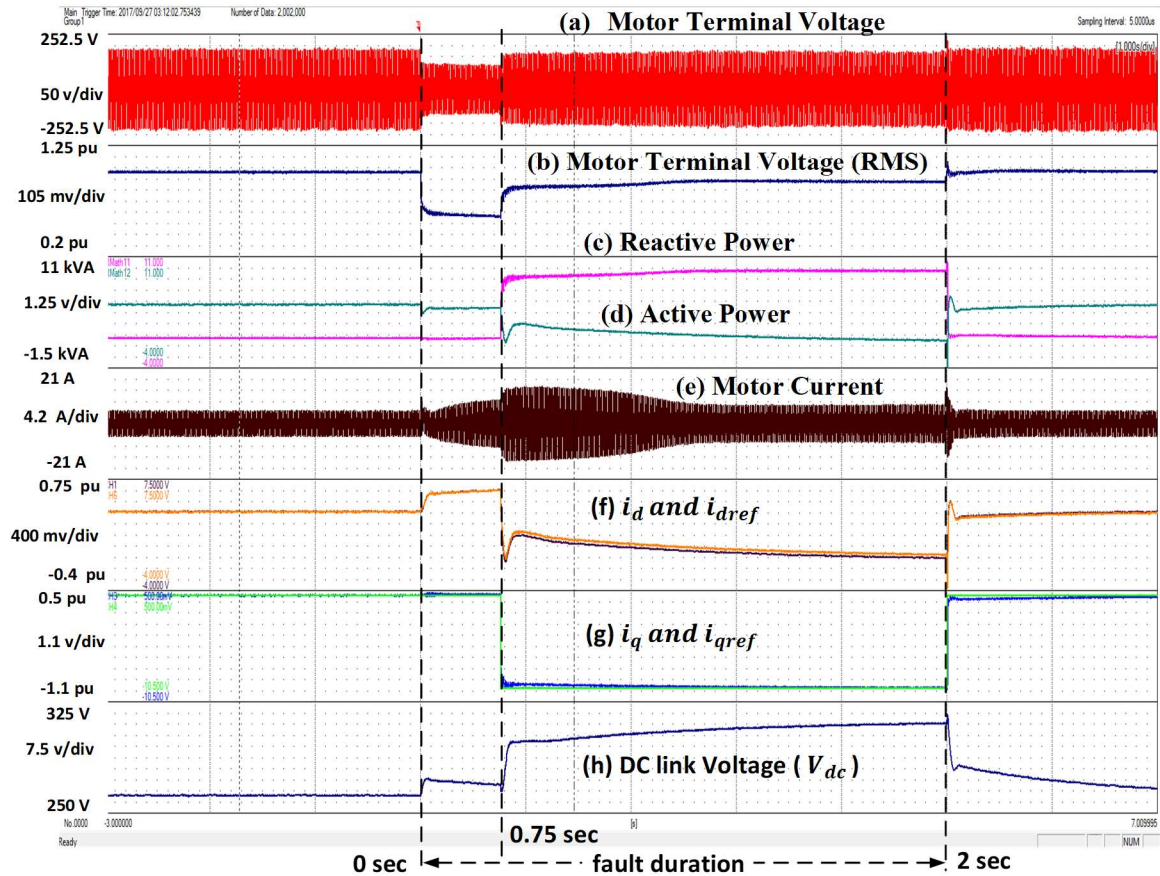
Figure 4-8. Response of the IM and the PV-STATCOM controller with a 750 msec communication delay for a large disturbance at motor terminal.

t < 0 sec. The motor terminal voltage is 1.02 pu. The motor is operating in steady state and consuming 8A. The PV solar farm is injecting 4.2 kW at unity power factor.

t = 0 sec. A three-phase disturbance is applied at motor terminal by connecting a 10 kvar inductive load. Due to the large load connection, the motor terminal voltage drops from 1 pu to 0.58 pu as shown in Figure 4-8 (b). The PV system rides through the fault and injects the maximum available active power as illustrated in Figure 4-8 (c). This PV active power is however slightly reduced due to the drop in the terminal voltage. The reactive power output of PV inverter is zero as seen in Figure 4-8 (c) as the PV system operates at unity power factor. Due to reduced terminal voltage, the motor consumes a large reactive power and its current increases to 12 A.

t = 0.75 sec. The PV-STATCOM controller detects the drop in motor voltage after the communication delay of 750 msec and switches to PV-STATCOM operation. The PV-STATCOM continues injecting 10 kvar in this interval. The motor terminal voltage gradually increases to 0.9 pu. The motor current initially increases but soon stabilizes at 8A with rise in terminal voltage.

t = 2 sec. The large load is disconnected. The motor terminal voltage starts increasing. The PV-STATCOM controller stops dynamic reactive power support and ramp up the active power as the motor terminal voltage recovers to its pre-fault level. The motor remains stable during the disturbance and continues stable operation after disturbance by providing pre-fault load torque.

The zoomed images of transients during initiation of disturbance (t=0 s) and those during termination of disturbance (t=2 s) are shown in Figure 4-9 and Figure 4-10, respectively.
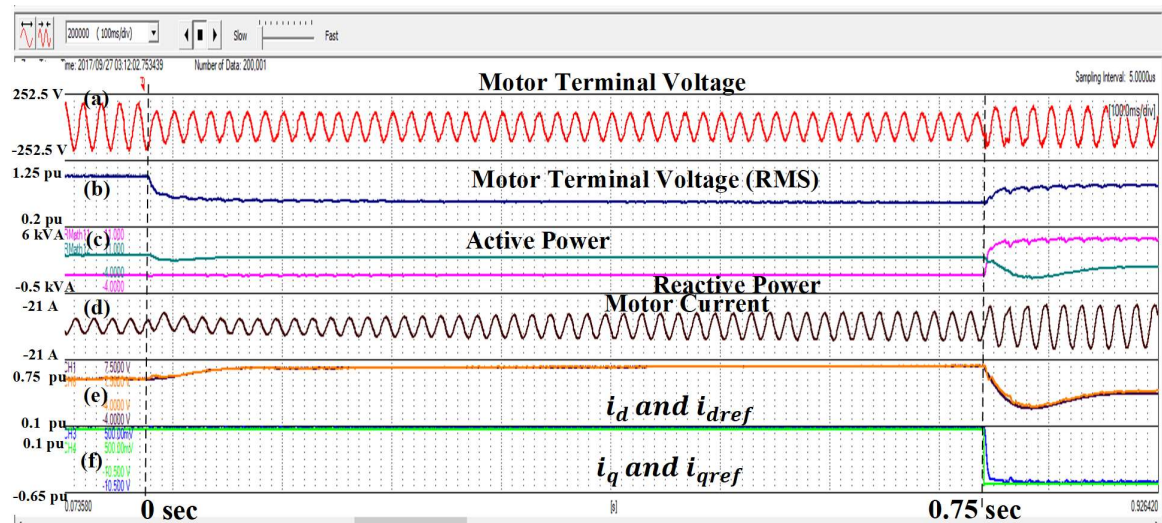
Figure 4-9. Zoomed response of the IM and the PV -STATCOM controller with a 750 msec delay for a large disturbance at motor terminal at initiation of disturbance (t = 0 s).
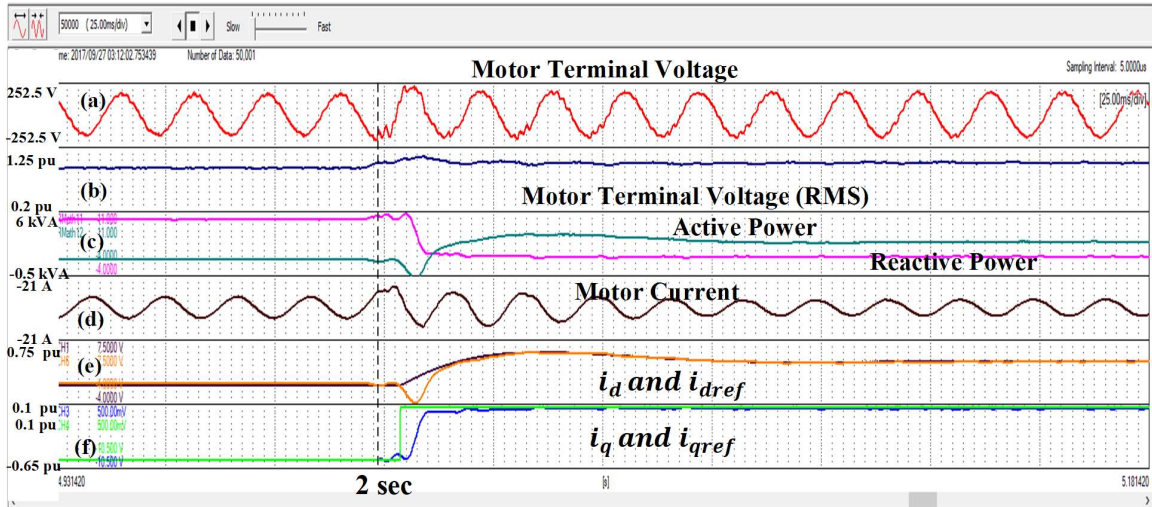
Figure 4-10. Zoomed response of the IM and the PV -STATCOM controller with a 750 msec delay for a large disturbance at motor terminal at termination of disturbance (t = 2 s).

The PV-STATCOM controller is able to respond to the disturbance and inject full reactive power within half a cycle as shown in Figure 4-9 (c). The PV-STATCOM is further able to ramp active power within a cycle with minimal distortion in the system voltage as depicted in Figure 4-10. This rapid response of PV-STATCOM, matches that of actual STATCOMs.

This field test demonstrates that the proposed that the PV-STATCOM can effectively stabilize the remotely located critical motor even with a communication delay of 750 ms.

4.4.3   PV solar farm operating as PV-STATCOM at night

Figure 4-11 (a)-(h) illustrate the motor terminal voltage, motor terminal RMS voltage, reactive and active power output of PV-STATCOM, motor current, i_d and i_{dref}, i_q and i_{qref} of PV-STATCOM, and DC link voltage respectively.
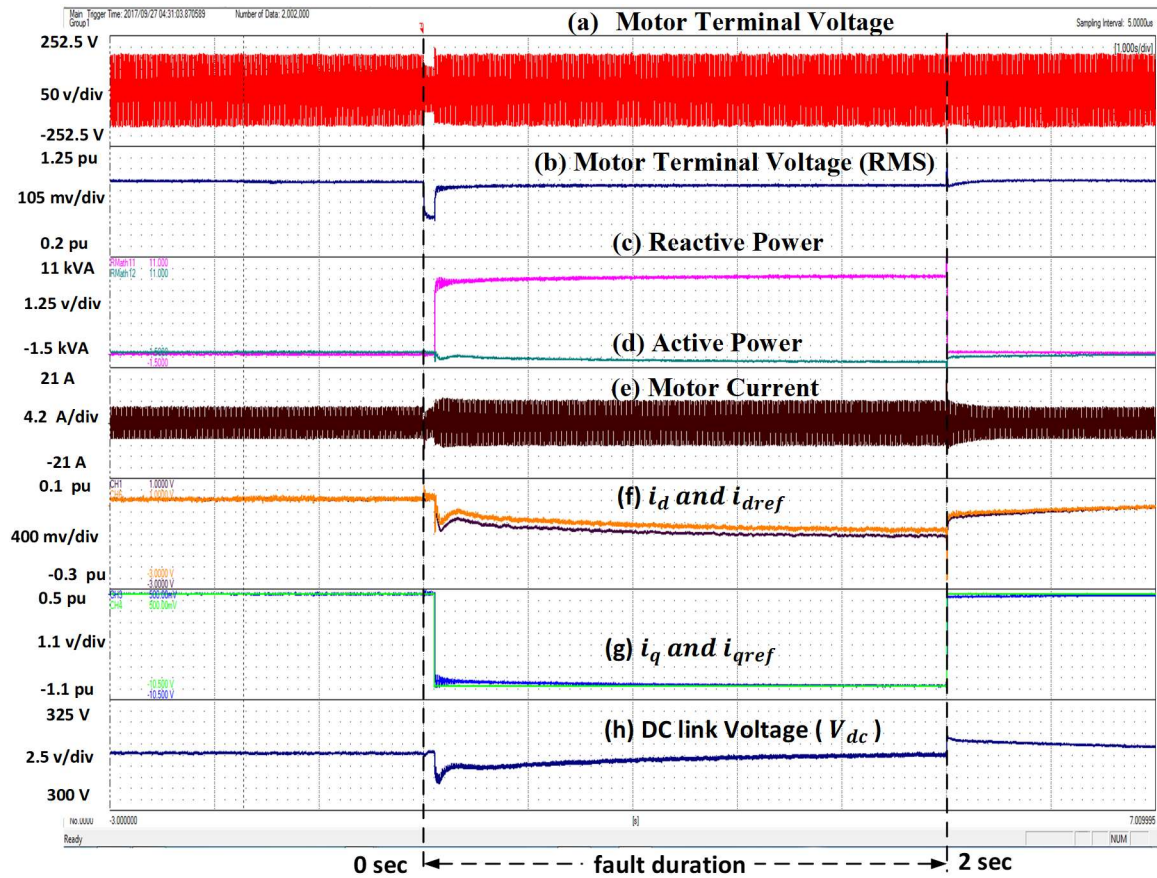
Figure 4-11. Response for PV-STATCOM operation at night.

Initially PV system is idle. As soon as it detects a drop in V_m due to the large disturbance, the PV-STATCOM controller initiates dynamic reactive power support and ensures continuous stable operation of IM. When the large load is switched off, the PV system stops reactive power support. The PV-STATCOM control thus successfully stabilizes the IM at night during a large disturbance which would have otherwise destabilized the motor.

4.5 Conclusion

This chapter presents the first time in Canada (and first in the world, to the best of authors' knowledge) field demonstration of a novel PV solar farm control as a STATCOM, termed PV-STATCOM. This novel control is demonstrated on a 10 kW PV solar farm installed in the utility network of Bluewater Power Distribution Corporation, Sarnia, ON, for stabilizing a critical 5 hp induction motor both during night and day. The first field demonstration of PV-STATCOM for stabilizing a locally connected critical motor was

performed on 13th Dec. 2016. The second field demonstration of PV-STATCOM for stabilizing a remotely connected critical motor was performed subsequently.

A large disturbance is initiated by switching a 10 kvar inductive load at PCC, both during night and day. Following are the conclusions of the first field demonstration studies:

1) The switching of large inductive load causes a drop in the PCC voltage to about 0.5 pu both during night and day. The motor becomes unstable and stalls in both cases.

2) The PV-STATCOM control on the solar farm successfully ensures stable operation of the motor. The motor continues to operate in a stable manner despite the switching of the large load both during night and day.

Following are the conclusions of the second field demonstration:

1) The dynamic reactive power support according to the German Grid Code (BDEW) fails to stabilize the critical induction motor located 16 km away from the PV solar farm.

2) The PV-STATCOM successfully stabilizes a critical induction motor even if it is located 16 km away from the PV solar farm, both during night and day

3) The PV-STATCOM control is effective even if the delay in communication of motor voltage control signal to solar farm site is 750 ms, which is 7 times more than actual delay in real conditions.

4) The PV-STATCOM regulates the voltage to 1 pu in about 1.4 cycles, both during night and day. This speed of response is identical to actual STATCOMs

5) During daytime, the PV-STATCOM restores the active power generation of the solar farm from zero to its pre-disturbance level in less than 3 cycles after the large load is switched off.

The PV-STATCOM is thus shown to be a new smart inverter, which:

1) provides dynamic voltage control in 1-2 cycles, whereas the present smart inverters provide voltage control (volt-var or volt-watt) in 1-3 seconds [20], and

2) provides dynamic voltage control at night, which conventional smart inverters do not [20].

The PV-STATCOM is further a new FACTS device, which:

1) provides dynamic voltage control with a similar rapid response as a STATCOM [9, 10], and

2) is about 50-100 times lower cost than an equivalent sized STATCOM or SVC. This is because PV-STATCOM involves only installing additional novel controls on the inverter in-use and the already existing electrical infrastructure (substation, transformer, switchgear, buswork, protection systems, etc.) of a PV solar farm.

Chapter 5

5 Coordinated Active and Reactive Power Control of PV-STATCOM for stabilizing a Remote Critical Induction Motor

5.1 Introduction

Dynamic active and reactive power support according to the sensitivity of voltage to active and reactive power output of PV solar farm can ensure faster voltage recovery than the reactive power support alone as shown in Sec. 1.6.2.1. Further, the active and reactive power control can minimize the amount of active power curtailed for providing dynamic voltage support. Thus, a coordinated active and reactive power control of PV-STATCOM for preventing the instability of a critical induction motor (IM) located remotely from the solar farm in a distribution feeder, is presented in this chapter.

At the occurrence of a network fault that can likely destabilize the critical IM, the proposed control strategy intelligently chooses the active and reactive power references based on the latest measured sensitivity of IM terminal voltage to the active and reactive power output of the PV solar farm. Once satisfactory voltage conditions are re-established for stable operation of IM, the solar farm autonomously returns to its pre-disturbance real power production level. The performance of remotely located PV-STATCOM, incorporating detailed model of a realistic medium sized PV plant and control signal communication delays, is further compared with other smart inverter control strategies for dynamic voltage support. The effectiveness of the proposed control strategy is tested through simulation studies on a 27.6 kV feeder in Ontario, Canada. The implementations of the proposed PV-STATCOM control at plant level and inverter level are compared. The impacts of PV plant parameters, and system parameters on system stability for various modes of the proposed controller are studied. Subsequently, design guidelines for PV-STATCOM controller for various system conditions are presented.

5.2 Study System

A realistic 45 km long 27.6 kV feeder in Ontario, Canada [179] is considered as the study system for testing the effectiveness of the proposed controller.
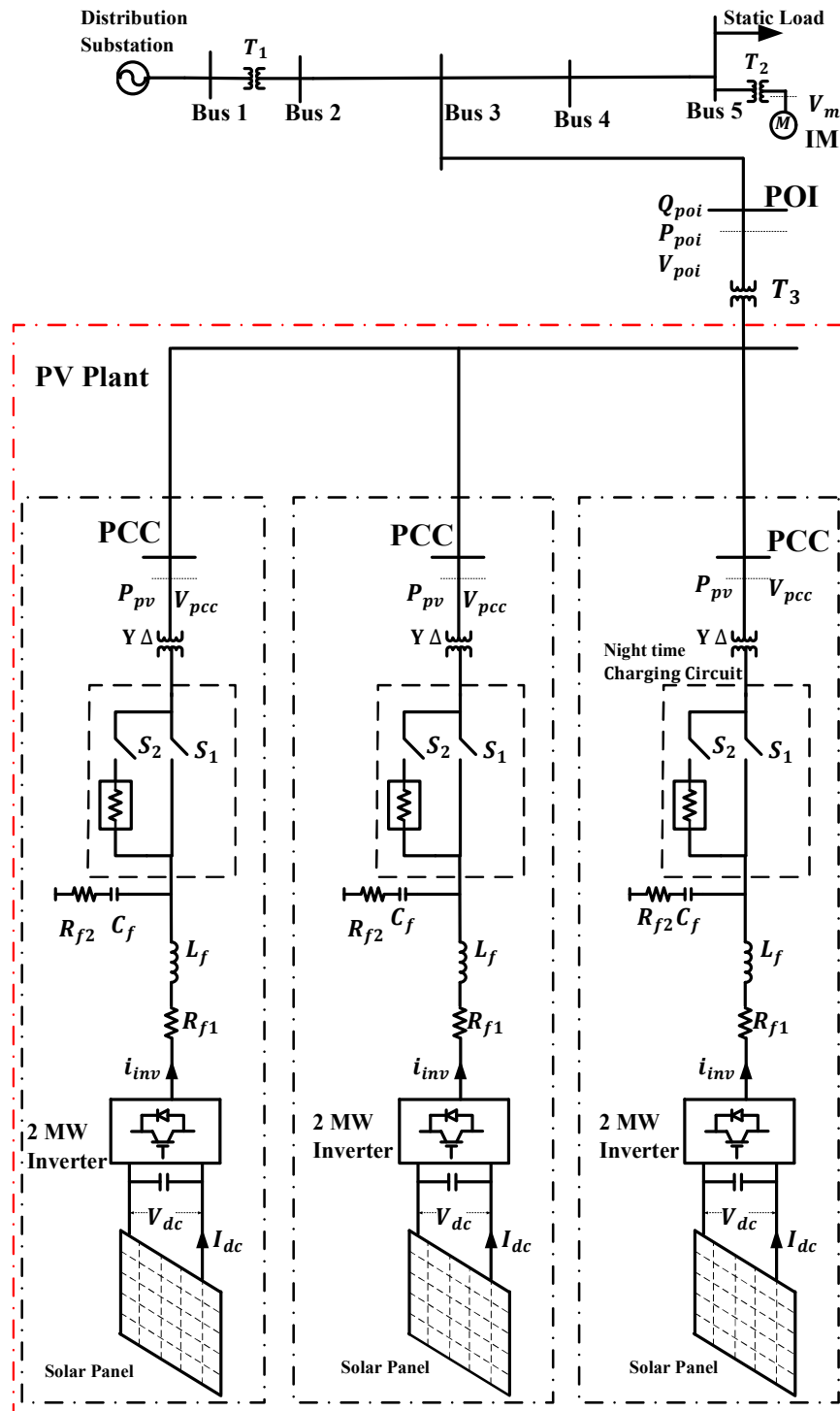
Figure 5-1. Single Line Diagram of the study system.

The single line diagram of the study system is shown in Figure 5-1. The transformer T_1 is rated 115 kV/27.6 kV, 20 MVA with 5% impedance. The distribution lines are

represented by their equivalent pi models. A total load of 5.3 MVA at 0.9 power factor is connected at feeder end. For simulation studies, 50% of loads are modelled as IM loads and other 50% as voltage dependent static loads (SL). The IM loads are rated at 4 kV [180] and are connected through a transformer T_2 rated 27.6/4 kV and 5% impedance.

A 6 MW PV solar farm is connected to the feeder at bus 3 which is 25 km away from the IM loads. Utility scale PV plants have multiple inverter units, which are connected to the substation transformer using collector cables. Hence, the 6 MW PV system is modelled as a PV plant with three 2 MW inverters. The inverter output power is fed to the substation transformer using MV collector cables. The cables are represented by their equivalent π models.

The inductor L, capacitor C and inductance of $\Delta - Y$ transformer constitutes LCL filter of the PV inverter. R_{f1} and R_{f2} represents the resistance of the inductor and capacitor respectively. To provide 24/7 PV-STATCOM operation, modifications are made in the PV inverter system. The dc link capacitor is charged from the real power output of PV solar panels during start up in daytime. But at night, the PV panel is idle, and therefore a charging circuit is added for nighttime dc link capacitor charging. This is accomplished by keeping switch S_2 on and S_1 off. Once the capacitor voltage reaches the peak of ac phase voltage, switch S_1 is turned on, and S_2 is turned off. The PV inverter thus become ready to function as a STATCOM at night.

PV solar plants have two layers of control. The outer plant level control (PLC) decides the operating set points for all the inverter units based on the commands from the system operator. These setpoints are determined based on frequency or voltage control requirement per grid codes and Standards [87, 90]. The plant level quatities are measured at the point of interconenction (POI), which is at the HV terminal of the substation transformer T_3. The voltage, active and reactive power at POI are denoted as V_{poi}, P_{poi}, and Q_{poi} respectively.

The inner inverter level control (ILC) generates the switching signals for inverter based on: i) the plant level signals, ii) local control units such as MPPT, and iii) inverter level grid supporting functions [87, 90]. The inverter level quatities are measured at the point of

common coupling (PCC), which is at the HV terminal of the $\Delta - Y$ transformer at the inverter unit. The voltage, active and reactive power at PCC are denoted as V_{pcc}, P_{pcc}, and Q_{pcc} respectively.

The voltage at the motor terminal is denoted as V_m. The motor terminal voltage is measured and communicated (through a fiber optic cable) to the PV-STATCOM controller incurring a delay in the process. This overall delay includes: i) the communication delay between motor terminal and PV-STATCOM, ii) the communication delay between plant level controller and individual inverter controllers in a PV solar farm, and iii) voltage measurement delay. The latency for fiber optic cable is $3.34\,\mu s/km$ [178] and the communication delay incurred in a PV solar farm plant control is approximately 100 ms [88]. Thus, the delay in the study system with a distance of about 25 km between the IM and the PV solar farm is 100.08 ms and is approximated as 100 ms.

5.3   PV-STATCOM Controller

Figure 5-2 (a) shows the single line diagram of the Study System in which the detailed inverter controller is depicted for only one of the three 2 MW inverters. The inverter controllers for the other two inverters are similar, and hence not shown here. Figure 5-2 (b) and (c) depict the conventional PV inverter controller and the proposed PV-STATCOM controller, respectively. Figure 5-2 (b) shows the structure of a conventional PV inverter control. It consist of dc link voltage controller, power factor controller, inner current controller and PLL, as discussed in Sec. 2.4.

The proposed PV-STATCOM controller is illustrated in Figure 5-2 (c). It consists of: i) Operation Mode selector, ii) Active Power Controller, iii) Reactive Power Controller, and iv) Night time Voltage Controller.

5.3.1   Operation Mode Selector

The PV-STATCOM controller operates in three modes: Mode 1, 2 and 3. The real/active and reactive power outputs of the PV solar farm at noon in different modes are conceptually depicted in Figure 5-3 (whereas actual outputs are described in Sec. 5.5 e.g., in Figure 5-9).

The operating modes are decided by Mode Selector by monitoring V_{pcc}, P_{pcc} and $Q_{pcc.}$ Mode 0 is the normal pre-fault/disturbance operating mode of the solar farm.
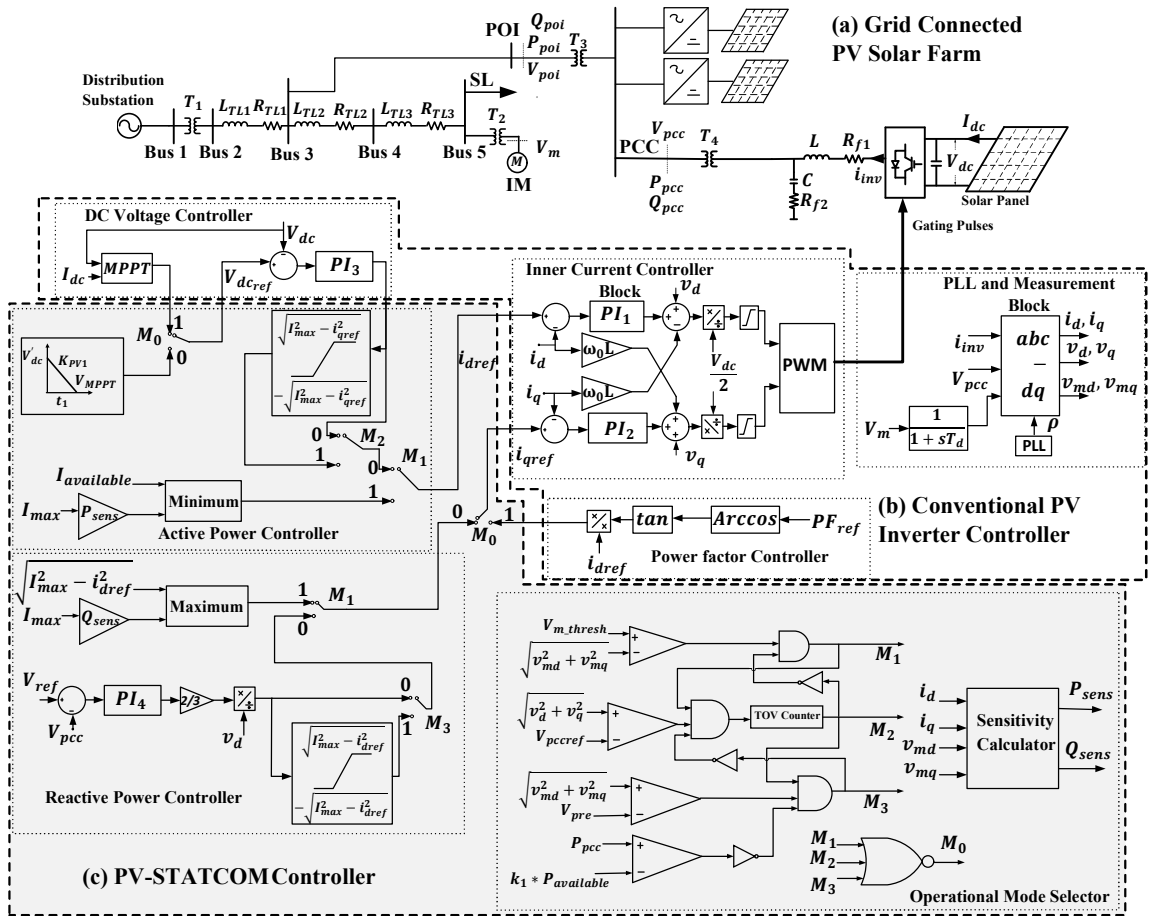
Figure 5-2. Single Line Diagram of a grid connected PV Solar Farm and the architecture of the proposed PV-STATCOM controller implemented at inverter level.
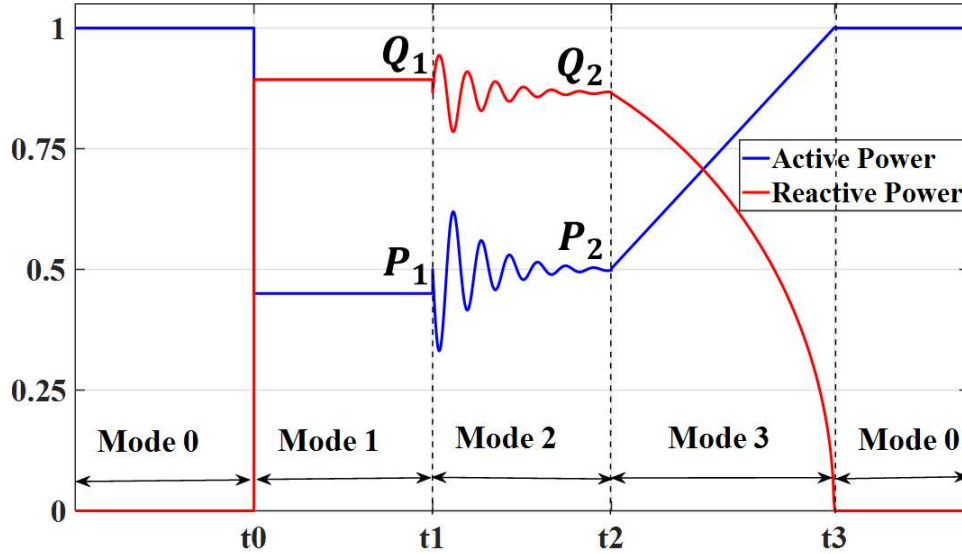
Figure 5-3. Output of PV solar farm with the proposed control.

5.3.1.1   Mode 0 (represented by flag M_0)

In this mode, during day time, the PV system generates the maximum available active power ($P_{available}$) at the power factor specified by the system operator. During night time, it regulates V_{dc} at $V_{dcrated}$ and remains on standby to respond to any system disturbance.

5.3.1.2   Mode 1 (represented by flag M_1)

This is the Variant 2 of the Full PV-STATCOM mode. In this mode, the PV plant injects active power P_1 and reactive power Q_1 based on the latest active and reactive power sensitivity at IM terminal. If $P_1 < P_{available}$, active power output is curtailed to P_1 (as shown in Figure 5-3) and reactive power is set to Q_1. However, if $P_1 > P_{available}$, active power output is set to $P_{available}$, and the remaining inverter capacity is used for reactive power injection, which may be different than Q_1.

If, due to a system fault/disturbance, V_m goes below a threshold voltage V_{m_thresh}, Mode Selector enables Mode 1 operation by setting M_1 signal high. V_{m_thresh} is the low voltage that results from a fault/disturbance which is sufficient to cause IM instability. This voltage is system dependent and determined from off-line simulation studies for the system under study. $V_{m\_thresh} = 0.8$ pu for our study system.

The PV plant operates in Mode 1 till V_{pcc} increases to just below the utility TOV limit V_{TOVL}. This enhanced voltage support helps in fast voltage recovery. Once TOV limit is reached, Mode 1 operation is disabled, and Mode 2 operation is initiated by setting M_1 signal low and M_2 signal high. A TOV counter is used to detect TOV limit violation. For instance, a voltage between 1.06 pu and 1.3 pu is permitted for a period of 166 ms [23]. The counter is activated (output is set high) when V_{pcc} crosses utility's upper steady state voltage limit V_{pccref} (=1.06 pu, here). The counter is kept activated for 150 ms (to be safely within the utility limit of 166 ms [90]).

5.3.1.3   Mode 2 (represented by flag M_2)

This is the Variant 1 of the Full PV-STATCOM mode. In this mode which gives preference to reactive power, the PV-STATCOM control provides reactive power support Q_2 with the objective of maintaining V_{pcc} at utility's upper steady state voltage limit V_{pccref} (=1.06 pu, here). If active power was curtailed to P_1 in Mode 1, it is increased to P_2 using the inverter capacity remaining after reactive power injection Q_2. It is noted that $P_2 <$ $P_{available}$. Even though V_{pcc} reaches V_{pccref}, motors still need reactive power support for their speeds to return to their pre-fault stable operating state, as in Mode 0. Mode 2 operation is therefore continued till reactive power support is no longer required for motor stabilization. This mode of operation is continued till V_m reaches at least k_1 times pre disturbance IM terminal voltage (V_{pre}). In this study $k_1 = 0.96$. Once this condition is satisfied, Mode 2 operation is disabled, and Mode 3 operation is initiated.

5.3.1.4   Mode 3 (represented by flag M_3)

This is the Partial STATCOM mode. In this mode active power is given preference. The objective is to ramp active power from P_2 to the pre-disturbance solar power level $P_{available}$ at a high rate. An important aspect of this control is that during power ramp up, voltage control is simultaneously performed to maintain V_{pcc} at V_{pccref} (=1.06 pu) using inverter capacity remaining after real power ramp up. This unique control prevents occurrence of any unwanted voltage oscillations at POI while ensuring a fast ramp up. Mode 3 operation is continued till P_{pcc} reaches at least k_1 times $P_{available}$. In this study $k_1 = 0.96$.

5.3.2   Sensitivity Calculator

This block calculates the real and reactive power sensitivities (P$_{sens}$, and Q$_{sens}$) of IM terminal voltage (V_m) by monitoring the change in V_m on injection of small amount of real and reactive currents. These sensitivities depend upon the effective R/X ratio. The X and R change due to system conditions e.g. switching of lines/transformers, turning on/off of distributed generators, etc. To accommodate these system changes, P$_{sens}$ and Q$_{sens}$ are updated periodically, say every 15 minutes, based on system operation. There is a delay incurred in the measurement and communication of V_m to the PV plant controller, which is considered as 100 msec in study [88]. This delay is considered while computing R and X according to (1) and (2) respectively, for accurate calculation of P$_{sens}$ and Q$_{sens}$.

The effective reactance X' is calculated by injecting 10% of i_q and noting the change in terminal voltage V_m of the remotely located induction motor, according to (5-1).

$$X' = \frac{\Delta V_m}{\Delta i_q}$$

(5-1)

The effective resistance R' is calculated by varying i_d by 10% and noting the change in V_m as given in (5-2).

$$R' = \frac{\Delta V_m}{\Delta i_d}$$

(5-2)

Normalized P_{sens} and Q_{sens} are calculated using (5-3) and (5-4) respectively from updated X' and R'.

$$P_{sens} = \frac{R'}{\sqrt{R'^2 + X'^2}}$$

(5-3)

$$Q_{sens} = \frac{X'}{\sqrt{R'^2 + X'^2}}$$

(5-4)

5.3.3 Active Power Controller

This block controls the active power output of the PV plant for the PV-STATCOM control according to the various modes of operation. This block controls the active power by generating the DC voltage reference (V_{dcref}) and *d axis* current reference (i_{dref}) for the conventional DC link controller and inner current controller of the inverter respectively.

5.3.4 Reactive Power Controller

This block generates the *q axis* current reference for the various modes of operation of PV-STATCOM controller. It consists of PCC voltage controller and a *q axis* current reference generator.

5.3.5 Calculation of Current and Voltage References.

The active power controller and reactive power controller blocks computes the references for the various modes of operation as described below.

5.3.5.1 Reference Calculation for Mode 1

In this mode, PV solar farm injects active power P_1 and reactive power Q_1 as per the latest P_{sens} and Q_{sens}. If calculated $P_1 > P_{available}$, the active power controller block sets i_{dref} to $I_{available}$ ($= P_{available} /(1.5 v_d)$). The remaining inverter capacity is utilized to inject reactive power and i_{qref} is set by reactive power controller block to $\sqrt{(I^2_{max} - i^2_{dref})}$, where I_{max} is the rated inverter current. However, if $P_1 < P_{available}$, active power is curtailed to P_1. Correspondingly i_{dref} is set to $I_{max} * P_{sens}$, and i_{qref} is set to $I_{max} * Q_{sens}$.

$$i_{dref} = \text{minimum}(\, I_{available}, \quad I_{max} * P_{sens}\,) \qquad (5\text{-}5)$$

$$i_{qref} = \text{minimum}\left(\sqrt{I^2_{max} - i^2_{dref}}, I_{max} * Q_{sens}\right) \qquad (5\text{-}6)$$

5.3.5.2   Reference Calculation for Mode 2

In this mode, i_{qref} is generated by PCC voltage controller to regulate V_{pcc} to V_{pccref}. If active power was curtailed during Mode 1 operation to P_1, the inverter will increase active power to P_2 (as described in Mode 2 operation) by using the remaining inverter capacity. The active power is ramped by varying the DC link voltage reference from the DC voltage at the initiation of Mode 2 (V'_{dc}) to the MPPT voltage of the PV panel (V_{MPPT}) by the DC link ramp generator in active power controller. The priority is assigned to reactive power, by limiting *d axis* current reference generated by DC link voltage controller according to (5-7).

$$i_{dref\_limiter} = \pm \sqrt{I_{max}^2 - i_{qref}^2} \qquad (\text{5-7})$$

5.3.5.3   Reference Calculation for Mode 2

Active power is ramped up from P_2 to $P_{available}$ by the DC link ramp generator in active power controller. The remaining inverter capacity is simultaneously used for regulating V_{pcc} at V_{pccref}. The i_{qref} generated by PCC voltage controller is limited by the saturation block using (5-8), to ensure that the maximum current rating of inverter is not violated.

$$i_{qlimit} = \pm \sqrt{i_{max}^2 - i_{dref}^2} \qquad (\text{5-8})$$

5.4   Implementation of the proposed control strategy on a realistic solar PV plant

The proposed control strategy can be either implemented at Plant Level controller (PLC) or Inverter level controller (ILC) of the PV plant. The implementation strategy for both controllers are discussed in this section.

5.4.1   Plant Level Controller (PLC)

If the proposed control is implemented at PLC, the controller monitors motor terminal voltage (V_m), and voltage (V_{poi}), active (P_{poi}), and reactive power (Q_{poi}), at plant substation to decide the modes of operation. In Mode 1, the PLC gives reactive and real

current reference to the inverter controllers based on the P_{sens} and Q_{sens} measured at POI. In Mode 2, and Mode 3, the PLC voltage controller generates the reactive power set points to the individual inverters for the POI voltage (V_{poi}) control and communicate them to all inverter controller units. As the control is done at plant level, the PLC level voltage controller causes a large closed loop delay [87, 89]. This delay is considered as 500 ms in this study [87].

5.4.2   Inverter Level Controller (ILC)

If the proposed control is implemented at ILC, the controller monitors motor terminal voltage (V_m), and voltage (V_{pcc}), active (P_{pcc}), and reactive power (Q_{pcc}), at inverter terminal (measured at HV side of the inverter transformer) to decide the modes of operation. As the PV plant has dedicated communication channels between PLC and ILC, the V_m received by the PLC can be send to ILC using the same communication channel if the control is implemented in ILC.

In Mode 1, the ILC calculates reactive and real current reference to the inverter controllers based on the P_{sens} and Q_{sens} measured at POI, which is provided by the PLC periodically (every 15 minutes in this study). In Mode 2, and Mode 3, all the inverter controllers do the control of its PCC voltage independently.

5.5   Simulation Studies

The simulation studies of the proposed PV-STATCOM controller are done on MATLAB Simulink. The effectiveness of the proposed control strategy is tested for stabilizing critical IM, and it is further compared with other smart inverter control strategies. The performance is tested in systems with various X/R ratios. The comparison studies are done at PLC and ILC to find the best method for its implementation.

5.5.1   Performance of the proposed PV-STATCOM control

The effectiveness of the proposed PV-STATCOM controller for stabilizing a remotely located critical IM for a 100 ms LLL-G fault at Bus 4 of the study system (10 km from the IM terminal) is shown in Figure 5-4.

Figure 5-4 (a) – (e) depicts IM terminal RMS voltage, POI RMS voltage, the active power output of PV solar farm, the reactive power output of PV solar farm, and motor speed respectively.
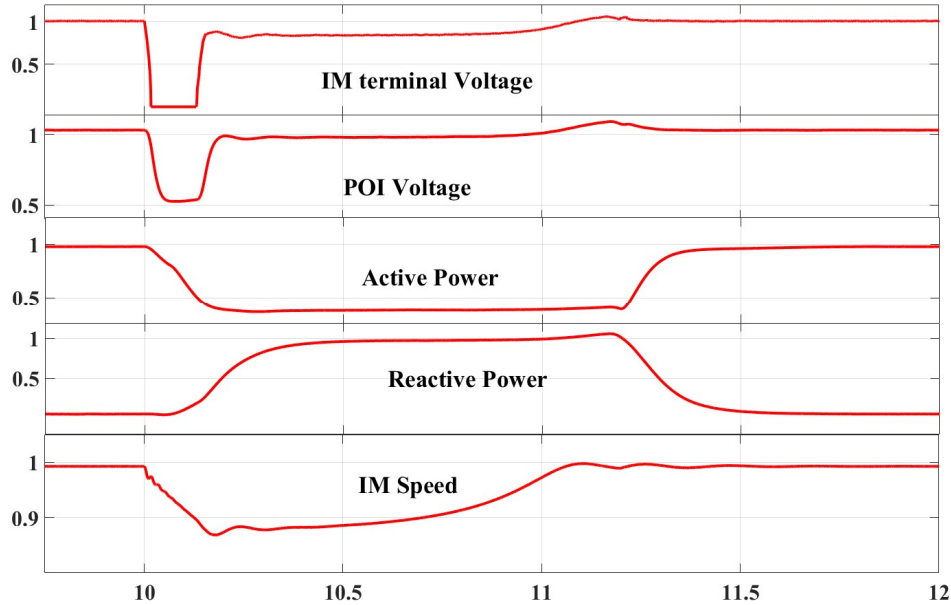
Figure 5-4. Response of the PV-STATCOM and IM.

t < 10 s. The PV plant is operating in Mode 0 by generating 1 pu active power at unity power factor. The PCC voltage is 1.03 pu and motor terminal voltage is 1 pu. The motor is operating at steady state by generating 0.75 pu electromagnetic torque at a slip of 0.03 pu.

t = 10 s. A large disturbance is created at the motor terminal. Due to the large disturbance, V_{poi} and V_m drops to 0.52 pu and 0.02 pu respectively, The PV active power reduces due to the drop-in voltage. The motor speed drops and the torque become oscillatory.

t = 10.12 s. Due to the communication delay, the PV solar farm does not respond for the drop in V_m till 10.12 s. The sensitivity calculator calculates the P_{sens} and Q_{sens} in steady state as discussed in Sec. 5.3.2. The i'_{dref} based on latest P_{sens} is 0.375, which is lower than the $I_{available}$, and thus i_{dref} is set at 0.375 pu. The i_{qref} is set at 0.92 pu, which is corresponding to the Q_{sens}. The PV solar farm injects 0.89 pu reactive power and 0.36 pu active power to the grid at PCC. The measured power at PCC is lower than the reference,

because the PCC voltage is only 0.9 pu. Due to the P and Q injection, the motor speed starts to accelerate back to steady state value and it generate 0.75 pu electromagnetic torque.

t = 11.12 s. The PV plant continues Mode 1 operation till the TOV limit specified by [90] is violated. Due to this novel feature of extended voltage support, the IMs start recovering. The PV-STATCOM controller switches to Mode 2 operation at 11.12 s.

The V_{PCC} is regulated at 1.06 pu in this mode. The reactive power output of the PV plant is controlled to keep V_{poi} at 1.06 pu. The active power is ramped to the maximum available capacity using the remaining inverter capacity.

t = 11.2 s: The IM terminal voltage recovers to pre fault voltage at 11.2 s. Thus, the controller starts Mode 3 operation to ramp up the active power to the maximum available capacity at a ramp rate of 100 pu/sec. POI voltage is regulated at 1.06 pu to prevent voltage transients due to fast ramp up of active power.

t = 11.28 s: The PV power reaches maximum available capacity of 1 pu at 11.28 s. The controller initiates the Mode 4 operation by generating maximum available solar power.

This study shows that the proposed PV-STATCOM control can ensure fast recovery of remotely located IM. The proposed control can provide this critical service with minimal curtailment of active power.

5.5.2   Need for Measurement of IM terminal voltage

To investigate the requirement of IM terminal voltage as the triggering signal for the proposed control strategy, the distance between PV and IM is increased to 40 km and LLL-G fault is applied for 100 ms at 5 km from the IM (35 km from PV plant). The result of this study is shown in Figure 5-5.

Figure 5-5 (a) – (e) depicts IM terminal RMS voltage, POI RMS voltage, the active power output of PV solar farm, the reactive power output of PV solar farm, and motor speed respectively.

Due to the fault, the IM terminal voltage drops to 0.01 pu voltage. Due to the severe drop of voltage, the IM torque becomes oscillatory and speed reduces.
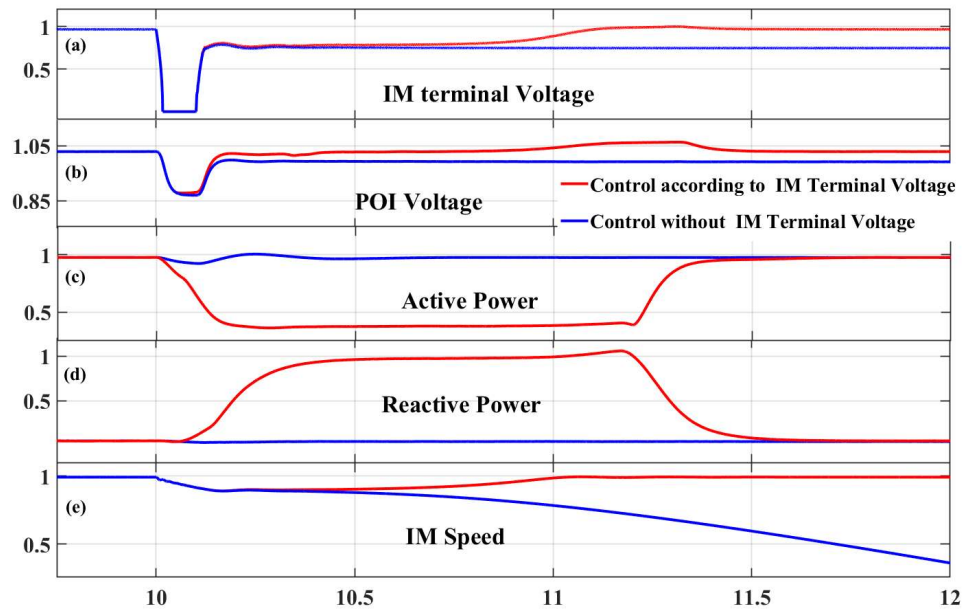
Figure 5-5. Response of the PV Plant with and without the measurement of IM terminal voltage.

5.5.2.1   Without monitoring IM terminal voltage

The PV plant voltage drops to 0.87 pu due to the fault, and it recovers to 0.99 pu after the clearance of fault. As the PV plant is experiencing low voltage of 0.87 pu for a duration of 100 ms only, the PV plant rides through the fault by maintaining the steady state operation. But the IM experience a severe voltage drop across its terminal and thus the IM become unstable as shown in Figure 5-5 (e).

5.5.2.2   Control based on monitoring IM terminal voltage

As the drop in IM terminal voltage is severe, the controller initiates PV-STATCOM operation, as soon as it detects the voltage drop. Due to the fast support according to the proposed control strategy, the IM recovers and continues its stable operation.

The following conclusions can be inferred from this study, (i) if the PV plant is located far from the IM and a fault happen near to IM terminal, the severity of that fault will not

be visible in the PV terminal voltage, and a control strategy based on PV terminal voltage fails to ensure stable operation of IM, (ii) even in the case of very remotely located IM (40 km in this study), the proposed control strategy can ensure stable operation of the critical IM for a severe fault at IM terminal.

5.5.3   Comparison with other smart inverter control strategies

According to the German BDEW code, during a voltage disturbance, the PV plant is required to inject 2% reactive current per 1% voltage drop for a voltage drop below 0.9 pu [91]. A voltage support strategy based on injecting real and reactive power in 1: 1 ratio is proposed in [101]. The proposed control strategy is compared with the above two methods. An LLL-G fault is applied for 100 ms at 10 km from the IM terminal. The PV is located at 25 km from the IM terminal. The result of this study is shown in Figure 5-6.

Figure 5-6 (a) – (e) depicts IM terminal RMS voltage, POI RMS voltage, the active power output of PV solar farm, the reactive power output of PV solar farm, and motor speed respectively.
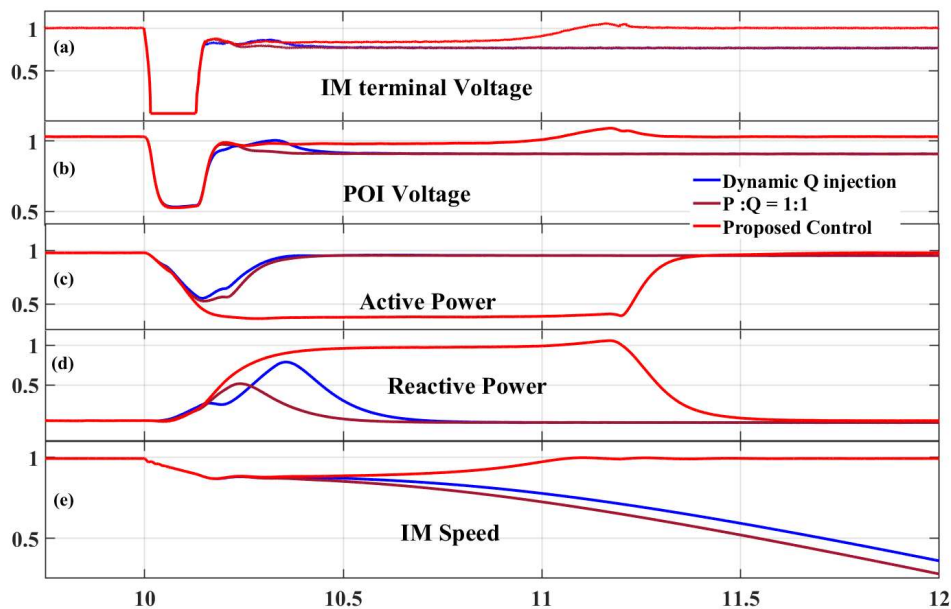
Figure 5-6. Comparison of proposed method with other smart inverter control strategies.

Due to the fault, the motor terminal voltage drops to 0.01 pu and the PV terminal voltage drops to 0.52 pu.

5.5.3.1　Case 1: Voltage support according to BDEW [91]

Due to the drop in PV terminal voltage, the PV inverters inject 0.76 pu reactive current, and inject active power using the remaining capacity. The PV plant continues this support till the PV terminal voltage recovers to 0.9 pu. Once the voltage stays above 0.9 pu for two cycles, the PV inverters curtails reactive support and resume UPF operation by increasing the active power to the maximum available capacity. The IM terminal voltage recovers to 0.82 pu only, when the PV curtails the reactive power support. Due to the low voltage, the IM speed drops and finally it stalls.

5.5.3.2　Case 2: Voltage support according to P and Q in 1:1 ratio [101]

Due to the drop in PV terminal voltage, the PV plant starts injecting 0.707 pu real and reactive power. Due to the dynamic support from the PV plant, the PV voltage starts rising. As the fault is cleared, the PV terminal voltage increases, and once the PV voltage reaches 1 pu, the PV stops the voltage support and resumes its normal operation by ramping the active power to the maximum available capacity. Similar to BDEW, the IM terminal voltage is not recovered when the PV curtails its support, and eventually the motor stalls.

5.5.3.3　Case 3: Voltage Support according to Proposed Control

The PV initiates the voltage control strategy as explained in section 5.5.1. The performance of the PV plant and IM are discussed in detail for this control strategy in Sec. 5.5.1. The voltage control according to proposed control strategy is able to ensure stable operation of the IM as shown in Figure 5-6.

The studies are extended to find the capacity of STATCOM needed at IM terminal for stable operation of the motor, when the PV is operating according to control strategies discussed in Case 1 and Case 2, and the results are shown in Table 5.1.

The voltage control strategy according to BDEW requires 3.2 Mvar STATCOM to be connected at IM terminal to ensure a recovery of IM similar to the proposed control strategy. The control according to 1:1 injection of P and Q requires 2.5 Mvar STATCOM to be connected at IM terminal to provide the same performance.

Table 5.1. Comparison of different smart inverter control strategies.

Sl. No	Control Strategy	Rating of STATCOM required at IM terminal
1	BDEW	3.2 Mvar
2	P and Q in 1:1 ratio	2.5 Mvar
3	Proposed Control	Not required

This study shows that, the proposed control strategy can ensure the stable operation of IM even in the cases, where existing smart inverter control strategies failed. To ensure the same performance as the proposed control strategy, the voltage control according to BDEW, and P and Q in 1:1 ratio has to install 3.2 Mvar and 2.5 Mvar statcom at IM terminal, which are expensive devices. Thus, the proposed control strategy has the added advantage of helping the industries to eliminate the installation of expensive FACTS devices for critical IM support.

5.5.4 Performance of the proposed controller in systems with various X/R ratios.

The effectiveness of the proposed controller to ensure stable operation of critical IM is tested in systems with various X/R ratios and results are shown in Figure 5-7. The studies are done in system with X/R =1, 2 and 3, to cover the typical X/R ratios of MV network.

Figure 5-7 (a) – (e) depicts IM terminal RMS voltage, POI RMS voltage, the active power output of PV solar farm, the reactive power output of PV solar farm, and motor speed respectively.

The studies are done to test the capability of the proposed controller to effectively estimate the real and reactive power sensitivity of IM terminal voltage and how the control can ensure the recovery of IM in various systems.
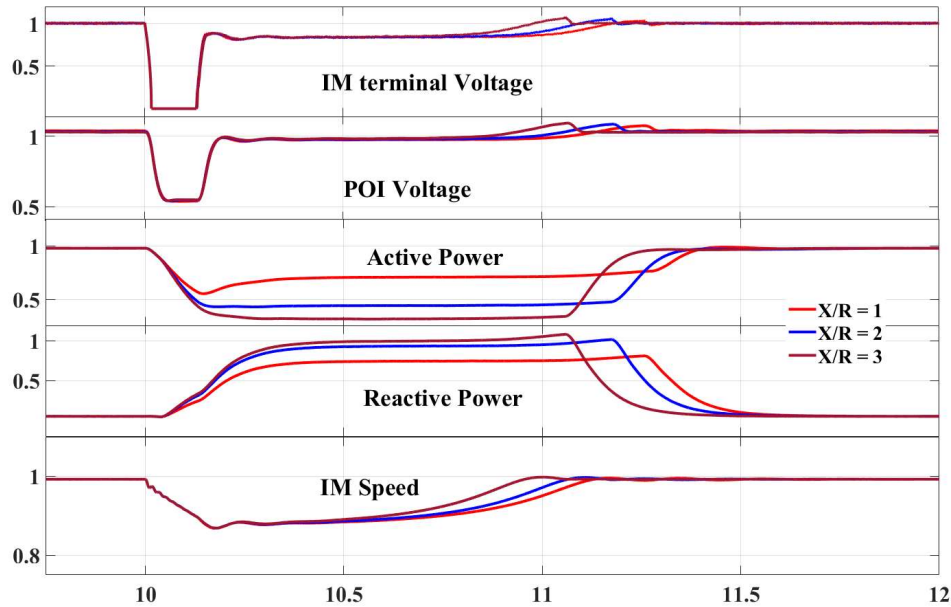
Figure 5-7. Performance of the proposed controller in systems with various X/R ratios.

It can be observed that the controller is able to estimate the P_{sens} and Q_{sens} in various systems and inject real and reactive power according to the P_{sens} and Q_{sens}. In system with X/R =1, the controller injects P = 0.707 pu and Q = 0.707 pu. The P and Q are 0.447 pu and 0.89 pu for X/R =2. In system with X/R =3, it injects 0.316 pu active power and 0.94 pu reactive power. The proposed controller is able to ensure stable operation in all the cases considered as seen in Figure 5-7.

The tests confirm that the proposed controller is able to intelligently choose the real and reactive power reference according to the system X/R ratio to ensure the stable operation of the critical IM.

5.5.5   Comparison of Plant Level and Inverter Level Control

The proposed controller can be implemented at Plant level (PLC) or Inverter level (ILC) of a PV plant. Detailed simulation studies are done by implementing the control strategy in both plant level and inverter level, to find the best location for implementation. The response of the IM and PV plant level parameters are shown in Figure 5-8, and inverter level parameters are depicted in Figure 5-9 for both plant level and inverter level control.

Figure 5-8 (a) – (e) depicts IM terminal RMS voltage, POI RMS voltage, the active power output of PV solar farm, the reactive power output of PV solar farm, and motor speed, respectively. Figure 5-9 (a) – (f) illustrates PCC voltage, and real and reactive power output of inverter 1, PCC voltage, and real and reactive power output of inverter 2, PCC voltage, and real and reactive power output of inverter 3, respectively.
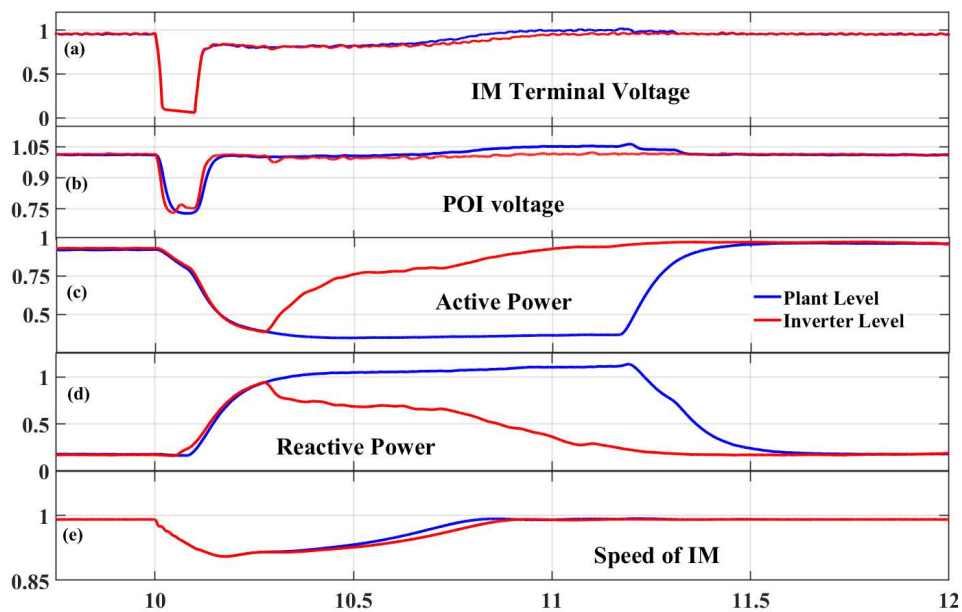
Figure 5-8. IM and Plant Parameters for Plant Level and Inverter Level Control.

The PLC control can ensure a marginally faster recovery of IM terminal voltage and speed compared to ILC. The POI voltage is controlled in PLC, whereas PCC voltage is controlled in ILC. Thus, the losses in collector system, substation transformer etc., are compensated in PLC, and causes faster recovery compared to ILC.

In PLC, PV plant continues Mode 1 operation till the POI voltage reaches TOV limit, whereas in ILC, the Mode 1 operation is continued till PCC voltage violates the TOV limit. Due to the impedance of collector system and transformer, the POI voltage recovers slower compared to PCC voltage of Inverter. Thus, if the controller is implemented in PLC, the Mode 1 operation is continued till 11.2 s, but in ILC the Mode 1 operation is done till 10.21 s. Thus, in PLC control, longer duration of Mode 1 operation is required compared to ILC. This leads to higher curtailment of active power in PLC compared to ILC.
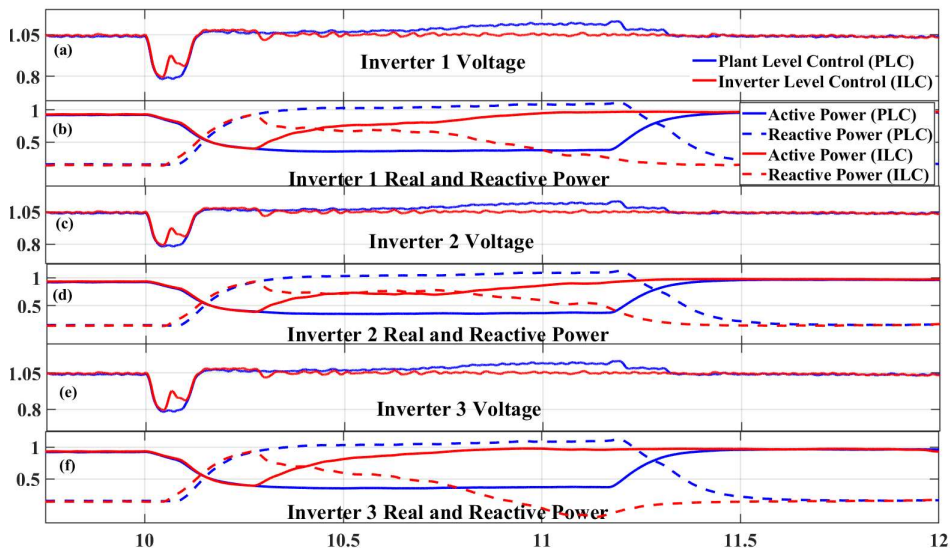
Figure 5-9. Inverter Parameters for Plant Level and Inverter Level Control.

In PLC, the inverter terminal voltage violates the TOV limit and experience overvoltage for a longer duration. This can lead to tripping of inverter level voltage protection. The amount and duration of overvoltage experienced by each inverter depends upon the length of collector cable for corresponding inverter and its transformer impedance. As these quantities varies for each inverter, it is difficult to estimate the duration and depth of overvoltage for each inverter without detailed simulation studies. In ILC, as the voltage control is done at PCC of each inverter, none of the inverters will violate the TOV limit.

This study shows that the control done at PLC can ensure faster recovery compared to ILC, but it comes at a cost of over voltage at inverter terminals and curtailment of higher

active power. Whereas, if the control is done at ILC, it can ensure stable operation of IM with less amount of active power curtailment and without overvoltage issues.

5.6 Small Signal Studies

The detailed time domain simulation study showed that it is more beneficial to implement the proposed control strategy at inverter level. In a utility scale PV plant, there are multiple inverters in vicinity and independent control of these inverters can cause unnecessary interactions and could cause unstable operation. To perform the stability analysis of the control at inverter level, small signal model of the study system is developed and eigen value analysis is done for the variation of PV plant and system parameters. The parameters are varied between the typical range of them in a medium sized utility scale PV plants connected to a distribution network. In the proposed control strategy, the inverters operate in different modes of operation as discussed before, and thus the interactions could be different in each mode. In Mode 1 and Mode 4, operation the PV inverters inject active power and control the reactive power either at power factor specified by user (Mode 0), or according to real and reactive power sensitivity (Mode 1). In Mode 2 and Mode 3, the inverter does PCC voltage control and inject active power.

To study the possible interactions in all Modes, eigen studies are done for two cases,

1. *Case 1:* inverter injecting active power and providing reactive power according to the reactive power sensitivity. It represents Mode 0 and Mode 1 operation of the proposed PV-STATCOM control. The developed model for Case 1 has 75 states.

2. *Case 2:* inverter injecting active power and controlling PCC voltage. It represents the Mode 2 and Mode 3 operation. The developed model for Case 2 has 78 states.

The small signal model is developed in MATLAB, and it is verified by comparing its step response with the response of the detailed switching model in PSCAD. The step response of PCC voltage controller of inverter 1 and DC link voltage controller of inverter 3 for an underdamped response and oscillatory response, are shown in Figure 5-10 and Figure 5-11, respectively.
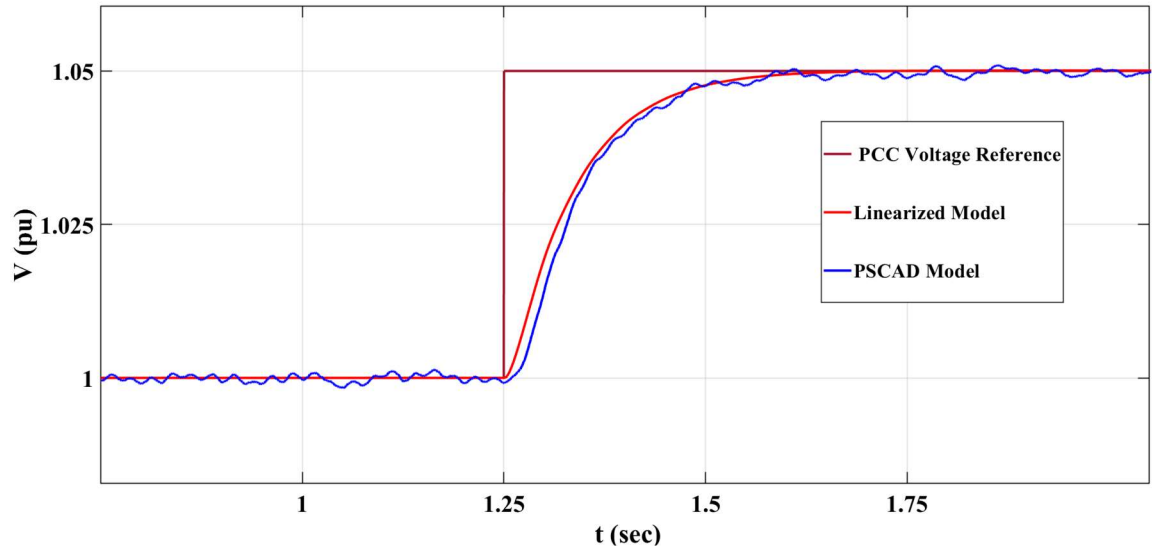
Figure 5-10. Step Response of Linearized and Detailed Model for a step change of Reference for PCC Voltage Controller of Inverter 1.
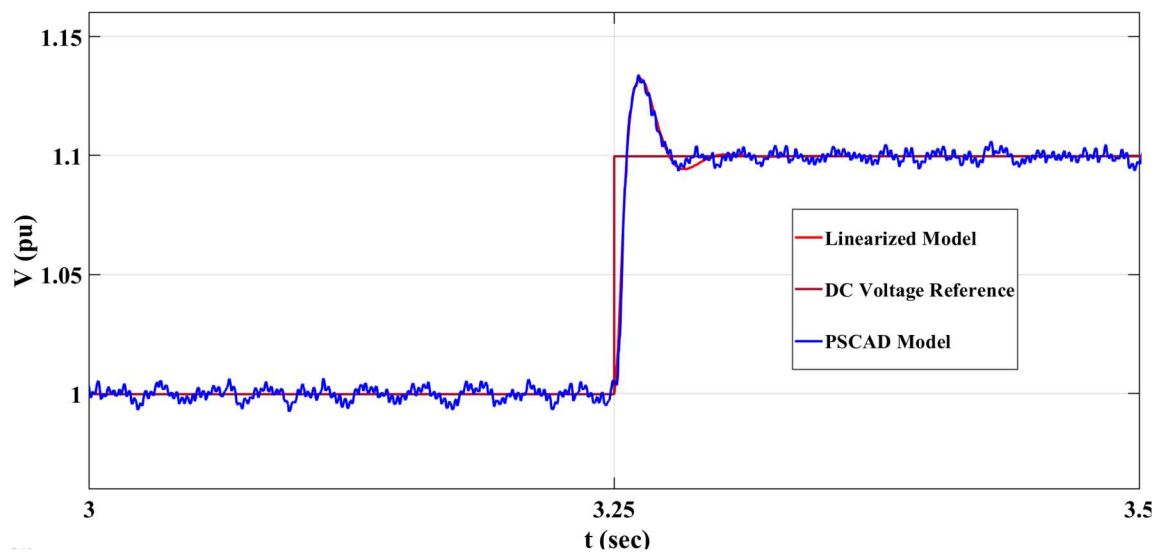
Figure 5-11. Step Response of Linearized and Detailed Model for a step change of Reference for DC Voltage Controller of Inverter 3.

5.6.1 Impact of PV plant parameters

The sensitivity of the controller for the variation of the PV plant parameters is analyzed in this section. The plant parameters considered are distance between inverters, and the

active power output of the inverters. The bandwidth of DC link voltage controller and PCC voltage controller are 50 Hz for both studies. The SCR and X/R are 3 each.

5.6.1.1 Effect of distance between Inverters

To study the sensitivity of the PV system for the variation of the distance between the inverters, the length of the collector cables connecting inverters to the substation transformer are varied. The length is varied between 100 meters to 1 km, to cover the possible distances between the inverters in a realistic medium sized utility scale PV plant. Various combination of distances is selected in such a way that it covers the different possible cases. The dominant eigen values for Case 1 and Case 2 for the variation of the distance between inverters are shown in Figure 5-12 and Figure 5-13 respectively.
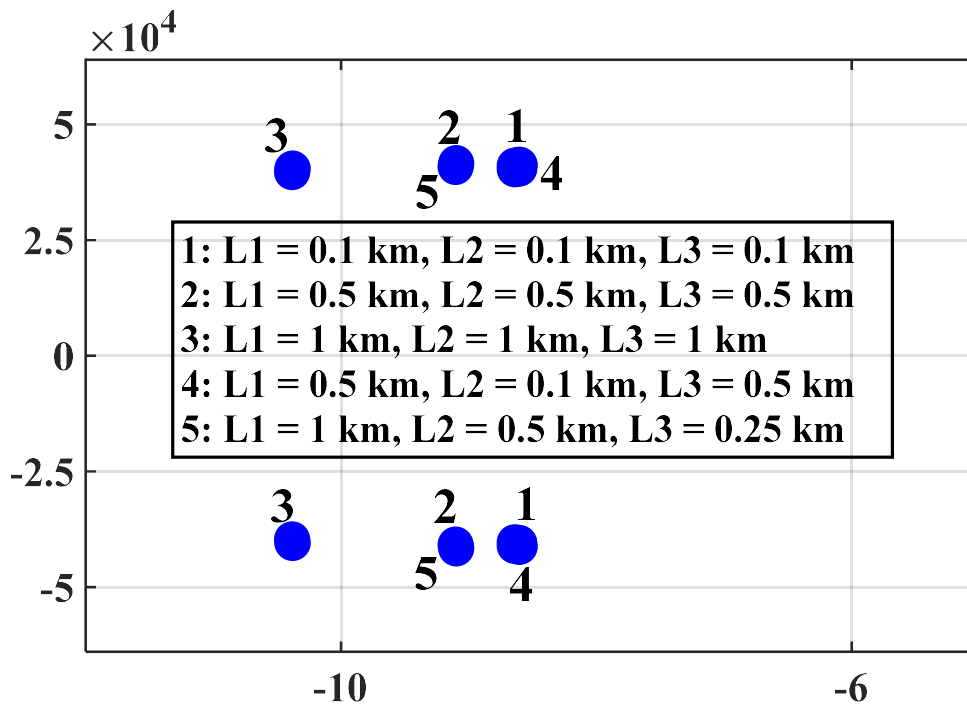
Figure 5-12. Eigen Values for the variation of distance between Inverters for Case 1.
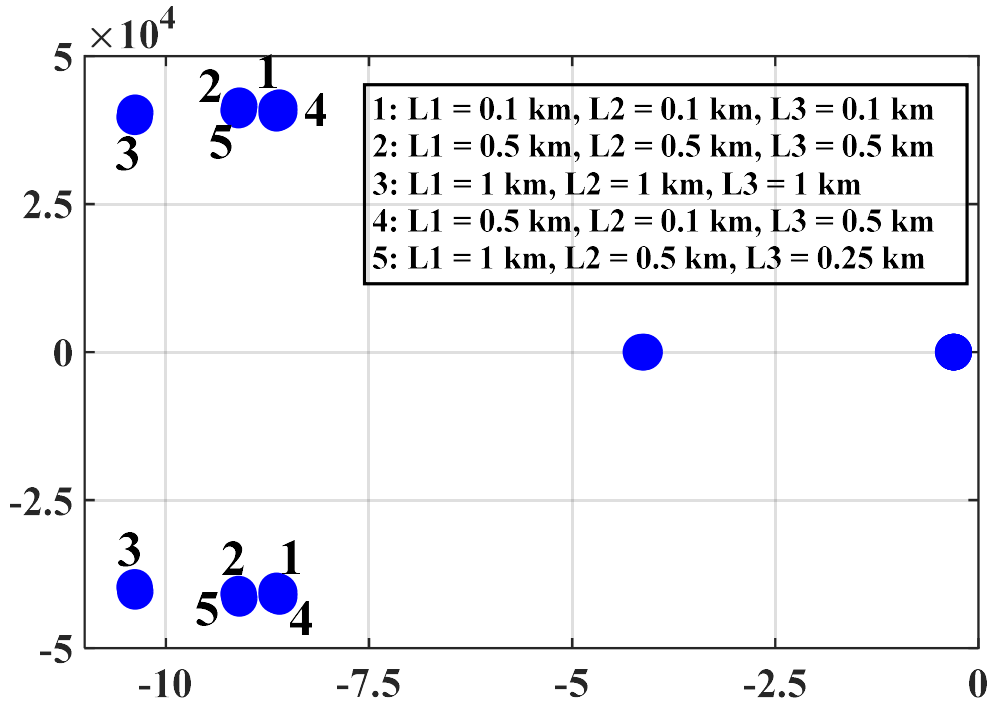
Figure 5-13. Eigen Values for the variation of distance between Inverters for Case 2.

Loci of one pair of pole varies with the change in distance between inverters for both cases, and this mode has highest damping when the distance between inverters are high. The participation factor analysis showed that, this mode is influenced by the states corresponding to inverter transformer currents, collector cable currents and voltage at collector cable terminals.

5.6.1.2   Effect of PV solar power

The sensitivity of the eigen values for the variation of PV power is studied and the locus of the dominant eigen values for Case 1 for the variation of PV power is depicted in Figure 5-14 (a). The behaviour is identical for Case 2, and thus not shown here.

The different operating scenarios considered are, all the inverters at maximum solar irradiance, night time operation (no active power), all the inverters operating in partial output (P = 0.5 pu), and two cases corresponding to partial clouding effect. To represent clouding effect, following conditions are considered, one inverter is producing lower power compared to other two inverters due to partial clouding, and all the three inverters operating at different power outputs.
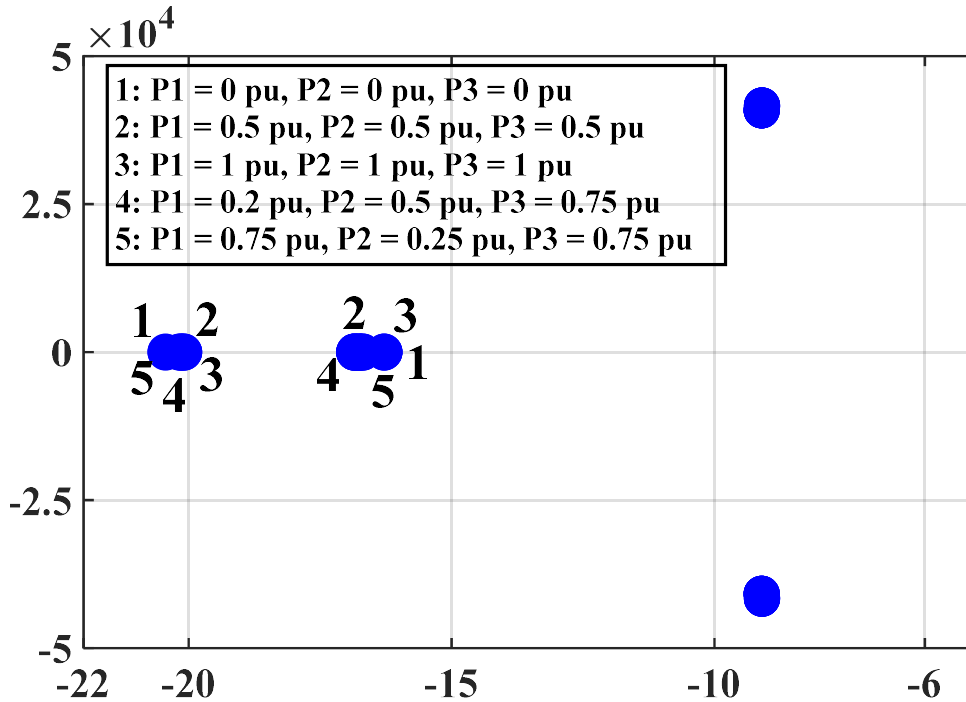
Figure 5-14. Eigen Values for the variation of PV solar power for Case 1.

The operation of the different modes of the proposed controller is not significantly affected by the variation of the PV power, and thus the proposed controller can ensure stable operation irrespective of the active power output of each inverter.

5.6.2   Impact of System Parameters

The impact of system parameters on the performance of a PV plant equipped with the proposed controller is investigated in this section. The studies are done for the variation of system strength and X/R ratio of the distribution feeder. The bandwidth of DC link voltage controller and PCC voltage controller are 50 Hz for both studies. All inverters are generating 0.8 pu active power each, and the collector cables 300 m long.

5.6.2.1   Effect of System Strength

The short circuit ratio (SCR) is varied at the POI of the PV plant to study the impact of system strength on the performance of the controller. The SCR is varied between 2 (weak system) to 12 (strong system) to study the impact. The locus of the eigen values for the

Case 1 and Case 2 for the variation of SCR is shown in   Figure 5-15 and Figure 5-16 respectively.
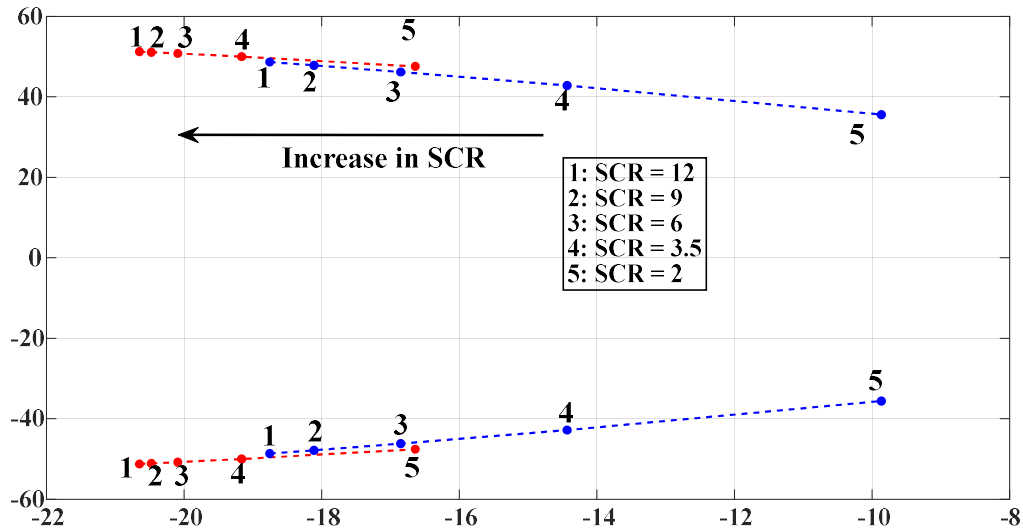
Figure 5-15. Eigen Values for the variation of system strength for Case 1.
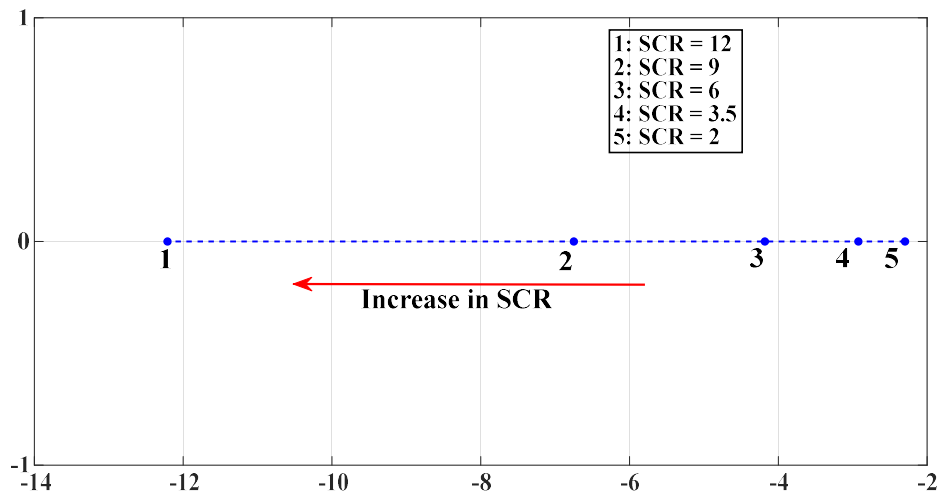
Figure 5-16. Eigen Values for the variation of system strength for Case 2.

In Case 1, a pair of eigen values moves towards right with the reduction in system strength. This pair of eigen value has higher damping in stronger system and its damping reduce with reduction in the system strength. The third sensitive pole also shows the same trend and moves right with the reduction in system strength.

For Case 2, the behavior is identical to Case 1, and a pole moves right with the reduction in system strength.

5.6.2.2   Effect of System X/R

The X/R ratios of the distribution lines are varied between one to three to study the sensitivity of the PV system with the proposed controller on system X/R ratio. The locus of the dominant roots for Case 1 and Case 2 for the variation of system X/R ratio is depicted in Figure 5-17 and Figure 5-18 respectively.
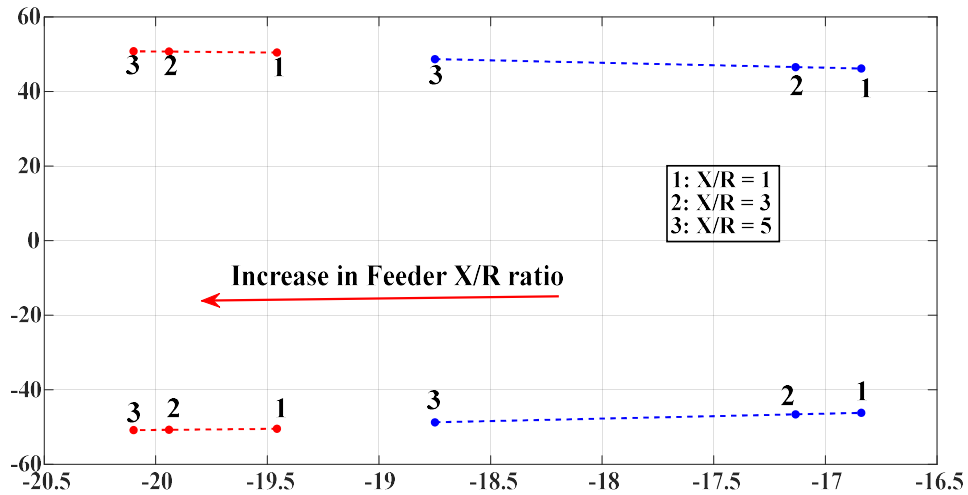
Figure 5-17. Eigen Values for the variation of X/R ratios of distribution lines for Case 1.
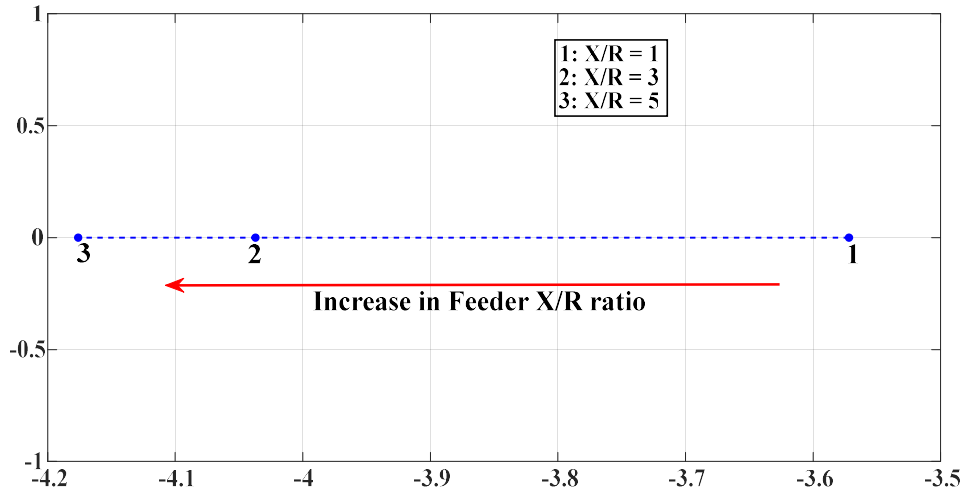
Figure 5-18.Eigen Values for the variation of X/R ratios of distribution lines for Case 2.

The dominant poles showed same behaviour with the variation of X/R ratio in both cases. The variation in feeder X/R has slight impact on the poles and the dominant poles moves towards right, with the reduction in X/R ratios.

5.7   Conclusion

A comprehensive control strategy for the PV-STATCOM control of a PV solar farm for providing support to a critical induction motor connected to a remote location at the same bus is presented in this chapter. The proposed control strategy measures the sensitivity of IM terminal voltage to the active and reactive power output of the PV solar farm in regular intervals. During a disturbance, it provides real and reactive power according to the measured sensitivity of IM terminal voltage to the active and reactive power output of the PV solar farm. Even during low active power generation, the controller modulates the active and reactive power within the available capacity to ensure fast recovery of IM.

Extensive simulation studies of the proposed controller, considering a realistic model of PV solar farm with the various delays incurred, are done in MATLAB Simulink. The simulation studies show that the proposed controller can ensure,

(i)   Stable operation of the critical IM, even for systems with various $\frac{X}{R}$ ratios.

(ii) fast recovery of the IM in cases, where other smart inverter strategies failed.

Simulation studies using a realistic model of a medium sized PV plant showed that, the implementation of proposed controller in inverter level can stabilize IM with minimal active power curtailment and no overvoltage issue at inverter terminal, whereas implementation at plant level control can cause overvoltage at inverter terminal and requires higher active power curtailment.

Small Signal studies of a medium sized utility scale PV plant connected to distribution system, with PV-STATCOM control done at inverter level showed that,

(i)   the typical distance between inverters (usually 100 m – 1km) in a medium sized PV plant has small effect on the stability of the proposed controller.

(ii) the PV power level has no effect on the stability of the proposed controller.

(iii) the X/R ratio of feeder has small effect on the stability of the proposed controller.

(iv) the controller is more stable in a stronger system.

Chapter 6

6   Mitigation of Fault Induced Delayed Voltage Recovery (FIDVR) by PV-STATCOM

6.1   Introduction

This chapter presents a novel day-and- night control of large PV solar farm as PV-STATCOM for FIDVR alleviation. The proposed control involves dynamic modulation of both reactive and real power during day, and of reactive power during night. The active and reactive power output of solar farm are based on the sensitivity of solar plant voltage to active and reactive power injections. Enhanced voltage control up to utility Transient Overvoltage Limit is utilized. Eigenvalue analysis is done to study the sensitivity of proposed controller performance to various power system and PV plant parameters. Extensive PSCAD simulation studies of FIDVR are performed in a realistic power transmission system with large-scale PV plant and comprehensive IM loads. It is shown that the proposed PV-STATCOM control: (i) mitigates FIDVR even if solar farm is located more than 100 km from motor loads, (ii) is more effective than reactive power support required by German Grid Code, (iii) is equally effective as a STATCOM connected locally at motor loads, and iv) stabilizes motors at night which is beyond Grid Code requirements.

6.2   Study System

The single line diagram of the study system is shown in Figure 6-1. This system has been created by incorporating different features of realistic systems in which FIDVR has been experienced [61, 182]. An important factor in considering these systems is that a FACTS device such as SVC was necessarily required for FIDVR mitigation. The validity of this system was ensured by checking that it provided an FIDVR scenario very similar to the event reported in Barrow County [61].

The study system comprises a 200 km single circuit radial transmission system having four 138 kV line sections of 50 km each. These 138 kV line sections are represented as equivalent pi models. L_1, L_2, L_3, L_4, and R_1, R_2, R_3, R_4 represent the inductances and resistances of the different transmission line sections, respectively. Capacitances C_1, C_2,

C_3, C_4 and C_5 represent the sum of transmission line capacitance and shunt capacitor at various sections of the 138-kV line. This radial transmission system is supplied by a 230-kV transmission system at transformer station T_1. The Thevenin equivalent impedance of the 230-kV network is represented by inductance L_g and resistance R_g. A 75 MW PV solar farm is connected to the middle of the 138-kV transmission system. The 138-kV transmission line feeds a total load of 80 MVA through 138/27.6 kV transformer T_2. The load consists of a static load component of 40 MVA and dynamic load component of 40 MVA, both at 0.9 pf. The voltage dependent model is used to represent the static load L_s. The dynamic load comprises 25% of Type A (compressor motors in commercial cooling and refrigeration systems), 25% of Type B (fan motors in residential and commercial buildings), 25% of Type C (direct connected pump motors in commercial buildings) and 25% of Type D (residential air conditioner) motors [3]. The IM parameters are taken from [180, 181]. The IMs are rated at 4 kV and are connected to T_2 through a 27.6/4 kV transformer T_3. The capacitor C_{PF} represents the power factor correction capacitor.
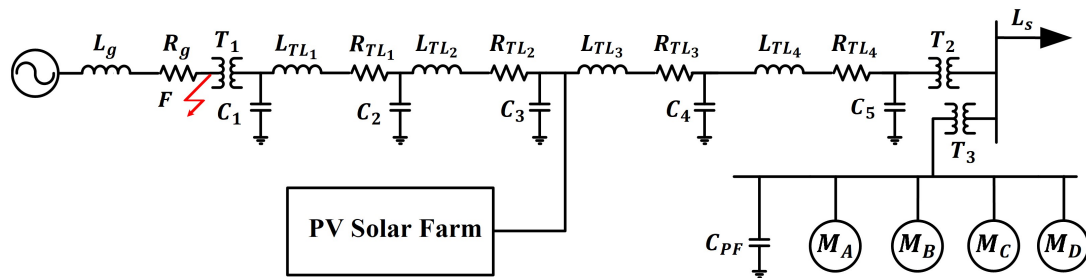
Figure 6-1. Single line diagram of the study system.

6.3 Structure of a Large PV Solar Farm

In this study, the large-scale 75 MVA solar plant is modelled as a single equivalent inverter with inverter controller, plant controller and plant communication delays [87, 88] as depicted in Figure 6-2 (a). The inverter terminal voltage is 0.6 kV, which is stepped up to 27.6 kV using inverter pad mount transformers. The PV plant power is fed to the network through 27.6/138 kV plant transformer. The delay incurred during the measurement process in PV plant is approximated as 10 ms [87]. The collector cable is modelled by its

equivalent π model. The inductance, capacitance, and resistance of the cable are denoted as L_c, C_c, and R_c, respectively.

A large PV plant has both Power Plant Control (PPC) and individual Inverter Level Controllers (ILC). As the plant level controller is slow, grid supporting functions like LVRT and dynamic reactive power support are performed by ILC [87]. In this study as well, since the proposed PV-STATCOM controller is for dynamic voltage support, it is implemented at ILC.

6.4 Proposed PV-STATCOM Control

The proposed PV-STATCOM controller is shown in Figure 6-2 (b). It generates i_{dref} and i_{qref} for providing fast system support during a disturbance. These current references are subsequently transmitted to the conventional inverter controller. The controller consists of: (i) Mode Selector, (ii) Sensitivity Calculator and (iii) Current Reference Calculator.

6.4.1 Mode Selector

The PV-STATCOM controller operates in three modes: Mode 1, 2 and 3. The real/active and reactive power outputs of the PV solar farm at noon in different modes are conceptually depicted in Figure 5-3 (whereas actual outputs are described in Sec. 6.6 e.g., in Figure 6-8). The operating modes are decided by Mode Selector by monitoring V_{pcc}, P_{pcc} and $Q_{pcc.}$ Mode 0 is the normal pre-fault/disturbance operating mode of the solar farm.

6.4.1.1 Mode 0 (controlled by Mode 0 signal)

In this mode, the inverter generates real and reactive power according to real power $P_{available}$ and reactive power Q_{cmd} references provided by PPC. $P_{available}$ corresponds to available solar irradiance. In Figure 5-3, $P_{available} = 1$ pu at noon.

6.4.1.2 Mode 1 (controlled by Mode 1 signal)

In this mode, PV solar farm injects active power P_1 and reactive power Q_1 in proportion to effective R/X ratio at POI. If $P_1 < P_{available}$, active power output is curtailed to P_1 (as shown in Figure 5-3) and reactive power is set to Q_1. However, if $P_1 > P_{available}$, active

power output is set to $P_{available}$, and the remaining inverter capacity is used for reactive power injection, which may be different than Q_1.

If, due to a system fault/disturbance, V_{pcc} goes below a threshold voltage V_{thresh}, Mode Selector enables Mode 1 operation by setting Mode 1 signal high. V_{thresh} is the low voltage that results from a fault/disturbance which is sufficient to initiate an FIDVR event leading to shutdown of motors. This voltage is system dependent and determined from off-line simulation studies for the system under study. $V_{thresh} = 0.75$pu for our study system.
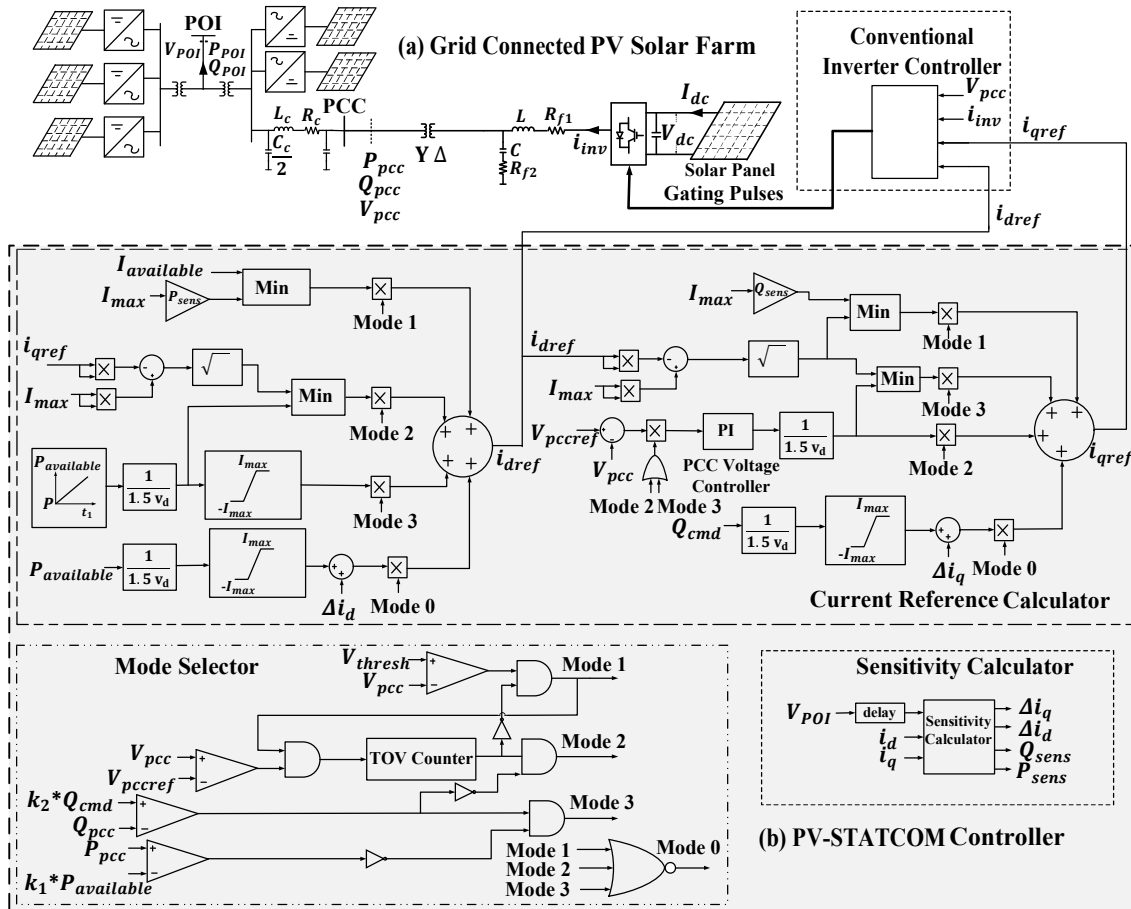
Figure 6-2. Single Line Diagram of a large PV plant with the proposed PV-STATCOM controller.

The PV plant operates in Mode 1 till V_{pcc} increases to just below the utility TOV limit V_{TOVL}. This enhanced voltage support helps in fast voltage recovery. Once TOV limit is reached, Mode 1 operation is disabled, and Mode 2 operation is initiated by setting Mode 1 signal low and Mode 2 signal high. A TOV counter is used to detect TOV limit violation. For instance, a voltage between 1.06 pu and 1.3 pu is permitted for a period of 166 ms [23]. The counter is activated (output is set high) when V_{pcc} crosses utility's upper steady state voltage limit V_{pccref} (=1.06 pu, here). The counter is kept activated for 150 ms (to be safely within the utility limit of 166 ms [90]).

6.4.1.3   Mode 2 (controlled by Mode 2 signal)

In this mode which gives preference to reactive power, the PV-STATCOM control provides reactive power support Q_2 with the objective of maintaining V_{pcc} at utility's upper steady state voltage limit V_{pccref} (=1.06 pu, here). If active power was curtailed to P_1 in Mode 1, it is increased to P_2 using the inverter capacity remaining after reactive power injection Q_2. It is noted that $P_2 < P_{available}$. Even though V_{pcc} reaches V_{pccref}, motors still need reactive power support for their speeds to return to their prefault stable operating state, as in Mode 0. Mode 2 operation is therefore continued till reactive power support is no longer required for motor stabilization. A practical way of checking is that Q_{pcc} becomes equal to k_2 times pre-disturbance value Q_{cmd}. In this study k_2=1.1. Once this condition is satisfied, Mode 2 operation is disabled, and Mode 3 operation is initiated.

6.4.1.4   Mode 3 (controlled by Mode 3 signal)

In this mode that gives preference to active power, the objective is to ramp active power from P_2 to the pre-disturbance solar power level $P_{available}$ at a high rate (100 pu/s, here) in a time period t_1. An important aspect of this control is that during power ramp up, voltage control is simultaneously performed to maintain V_{pcc} at V_{pccref} (=1.06 pu) using inverter capacity remaining after real power ramp up. This unique control prevents occurrence of any unwanted voltage oscillations at POI while ensuring a fast ramp up. Mode 3 operation is continued till P_{pcc} reaches at least k_1 times $P_{available}$. In this study $k_1 = 0.96$.

6.4.2 Sensitivity Calculator

This block calculates the real and reactive power sensitivities (P_{sens}, and Q_{sens}) of POI voltage by monitoring the change in POI voltage on injection of small amount of real and reactive currents. These sensitivities depend upon the effective R/X ratio. The X and R change due to system conditions e.g. switching of lines/transformers, turning on/off of distributed generators, etc. To accommodate these system changes, P_{sens} and Q_{sens} are updated periodically, say every 15 minutes, based on system operation. There is a delay incurred in the measurement and communication of V_{POI} to the ILC, which is considered as 100 msec in study [88]. This delay is considered while computing R and X according to (1) and (2) respectively, for accurate calculation of P_{sens} and Q_{sens}.

Effective R is calculated by varying i_d by a small amount Δi_d (e.g. 10% i_{dmax}) and noting the change ΔV_{POI} as below (6-1).

$$R = \frac{\Delta V_{POI}}{\Delta i_d} \qquad (6\text{-}1)$$

Effective X is calculated by injecting a small current Δi_q (e.g. 10% i_{qmax}) and noting the change ΔV_{POI} as below.

$$X = \frac{\Delta V_{POI}}{\Delta i_q} \qquad (6\text{-}2)$$

Normalized P_{sens} and Q_{sens} are then calculated as:

$$P_{sens} = \frac{R}{\sqrt{R^2 + X^2}} \qquad (6\text{-}3)$$

$$Q_{sens} = \frac{X}{R} * P_{sens} \qquad (6\text{-}4)$$

6.4.3 Current Reference Calculator

This block computes i_{dref} and i_{qref} for the inverter based on the mode of operation, as described below.

6.4.3.1   Reference Calculation for Mode 1

As stated earlier, in this mode the PV solar farm injects active power P_1 and reactive power Q_1 in the ratio of effective R/X ratio at POI. If calculated $P_1 > P_{available}$, the inverter sets i_{dref} to $I_{available}$ ($= P_{available}/(1.5v_d)$). The remaining inverter capacity is utilized to inject reactive power and i_{qref} is set to $\sqrt{(I^2_{max} - i^2_{dref})}$, where I_{max} is the rated inverter current. However, if $P_1 < P_{available}$, active power is curtailed to P_1. Correspondingly i_{dref} is set to $I_{max}*P_{sens}$, and i_{qref} is set to $I_{max}*Q_{sens}$.

$$i_{dref} = \text{minimum}(\,I_{available}, \quad I_{max} * P_{sens}\,) \qquad (6\text{-}5)$$

$$i_{qref} = \text{minimum}\left(\sqrt{I^2_{max} - i^2_{dref}}\,, I_{max} * Q_{sens}\right) \qquad (6\text{-}6)$$

6.4.3.2   Reference Calculation for Mode 2

In this mode, i_{qref} is generated by PCC voltage controller to regulate V_{pcc} to V_{pccref}. If active power was curtailed during Mode 1 operation to P_1, the inverter will increase active power to P_2 (as described in Mode 2 operation). i_{dref} is obtained by dividing active power by $1.5v_d$.

6.4.3.3   Reference Calculation for Mode 3

Active power is ramped up from P_2 to $P_{available}$ at a fast rate. The corresponding i_{dref} is obtained by dividing active power by $1.5v_d$. Voltage control is simultaneously performed with reactive power exchange using remaining inverter capacity. Correspondingly, i_{qref} is generated as below:

$$i_{qref} = \text{minimum}(\,I_{VC}, \quad \sqrt{I^2_{max} - i^2_{dref}}\,) \qquad (6\text{-}7)$$

where, I_{VC} is reactive current required by voltage controller to maintain V_{pcc} at V_{pccref}.

6.4.3.4   Reference Calculation for Mode 0

In this mode, inverter generates current references $I_{available}$ and I_Q from $P_{available}$ and Q_{cmd} signals provided by the power plant controller. i_{dref} and i_{qref} are then calculated as

$$i_{dref} = I_{available} + \Delta i_d \qquad (6\text{-}8)$$

$$i_{qref} = I_Q + \Delta i_q \qquad (6\text{-}9)$$

where, Δi_d and Δi_q are the incremental currents provided by the sensitivity calculator to calculate P$_{sens}$ and Q$_{sens}$, respectively; and $I_Q = Q_{cmd}/(1.5v_d)$.

6.5   Sensitivity Studies

The linearized model of the study system with PV-STATCOM controller is developed in *dq* reference frame in MATLAB. The developed model has 59 states for Mode 1 and Mode 0 operation, and 60 states for other modes of operation. The linearized model is validated by comparing its step response with the nonlinear system model in PSCAD software. The responses of the linear and nonlinear models for a 10% step change in PCC voltage reference for an underdamped response case are shown in Figure 6-3 which match very well. This close correlation validates the linearized model.
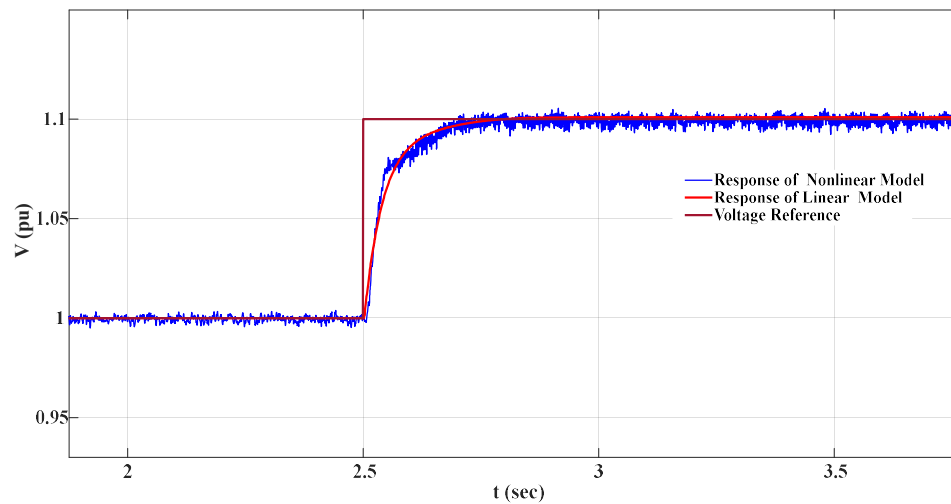
Figure 6-3. Verification of developed small signal model.

As described earlier, the proposed PV-STATCOM controller is based on modulating active and reactive power based on POI voltage sensitivity to active and reactive currents. Hence, the controller sensitivity is tested with respect to both system *X/R* ratio and PV plant

cable *X/R* ratio. Sensitivity studies are also conducted with respect to varying active power levels, since PV plant power varies throughout the day. Loci of sensitive roots are shown for Mode 1 and Mode 0 operations here. The locus of dominant modes for other operating modes (Mode 2 and 3) also depict similar behavior, and hence not presented here.

6.5.1   Sensitivity of controller for variation of system X/R ratio

The loci of sensitive roots with respect to variation of *X/R* ratio between 2 to 9.5 is depicted in Figure 6-4. One dominant mode is seen to become less damped with increasing X/R ratio.
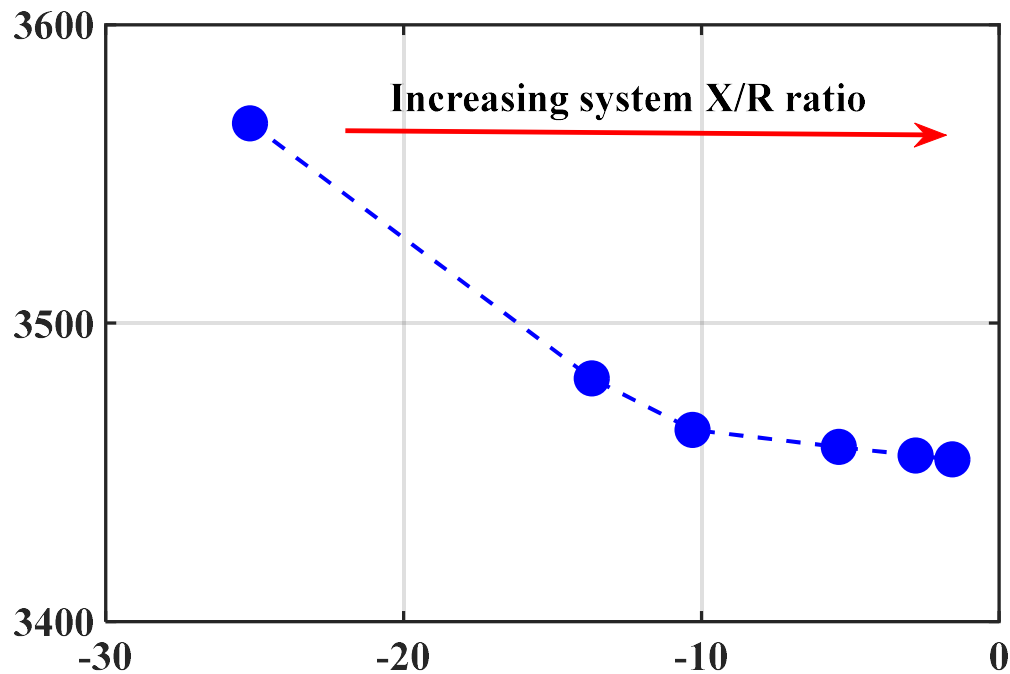
Figure 6-4. Variation of dominant eigen values for varying system X/R ratio.

6.5.2   Sensitivity of controller for variation of PV farm cable X/R

Typically, X/R ratios of cables in PV plant is less than 2, which is lower than the system X/R ratio. Hence, the cable can have a different impact than system impedance on controller performance. The cable X/R is varied between 0.5 to 7.5, and the loci of sensitive roots are shown in Figure 6-5. The root affected by variation in system X/R shows the same trend with variation in cable X/R. System stability is reduced by increase in cable X/R

similar to system X/R. It is further observed that cable X/R affects two more roots which were not affected by the variation in system X/R. It is thus seen that cable impedance has higher impact than system impedance on stability of PV plants equipped with PV-STATCOM controller.
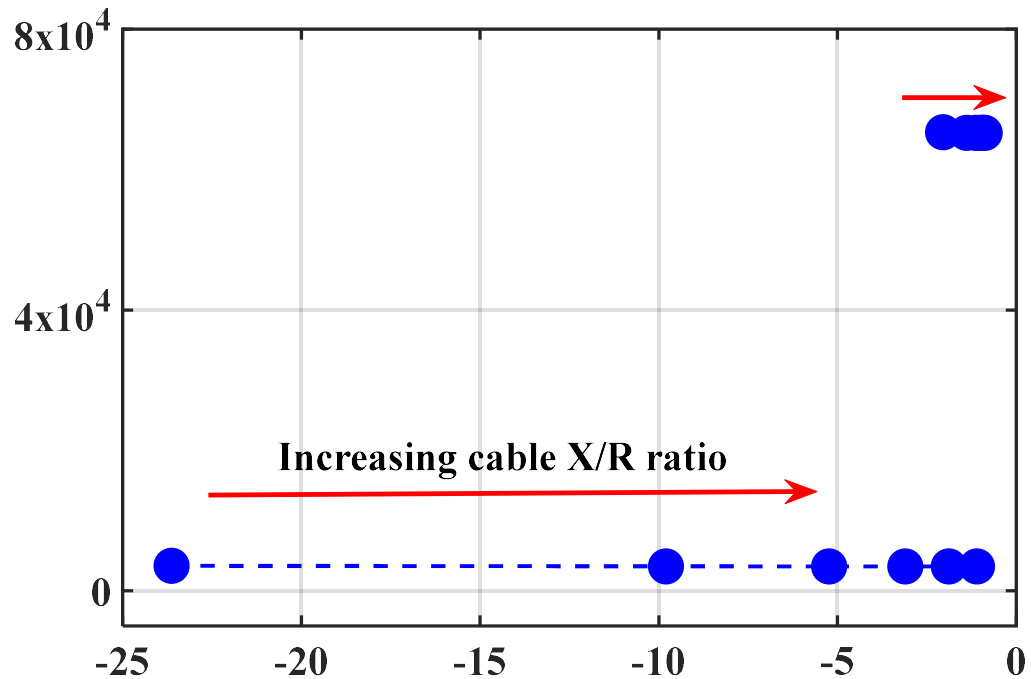
Figure 6-5. Variation of dominant eigen values for varying cable X/R

6.5.3   Sensitivity of controller for variation of PV active power

In the proposed control, PV system can operate in two different states (i) $P_1 < P_{available}$ or ii) $P_1 > P_{available}$.   If $P_1 > P_{available}$ two roots move towards right reducing their damping, as shown in Figure 6-6. This demonstrates that the proposed control is more stable when PV plant is producing higher power than the level determined by plant sensitivity to real power.
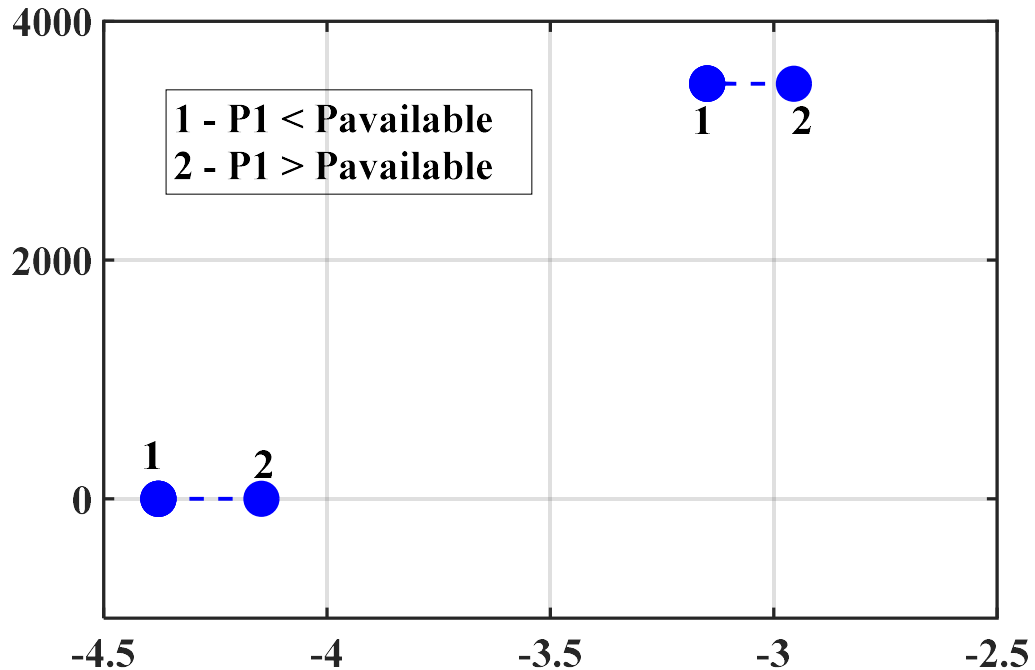
Figure 6-6. Variation of dominant eigen values for varying PV active power.

6.6 Simulation Results

This section presents EMTDC/PSCAD simulation studies of the performance of proposed PV-STATCOM control for FIDVR mitigation under widely-different operating conditions. In all these studies, the PV plant is initially providing its rated power output of 75 MW (1 pu) i.e. at full noon operation. An LLL-G fault is initiated at the middle of transmission line between PV plant and 138/27.6 kV substation (i.e., 50 km away from the motors), and is cleared in 100 ms.

6.6.1   Response of IMs for LLL-G fault with no PV plant control

This case is studied to demonstrate the FIDVR phenomenon in absence of any PV system control. The PV solar farm is considered to operate at unity power factor (UPF). The responses of IMs and PV plant are shown in Figure 6-7. Figure 6-7 (a)-(c) depict PCC voltage V_{pcc} (rms) and 27.6 kV bus voltage (rms); active power (P_{POI}) and reactive power (Q_{POI}) output of PV solar farm (pu); and speeds of the type A-D motors (pu), respectively. The active power from PV farm reduces due to fault-induced drop in voltage. The non zero Q_{POI} is due to collector cable capacitance. When fault is cleared, the PCC voltage and 27.6

kV bus recover only up to 0.86 pu and 0.65 pu, respectively, even after 2s, thus causing an FIDVR event. This is due to excessive reactive power drawn by the motors. All motor speeds decline steadily, and motors eventually stall.
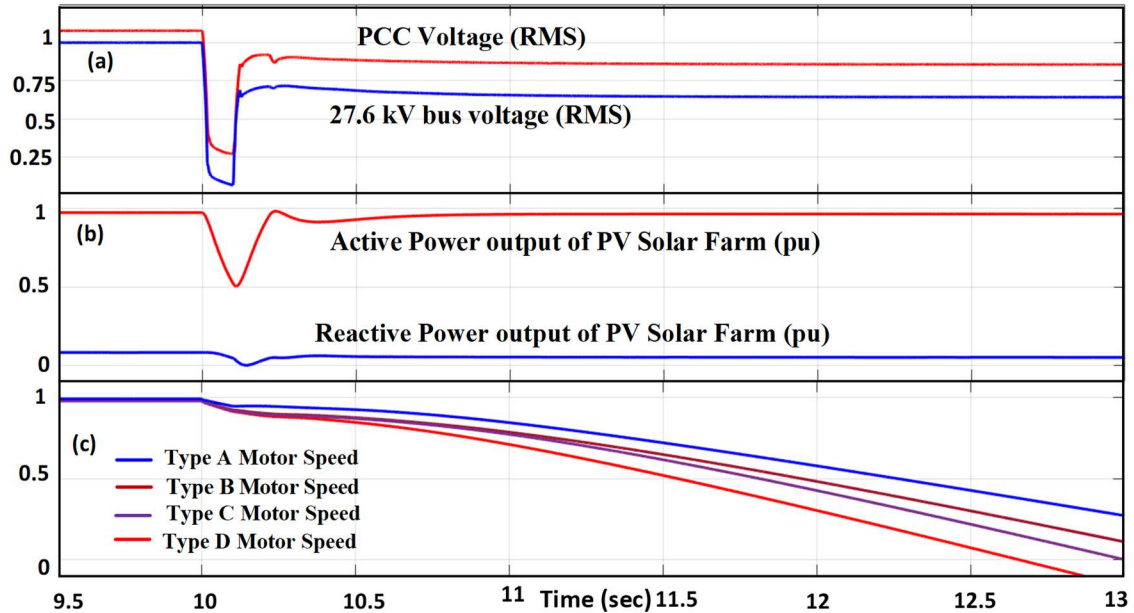
Figure 6-7. Response of IMs with PV plant without any control.

6.6.2   Performance of proposed PV-STATCOM controller

The performance of the 75 MW PV plant with the proposed PV-STATCOM controller is shown in Figure 6-8. Figure 6-8 (a)-(g) depict V_{pcc}, and 27.6 kV bus voltage (rms), P_{POI}, and Q_{POI} (pu), i_d and i_q, electromagnetic torque (pu), and speed of the type A-D motors (pu), power consumed by loads, and the operating mode signals of the controller, respectively.

t < 10 s. The PV plant is operating in Mode 0 by generating 1 pu active power at UPF. V_{pcc} is 1.03 pu and the voltage at LV side of 138/27.6 kV substation is 1 pu. The different motors are operating at steady state with torques between 0.88 - 0.92 pu and slips within 3%. The total load power at 27.6 kV bus is 79 + j12.5 MVA.

t = 10 s. The faults is applied, due to which V_{pcc} and 27.6 kV bus voltages drop to 0.28 pu and 0.12, pu respectively. The motor torques become oscillatory and their speeds reduce. The static load consumption also reduces due to reduction in voltage.

t = 10.02s. The V_{pcc} threshold is violated at 10.01 s. As the measurement delay in PV plant is 10 ms, the PV-STATCOM controller detects the drop in voltage at 10.02 s and changes the mode of operation to Mode 1. The latest *X/R* measured at POI is 2.46, so the controller sets i_{dref} =0.3765 pu and i_{qref} =0.926 pu, as explained in Sec. 6.4.
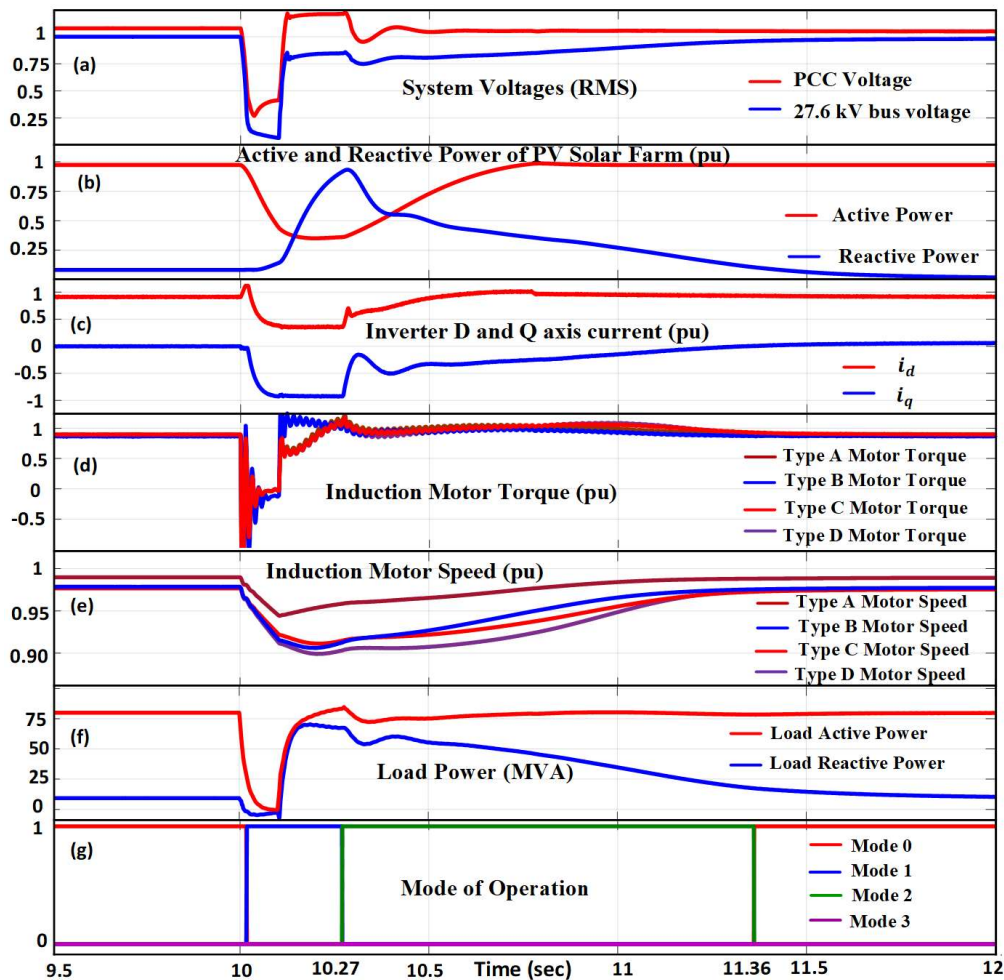
Figure 6-8. Response of the large PV plant with proposed PV-STATCOM control.

t = 10.1s. The fault is cleared at 10.1s. Due to fault clearance, both V_{pcc} and distribution substation voltage increase. Due to P and Q injection by PV-STATCOM, the PCC voltage crosses the steady state limit of 1.06 pu at 10.13s and increases to 1.2 pu.

t = 10.28s. The PV plant continues Mode 1 operation till V_{TOVL} is violated. Due to this novel feature of extended voltage support, the IMs start recovering. The PV-STATCOM controller switches to Mode 2 operation at 10.28s. The reactive power output of PV plant is controlled to regulate V_{pcc} at 1.06 pu in this mode. i_{dref} and i_{qref} are limited within ± 0.3765 pu and ± 0.926 pu, respectively, to provide fast recovery. The PV system injects 0.9 pu reactive power and 0.35 pu active power at 10.28s. As IMs start recovering, their reactive power demand reduces and consequently, the reactive power required to maintain V_{pcc}, also reduces. The active power of the PV plant is also increased.

t= 11.36s. The IMs reach steady state speed at 11.36s. Due to this, the reactive power Q_{pcc} required to keep V_{pcc} at 1.06 pu falls within k_2 (=1.1) times pre-fault reactive power output of PV plant, and eventually i_q reduces to zero. The PV-STATCOM then changes the mode of operation to Mode 0. As PV active power has reached the maximum power already (at 10.77 s) in Mode 2, Mode 3 operation is skipped. The PV system starts operating at UPF by injecting 1 pu active power to the grid. The IMs resume normal steady state operation and total load consumption reaches its pre-fault level.

The proposed PV-STATCOM controller successfully stabilizes the motors during the severe fault and helps in system voltage recovery in 1.36s, which is within the 2s limit set by North American Electric Reliability Corporation (NERC) for not to be characterized as FIDVR event [5]. Furthermore, the PV plant provides this FIDVR alleviation with an energy curtailment (area of real power dip) of only 12 MWs over 1.36s (equivalent to 3.33 kWh).

6.6.3   Advantage of enhanced voltage support up to TOV limit

The performance of PV-STATCOM controller with and without utilizing the proposed enhanced voltage control up to the TOV limit, is compared in terms of time taken for distribution substation voltage recovery, amount of PV power curtailed, and amount of IM

loads becoming unstable. The results are stated in Table 6.1 from which the efficacy of proposed enhanced PV-STATCOM control is clearly evident.

This study shows that with the proposed control, even if the inverter experiences an overvoltage for 9 - 10 cycles, a fast recovery of system voltage and motor stabilization is achieved with minimal PV power curtailment. The High Voltage Ride Through (HVRT) of IEEE Std. 1547-2018 [90] requires the inverter to remain connected even for a voltage range of 1.06 pu - 1.3 pu, and hence all PV inverters will be designed to operate in this voltage range. The proposed enhanced PV-STATCOM control is thus compliant with [90] and can be implemented without modification in existing inverters.

Table 6.1. Comparison of performance of controller with and without TOV support.

	Time taken for 27.6 kV bus voltage to recover to		Total PV energy lost or curtailed	Total IMs becoming unstable
	0.9 pu	**Pre-fault**		
With TOV control	0.96 s	1.36 s	12 MWs (=3.33kWh)	0 MVA
Without TOV control	1.21 s	Voltage does not recover	19.45 MWs (=5.4 kWh)	17.5 MVA

6.6.4   Comparison of Proposed PV STATCOM Controller and other smart inverter controls

The performance of the proposed PV-STATCOM controller is compared with other smart inverter technologies viz. (i) dynamic reactive current injection required under German Grid Code (BDEW) [91], and (ii) only reactive power control of PV-STATCOM [138]. According to [91], the PV inverter needs to inject minimum 2% reactive current per 1% voltage drop below 0.9 pu. In this study, the inverter is set to inject 4% reactive current per 1% voltage drop, which is double the minimum requirement set by BDEW. In only reactive power control of PV-STATCOM [138], active power is autonomously curtailed to zero during a disturbance and the entire inverter capacity is utilized for providing

reactive power support. The study results are shown in Figure 6-9. Figure 6-9 (a)-(e) depict PCC voltage (rms), 27.6 kV bus voltage (rms), active power output of PV solar farm (pu), reactive power output of PV solar farm (pu), speed of type D IM (pu), respectively. Speed of only type D IMs is shown as they have lower inertia and are more prone to instability compared to Type A-C motors.

Proposed PV-STATCOM Control: The performance is same as already discussed in Sec. 6.6.2. The system voltage reaches steady state at 11.58 s, and FIDVR is avoided.

Dynamic reactive current injection: V_{pcc} increases to 0.85 pu at 10.5 s, and thus i_q is reduced from 1 pu to 0.2 pu. This reactive support is inadequate, and the IMs eventually stall. The 27.6 kV bus voltage recovers only to 0.676 pu causing FIDVR.
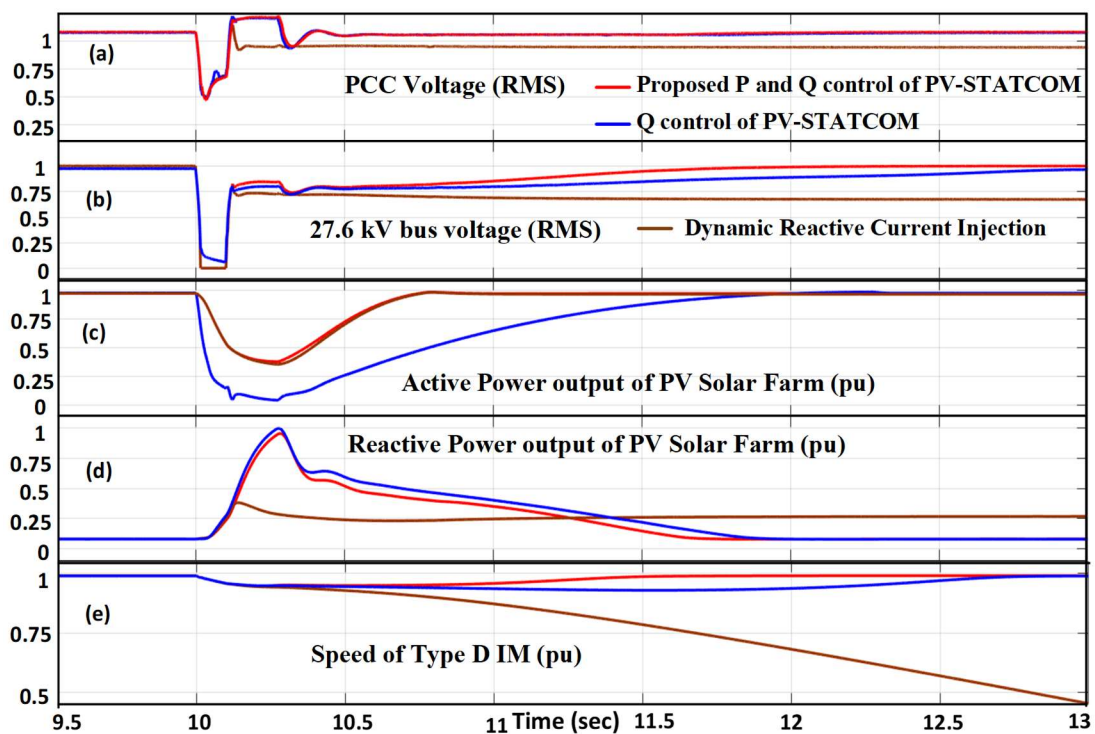
Figure 6-9. Comparison of PV-STATCOM and other smart inverter controls

Reactive power control of PV-STATCOM: The PV plant continues providing reactive power support till the TOV limit, and then switches to closed loop voltage control i.e., regulating V_{pcc} to V_{pccref} (=1.06 pu). The system voltage recovers at 12.7 s and the motor

is stabilized. However, since the voltage recovery takes more than 2s per NERC [3], FIDVR is technically not prevented.

This study thus shows that among all the investigated smart inverter controls, the proposed P and Q control of PV-STATCOM control is most effective in FIDVR mitigation.

6.6.5   Comparison of PV STATCOM Controller and STATCOM

Typically, an SVC or STATCOM is installed close to the distribution substation for FIDVR alleviation, as described in Sec. 1.3.3. In this section, a performance comparison is presented of: i) 75 MW PV plant operating with proposed PV-STATCOM controller with no STATCOM connected at the distribution substation, and ii) 75 MW PV plant operating according to BDEW LVRT requirements by injecting 4% reactive current per 1% voltage drop for voltage below 0.9 pu [91] with a 34 Mvar STATCOM located at the distribution substation. The results of this study are shown in Figure 6-10. Figure 6-10 (a)-(e) depict V_{pcc}, 27.6 kV bus voltage (rms), active power output of PV solar farm (pu), reactive power output of PV solar farm (pu) and STATCOM, and the speed of type D IM (pu), respectively.
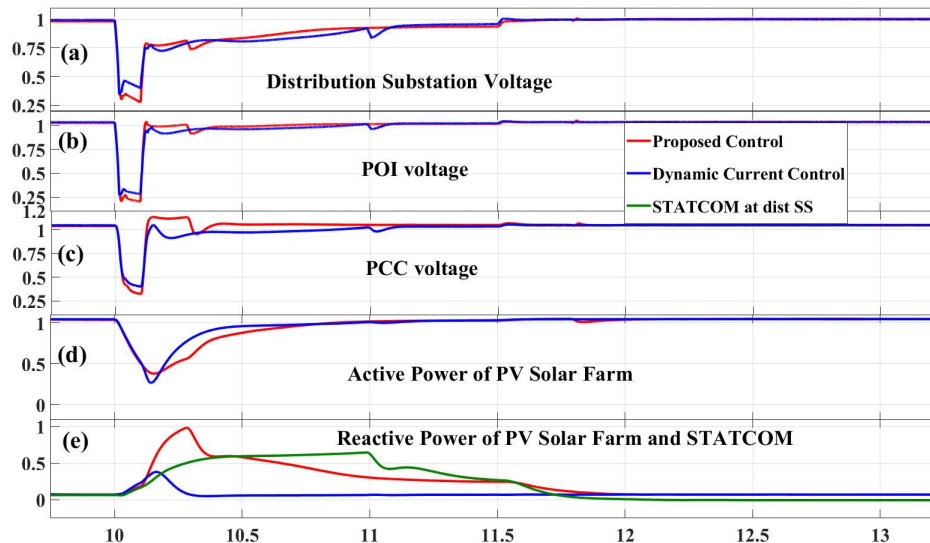
Figure 6-10. Comparison of PV STATCOM Controller and actual STATCOM.

This study shows that a 34 Mvar STATCOM needs to be installed at the distribution substation to mitigate FIDVR, even with 75 MW PV solar providing reactive power

support as per [91]. However, the same FIDVR mitigation can be accomplished by the 75 MW solar farm with proposed PV-STATCOM control, even if it is located 100 km away from the distribution substation. This demonstrates that the PV solar farm equipped with the proposed PV-STATCOM controller can eliminate the need for installing a STATCOM.

A PV-STATCOM (i.e., a PV solar plant with the proposed PV-STATCOM controls) is expected to be about 50 times cheaper than an equivalent sized STATCOM. This is because the PV-STATCOM is a relatively small addition in control system with associated measurements and protection system, superimposed on the existing inverters, electrical substation, bus work, breakers, protection systems, and civil works of a PV plant, which transforms the existing solar plant into a STATCOM. Even though in this study, a PV-STATCOM is shown to eliminate the need of a half-size STATCOM, the financial savings can be significant.

6.6.6   Nighttime Performance of PV-STATCOM controller

Figure 6-11 (a)-(e) depict V_{pcc}, 27.6 kV bus voltage (rms), P_{POI} and Q_{POI} (pu), and the speed of all IMs (pu), respectively for an LLL-G fault at the middle of transmission line between PV plant and 138/27.6 kV substation, at night. Performances of PV system both with and without the PV-STATCOM control are illustrated.

As soon as PV-STATCOM controller detects the fault, it initiates dynamic voltage support, as discussed in Sec. 6.4. Since at night the available active power is zero, the controller uses full inverter capacity to inject reactive power. Once the TOV limit is violated, the controller initiates Mode 2 operation by regulating PCC voltage V$_{pcc}$ to V$_{pccref}$ (=1.06 pu). Due to PV-STATCOM support, the 27.6 kV bus voltage recovers and Q_{pcc} falls within k_2 (=1.1) times pre-fault reactive power output of PV plant. i_q eventually reduces to zero and the controller stops Mode 2 operation. Mode 3 operation is skipped, as the active power is zero. The controller initiates Mode 0 and remains on standby to provide grid support during any next disturbance. Without the support of PV-STATCOM control, neither PCC voltage nor 27.6 kV bus voltage recovers and all motors stall.
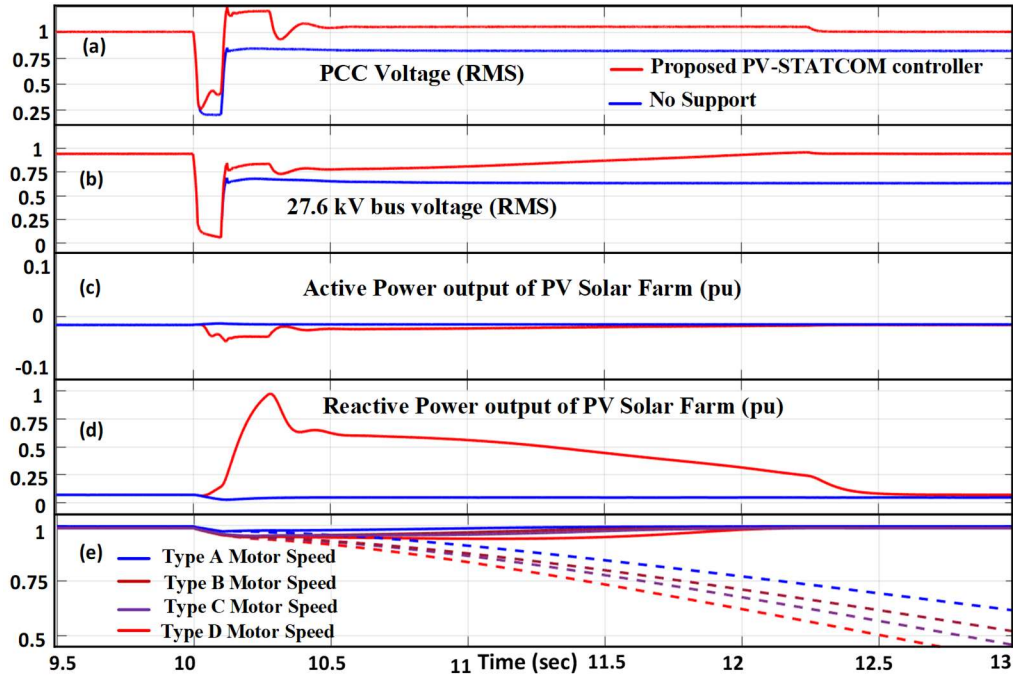
Figure 6-11. Performance of PV-STATCOM Controller at night.

The proposed PV-STATCOM controller thus successfully helps voltages to recover and stabilizes motors at night.

6.6.7 Performance of the proposed PV-STATCOM controller for faults at various locations

The response of the 75 MW PV plant with the proposed PV-STATCOM controller for faults at various locations are shown in Figure 6-12. For this study, LLL-G fault for 100 msec is applied 150 km away from the 138/27.6 kV substation (case 1), 100 km away (i.e., at PV plant terminal) (case 2), 50 km away from the substation (case 3), HV side of the 138/27.6 kV transformer (case 4), and LV side of the 138/27.6 kV transformer (case 5). Figure 6-12 (a)-(e) depict the POI voltage (rms), 27.6 kV bus voltage (rms), active power output of PV solar farm (pu), reactive power output of PV solar farm (pu), and the speed of type D IM (pu), respectively. The speed of only type D motors is shown, as they have lower inertia among all the motors, and are more prone to stall during a voltage disturbance.

t < 10 sec. The system is operating in same steady state condition for all the cases. The PV plant is operating in Mode 4 by generating 0.97 pu active power at UPF. The V_{POI} is 1.06

pu and the voltage at LV side of 138/27.6 kV substation is 1 pu. The different motor loads are operating at steady state with torque between 0.88 – 0.92 pu and slips within 3%. The total load consumed at 27.6 kV bus is $79 + j12.5$ MVA.

An LLL-G fault is applied at various locations as stated above at t = 10 sec. Due to the fault, the V_{POI} drops to 0.14 pu, 0.13 pu, 0.31 pu, 0.42 pu and 0.49 pu for case 1-5, respectively. The 27.6 kV bus voltage falls to 0.22 pu, 0.21 pu, 0.12 pu, 0.07 pu and 0 pu for case 1-5, respectively.
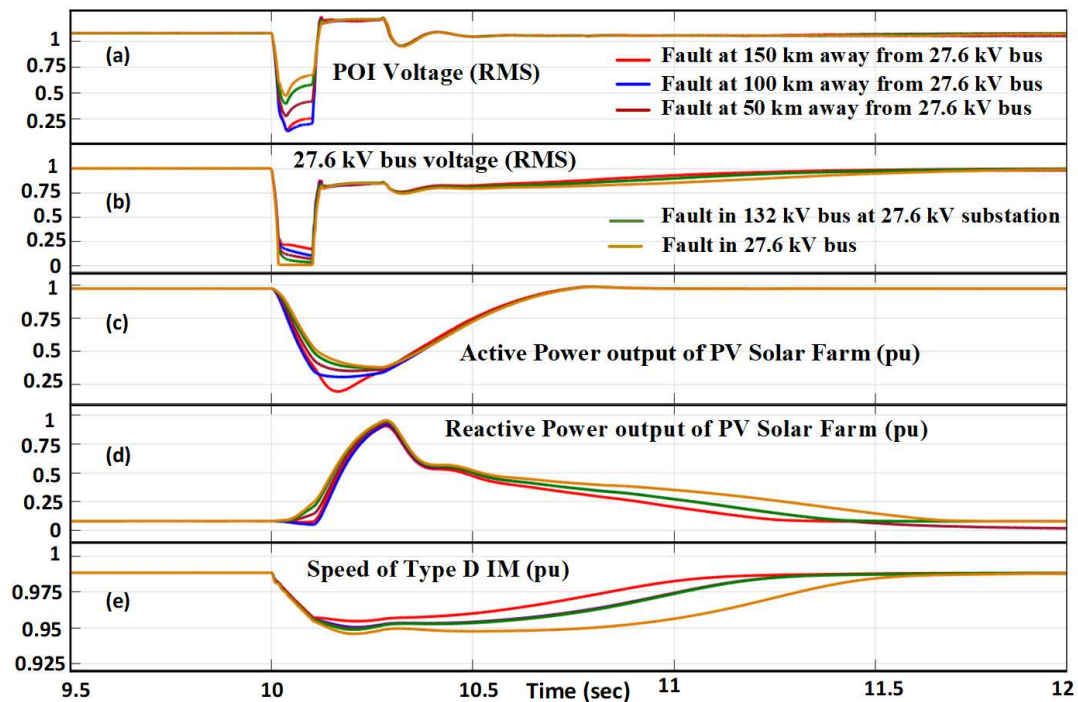
Figure 6-12. Response of 75 MW PV plant with the proposed PV-STATCOM controller for 3-phase to ground fault at various locations.

The fault is cleared at 10.1 sec. The closed loop delay for a large PV plant is 100 msec [88], hence the inverter currents i_d and i_q become 0.3765 pu and 0.926 pu, respectively at 10.11 sec. Due to fault clearance, the POI and 27.6 kV bus voltages rise. The IM's torque increases, and slope of the speed decline reduces.

The system voltage recovers at 11.26 sec for case 1 and PV-STATCOM controller switches to Mode 4 operation. The voltage recovers for cases 2-4 at 11.32 s, 11.36 s, 11.4 s, and 11.58 s, respectively.

This study shows that PV solar plant with the proposed PV-STATCOM control is able to provide fast voltage recovery for a severe disturbance such as LLL-G fault at all buses including the load terminal (case 5). In all cases, the maximum PV energy curtailed for providing this critical support is approximately 72 MWs, which is equivalent to only 20 kWh.

6.6.8 PV-STATCOM performance for various system strengths

Studies are done on systems with varying Short Circuit Ratios (SCR). Due to voltage support from PV solar farm with proposed PV-STATCOM controller, the 27.6 kV bus voltage recovers in 11.18s, 11.30s, 11.36s and 11.9s, respectively for SCRs of 6, 4.8, 2.8, and 1.6, respectively. This study confirms that PV-STATCOM control can help in fast voltage recovery in both strong and weak systems and prevent FIDVR.

6.7 Conclusion

A novel control of large PV solar farm as PV-STATCOM for providing enhanced voltage support utilizing both reactive and active power modulation to alleviate FIDVR is presented. The study system comprises a 138 kV transmission network with a 75 MW PV solar farm installed midline and feeding 40 MVA voltage dependent static load and 40 MVA induction motor loads of different types. The PV solar plant injects active and reactive power in proportion to sensitivity of POI voltage to real and reactive power. A linearized system model is developed for performing various sensitivity studies, which is validated by PSCAD simulations. Extensive PSCAD simulation studies demonstrate that the proposed PV-STATCOM control:

(i) mitigates FIDVR even if solar farm is more than 100 km away from the distribution substation with motor loads.

(ii) is more effective than i) reactive power support required by the German Grid Code, and ii) PV-STATCOM with only reactive power control

(iii) on the 100-km remote 75 MW solar farm ensures similar FIDVR mitigation as a 34 Mvar STATCOM connected locally at the distribution substation with motor loads.

(iv) Successfully alleviates FIDVR for: i) wide ranging system strengths, and ii) different fault locations

(v) Provides voltage recovery at night. This functionality is beyond the requirements of present day Grid Codes.

Chapter 7

7 Stability Analysis of Two PV-STATCOMs

7.1 Introduction

The stability analysis of two PV plants, with PV-STATCOM control, connected to a medium voltage realistic feeder is presented in this chapter. Studies are done for (i) PV-STATCOM control performed at plant level, and (ii) PV-STATCOM control performed at inverter level. Studies are done to compare the application of equivalent model and detailed model of PV plants for stability analysis. The need for detailed modeling of PV plants for stability analysis of the system, is examined. Furthermore, studies are done to test the sensitivity of proposed PV-STATCOM controller performance to various power system and PV plant parameters.

7.2 Study System

A realistic 45 km long 27.6 kV feeder in Ontario, Canada [179] is considered as the study system for studying the interactions between two PV plants in a medium voltage distribution system.

The single line diagram of the study system is shown in Figure 7-1. The transformer T_1 is rated 115 kV/27.6 kV, 20 MVA with 5% impedance. The distribution lines are represented by their equivalent pi models. A total load of 5.3 MVA at 0.9 power factor is connected at the feeder end. For simulation studies, 50% of loads are modelled as IM loads and other 50% as voltage dependent static loads (SL). The IM loads are rated at 4 kV [180] and are connected through transformer T_2 rated 27.6/4 kV and 5% impedance.

A 6 MW PV solar farm is connected to the feeder at Bus 3 and a 4 MW solar farm is connected to Bus 4. The 6 MW plant and 4 MW plant consists of three and two 2 MW inverters, respectively. The inverters and collector cables of 6 MW PV plant are represented as Inv 1x and Cable 1x, respectively, where x is an index for the inverter unit. Similarly, inverters and collector cables of 4 MW PV plant are denoted as Inv 2x and Cable 2x, respectively.
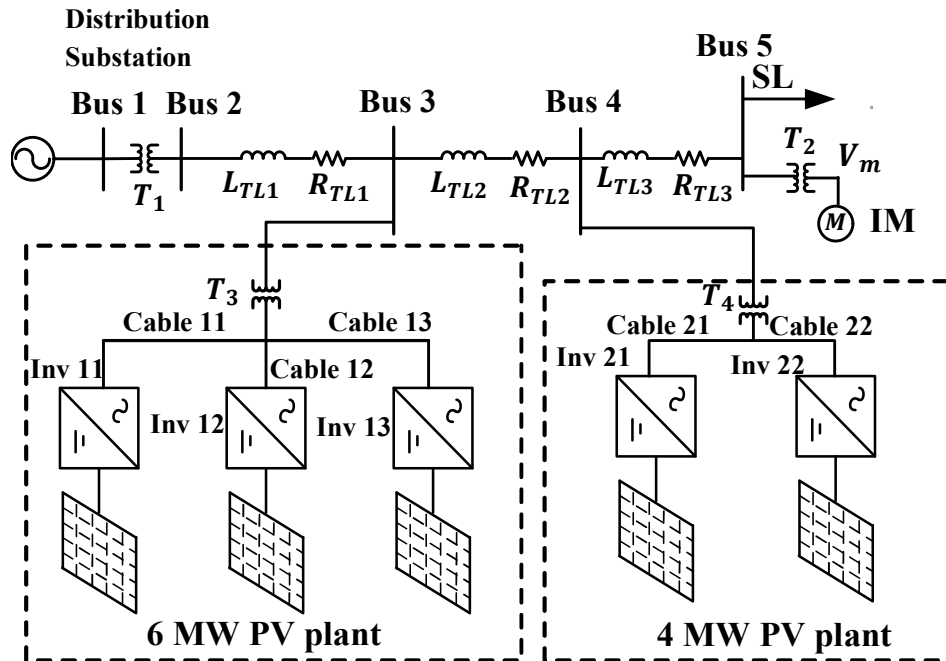
Figure 7-1. Single Line Diagram of the study system.

7.3 Modeling of the PV plant

A PV plant consists of multiple inverters which can be either modelled in detail or as an equivalent model. Typically, they are represented by their equivalent single inverter model as discussed in Sec. 2.5 [87]. For studying the transients that occur within the plant, the PV plant is modelled in detail with detailed models of inverters, filter, collector system and pad mount transformers etc. as discussed in Sec. 2.3. The detailed model of the 6 MW PV plant used in this study is described in Sec. 5.2.

7.4 Small Signal Model

The modeling of the study system is discussed in this section. The nonlinear model of study system is developed in MATLAB from the differential equations of various components described in Chapter 2. The developed model is linearized around an operating point using MATLAB control system toolbox.

The linearized model is validated by comparing its step response with the nonlinear system model in PSCAD software. The responses of the linear and nonlinear models for a 10% step change in PCC voltage reference, and 10% step change for DC link voltage

reference for an underdamped response case and oscillatory response case, are shown in Figure 7-2 and Figure 7-3, respectively. It is observed that the responses of linearized and detailed time domain model match very well in both cases. This close correlation validates the linearized model.
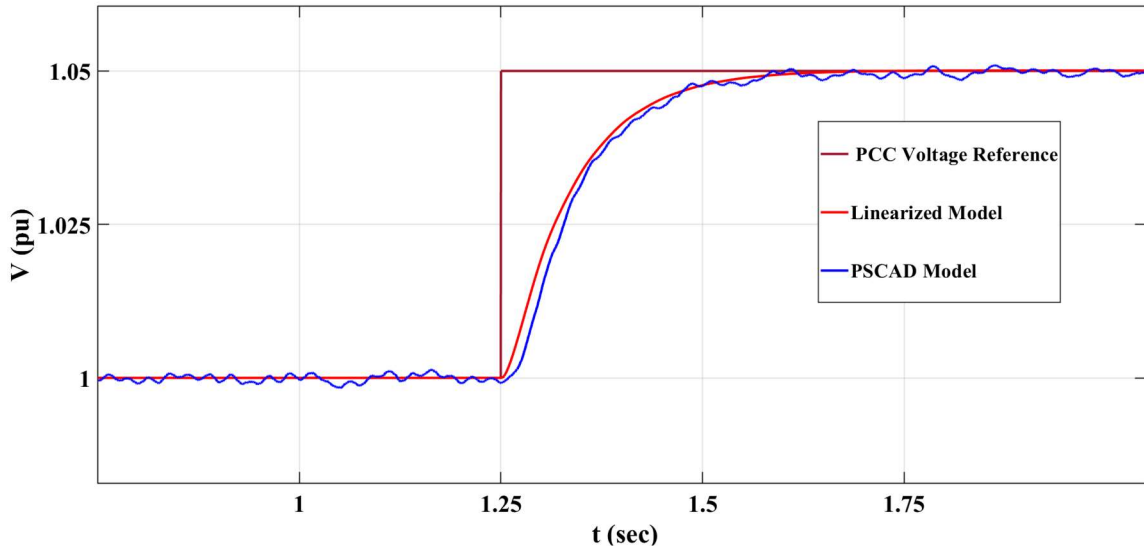
Figure 7-2. Response of Linearized model and PSCAD model for a step change of Reference for PCC Voltage Controller of an inverter of 6 MW PV plant.
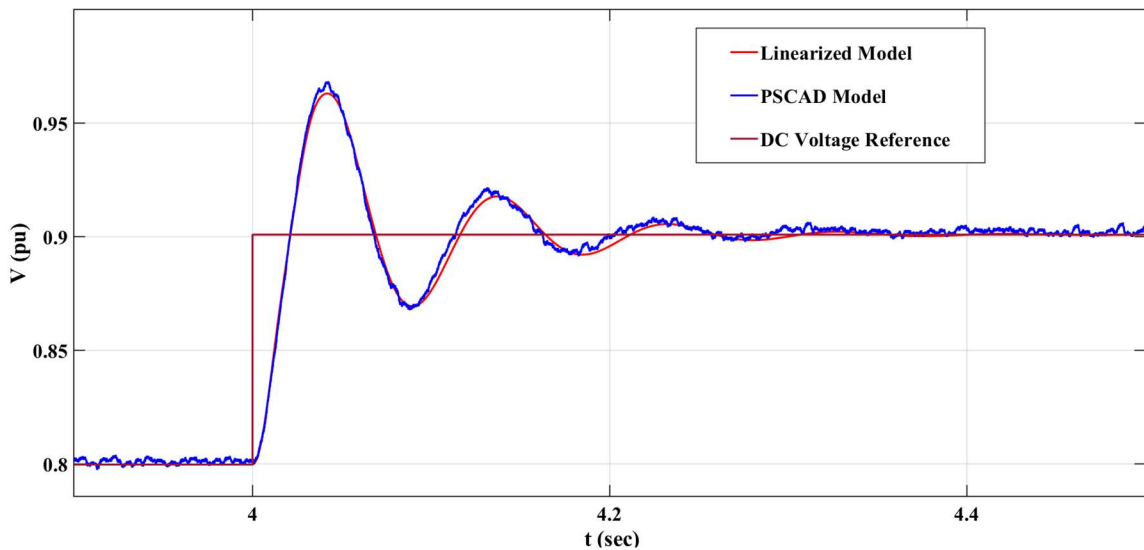
Figure 7-3. Response of the Linearized model and PSCAD model for step change of Reference for DC link Voltage Controller of an inverter of 4 MW PV plant.

7.5   Comparison of Equivalent Model and Detailed Model of PV Plant for Stability Studies

Utility scale PV plant consists of multiple inverters which are typically modelled as a single equivalent PV plant model for stability studies. In this section, the equivalent model and detailed model are compared in terms of their application for small signal studies. Since the interactions between Volt-Var controllers are reported widely in literature [152-155, 157], the PV plants in study system are equipped with Volt-Var control for the comparison study.

For the equivalent PV plant model, the 6 MW and 4 MW plants are modelled with their corresponding equivalent PV plant models. The detailed model of PV plant includes individual models of all inverters and their filters, the inverter level transformers, all the collector cables and plant transformer.

The block diagram of a Volt-Var controller is shown in Figure 7-4. The delay and slope of the Volt-Var control are user settable. The slope of the Volt-Var controller is defined as in (7-1).
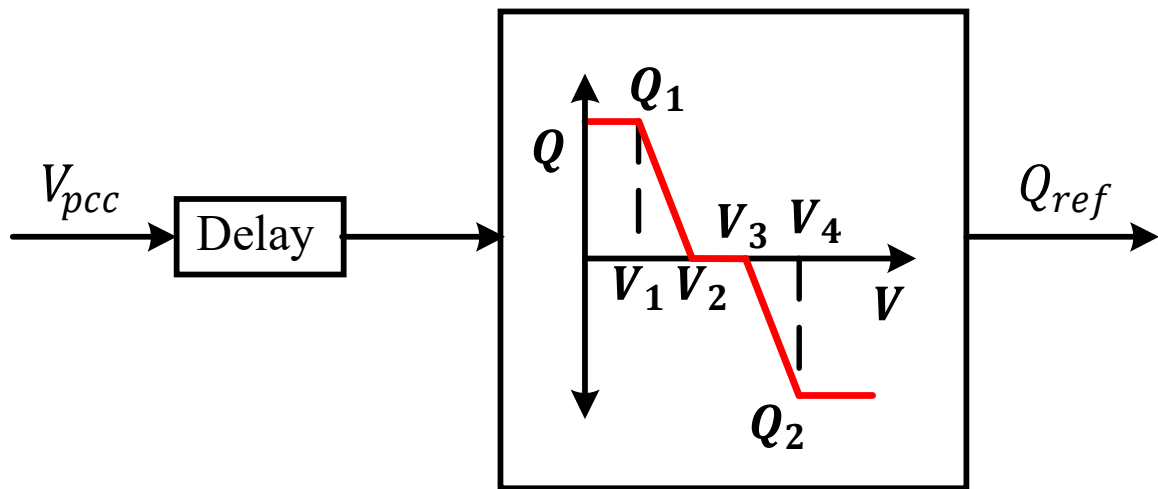
Figure 7-4. Block diagram of Volt-Var Controller.

$$Slope = \frac{Q_1 - 0}{V_1 - V_2} \text{ for Capacitive Reactive power injection} \qquad (7\text{-}1)$$

$$\text{Slope} = \frac{Q_2 - 0}{V_4 - V_3} \text{ for Inductive Reactive power injection}$$

7.5.1   Response of Equivalent Model

The PV plants are modelled with their corresponding equivalent models and the system response is studied for both a small and large slope.
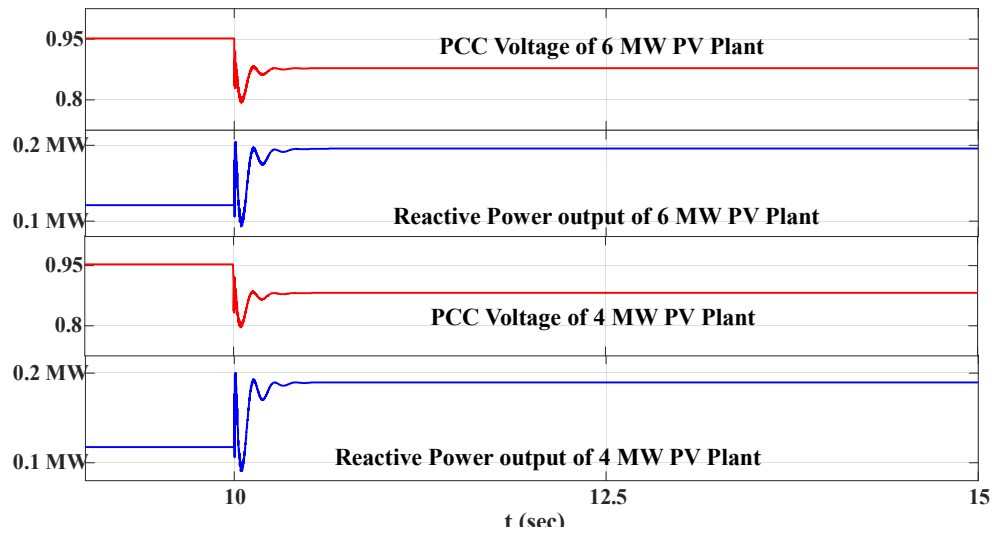
Figure 7-5. Response of equivalent model with Volt-Var characteristic of slope = 2
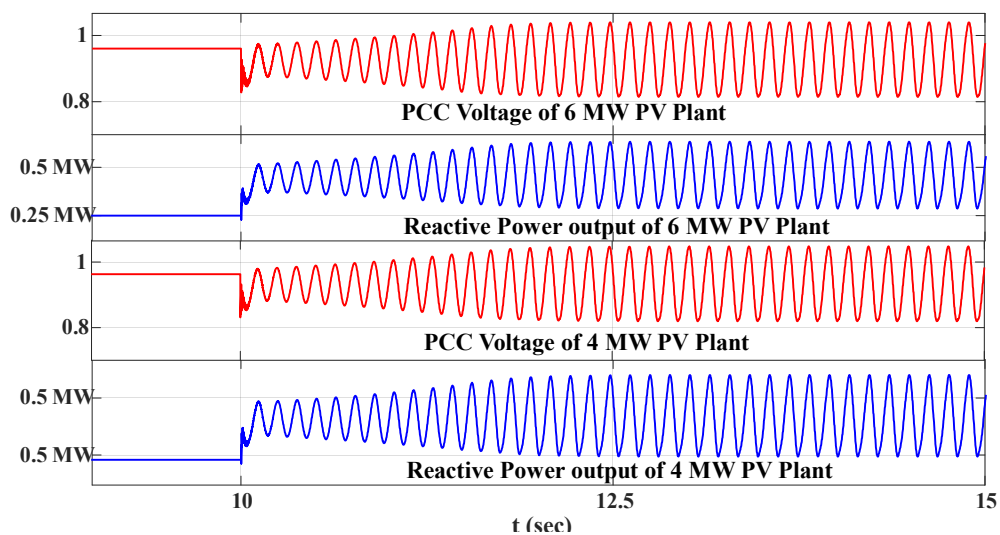
Figure 7-6. Response of equivalent model with Volt-Var characteristic of slope = 7.5

The distance between the two PV plants is 5 km and both are assumed to generate 0.8 pu of their rated capacity active power. The delay is set at 100 ms for Volt-Var controllers of both PV Plants. A load of 0.4 + j1.5MVA is switched at 10s. The response of both PV plants with equivalent models for a slope of 2 and 7.5 are shown in Figure 7-5 and Figure 7-6, respectively.

For a small slope (slope = 2), the system is stable as shown in Figure 7-5. When a large slope (slope = 7.5) is used, the system becomes unstable for the same load change. This shows that as the slope increases, the stability of the system reduces. This result matches with the findings reported in literature [152, 153, 155].

7.5.2   Response of Detailed Model

The detailed model of 6 MW and 4 MW PV plants are used in this study to compare their response with the response of the equivalent models described above.
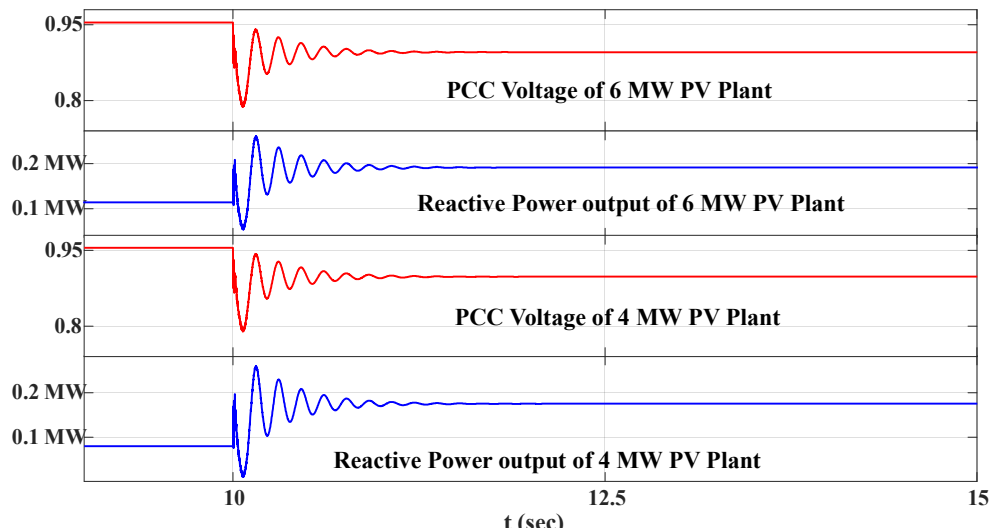
Figure 7-7. Response of detailed model with Volt-Var characteristic of slope = 2

The distance between the two PV plants is 5 km and both are assumed to generate 0.8 pu of their rated capacity active power. The delay is set at 100 ms for Volt-Var controllers of both PV Plants. A load switching is done at 10s and the response of both the PV plants with the equivalent plant models for a slope of 2 and 7.5 are shown in Figure 7-7 and Figure 7-8, respectively.

The system is seen to be stable for both the slopes, even though slightly more oscillations are observed in case of large slope of 7.5 as compared to small slope of 2.
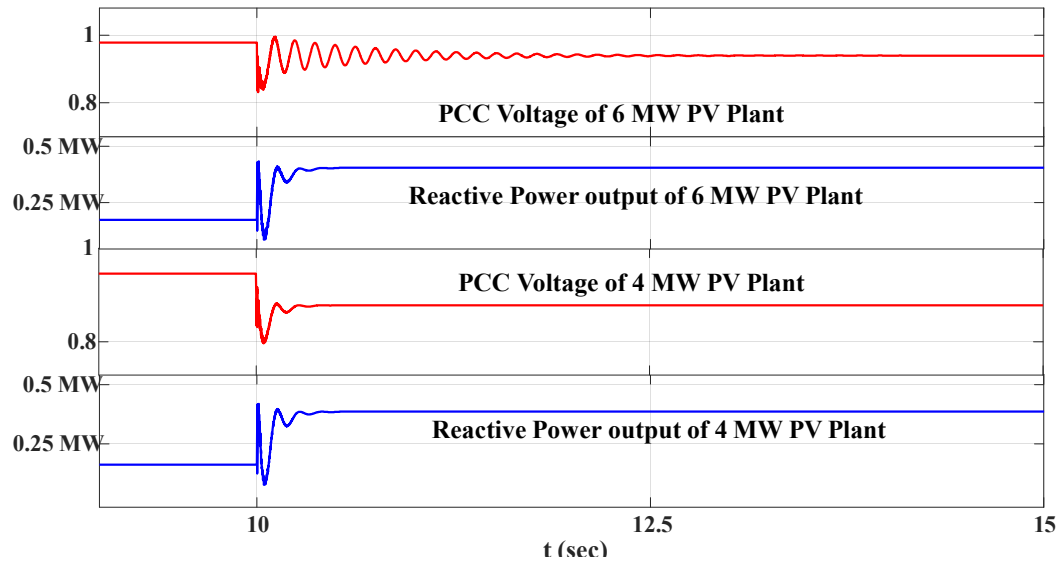
Figure 7-8. Response of detailed model with Volt-Var characteristic of slope = 7.5

By comparing the response of the equivalent and detailed model for slope = 7.5, it is observed that the equivalent model shows unstable operation while the detailed model shows stable operation for the same slope. This implies that the equivalent model can potentially show unstable operation for slopes for which the PV plant is actually stable. Thus, if equivalent model is used for stability analysis, it could give incorrect and pessimistic information about the stability of the system. A low value of slope of the Volt-Var controller will unnecessary be selected, resulting in a slower PV plant response.

The eigen value analysis also shows the same result. The dominant poles of detailed and equivalent model are -6.72±j51.13 and -0.4±j68.13, respectively. This further confirms that the equivalent model provides pessimistic and inaccurate information about the stability of system.

Therefore, detailed model of PV plants should be utilized for stability analysis of the controller, as equivalent model fails to give correct information on the stability of system.

7.6   Stability Analysis of Two PV-STATCOM controllers

The proposed PV-STATCOM controller can be implemented either at Plant Level Controller (PLC) or at the Inverter Level Controller (ILC). The structure of Plant Level Control and Inverter Level Controllers are discussed in detail in Chapter 1.5.2. Small signal studies of the PV-STATCOM controller implemented at PLC and ILC are now performed to assess the impact of different system and plant level parameters on the stability of the system with multiple PV-STATCOMs.

Based on the results of the previous section, the studies in this section are conducted using detailed model of the PV plants.

7.6.1   PV-STATCOM control implemented at Plant level

The interactions between adjacent PV plants; and the influence of system and PV plant parameters when the proposed PV-STATCOM control is implemented at PLC are studied in this section.

7.6.1.1   Impact of Speed of Voltage Controller

The maximum switching frequency of a typical 2 MW inverter is limited to 2 kHz to reduce switching losses, and hence the inverters are switched at 2 kHz in this study. The bandwidth of the inner current controller should be at least 10 times lower than the switching frequency [172] and therefore the current controllers are designed with a bandwidth of 200 Hz. The outer voltage controller's bandwidth should be at least four times lower than the current controller bandwidth i.e, 50 Hz. In this study, the bandwidth of voltage controller is varied between 5 Hz and 50 Hz, which covers the range of the possible bandwidths of the voltage controller of a 2 MW PV inverter. The dominant eigen values of the system for variation in voltage controller bandwidth are depicted in Figure 7-9. The bandwidth of the voltage controllers of both plants are changed, simultaneously.

The relation between the bandwidth and parameters of the PI controller for voltage controller can be approximately given as [183],

$$K_{Pvc} = \frac{BW_{vc}}{BW_{cc}w_nL_g} \tag{7.1}$$

$$K_{Ivc} = \frac{BW_{vc}}{w_nL_g} \tag{7.2}$$

where,

BW_{vc} = bandwidth of the AC voltage controller

BW_{cc} = bandwidth of the Current controller (200 Hz in this study)

w_n = system frequency

L_g = Thevenin inductance at PV solar farm terminal.

As per (7.2), speed of response is directly proportional to bandwidth of the controller, because speed is determined by the integral gain (K_{Ivc}), and (7.2) implies that integral gain (K_{Ivc}) is linearly proportional to bandwidth.

The PV-STATCOM control performed at PLC experiences a delay, which includes the communication delay between plant level controller and inverter level controller, measurement delay, etc. In a PV plant, this delay lies between 0.1 s – 1.5 s [87, 88]. In this study, the delay is set as 1 s. The $\frac{X}{R}$ ratio of the feeder is 3, and the SCR at Bus 3 is considered to be 3. The distance between the PV plants is 5 km.
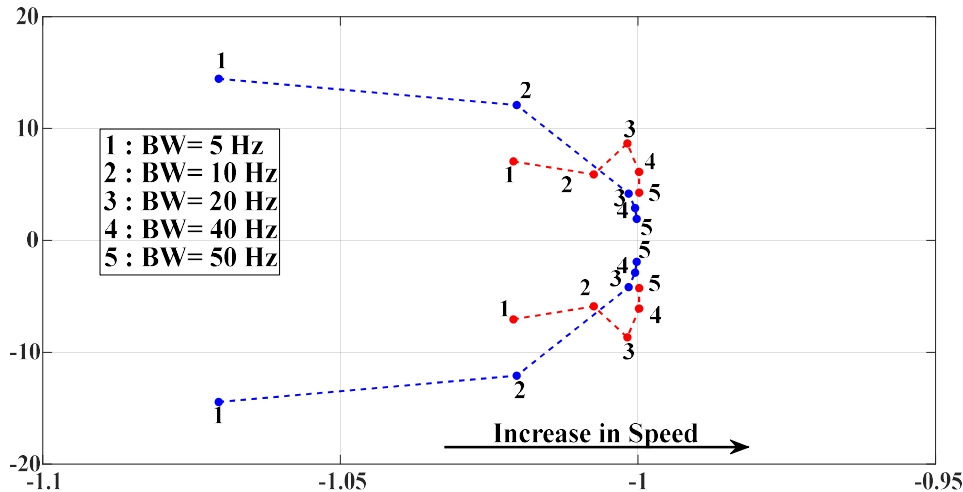
Figure 7-9. Variation of dominant eigen values for varying voltage controller bandwidth.

The poles shift to the right as controller speed is increased (i.e., with increasing bandwidth (BW)), as seen in Figure 7-9. The frequency and damping of this mode also reduce with increase in controller speed.

7.6.1.2   Impact of Plant Level Controller delay

In a PV-STATCOM, the communication of control instructions from PV-STATCOM controller installed at Plant Level Controller to Inverter Level Controllers experiences a delay. This delay is a part of the voltage control path and thus could have an impact on the controller performance. In order to study the impact of this delay, the plant level delay is varied between 0.1 s – 0.9 s and the loci of dominant poles for this variation of delay are presented in Figure 7-10. In this study, the voltage controller bandwidth is set at 50 Hz. The system conditions are same as in the previous study.

The variation in plant level delay has impact on two critical modes, and they show opposite behavior. One mode tends to become unstable with increase in delay, and other mode becomes stable with increase in delay. For the system considered, a delay greater than 0.9 s is required to ensure stable operation.
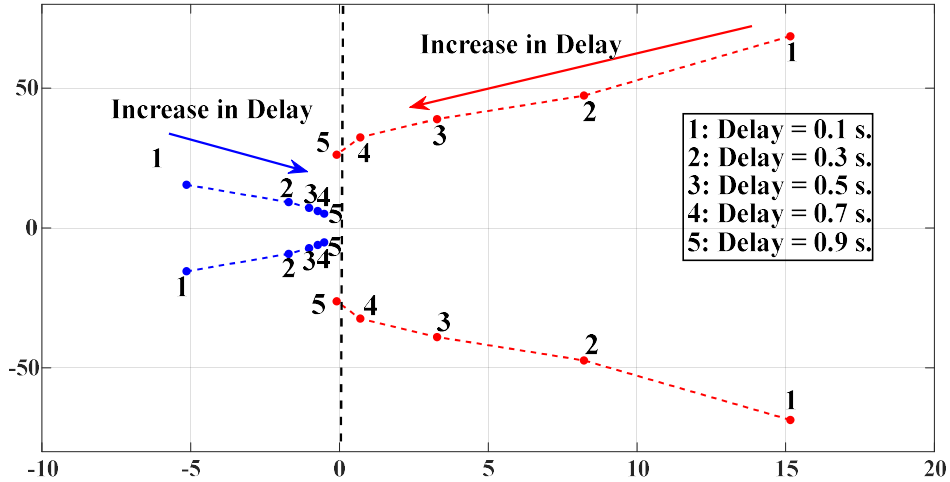
Figure 7-10. Variation of dominant eigen values for varying plant level delay.

7.6.1.3   Impact of PV plant output power

The poles of the system for variation of PV plant output active power is depicted in Figure 7-11. The different cases of PV power levels considered in this study are: (i) when both PV plant are producing high power (0.9 pu), (ii) when both are producing 0.5 pu power, (iii) night time operation (zero active power), (iv) partial shading on 6 MW PV plant, (v) partial shading on 4 MW PV plant.

Figure 7-11. Variation of dominant eigen values for varying PV plant output power.

In this study, the voltage controller bandwidth and plant level delay are set at 50 Hz and 1 s respectively. The other system conditions are same as in the previous study.

From Figure 7-11, it is observed that the level of active power output of PV plants has no significant impact on the interactions between the two PV plants while performing PV-STATCOM operation, implemented at PLC.

7.6.1.4   Impact of feeder $\frac{X}{R}$ ratio

The system $\frac{X}{R}$ is varied between 1-5 to study its influence on the interaction between PV plants while providing PV-STATCOM control at plant level. In this study, the voltage controller bandwidth and plant level delay are set at 50 Hz and 1 s respectively. The SCR at Bus 3 is 3. The results are shown in Figure 7-12.

With increasing $\frac{X}{R}$, as the network becomes more inductive, the sensitive pole shifts to the right slightly reducing the modal damping. The variation in $\frac{X}{R}$ ratio has however no effect on the frequency of the sensitive mode.

Figure 7-12. Variation of dominant eigen values for varying system $\frac{X}{R}$ ratio.

7.6.1.5　　Impact of system strength

The effect of system strength is evaluated by varying the short circuit ratio (SCR) at Bus 3 from 2 (weak system) to 12 (very strong system). In this study, the voltage controller bandwidth and plant level delay are set at 50 Hz and 0.5 s respectively. The $\frac{X}{R}$ ratio of feeder is 3. The result of this study is presented in Figure 7-13.
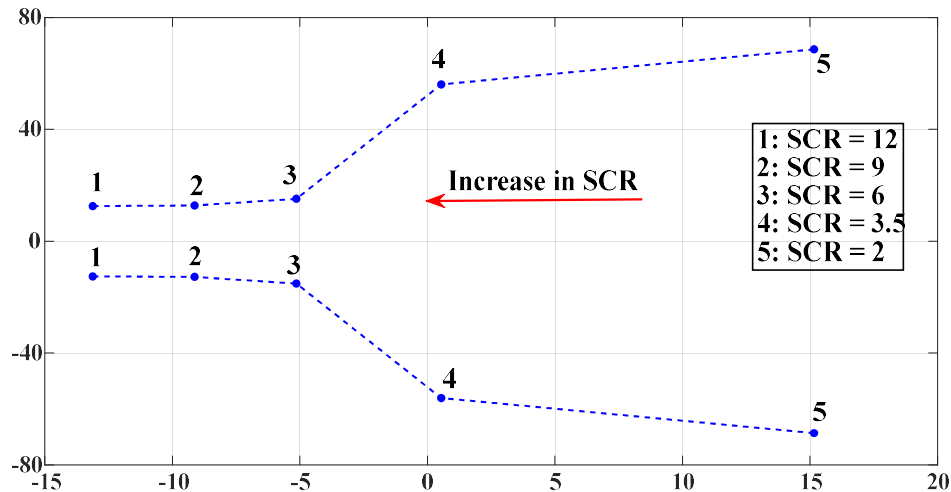
Figure 7-13. Variation of dominant eigen values for varying system strength.

Two pairs of poles are affected by variation in system strength. One pair of pole moves to the right reducing its stability with decreasing system strength. The other pair of pole shifts left with the reduction in system strength. For SCR less than 3.5, the first pair of pole moves to right half plane, causing unstable operation. The time domain response of the system with SCR =3 and delay = 0.5 s, for a step change in voltage reference is shown in Figure 7-14. This confirms that fast control at PLC can cause unstable operation in a weak system. The participation factor analysis of the unstable mode is depicted in Table 7.1. It is seen that this mode is caused due to interaction between the voltage controllers and delay of both PV plants. These results show that the speed of the controller should be reduced in a weak system to ensure stable operation.
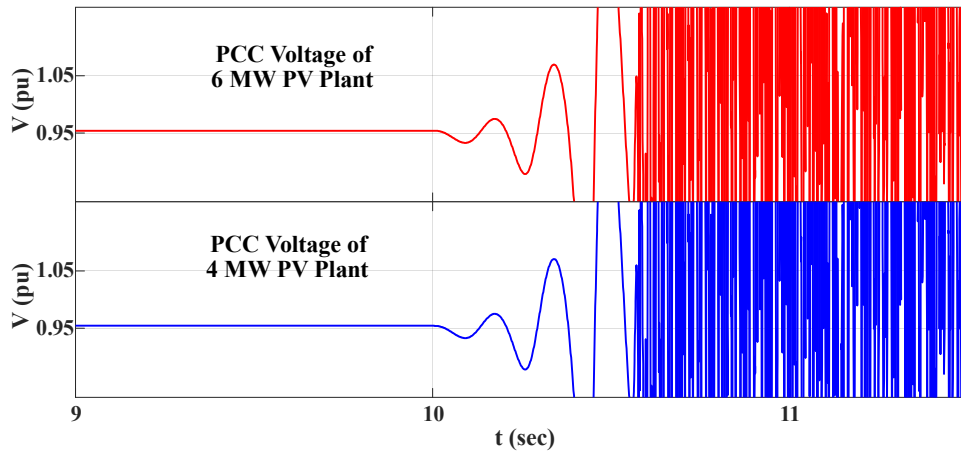
Figure 7-14. Both PV plant terminal voltages for a step change in Voltage reference in a system with SCR = 3.

Table 7.1. Participation factors of unstable mode.

Sl. No	State	Participation factor
1	Voltage controller of PV plant 1	14.19%
2	Delay of Voltage Controller of PV plant 1	13.83%
3	Voltage controller of PV plant 1	22.24%
4	Delay of Voltage Controller of PV plant 1	21.67%

7.6.1.6   Impact of distance between PV plants

The effect of distance between the PV plants on system stability is assessed by varying the distance between them and the results are illustrated in Figure 7-15. The total length of the study feeder is 45 km. The distance between the PV plants is varied between 2.5 km to 32.5 km to cover as wide range of distance as possible. The SCR at Bus 3 is kept constant in this study by not varying the length of feeder between Bus 1 and Bus 3 of Figure 7-1.

In this study, the voltage controller bandwidth and plant level delay are set at 50 Hz and 1 s, respectively. The $\frac{X}{R}$ ratio of feeder and SCR at bus 3 are kept at 3 and 3, respectively.
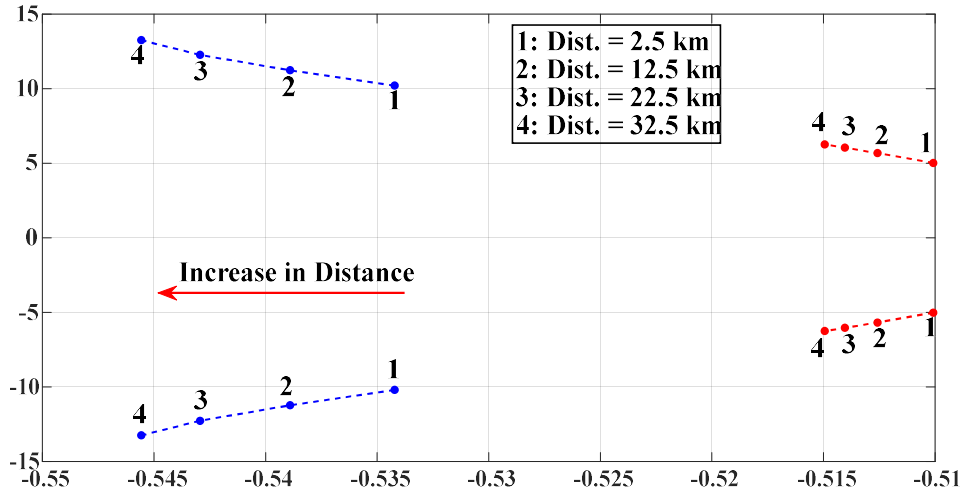
Figure 7-15. Variation of dominant eigen values for varying distance between PV plants.

Two sensitive poles shift rightwards with reduction in distance between the PV plants. This shows that the two PV plants will tend to interact adversely as the distance between them decreases.

7.6.2   PV-STATCOM control performed at Inverter level

The interactions between adjacent PV plants; and the influence of system and PV plant parameters when the proposed PV-STATCOM control is implemented at inverter level control (ILC), is studied in this section. In ILC, each inverter does the voltage control at its PCC, autonomously. In this study, the speed of all voltage controllers is kept at same value.

7.6.2.1   Impact of Speed of Voltage Controller

The bandwidth of the voltage controller is varied between 50 Hz– 5 Hz to study the impact of speed of voltage controllers on the interaction between PV plants. In this study, the $\frac{X}{R}$ ratio of feeder and SCR at bus 3 are kept at 3 and 3 respectively. The distance between PV plants is 5 km. The results are depicted in Figure 7-16.
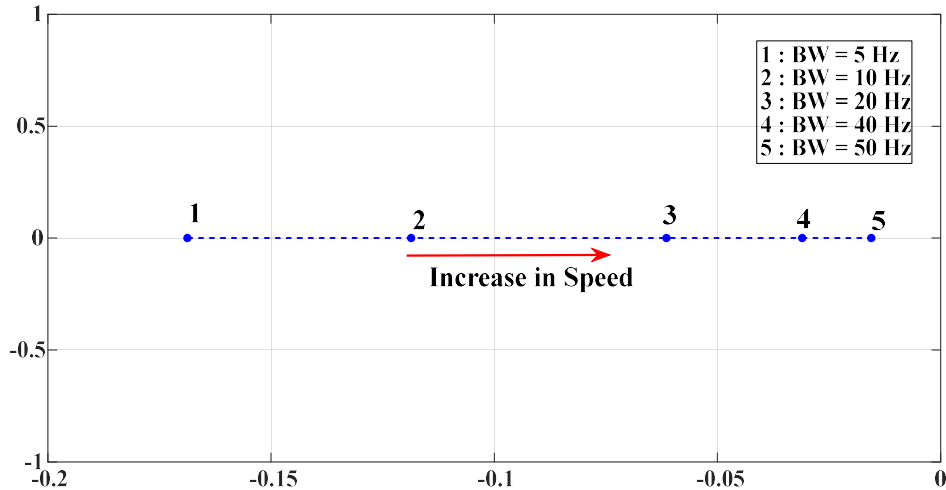
Figure 7-16. Variation of dominant eigen values for varying speed of voltage controller.

It is seen that as the controller speed increases the dominant poles shift rightwards reducing system stability. A slower voltage controller ensures more stable operation. Thus, the speed (bandwidth) of the voltage controller should be designed considering this stability issue.

Table 7.2. Participation factor of dominant mode for PV-STATCOM control done at inverter level.

Sl. No	State	Participation factor
1	Voltage controller of inverter 1 of PV plant 1	20.95%
2	Voltage controller of inverter 2 of PV plant 1	20.95%
3	Voltage controller of inverter 3 of PV plant 1	21.02%
4	Voltage controller of inverter 1 of PV plant 2	18.52%
5	Voltage controller of inverter 2 of PV plant 2	18.56%

The participation factor analysis of the sensitive mode shows that this mode is affected by all the five voltage controllers almost equally, as shown in Table 7.2. It is expected that the interaction between the voltage controllers within the plant will be higher compared to the interaction between the voltage controllers of different PV plants. This is because the voltage controllers within the plant are located more closely, and their voltage regulating terminals are separated by only by short collector cables. This participation factor analysis shows that even if PV plants are located 5 km apart, the inverter level voltage controllers of adjacent voltage controllers tend to adversely interact each other. Thus, the design of the inverter level controllers should be done considering this interaction between plants to ensure stable operation.

7.6.2.2   Impact of varying PV Power

The sensitivity of the critical system poles to variation of PV plant output active power is studied in this section. The different cases of PV power levels considered in this study are: (i) when both PV plant are producing high amount of power (0.9 pu), (ii) when both are producing 0.5 pu power, (iii) night time operation (zero active power), (iv) partial shading on 6 MW PV plant, (v) partial shading on 4 MW PV plant. Similar to PV-STATCOM control implemented at PLC, the PV active power output has no significant effect on stability when the control is done at ILC. The response is identical to Figure 7-11, and thus not shown here.

7.6.2.3   Impact of feeder $\frac{X}{R}$ ratio

The $\frac{X}{R}$ ratio of the feeder is varied between one to five, to assess the impact of $\frac{X}{R}$ ratio, and the results are illustrated in Figure 7-17. In this study, the SCR at bus 3 is 3. The distance between PV plants is 5 km, and the voltage controller bandwidth is 50 Hz.

When the control is done at inverter level, a pole moves left with increase in $\frac{X}{R}$ ratio. The variation of $\frac{X}{R}$ ratio has a very small impact on the dominant pole.

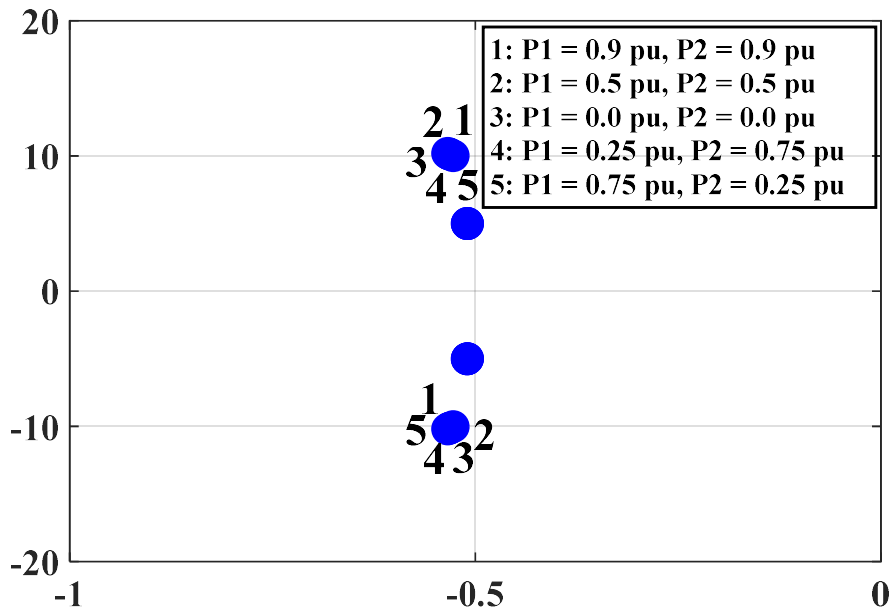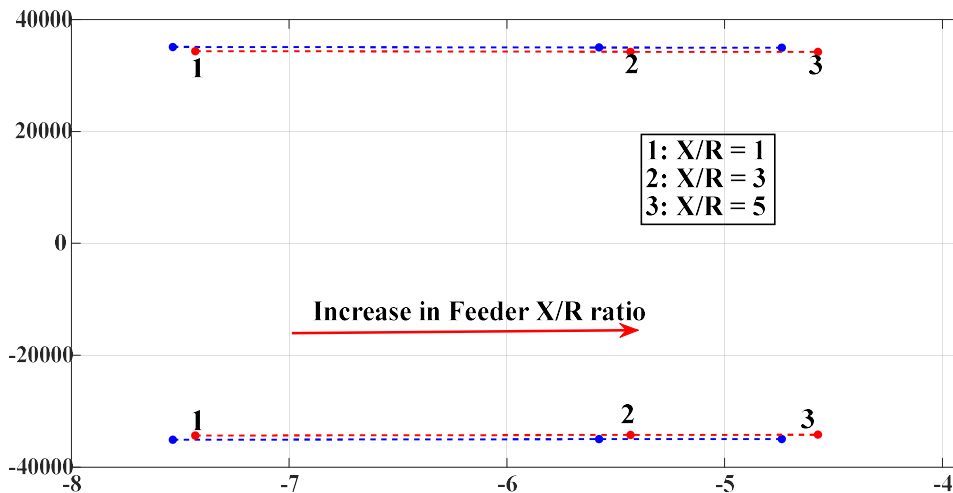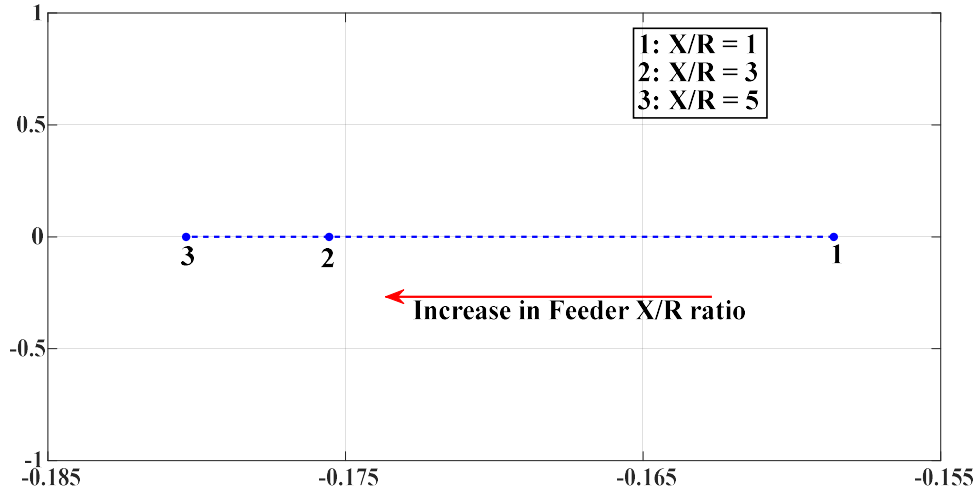**Figure 7-17. Variation of dominant eigen values for varying X/R ratio**

7.6.2.4   Impact of system strength

The effect of system strength on the interaction for ILC is done by varying the SCR between 2 (weak system) and 12 (strong system). In this study, the $\frac{X}{R}$ ratio of the feeder is 3. The distance between PV plants is 5 km, and the voltage controller bandwidth is 50 Hz. The results of this study are presented in Figure 7-18.
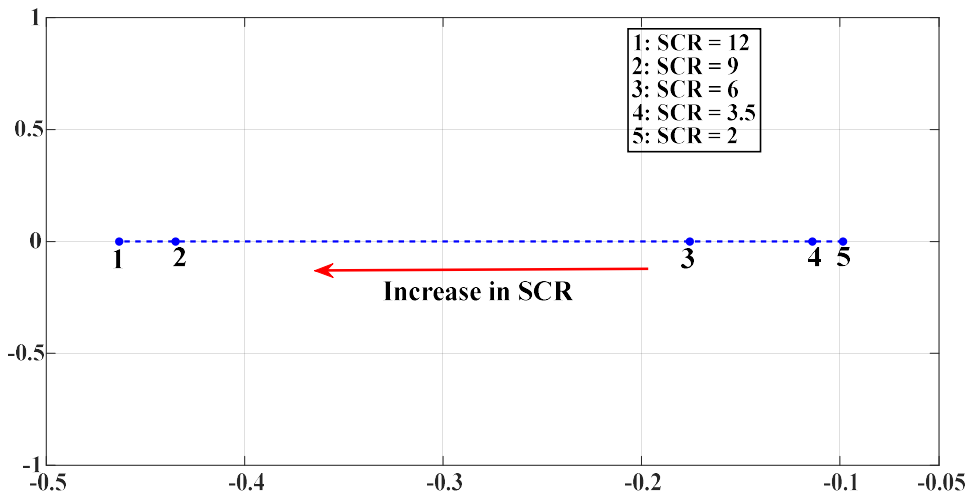
Figure 7-18. Variation of dominant eigen values for varying system strength.
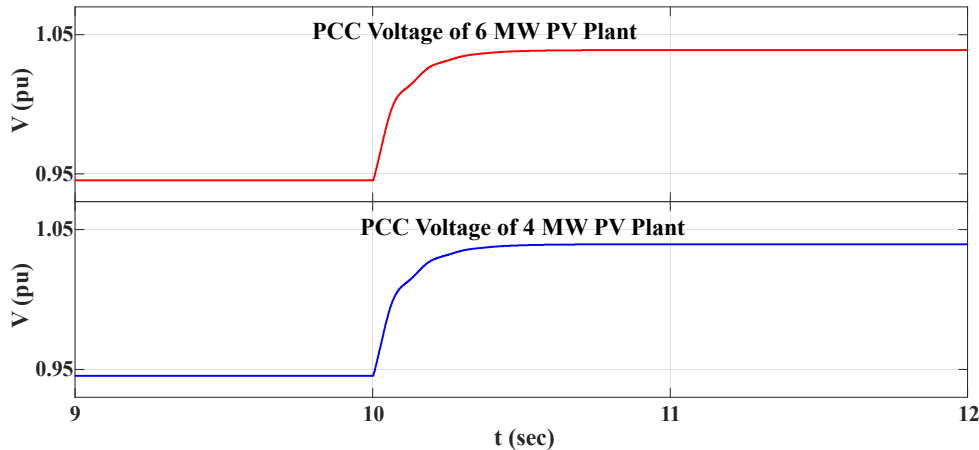
Figure 7-19. Terminal Voltages of both PV plants for a step change in Voltage reference for SCR = 3, at Bus 3.

The inverter level control is more stable in a stronger system. The stability reduces as the system strength is decreased. In ILC, the system is stable for all the values of SCR considered, whereas the system become unstable for SCR less than 3.5 in plant level control.

The POI voltage of both PV plants for a step change in voltage reference for SCR =3, is shown in Figure 7-19. Comparing the eigen values and time domain response of both ILC and PLC, it can be concluded that in a weaker system the PLC control can causes unstable operation, whereas ILC can ensure stable operation for the same speed of response, even in a system with low SCR.

7.6.2.5   Impact of distance between PV plants

The effect of distance between the PV plants on the interaction between PV-STATCOM controllers is assessed by varying the distance between them. The result is illustrated in Figure 7-20. The total length of the feeder considered is 45 km, and the distance between the PV plants are varied between 2.5 km to 32.5 km to cover the widest possible range of distance in the study system. The SCR at Bus 3 is kept constant in this study by not varying the length of feeder between Bus 1 and Bus 3 of Figure 7-1.

In this study, the $\frac{X}{R}$ ratio of the feeder is 3. The SCR at Bus 3 is 6, and the voltage controller bandwidth is 50 Hz.
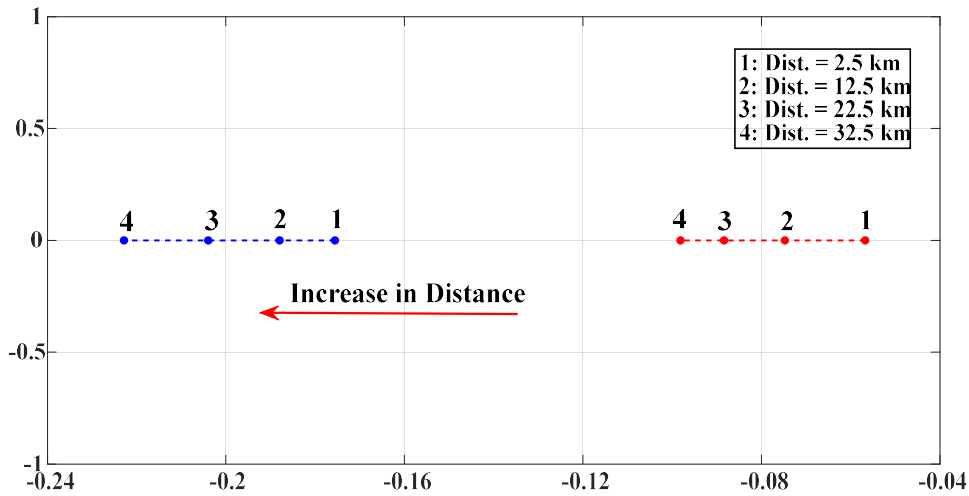
Figure 7-20. Variation of dominant eigen values for varying distance between PV plants.

It is seen that the PV plants tend to interact adversely as their distance between them decreases.

7.7 Summary of impact of various parameters on location of PV-STATCOM control.

The summary of the impact of key parameters on the performance of the two PV plants when the PV-STATCOM control is performed at plant level and inverter level, is presented in Table 7.3.

Table 7.3. Impact of various parameters on location of PV-STATCOM control

Sl. No	Parameter	PV-STATCOM at plant level	PV-STATCOM at inverter level
1	Speed of Controller	Stability reduces with faster control	Stability reduces with faster control

2	$\frac{X}{R}$ ratio of the feeder	Critical pole is affected slightly	Critical pole is affected slightly
3	System Strength	Tends to become unstable in a weak system	Stable in even weak system
4	Distance between the PV plants	Interaction increases with closeness	Interaction increases with closeness

7.8 Conclusion

The stability analysis of two PV-STATCOMs connected to a medium voltage realistic feeder is presented. The study system comprises of a 6 MW and 4 MW PV plants connected in a 45 km realistic feeder in Ontario, Canada, feeding 5.3 MVA load at 0.9 power factor.

Initial studies are done using detailed model and equivalent model of PV plant for Volt-Var control to compare the application of detailed and equivalent PV Plant model for stability analysis. Studies shows that if equivalent model is used for controller design, it will result in undesirable slowdown of controller. Thus, it is recommended to use detailed model.

The stability analysis of the PV plants for PV-STATCOM control implemented at plant level and inverter level are done. The influence of different parameters on stability is further done. The small signal analysis showed that

(i) If the controller is implemented at plant level, the controller could become unstable in a weak system, whereas inverter level control can ensure stable operation even in a system with low SCR.

(ii) Two critical modes are influenced by the plant level delay. One tends to become unstable with increase in delay, whereas other become stable with increase in delay. Thus, based on the studies performed, impact of delay should be analyzed system by system case.

Chapter 8

8 Conclusions and Future Work

Induction motors (IM) are globally used in several critical operations such as petrochemicals, mining, process control, etc., where their shutdown, even temporarily, during system faults can cause significant financial loss to industries. System faults can also lead to Fault Induced Delayed Voltage Recovery (FIDVR) causing service disruption to a large number of customers. Dynamic reactive power compensators such as SVC and STATCOM are conventionally employed to mitigate these issues, however, these devices are very expensive.

PV solar plants are growing at an unprecedented rate globally and are quite likely to be installed near such critical motors. This thesis presents several novel applications of a patented technology of utilizing PV solar plants, both during night and day, as STATCOM, termed PV-STATCOM, for mitigating above issues at about 50 times lower cost than equivalent-size STATCOMs.

A reactive power modulation based PV-STATCOM control is developed to stabilize remotely located critical motor both during night and day in a realistic distribution feeder in Ontario. The performance of the proposed control is compared with reactive power support proposed in the pioneering German Grid code. This control is field demonstrated for first time in Canada (and perhaps in world) on the 10 kW PV solar system connected in the utility network of Bluewater Power Distribution Corporation, Sarnia, Ontario.

Another novel control strategy based on active and reactive power modulation of PV-STATCOM is developed. Its effectiveness compared to a simple reactive power based PV-STATCOM control in a realistic utility network is investigated through MATLAB and PSCAD simulation studies.

A new real and reactive power control of PV-STATCOM is proposed to alleviate FIDVR. The efficacy of the proposed PV-STATCOM control on solar farm located 100 km away from a cluster of motors in a realistic transmission network is studied. The PV-

STATCOM capability is examined for a wide range of system parameters and operating conditions through Electromagnetic Transients simulation studies using PSCAD software.

A comprehensive sensitivity and stability analysis of single and two PV-STATCOMs connected to a distribution network is performed with: i) equivalent and detailed PV-STATCOM model, and ii) PV-STATCOM control implemented both at plant level and inverter level. The effectiveness of detailed modeling and controller location, and impact of different parameters causing adverse interaction, are investigated.

8.1   Modeling of Grid Connected PV System

A detailed nonlinear model of a PV solar farm is presented in Chapter 2. The modeling of various components of PV system viz., solar panels, inverter, filter, transformer, collector cables, etc., is described. The design procedure for various components is presented. The overview of the novel PV-STATCOM controller is presented and the design of controllers of its various control units is described. The detailed and equivalent models of utility scale PV solar farm are introduced and the procedure for designing various components of the equivalent model is presented.

8.2   PV-STATCOM Control for Stabilizing a Remote Critical Induction Motor

In chapter 3, a novel reactive power control of PV-STATCOM for stabilizing a remote critical induction motor is presented. The developed control provides enhanced voltage support utilizing the transient overvoltage voltage limit, and thus helps in fast recovery of induction motor voltage. The proposed controller provides a new fast active power ramp-up with simultaneous dynamic voltage control. Extensive simulation studies on the 10 kW PV solar farm connected in the utility network of Bluewater Power Distribution Corporation, Sarnia, shows that the proposed control can ensure stable operation of the critical IM, even for cases in which reactive power support according to German Grid Code fails to stabilize the motor. The remotely located PV-STATCOM control is as effective as a locally connected STATCOM at IM terminal. The proposed PV-STATCOM control can thus eliminate the need for installing an expensive STATCOM for IM stabilization.

Simulation studies on a realistic 27.6 kV distribution feeder in Ontario, shows that the proposed PV-STATCOM controller can ensure stable operation of a remote IM, even if located 20 km away, for a wide range of system strengths, feeder X/R ratios, distances between PV plant and IM, and voltage sag depths.

8.3   Night and Day Field Demonstration of PV-STATCOM Technology for Stabilizing Critical Induction Motor

Chapter 4 presents the first time in Canada (and first in the world, to the best of author's knowledge) night and day field demonstration of the patented PV-STATCOM technology. The PV-STATCOM technology is demonstrated on a 10 kW PV solar farm connected to the utility network of Bluewater Power Distribution Corporation, Sarnia, Canada.

The German Grid Code [93], which is the pioneering grid code for smart inverters, requires dynamic reactive power support during low voltage ride through, whereas it is optional in the recently adopted IEEE 1547- 2018. Simulation and field studies show that the PV-STATCOM can stabilize a 5 hp induction motor located 16 km away from the PV solar farm, whereas reactive power support by PV solar farm according to the German Grid Code fails to do so.

The PV-STATCOM control is shown to be effective even with a large 750 ms delay in communication of motor terminal voltage signal to PV solar farm location, which is 7 times more than the communication delay in real conditions. The application of PV-STATCOM to stabilize the critical induction motor is demonstrated for both day and night. It is shown that PV-STATCOM can provide dynamic voltage control in 1-2 cycles, which is identical to the speed of response of commercial STATCOMs. With the proposed PV-STATCOM control, active power can be ramped up to its pre disturbance level within 3 cycles after the recovery of motor voltage.

8.4   Coordinated Active and Reactive Power Control of PV-STATCOM for Stabilizing a Remote Critical Induction Motor

A novel control strategy for PV-STATCOM using combined active and reactive power modulation is presented in Chapter 5. The control strategy proposed in Chapter 3 is modified and a patented control based on active and reactive power modulation is presented in this chapter. The controller measures the sensitivity of motor terminal voltage to injection of active power and reactive power by PV-STATCOM, at regular intervals. During a disturbance, the PV-STATCOM provides real and reactive power according to the latest measured sensitivities, PV solar farm active power output and terminal voltage of PV inverters. Extensive simulation studies using a realistic model of utility scale PV solar farm, including communication delays, shows that the combined real and reactive power control of PV-STATCOM can ensure a fast recovery of motor terminal voltage. The combined active and reactive support can provide enhanced voltage recovery as compared to reactive power support alone.

The simulation studies using a detailed model of PV solar farm further showed that implementation of proposed PV-STATCOM control at inverter level can minimize the amount of active power curtailed and can avoid over voltage at inverter terminal. Whereas, implementation at plant level can cause over voltage at inverter terminal and require more active power curtailment.

Small signal studies of a medium sized utility scale PV plant connected to distribution system, with PV-STATCOM control done at inverter level shows that the system is more stable for: i) system with higher X/R ratio, ii) system with higher strength (short circuit level), and iii) maximum distance between inverters in the PV plant.

8.5   Mitigation of Fault Induced Delayed Voltage Recovery (FIDVR) by PV-STATCOM

A novel control strategy based on the dynamic modulation of active and reactive power of PV-STATCOM for mitigation of FIDVR in a cluster of induction motors located about 100 km away, is presented in this chapter. The proposed control strategy is based on

the modulation of real and reactive power during daytime and modulation of reactive power during night. The controller modulates active and reactive power according to the sensitivity of the solar plant voltage for active and reactive power output of PV plant. The PV-STATCOM provides dynamic voltage support in three modes which are decided based on PV plant terminal voltage, active power output of PV plant, and PV inverter terminal voltage.

Extensive simulation studies using the equivalent model of a 75 MW PV solar farm connected to a 138 kV transmission network, shows that the proposed PV-STATCOM control can mitigate FIDVR, and is more effective than i) reactive power support per German Grid Code, and ii) active and reactive power modulation in 1:1 ratio, as proposed in recent literature.

This study shows that the proposed PV-STATCOM control: i) provides a better performance than German Grid Code, and ii) eliminates the need of local STATCOM for achieving the same objective, bringing substantial cost-saving.

8.6   Stability Analysis of Two PV-STATCOMs

This chapters presents the stability analysis of two PV-STATCOMs connected to a realistic 27.6 kV distribution feeder in Ontario, Canada. The suitability of equivalent and detailed model of a utility scale PV solar plant for stability analysis is investigated. A power system which is demonstrated to be stable using detailed PV system model is shown as unstable by use of equivalent model. It is therefore recommended that detailed model be used for controller design.

Stability analysis of PV-STATCOM control implemented both at Plant level and Inverter level are performed and the sensitivities of both the controllers to system parameters is studied. For both cases, stability reduces with faster control. For both implementations, the system is more prone to adverse control interaction when the distance between PV plants decreases.

The PV-STATCOM control when implemented at Plant level may result in unstable operation in weak systems with low system strength (SCR), whereas PV-STATCOM

controller implemented at Inverter level ensures stable operation even in such weak systems. Two critical modes are affected by the variation of plant communication delay, and display opposite stability behavior with increasing delay. One mode becomes unstable with decreasing delay while the other becomes unstable with increasing delay. Thus, the impact of plant level delay on system stability should be analyzed on system by system basis.

8.7 Discussion

- The PV-STATCOM is a new smart inverter as it provides real and reactive power modulation per the definition of smart inverters, but:

  i)   responds within 1-2 cycles (less than 33 msec) whereas conventional smart inverters (volt-var, volt-watt control, etc.) respond in 1-2 seconds, and

  ii)   provides dynamic reactive power modulation during night, which conventional smart inverters do not, and

  iii)   performs dynamic voltage control during power ramp-up resulting in faster ramping operation. The present grid codes and Standards do not envisage such a voltage control.

- The PV-STATCOM is indeed a new Flexible AC Transmission System (FACTS) device, as it performs dynamic voltage control with the same response speed as actual STATCOM and mitigates FIDVR in the same manner as STATCOM.

- The PV-STATCOM is however, about 50-100 times less costly than an equivalent sized STATCOM or SVC.

A solar farm mainly comprises: i) PV modules, ii) Voltage source converters (VSCs) i.e., inverters, and iii) its associated electrical/civil infrastructure (substation, transformer, switchgear, buswork, protection systems, etc.). On the other hand, an equivalent sized STATCOM essentially consists of: i) VSCs and ii) its associated electrical/civil infrastructure which is quite similar to that of a PV solar farm. If a utility has identified the need for installing a STATCOM, and if a similar size PV solar farm is available nearby, only an additional PV-STATCOM controller with its measurement circuitry needs to be installed on the existing VSCs of the solar farm to transform it into a STATCOM. This expense is very small considering that the cost of VSCs

hardware and their control system is only about 5-8% of the entire solar plant cost. The plant level control also constitutes 1-2% of the total PV plant cost. This makes a PV-STATCOM almost 50 times lower cost than an equivalent sized STATCOM.

- The proposed PV-STATCOM control can:

    i)   bring significant saving for utilities by reducing the need for expensive STATCOMs or SVCs for FIDVR mitigation and critical IM support, and

    ii)   opens new revenue making opportunities for solar plants for providing critical motor stabilization service and FIDVR mitigation on a 24/7 basis.

8.8   Contributions

- The application of a patented novel control of PV solar plants as a dynamic reactive power compensator STATCOM, termed, PV-STATCOM, is presented for stabilizing a remotely located critical induction motor on a 24/7 basis, over widely varying system conditions.

    Such a novel smart inverter control to provide dynamic reactive power support to remotely located critical induction motor is not available in the literature to the best of author's knowledge.

- The night and day application of PV-STATCOM technology to stabilize a remote critical induction motor is field-demonstrated on a 10 kW PV solar farm in the utility network of Bluewater Power Distribution Corporation Sarnia, Canada.

    The field demonstration of PV solar farm as PV-STATCOM to provide dynamic reactive power support is demonstrated on a utility network for the first time in Canada (and most likely the first time in world) to the best of author's knowledge.

- A novel control strategy based on the active and reactive power modulation of PV-STATCOM to provide dynamic voltage support to stabilize a remote critical induction motor is presented.

Such control of active and reactive power output of a PV solar farm considering the existing sensitivities of bus voltage to PV active and reactive power injections is not reported in literature before to the best of author's knowledge.

- A control strategy based on real and reactive power modulation of PV solar farm as PV-STATCOM to mitigate FIDVR in a cluster of induction motor loads located about 100 km away in a transmission network is proposed. The PV-STATCOM replaces the need of a new expensive STATCOM by almost half.

This control demonstrates for the first time that PV solar plants can reduce the need for actual STATCOMs and SVCs that are employed for mitigation of FIDVR.

- Comprehensive sensitivity and stability analysis of single and two distribution level PV-STATCOMs are performed with: i) equivalent and detailed PV-STATCOM model, and ii) PV-STATCOM control implemented at plant level and inverter level. The impact of modeling details, controller location and system parameters on controller interaction, are investigated.

Such a detailed stability analysis of PV plants and their control interactions have not been performed earlier to the best knowledge of author.

8.9 Publications

Journal papers

1. R. K. Varma, E. M. Siavashi, **S. Mohan** and T. Vanderheide, "First in Canada, Night and Day Field Demonstration of a New Photovoltaic Solar Based Flexible AC Transmission System (FACTS) Device PV-STATCOM for Stabilizing Critical Induction Motor," in *IEEE Access,* vol. 7, pp. 149479-149492, 2019.

2. R. K. Varma, S. A. Rahman, V. Atodaria, **S. Mohan** and T. Vanderheide, "Technique for Fast Detection of Short Circuit Current in PV Distributed Generator," in *IEEE Power and Energy Technology Systems Journal*, vol. 3, no. 4, pp. 155-165, Dec. 2016.

3. R. K. Varma, and **S. Mohan**, " Mitigation of Fault Induced Delayed Voltage Recovery (FIDVR) by PV-STATCOM," in *IEEE Trans. on Power Systems* (under review).

4. R. K. Varma, **S. Mohan** and T. Vanderheide, " Solar Farm control as PV-STATCOM for stabilization of Remote Critical Induction Motor," Paper ready to be submitted to *IEEE Journal on Photovoltaics*.

5. R. K. Varma, **S. Mohan** and T. Vanderheide, "Coordinated Active and Reactive Power control of PV-STATCOM for stabilization of Remote Critical Induction Motor," Paper ready to be submitted to *IEEE Access*.

Conference Papers:

1. Rajiv K. Varma, Ehsan Siavashi, **S. Mohan**, Hesamaldin Maleki, Sridhar Bala Subramanian, and Tim Vanderhide, "First in Canada Field demonstration of Night time motor stabilization by PV solar farm as PV-STATCOM", Proc. 2018 Solar Power International Conference, Anaheim, USA, Sep. 2018

2. **S. Mohan**, S. Hasan, Y. Gebremariam and R. K. Varma, "Increasing Hosting Capacity of PV Solar Systems using Smart Inverter Volt-Var Control," 2018 20th National Power Systems Conference (NPSC), Tiruchirappalli, India, 2018, pp. 1-6.

3. Rajiv K. Varma, Ehsan Siavashi, Hesamaldin Maleki, Reza Salehi, **S. Mohan**, Mahendra A.C., S. Arifur Rahman and T. Vanderheide, "PV-STATCOM: A Novel Smart Inverter for Transmission and Distribution System Applications", 7th International Conference on Integration of Renewable and Distributed Energy Resources", Niagara Falls, Canada, Oct. 24-28, 2016

4. Rajiv K. Varma and **S. Mohan**, "New PV Solar Farm Control as STATCOM (PV-STATCOM) for Stabilization of a Critical Motor Load", Proc. 2015 Solar Power International Conference, Anaheim, USA, Sep. 2015.

5. **S. Mohan**, and R. K. Varma, " Stability Analysis of Two PV power plants while providing Plant Level Voltage Control," Submitted for 2020 PES General Meeting, Montreal, Canada.

8.10 Future Work

Some of the work that can be carried out as part of future research is provided below:

- Development of a control strategy to provide dynamic voltage support using PV-STATCOM during unbalanced faults; and its field demonstration.

- Detailed analysis of interaction between inverters in the same plant and interaction between multiple PV plants using the small signal model developed.

- Development of a coordination strategy for PV-STATCOMs with wind plants and other FACTS devices in electrical proximity.

- Field demonstration of PV-STATCOM technology on a utility scale PV plant with multiple inverters, to study the behavior of such a large PV plant with the proposed PV-STATCOM control.

- Study of the impact of PV-STATCOM to mitigate FIDVR in a series compensated long transmission lines.

References

[1] B. Lesieutre, *et al.*, "Final Project Report Load Modeling Transmission Research," Lawrence Berkeley National Laboratory, California, 2010.

[2] J. Eto. *et al.*, "US DOE Workshop on the Role of Residential AC in Contributing to Fault-Induced Delayed Voltage Recovery (FIDVR)", 2008.

[3] J. Eto. *et al.*, 2015 Workshop on Fault-Induced Delayed Voltage Recovery (FIDVR) & Dynamic Load Modeling., 2015.

[4] R. J. Bravo, R. Yinger, and P. Arons, "Fault Induced Delayed Voltage Recovery (FIDVR) indicators," in *2014 IEEE PES T&D Conference and Exposition*, 2014, pp. 1-5.

[5] NERC, "A Technical Reference Paper Fault-Induced Delayed Voltage Recovery," NERC, Princeton, 2009.

[6] EPRI, "The Cost of Power Disturbances to Industrial and Digital Economy Companies," Electric Power Research Institute, California, 3002000476, Mar 2013.

[7] O. V. Thorsen and M. Dalva, "A survey of faults on induction motors in offshore oil industry, petrochemical industry, gas terminals, and oil refineries," *IEEE Transactions on Industry Applications,* vol. 31, pp. 1186-1196, 1995.

[8] A. A. Mahmoud, T. H. Ortmeyer, R. G. Harley, and C. Calabrese, "Effects of Reactive Compensation on Induction Motor Dynamic Performance," *IEEE Transactions on Power Apparatus and Systems,* vol. PAS-99, pp. 841-846, 1980.

[9] N. G. Hingorani and L. Gyugyi, *Understanding FACTS*. New York: IEEE Press, 1999.

[10] R. M. Mathur and R. K. Varma, *Thyristor-Based FACTS Controllers for Electrical Transmission Systems*. New York: Wiley-IEEE Press, 2002.

[11] R. M. Hamouda, M. R. Irvani, and R. Hackam, "Co-ordination of thyristor-controlled VAr compensator and auxiliary controller of excitation system for small signal stability enhancement," *Canadian Journal of Electrical and Computer Engineering,* vol. 14, pp. 55-62, 1989.

[12] M. O. Brien and G. Ledwich, "Static reactive-power compensator controls for improved system stability," *IEE Proceedings C - Generation, Transmission and Distribution,* vol. 134, pp. 38-42, 1987.

[13] C. A. Canizares and Z. T. Faur, "Analysis of SVC and TCSC controllers in voltage collapse," *IEEE Transactions on Power Systems,* vol. 14, pp. 158-165, 1999.

[14] I. A. Hiskens and C. B. McLean, "SVC behaviour under voltage collapse conditions," *IEEE Transactions on Power Systems,* vol. 7, pp. 1078-1087, 1992.

[15] Y. Mansour, X. Wilsun, F. Alvarado, and R. Chhewang, "SVC placement using critical modes of voltage instability," *IEEE Transactions on Power Systems,* vol. 9, pp. 757-763, 1994.

[16] A. J. P. Ramos and H. Tyll, "Dynamic performance of a radial weak power system with multiple static VAr compensators," *IEEE Transactions on Power Systems,* vol. 4, pp. 1316-1325, 1989.

[17] J. L. Sancha, J. L. Fernandez, A. Cortes, and J. T. Abarca, "Secondary voltage control: analysis, solutions and simulation results for the Spanish transmission system," *IEEE Transactions on Power Systems,* vol. 11, pp. 630-638, 1996.

[18] O. T. Tan and R. Thottappillil, "Static VAr compensators for critical synchronous motor loads during voltage dips," *IEEE Transactions on Power Systems,* vol. 9, pp. 1517-1523, 1994.

[19] G. Ledwich and T. A. George, "Negative-phase-sequence reduction with adjacent static reactive-power compensators," *IEE Proceedings - Electric Power Applications,* vol. 141, pp. 259-263, 1994.

[20] S. Lee and C. Wu, "Reactive power compensation and load balancing for unbalanced three-phase four-wire system by a combined system of an SVC and a series active filter," *IEE Proceedings - Electric Power Applications,* vol. 147, pp. 563-578, 2000.

[21] P. K. Dash, P. C. Panda, A. M. Sharaf, and E. F. Hill, "Adaptive controller for static reactive-power compensators in power systems," *IEE Proceedings C - Generation, Transmission and Distribution,* vol. 134, pp. 256-264, 1987.

[22] C. Jen-Hung, L. Wei-Jen, and C. Mo-Shing, "Using a static VAr compensator to balance a distribution system," *IEEE Transactions on Industry Applications,* vol. 35, pp. 298-304, 1999.

[23] I. Hosono, M. Yano, M. Takeda, S. Yuya, and S. Sueda, "Suppression and Measurement of Arc Furnace Flicker with a Large Static Var Compensator," *IEEE Transactions on Power Apparatus and Systems,* vol. PAS-98, pp. 2276-2284, 1979.

[24] B. T. Ooi and M. H. Banakar, "Co-Ordination of Static Var Compensators With Long Distance Radial Transmission System for Damping Improvement," *IEEE Power Engineering Review,* vol. PER-4, pp. 24-24, 1984.

[25] Y. Hsu and C. Wu, "Design of PID static VAr controllers for the damping of subsynchronous oscillations," *IEEE Transactions on Energy Conversion,* vol. 3, pp. 210-216, 1988.

[26] A. E. Hammad and M. El-Sadek, "Application of a Thyristor Controlled Var Compensator for Damping Subsynchronous Oscillations in Power Systems," *IEEE Transactions on Power Apparatus and Systems,* vol. PAS-103, pp. 198-212, 1984.

[27] E. Zhou, "Application of static VAr compensators to increase power system damping," *IEEE Transactions on Power Systems,* vol. 8, pp. 655-661, 1993.

[28] G. Wolf, T. Duane, and D. Martin, "Modifying Blackwater HVDC for voltage control capability without power transfers," *IEEE Transactions on Power Delivery,* vol. 14, pp. 1482-1487, 1999.

[29] O. B. Nayak, A. M. Gole, D. G. Chapman, and J. B. Davies, "Dynamic performance of static and synchronous compensators at an HVDC inverter bus in a very weak AC system," *IEEE Transactions on Power Systems,* vol. 9, pp. 1350-1358, 1994.

[30] Y. Xue and X. Zhang, "Reactive Power and AC Voltage Control of LCC HVDC System With Controllable Capacitors," *IEEE Transactions on Power Systems,* vol. 32, pp. 753-764, 2017.

[31] A. E. Hammad and M. Z. El-Sadek, "Prevention of transient voltage instabilities due to induction motor loads by static VAr compensators," *IEEE Transactions on Power Systems,* vol. 4, pp. 1182-1190, 1989.

[32] O. T. Tan, G. C. Paap, and M. S. Kolluru, "Thyristor-controlled voltage regulators for critical induction motor loads during voltage disturbances," *IEEE Transactions on Energy Conversion,* vol. 8, pp. 100-106, 1993.

[33] T. Lee, S. Hu, and Y. Chan, "D-STATCOM With Positive-Sequence Admittance and Negative-Sequence Conductance to Mitigate Voltage Fluctuations in High-Level Penetration of Distributed-Generation Systems," *IEEE Transactions on Industrial Electronics,* vol. 60, pp. 1417-1428, 2013.

[34] B. Blazic and I. Papic, "Improved D-StatCom control for operation with unbalanced currents and voltages," *IEEE Transactions on Power Delivery,* vol. 21, pp. 225-233, 2006.

[35] C. Hochgraf and R. H. Lasseter, "Statcom controls for operation with unbalanced voltages," *IEEE Transactions on Power Delivery,* vol. 13, pp. 538-544, 1998.

[36] A. Jain, K. Joshi, A. Behal, and N. Mohan, "Voltage regulation with STATCOMs: modeling, control and results," *IEEE Transactions on Power Delivery,* vol. 21, pp. 726-735, 2006.

[37] K. Li, J. Liu, Z. Wang, and B. Wei, "Strategies and Operating Point Optimization of STATCOM Control for Voltage Unbalance Mitigation in Three-Phase Three-Wire Systems," *IEEE Transactions on Power Delivery,* vol. 22, pp. 413-422, 2007.

[38] P. Rao, M. L. Crow, and Z. Yang, "STATCOM control for power system voltage control applications," *IEEE Transactions on Power Delivery,* vol. 15, pp. 1311-1317, 2000.

[39] P. S. Sensarma, K. R. Padiyar, and V. Ramanarayanan, "Analysis and performance evaluation of a distribution STATCOM for compensating voltage fluctuations," *IEEE Transactions on Power Delivery,* vol. 16, pp. 259-264, 2001.

[40] Q. Song and W. Liu, "Control of a Cascade STATCOM With Star Configuration Under Unbalanced Conditions," *IEEE Transactions on Power Electronics,* vol. 24, pp. 45-58, 2009.

[41] K. V. Patil, J. Senthil, J. Jiang, and R. M. Mathur, "Application of STATCOM for damping torsional oscillations in series compensated AC systems," *IEEE Transactions on Energy Conversion,* vol. 13, pp. 237-243, 1998.

[42] M. S. El-Moursi, B. Bak-Jensen, and M. H. Abdel-Rahman, "Novel STATCOM Controller for Mitigating SSR and Damping Power System Oscillations in a Series Compensated Wind Park," *IEEE Transactions on Power Electronics,* vol. 25, pp. 429-441, 2010.

[43] N. Mithulananthan, C. A. Canizares, J. Reeve, and G. J. Rogers, "Comparison of PSS, SVC, and STATCOM controllers for damping power system oscillations," *IEEE Transactions on Power Systems,* vol. 18, pp. 786-792, 2003.

[44] A. Ghosh and G. Ledwich, "Load compensating DSTATCOM in weak AC systems," *IEEE Transactions on Power Delivery,* vol. 18, pp. 1302-1309, 2003.

[45] Z. Saad-Saoud, M. L. Lisboa, J. B. Ekanayake, N. Jenkins, and G. Strbac, "Application of STATCOMs to wind farms," *IEE Proceedings - Generation, Transmission and Distribution,* vol. 145, pp. 511-516, 1998.

[46] S. W. Mohod and M. V. Aware, "A STATCOM-Control Scheme for Grid Connected Wind Energy System for Power Quality Improvement," *IEEE Systems Journal,* vol. 4, pp. 346-352, 2010.

[47] S. Bozhko, G. Asher, R. Li, J. Clare, and L. Yao, "Large Offshore DFIG-Based Wind Farm With Line-Commutated HVDC Connection to the Main Grid: Engineering Studies," *IEEE Transactions on Energy Conversion,* vol. 23, pp. 119-127, 2008.

[48] C. Han, A. Q. Huang, M. E. Baran, S. Bhattacharya, W. Litzenberger, L. Anderson*, et al.*, "STATCOM Impact Study on the Integration of a Large Wind Farm into a Weak Loop Power System," *IEEE Transactions on Energy Conversion,* vol. 23, pp. 226-233, 2008.

[49] "VarPro STATCOM Dynamic reactive power compensation Power quality solutions for heavy industry," ABB, New Berln, WI, USA, 2015.

[50] TMT&D, "STATCOM," Mistubishi Electric Power Products, Inc., Toyo, Japan.

[51] S. V. Kolluri, J. R. Ramamurthy, S. M. Wong, M. Peterson, P. Yu, and M. R. Chander, "Relay-based undervoltage load shedding scheme for Entergy's Western Region," in *2015 IEEE Power & Energy Society General Meeting*, 2015, pp. 1-5.

[52] H. Bai and V. Ajjarapu, "A Novel Online Load Shedding Strategy for Mitigating Fault-Induced Delayed Voltage Recovery," *IEEE Transactions on Power Systems,* vol. 26, pp. 294-304, 2011.

[53] A. Mahari and H. Seyedi, "A fast online load shedding method for mitigating FIDVR based on novel stability index," in *2013 21st Iranian Conference on Electrical Engineering (ICEE)*, 2013, pp. 1-6.

[54] W. Huang, K. Sun, J. Qi, and Y. Xu, "A new approach to optimization of dynamic reactive power sources addressing FIDVR issues," in *2014 IEEE PES General Meeting | Conference & Exposition*, 2014, pp. 1-5.

[55] M. Paramasivam, A. Salloum, V. Ajjarapu, V. Vittal, N. Bhatt, and S. Liu, "Dynamic optimization based reactive power planning to mitigate slow voltage recovery and short term voltage instability," in *2014 IEEE PES General Meeting | Conference & Exposition*, 2014, pp. 1-1.

[56] W. Huang, K. Sun, J. Qi, and Y. Xu, "Voronoi diagram based optimization of dynamic reactive power sources," in *2015 IEEE Power & Energy Society General Meeting*, 2015, pp. 1-5.

[57] W. Huang, K. Sun, J. Qi, and J. Ning, "Optimal Allocation of Dynamic Var Sources Using the Voronoi Diagram Method Integrating Linear Programing," *IEEE Transactions on Power Systems,* vol. 32, pp. 4644-4655, 2017.

[58] M. Paramasivam, A. Salloum, V. Ajjarapu, V. Vittal, N. B. Bhatt, and S. Liu, "Dynamic Optimization Based Reactive Power Planning to Mitigate Slow Voltage Recovery and Short Term Voltage Instability," *IEEE Transactions on Power Systems,* vol. 28, pp. 3865-3873, 2013.

[59] J. Qi, W. Huang, K. Sun, and W. Kang, "Optimal Placement of Dynamic Var Sources by Using Empirical Controllability Covariance," *IEEE Transactions on Power Systems,* vol. 32, pp. 240-249, 2017.

[60] G. Reed, B. Grainger, M. Kempker, P. Bierer, A. Such, R. Grubb*, et al.*, "Technical requirements and design of the Indianapolis power & light 138 kV southwest static var compensator," in *2016 IEEE/PES Transmission and Distribution Conference and Exposition (T&D)*, 2016, pp. 1-5.

[61] D. Sullivan, R. Pape, J. Birsa, M. Riggle, M. Takeda, T. Hitoshi*, et al.*, "Managing fault-induced delayed voltage recovery in Metro Atlanta with the Barrow County SVC," in *2009 IEEE/PES Power Systems Conference and Exposition*, 2009, pp. 1-6.

[62]   A. Boström, R. Grunbaum, M. Dahlblom, and H. V. Oheim, "SVC for reliability improvement in the NSTAR 115 kV cape cod transmission system," in *2013 IEEE Power & Energy Society General Meeting*, 2013, pp. 1-5.

[63]   S. Kolluri, M. Peterson, D. Mader, D. Sullivan, R. Hellested, J. Paramalingam*, et al.*, "Application of SVC in Entergy to Address FIDVR Problem," in *2018 IEEE/PES Transmission and Distribution Conference and Exposition (T&D)*, 2018, pp. 1-9.

[64]   I. A. Hamzah and J. A. Yasin, "Static Var compensators (SVC) required to solve the problem of delayed voltage recovery following faults in the power system of the Saudi electricity company, western region (SEC-WR)," in *2003 IEEE Bologna Power Tech Conference Proceedings*, 2003, p. 8 pp. Vol.4.

[65]   M. Du, M. Han, Z. Cao, F. Chu, and M. Ei-Kady, "Utilizing STATCON to Resolve Delayed Voltage Recovery Problem in SEC-WR," in *2009 Asia-Pacific Power and Energy Engineering Conference*, 2009, pp. 1-4.

[66]   A. H. Al-Mubarak, S. M. Bamsak, B. Thorvaldsson, M. Halonen, and R. Grunbaum, "Preventing voltage collapse by large SVCs at power system faults," in *2009 IEEE/PES Power Systems Conference and Exposition*, 2009, pp. 1-9.

[67]   A. H. Al-Mubarak, B. Thorvaldsson, M. Halonen, and M. Z. Al-Kadhem, "Hybrid and Classic SVC technology for improved efficiency and reliability in Saudi transmission grid," in *2014 IEEE PES T&D Conference and Exposition*, 2014, pp. 1-8.

[68]   A. H. Al-Mubarak, M. H. Khan, and M. Z. Al-Kadhem, "Dynamic Reactive Power Compensation for voltage support using Static VAR Compensator (SVC) In Saudi Arabia," in *2015 IEEE Electrical Power and Energy Conference (EPEC)*, 2015, pp. 484-490.

[69]   "United Nations Framework Convention On Climate Change :-Doha amendment to the Kyoto Protocol " 2013.

[70]   "*Solar Industry Data Solar Industry growing at a Record Pace*.", Accessed 5 Nov, 2018, Available: https://www.seia.org/solar-industry-data

[71]   "Snapshot of Global Photovoltaic Market 2018," International Energy Agency, 2018, Accessed 4 April, 2019.

[72]   S. Lacey, "*Global Solar Demand Monitor: Q2 2017",* Accessed 5 Nov, 2018. Available: https://www.greentechmedia.com/articles/read/global-solar-capacity-set-to-surpass-global-nuclear capacity#gs. ETy IUg

[73]   "Technology Roadmap: Solar Photovoltaic Energy," International Energy Agency, 2014.

[74]   "Renewable Energy in Canada," N. R. Canada, 2014.

[75] "*Installed Capacity of WInd Energy in Canada*", Accessed 18 March, 2018. Available: https://canwea.ca/wind-energy/installed-capacity/

[76] "*Canada's cumulative installed solar PV capacity 1992-2017*", Accessed 18 March, 2018. Available: https://www.statista.com/statistics/790547/cumulative-installed-solar-pv-power-capacity-in-canada/

[77] M. M. L. Bird, and D. Lew, "Integrating Variable Renewable Energy: Challenges and Solutions," 2013.

[78] M. H. Rashid, *Power Electronics Handbook*: Academic Press, 2001.

[79] R. I. Amirnaser Yazdani, *Voltage-Sourced Converters in Power Systems : Modeling, Control, and Applications*: Wiley, 2010.

[80] T. M. U. Ned Mohan, William P. Robbins, *Power Electronics: Converters, Applications, and Design*: Wiley, 2002.

[81] M. Liserre, F. Blaabjerg, and S. Hansen, "Design and control of an LCL-filter-based three-phase active rectifier," *IEEE Transactions on Industry Applications,* vol. 41, pp. 1281-1291, 2005.

[82] I. J. Gabe, V. F. Montagner, and H. Pinheiro, "Design and Implementation of a Robust Current Controller for VSI Connected to the Grid Through an LCL Filter," *IEEE Transactions on Power Electronics,* vol. 24, pp. 1444-1452, 2009.

[83] W. Cunping, Y. Xianggen, W. Minghao, L. Jian, X. Qing, and Z. Bin, "Structure and parameters design of output LC filter in D-STATCOM," in *Power System Technology (POWERCON), 2010 International Conference on*, 2010, pp. 1-6.

[84] M. A. Elgendy, B. Zahawi, and D. J. Atkinson, "Assessment of the Incremental Conductance Maximum Power Point Tracking Algorithm," *IEEE Transactions on Sustainable Energy,* vol. 4, pp. 108-117, 2013.

[85] M. A. G. d. Brito, L. Galotto, L. P. Sampaio, G. d. A. e. Melo, and C. A. Canesin, "Evaluation of the Main MPPT Techniques for Photovoltaic Applications," *IEEE Transactions on Industrial Electronics,* vol. 60, pp. 1156-1167, 2013.

[86] R. M. Linus and P. Damodharan, "Maximum power point tracking method using a modified perturb and observe algorithm for grid connected wind energy conversion systems," *IET Renewable Power Generation,* vol. 9, pp. 682-689, 2015.

[87] "WECC Solar Plant Dynamic Modeling Guidelines", WECC Renewable Energy Modeling Task Force, June 2014.

[88] "Demonstration of Essential Reliability Services by a 300 MW Solar Photovoltaic Power Plant," NREL, NREL/TP-5D00-67799, 2017.

[89] "Common Functions for Smart Inverters 4th Edition," Electric Power Research Institute, California 3002008217, Dec. 2016.

[90] "IEEE Standard for Interconnection and Interoperability of Distributed Energy Resources with Associated Electric Power Systems Interfaces," *IEEE Std 1547-2018 (Revision of IEEE Std 1547-2003),* pp. 1-138, 2018.

[91] "Technical Guideline: - Generating Plants Connected to the Medium-Voltage Network," BDEW, 2008.

[92] "Rule 21: -Generating Facility Interconnections," S. C. Edison, July 2014.

[93] B. Tamimi, C. Cañizares, and K. Bhattacharya, "Modeling and performance analysis of large solar photo-voltaic generation on voltage stability and inter-area oscillations," in *2011 IEEE Power and Energy Society General Meeting*, 2011, pp. 1-6.

[94] B. Tamimi, C. Cañizares, and K. Bhattacharya, "System Stability Impact of Large-Scale and Distributed Solar Photovoltaic Generation: The Case of Ontario, Canada," *IEEE Transactions on Sustainable Energy,* vol. 4, pp. 680-688, 2013.

[95] B. Bletterie, S. Kadam, R. Bolgaryn, and A. Zegers, "Voltage Control with PV Inverters in Low Voltage Networks—In Depth Analysis of Different Concepts and Parameterization Criteria," *IEEE Transactions on Power Systems,* vol. 32, pp. 177-185, 2017.

[96] X. Su, M. A. S. Masoum, and P. Wolfs, "Comprehensive optimal photovoltaic inverter control strategy in unbalanced three-phase four-wire low voltage distribution networks," *IET Generation, Transmission & Distribution,* vol. 8, pp. 1848-1859, 2014.

[97] S. Hashemi and J. Østergaard, "Methods and strategies for overvoltage prevention in low voltage distribution systems with PV," *IET Renewable Power Generation,* vol. 11, pp. 205-214, 2017.

[98] R. J. Bravo, "DER volt-VAr and voltage ride-through needs to contain the spread of FIDVR events," in *2015 IEEE Power & Energy Society General Meeting*, 2015, pp. 1-3.

[99] E. Z. Abdel-Aziz, J. Ishaq, A. M. Al-Khulayfi, and Y. T. Fawzy, "Voltage stability improvement in transmission network embedded with photovoltaic systems," in *2016 IEEE International Energy Conference (ENERGYCON)*, 2016, pp. 1-7.

[100] G. Lammert, J. C. Boemer, D. Premm, O. Glitza, L. D. P. Ospina, D. Fetzer*, et al.*, "Impact of fault ride-through and dynamic reactive power support of photovoltaic systems on short-term voltage stability," in *2017 IEEE Manchester PowerTech*, 2017, pp. 1-6.

[101] K. Kawabe, Y. Ota, A. Yokoyama, and K. Tanaka, "Novel Dynamic Voltage Support Capability of Photovoltaic Systems for Improvement of Short-Term Voltage Stability in Power Systems," *IEEE Transactions on Power Systems,* vol. 32, pp. 1796-1804, 2017.

[102] Q. C. Zhong and G. Weiss, "Synchronverters: Inverters That Mimic Synchronous Generators," *IEEE Transactions on Industrial Electronics,* vol. 58, pp. 1259-1267, 2011.

[103] N. N. F. Norhasmi, S. K. Raveendran, and V. K. Ramachandaramurthy, "Power Factor Control of Solar Photovoltaic Inverter as a Solution to Overvoltage," in *2018 IEEE PES Asia-Pacific Power and Energy Engineering Conference (APPEEC)*, 2018, pp. 751-756.

[104] M. N. Muhtazaruddin and G. Fujita, "Voltage control in PV grid connected mode for overvoltage reduction," in *2012 IEEE International Conference on Power System Technology (POWERCON)*, 2012, pp. 1-4.

[105] S. Pukhrem, M. Conlon, and M. Basu, "Mitigation of over-voltage fluctuation in medium voltage (MV) distribution feeder line with high PV plant penetration," in *2015 50th International Universities Power Engineering Conference (UPEC)*, 2015, pp. 1-5.

[106] A. Agrawal, K. Rahimi, R. P. Broadwater, and J. Bank, "Performance of PV generation feedback controllers: Power factor versus Volt-VAR control strategies," in *2015 North American Power Symposium (NAPS)*, 2015, pp. 1-6.

[107] S. Essaghir, M. Benchagra, and N. E. Barbri, "Power factor control of a photovoltaic system connected to grid under load variation," in *2017 International Conference on Electrical and Information Technologies (ICEIT)*, 2017, pp. 1-7.

[108] M. Emmanuel, R. Rayudu, and I. Welch, "Impacts of Power Factor Control Schemes in Time Series Power Flow Analysis for Centralized PV Plants Using Wavelet Variability Model," *IEEE Transactions on Industrial Informatics,* vol. 13, pp. 3185-3194, 2017.

[109] R. J. Bravo, S. A. Robles, and T. Bialek, "VAr support from solar PV inverters," in *2014 IEEE 40th Photovoltaic Specialist Conference (PVSC)*, 2014, pp. 2672-2676.

[110] P. Jahangiri and D. Aliprantis, "Distributed Volt/VAr control by PV inverters," in *2014 IEEE PES General Meeting | Conference & Exposition*, 2014, pp. 1-1.

[111] I. Abdelmotteleb, T. Gómez, and J. P. Chaves-Avila, "Benefits of PV inverter volt-var control on distribution network operation," in *2017 IEEE Manchester PowerTech*, 2017, pp. 1-6.

[112] M. A. Shuvra and B. H. Chowdhury, "Distributed voltage control of active MV distribution networks in the presence of high PV penetration," in *2018 IEEE Power*

& Energy Society Innovative Smart Grid Technologies Conference (ISGT), 2018, pp. 1-5.

[113] A. Safayet, P. Fajri, and I. Husain, "Reactive Power Management for Overvoltage Prevention at High PV Penetration in a Low-Voltage Distribution System," *IEEE Transactions on Industry Applications,* vol. 53, pp. 5786-5794, 2017.

[114] P. Jahangiri and D. C. Aliprantis, "Distributed Volt/VAr Control by PV Inverters," *IEEE Transactions on Power Systems,* vol. 28, pp. 3429-3439, 2013.

[115] M. G. Kashani, S. Bhattacharya, J. Matamoros, D. Kaiser, and M. Cespedes, "Autonomous Inverter Voltage Regulation in a Low Voltage Distribution Network," *IEEE Transactions on Smart Grid,* vol. 9, pp. 6909-6917, 2018.

[116] A. O. Connell and A. Keane, "Volt–var curves for photovoltaic inverters in distribution systems," *IET Generation, Transmission & Distribution,* vol. 11, pp. 730-739, 2017.

[117] M. E. Baran, H. Hooshyar, Z. Shen, and A. Huang, "Accommodating High PV Penetration on Distribution Feeders," *IEEE Transactions on Smart Grid,* vol. 3, pp. 1039-1046, 2012.

[118] M. Chamana and B. H. Chowdhury, "Optimal Voltage Regulation of Distribution Networks With Cascaded Voltage Regulators in the Presence of High PV Penetration," *IEEE Transactions on Sustainable Energy,* vol. 9, pp. 1427-1436, 2018.

[119] M. G. Kashani, M. Mobarrez, and S. Bhattacharya, "Smart inverter volt-watt control design in high PV penetrated distribution systems," in *2017 IEEE Energy Conversion Congress and Exposition (ECCE)*, 2017, pp. 4447-4452.

[120] V. T. Dao, H. Ishii, and Y. Hayashi, "Optimal smart functions of large-scale PV inverters in distribution systems," in *2017 IEEE Innovative Smart Grid Technologies - Asia (ISGT-Asia)*, 2017, pp. 1-7.

[121] T. M. Wanzeler, J. P. A. Vieira, P. Radatz, V. C. Souza, and D. C. Pinheiro, "Assessing the performance of smart inverter volt-watt and volt-var functions in distribution systems with high PV penetration," in *2018 Simposio Brasileiro de Sistemas Eletricos (SBSE)*, 2018, pp. 1-6.

[122] S. Sharma, A. Chandra, M. Saad, S. Lefebvre, D. Asber, and L. Lenoir, "Investigations on active control schemes of solar-PV power generation in a distribution feeder," in *IECON 2016 - 42nd Annual Conference of the IEEE Industrial Electronics Society*, 2016, pp. 4158-4163.

[123] M. G. Kashani, M. Mobarrez, and S. Bhattacharya, "Smart Inverter Volt-Watt Control Design in High PV-Penetrated Distribution Systems," *IEEE Transactions on Industry Applications,* vol. 55, pp. 1147-1156, 2019.

[124] M. Islam, N. Mithulananthan, and M. J. Hossain, "Dynamic Voltage Support by TL-PV Systems to Mitigate Short-Term Voltage Instability in Residential DN," *IEEE Transactions on Power Systems,* vol. 33, pp. 4360-4370, 2018.

[125] M. Islam, M. Nadarajah, and J. Hossain, "Short-term Voltage Stability Enhancement in Residential Grid with High Penetration of Rooftop PV units," *IEEE Transactions on Sustainable Energy,* pp. 1-1, 2018.

[126] M. M. Hasaneen, M. A. L. Badr, and A. M. Atallah, "Control of active/reactive power and low-voltage ride through for 40 kW three-phase grid-connected single-stage PV system," *CIRED - Open Access Proceedings Journal,* vol. 2017, pp. 1655-1659, 2017.

[127] S. Sajadian and R. Ahmadi, "ZSI for PV systems with LVRT capability," *IET Renewable Power Generation,* vol. 12, pp. 1286-1294, 2018.

[128] S. Fan, P. Chao, and F. Zhang, "Modelling and simulation of the photovoltaic power station considering the LVRT and HVRT," *The Journal of Engineering,* vol. 2017, pp. 1206-1209, 2017.

[129] K. Kawabe and K. Tanaka, "Analytical Method for Short-Term Voltage Stability Using the Stability Boundary in the P-V Plane," *IEEE Transactions on Power Systems,* vol. 29, pp. 3041-3047, 2014.

[130] G. Lammert, D. Premm, L. D. P. Ospina, J. C. Boemer, M. Braun, and T. V. Cutsem, "Control of Photovoltaic Systems for Enhanced Short-Term Voltage Stability and Recovery," *IEEE Transactions on Energy Conversion,* vol. 34, pp. 243-254, 2019.

[131] M. B, "NREL/SCE High-Penetration PV Integration Project: Report on Field Demonstration of Advanced Inverter Functionality in Fontana, CA," NREL, 2014.

[132] M. B and A. Gebeyehu, "Field Demonstration of Using Advanced PV Inverter Functionality to Mitigate the Impacts of High-Penetration PV Grid Integration on the Distribution System," presented at the 2015 IEEE 42nd Photovoltaic Specialist Conference (PVSC), 2015.

[133] F. Bell, A. Nguyen, M. McCarty, K. Atef, and T. Bialek, "Secondary voltage and reactive power support via smart inverters on a high-penetration distributed photovoltaic circuit," in *2016 IEEE Power & Energy Society Innovative Smart Grid Technologies Conference (ISGT)*, 2016, pp. 1-6.

[134] "Advanced Grid – Friendly Controls Demonstration Project for utility scale PV Power Plants," NREL, 2016.

[135] R. K. Varma, V. Khadkikar, and S. A. Rahman, "Utilization of Distributed Generator Inverters as STATCOM," US Patent Application PCT/CA2010/001419, 15 Sept, 2010.

[136] R. K. Varma, S. A. Rahman, and T. Vanderheide, "New Control of PV Solar Farm as STATCOM (PV-STATCOM) for Increasing Grid Power Transmission Limits During Night and Day," *IEEE Transactions on Power Delivery,* vol. 30, pp. 755-763, 2015.

[137] R. K. Varma and R. Salehi, "SSR Mitigation With a New Control of PV Solar Farm as STATCOM (PV-STATCOM)," *IEEE Transactions on Sustainable Energy,* vol. 8, pp. 1473-1483, 2017.

[138] R. K. Varma and E. M. Siavashi, "PV-STATCOM: A New Smart Inverter for Voltage Control in Distribution Systems," *IEEE Transactions on Sustainable Energy,* vol. 9, pp. 1681-1691, 2018.

[139] R. K. Varma, S. A. Rahman, V. Sharma, and T. Vanderheide, "Novel control of a PV solar system as STATCOM (PV-STATCOM) for preventing instability of induction motor load," in *2012 25th IEEE Canadian Conference on Electrical and Computer Engineering (CCECE)*, 2012, pp. 1-5.

[140] A. Hariri, M. O. Faruque, R. Soman, and R. Meeker, "Impacts and interactions of voltage regulators on distribution networks with high PV penetration," in *2015 North American Power Symposium (NAPS)*, 2015, pp. 1-6.

[141] A. Kulmala, S. Repo, and B. Bletterie, "Avoiding adverse interactions between transformer tap changer control and local reactive power control of distributed generators," in *2016 IEEE PES Innovative Smart Grid Technologies Conference Europe (ISGT-Europe)*, 2016, pp. 1-6.

[142] K. M. Muttaqi, A. D. T. Le, M. Negnevitsky, and G. Ledwich, "A Coordinated Voltage Control Approach for Coordination of OLTC, Voltage Regulator, and DG to Regulate Voltage in a Distribution Feeder," *IEEE Transactions on Industry Applications,* vol. 51, pp. 1239-1248, 2015.

[143] D. Ranamuka, A. P. Agalgaonkar, and K. M. Muttaqi, "Examining the Interactions between DG Units and Voltage Regulating Devices for Effective Voltage Control in Distribution Systems," *IEEE Transactions on Industry Applications,* vol. 53, pp. 1485-1496, 2017.

[144] M. I. Hossain, R. Yan, and T. K. Saha, "Investigation of the interaction between step voltage regulators and large-scale photovoltaic systems regarding voltage regulation and unbalance," *IET Renewable Power Generation,* vol. 10, pp. 299-309, 2016.

[145] H. Ravindra, M. O. Faruque, K. Schoder, M. Steurer, P. Mclaren, and R. Meeker, "Dynamic interactions between distribution network voltage regulators for large and distributed PV plants," in *PES T&D 2012*, 2012, pp. 1-8.

[146] M. Kraiczy, T. Stetz, and M. Braun, "Parallel Operation of Transformers With on Load Tap Changer and Photovoltaic Systems With Reactive Power Control," *IEEE Transactions on Smart Grid,* vol. 9, pp. 6419-6428, 2018.

[147] A. A. A. Radwan and Y. A. I. Mohamed, "Modeling, Analysis, and Stabilization of Converter-Fed AC Microgrids With High Penetration of Converter-Interfaced Loads," *IEEE Transactions on Smart Grid,* vol. 3, pp. 1213-1225, 2012.

[148] J. Schoene, V. Zheglov, M. Humayun, B. Poudel, M. Kamel, A. Gebeyehu, *et al.*, "Investigation of oscillations caused by voltage control from smart PV on a secondary system," in *2017 IEEE Power & Energy Society General Meeting*, 2017, pp. 1-5.

[149] M. J. Hossain, J. Lu, M. A. Mahmud, N. Mithulanthan, and H. R. Pota, "Dynamic interactions of PV units in low volatge distribution systems," in *2013 IEEE 8th Conference on Industrial Electronics and Applications (ICIEA)*, 2013, pp. 495-500.

[150] S. Mortazavian and Y. A. I. Mohamed, "Dynamic Analysis and Improved LVRT Performance of Multiple DG Units Equipped With Grid-Support Functions Under Unbalanced Faults and Weak Grid Conditions," *IEEE Transactions on Power Electronics,* vol. 33, pp. 9017-9032, 2018.

[151] F. Andrén, B. Bletterie, S. Kadam, P. Kotsampopoulos, and C. Bucher, "On the Stability of Local Voltage Control in Distribution Networks With a High Penetration of Inverter-Based Generation," *IEEE Transactions on Industrial Electronics,* vol. 62, pp. 2519-2529, 2015.

[152] M. G. Kashani, Y. Cho, and S. Bhattacharya, "Design consideration of volt-VAR controllers in distribution systems with multiple PV inverters," in *2016 IEEE Energy Conversion Congress and Exposition (ECCE)*, 2016, pp. 1-7.

[153] J. Smith and H. Li, "Potential interaction between smart inverters," in *Electric Power Research Institute (EPRI) Smart Inverter Workshop*, 2014.

[154] J. Smith, M. Rylander, and H. Li, "Determining recommended settings of smart inverters," in *Electric Power Research Institute (EPRI) Smart Inverter Workshop*, 2014.

[155] S. Chakraborty, A. Hoke, and B. Lundstrom, "Evaluation of multiple inverter volt-VAR control interactions with realistic grid impedances," in *2015 IEEE Power & Energy Society General Meeting*, 2015, pp. 1-5.

[156] M. J. Hossain, M. A. Mahmud, H. R. Pota, and N. Mithulananthan, "Design of Non-Interacting Controllers for PV Systems in Distribution Networks," *IEEE Transactions on Power Systems,* vol. 29, pp. 2763-2774, 2014.

[157] J. H. Braslavsky, L. D. Collins, and J. K. Ward, "Voltage Stability in a Grid-Connected Inverter With Automatic Volt-Watt and Volt-VAR Functions," *IEEE Transactions on Smart Grid,* vol. 10, pp. 84-94, 2019.

[158] H. A. V. Gutiérrez and M. G. Molina, "Analysis of voltage sags due to induction motors in distribution systems with high PV penetration," in *2017 IEEE PES*

Innovative Smart Grid Technologies Conference - Latin America (ISGT Latin America), 2017, pp. 1-6.

[159] W. R. Issa, M. A. Abusara, and S. M. Sharkh, "Impedance interaction between islanded parallel voltage source inverters and the distribution network," in *7th IET International Conference on Power Electronics, Machines and Drives (PEMD 2014)*, 2014, pp. 1-6.

[160] M. J. Hossain, T. K. Saha, N. Mithulananthan, H. R. Pota, and J. Lu, "Dynamic interactions among multiple DER controllers in distribution systems," in *2012 IEEE International Conference on Power System Technology (POWERCON)*, 2012, pp. 1-6.

[161] "1000 VDC Utility Scale Inverters," Yaskawa, Available: http://www.yaskawa.com.sg/product/solar-inverters/sgi-500-750xtm..

[162] "Inverter in large scale PV Plants," SMA Solar, Available: https://www.sma-america.com/products/solarinverters/sunny-central-1850-us-2200-us-2500-ev-us-2750-ev-us.html

[163] "ABB Central Inverters," ABB, Available: http://search.abb.com/library/Download.aspx?DocumentID=3AXD50000042985&LanguageCode=en&DocumentPartId=&Action=Launch

[164] D. Remon, A. M. Cantarellas, J. M. Mauricio, and P. Rodriguez, "Power system stability analysis under increasing penetration of photovoltaic power plants with synchronous power controllers," *IET Renewable Power Generation,* vol. 11, pp. 733-741, 2017.

[165] "A detailed performance model for Photvoltaic Systems," NREL,, NREL/JA-5500-54601, 2012.

[166] T. Esram and P. L. Chapman, "Comparison of Photovoltaic Array Maximum Power Point Tracking Techniques," *IEEE Transactions on Energy Conversion,* vol. 22, pp. 439-449, 2007.

[167] B. Subudhi and R. Pradhan, "A Comparative Study on Maximum Power Point Tracking Techniques for Photovoltaic Power Systems," *IEEE Transactions on Sustainable Energy,* vol. 4, pp. 89-98, 2013.

[168] M. H. Rashid, *Power Electronics Handbook*, fourth ed.: Butterworth-Heinemann, 2018.

[169] A. Yazdani, A. R. D. Fazio, H. Ghoddami, M. Russo, M. Kazerani, J. Jatskevich*, et al.*, "Modeling Guidelines and a Benchmark for Power System Simulation Studies of Three-Phase Single-Stage Photovoltaic Systems," *IEEE Transactions on Power Delivery,* vol. 26, pp. 1247-1264, 2011.

[170] A. Kashyap, "Small-signal Stability Analysis and Power System Stabilizer Design for Grid-Connected Photovoltaic Generation System," M.A.Sc, Carleton University, Ottawa, Canada, 2014.

[171] F. B. a. S. H. M. Liserre, "Design and Control of an LCL-Filter-Based Three-Phase Active Rectifier," *IEEE Transaction on Industry Applications,* vol. 41, pp. 1281-1291, 2005.

[172] A. Yazdani and R. Iravani, *Voltage Sourced Converters in Power Systems Modeling, Control and Applications*. New York: IEEE Press/Wiley, 2010.

[173] J. Foster, "Introduction to Transformerless Inverter," New Berln, WI, USA.

[174] "Conext CL- 60A Inverter - Solution Guide for Decentralized PV systems (For North America).", Available: https://solar.schneider-electric.com/product/conext-cl-60-a-string-inverter/

[175] S. G. Parker, B. P. McGrath, and D. G. Holmes, "Regions of Active Damping Control for LCL Filters," *IEEE Transactions on Industry Applications,* vol. 50, pp. 424-432, 2014.

[176] C. Schauder and H. Mehta, "Vector analysis and control of advanced static VAr compensators," *IEE Proceedings C - Generation, Transmission and Distribution,* vol. 140, pp. 299-306, 1993.

[177] S. Soni, "Solar PV Plant Model Validation for Grid Integration Studies," Masters Thesis, Arizona State University, USA, 2014.

[178] J. Coffey, "Latency in optical fiber systems," CommScope, Hickory, North Carolina, 2017.

[179] A. Mahendra, "Novel Control of PV Solar and Wind Farm Inverters as STATCOM for Increasing Connectivity of Distributed Generators," Masters thesis, Western University, Canada, 2013.

[180] Baldor Three Phase Severe Duty Motors. [Online]. Available: http://stevenengineering.com/tech_support/PDFs/92MOTOR_SEVERE_DUTY.pdf

[181] "Standard load models for power flow and dynamic performance simulation," *IEEE Transactions on Power Systems,* vol. 10, pp. 1302-1313, 1995.

[182] W. V. Wang, Z. Ming, and S. Wah, "Challenges to supplying large induction motor loads in a long radial transmission system," in *2015 IEEE Power & Energy Society General Meeting*, 2015, pp. 1-4.

[183] C. Li, "Impedance based stability analysis in power systems with multiple STATCOMs in Proximity," PhD thesis, Virginia Tech University, USA, 2018.

[184] Solarworld, "Sunmodule Plus SWA 285-290 Mono Black Data sheet," USA, Available: https://www.altestore.com/static/datafiles/Others/sw-285-290-mono-black-solar-datasheet.pdf.

Appendices

Appendix A: System and PV plant Data for the various study systems used.

A. 1. Parameters for the 10 kW PV solar farm connected to network of Bluewater Power Distribution Corporation, Sarnia.

Parameter	Value
Inductance connected between PV solar farm and network	5.107 mH
Inductance connected between PV solar farm and IM	3 mH
Transformer T_1	600/208 V, 10 kVA, X = 5%
Transformer T_2	208/140 V, 10 kVA, X = 5%

A. 2. 10 kW PV Inverter Parameters

Component		Value
Inverter Rating		10 kVA
PV panel Specification	MPPT Voltage	280 V
	MPPT Current	35.7 A
Filter Inductor		0.9 mH

Filter Capacitor	92 μF
Filter Resistor	0.45 Ω
DC link Capacitor	9000 μF
Switching Frequency	8 kHz

A. 3. Controller parameters for 10 kW PV Inverter

Component		Value
DC voltage controller	K_i	64.28
	K_p	0.77
PLL	$H(s)$	$\dfrac{3.8 * 10^3(s + 271.3 * 10^3)}{s(s + 373.2)}$
Current Controller	K_i	338.15
	K_p	0.778
PCC voltage controller	K_i	3.3*10^4
	K_p	0

A. 4. Parameters of 5 hp Induction Motor

Parameter	Value
Motor Rating	3.3 kVA, 460 V, 376.99 rad/s

Stator Resistance (pu)	0.0272
Resistance of first cage (pu)	0.0330
Stator Reactance (pu)	0.0901
Reactance of first cage (pu)	0.0901
Magnetizing Reactance (pu)	1.9376
Inertia (sec)	0.2
Load Torque (pu)	0.75

A. 5. Parameters for the realistic 27.6 kW distribution network, Ontario, Canada

Parameter	Value
Equivalent resistance of 115 kV network	0.0277 Ω
Equivalent reactance of 115 kV network	0.8595 Ω
Resistance of feeder	0.169 Ω/km
Reactance of feeder	0.4182 Ω/km
Substation Transformer	115/27.6 kV, 20 MVA, X = 5%
PV plant transformer	27.6/0.6 kV, 7 MVA, X = 5%
Induction Motor transformer	27.6/4 kV, 3 MVA, X = 5%

A. 6. Parameters for the equivalent 6 MW PV inverter model

Component		Value
Inverter Rating		6 MVA
PV panel Specification	MPPT Voltage	1500 V
	MPPT Current	4 kA
Switching Frequency		4 kHz

A. 7. Parameters for the pad mount transformer and collector cables for 6 MW PV plant

Parameter	Value
Pad mount transformer	27.6/0.6 kV, 10 MVA, X = 10%
Series impedance of the collector system	0.128+j0.12 Ω/km
Capacitance of the collector system	0.2 μF/km

A. 8. Controller parameters for the equivalent 6 MW PV inverter model

Controller Parameter		Value
PCC voltage controller	K_i	1.68*10^4
	K_p	0

Current Controller	K_i	3.17
	K_p	0.025
PLL	$H(s)$	$\dfrac{7.9(s + 271.3 * 10^3)}{s(s + 373.2)}$

A. 9. Parameters for the 2.6 MVA Induction Motor

Parameter	Value
Motor Rating	2.6 MVA, 4 kV, 376.99 rad/s
Stator Resistance (pu)	0.019
Resistance of first cage (pu)	0.00607
Resistance of second cage (pu)	0.0582
Stator Reactance (pu)	0.0795
Reactance of first cage (pu)	0.1706
Reactance of second cage (pu)	0.0795
Magnetizing Reactance (pu)	3.89
Inertia (sec)	0.95
Load Torque (pu)	0.85

A. 10. Parameters for the 2 MW PV inverter

Parameter		Value
Inverter Rating		2 MVA
PV panel Specification	MPPT Voltage	1500 V
	MPPT Current	1.33 kA
Filter Inductor		0.39 mH
Filter Capacitor		115 µF
Filter Resistor		0.39 Ω
DC link Capacitor		16000 µF
Switching Frequency		2 kHz

A. 11. Controller Parameters for the 2 MW PV inverter

Parameter		Value
DC voltage controller	K_i	8.314
	K_p	0.292
PLL	$H(s)$	$\dfrac{7.9(s + 271.3 * 10^3)}{s(s + 373.2)}$
Current Controller	K_i	7.9732
	K_p	0.067

PCC voltage controller	K_i	1.6*10^4
	K_p	0

A. 12. Parameters for the 138 kV transmission network

Parameter	Value
Resistance of 138 kV Transmission Line	0.077 Ω/km
Reactance of 138 kV Transmission Line	0.205 Ω/km
Susceptance of 138 kV Transmission Line	7.59 µS/km
Substation Transformer (230 kV/138 kV)	230/138 kV, 200 MVA, X = 10%
PV plant transformer (27.6 kV/138 kV)	27.6/138 kV, 100 MVA, X = 8.5%
Load end transformer (138 kV/27.6 kV)	27.6/138 kV, 100 MVA, X = 8.5%
Induction Motor transformer (27.6 kV/4 kV)	27.6/4 kV, 50 MVA, X = 6%

A. 13. Parameters for the equivalent model of 75 MW PV solar farm

Component	Value
Inverter Rating	75 MVA

DC link Voltage	1500 V
Switching Frequency	2 kHz
Equivalent impedance of pad mount transformer (in 100 MVA and 34.5 kV base)	0.05 pu
Equivalent series impedance of the collector system (in 100 MVA and 34.5 kV base)	0.049+0.0261i pu
Equivalent susceptance of the collector system (in 100 MVA and 34.5 kV base)	0.032 pu

A. 14. Controller Parameters for the equivalent model of 75 MW PV solar farm

Controller Parameter		Value
PCC voltage controller	K_i	9.964*10^3
	K_p	62.3
Current Controller	K_i	699
	K_p	2.1

A. 15. Typical Parameters for a solar panel [184]

Parameter	Value
Maximum Power	285 W

Open circuit voltage	39.2 V
Maximum power point voltage	32 V
Short circuit current	9.52 A
Maximum power point current	9 A
Module efficiency	17%

Appendix B: Design of Filter and Controller parameters for the 10 kw PV plant connected to Bluewater Power Distribution System, Sarnia, Canada.

The design of different components for the 10 kw PV plant is presented below.

Design of Filter

The filter components are designed using the strategy discussed in Sec. 2.3.3.

For the Bluewater System, $V_{dc} = 280$ volt, rated line – line voltage at ac terminal of inverter $V_{LL} = 120$ V, Inverter rated power $S_n = 10$ kVA, nominal system frequency $f_0 = 60$ Hz, and switching frequency $f_s = 8$ kHz.

The filter inductor L_f is designed to limit the inverter current ripple to 10%.

$$L_f = \frac{V_{dc}}{8 * \Delta i_{max} * f_s} \qquad (0\text{-}1)$$

$$i_{max} = \frac{S_n}{\sqrt{3}*V_{LL}} = \frac{10*10^3}{\sqrt{3}*120} = 48.11\ A \qquad (0\text{-}2)$$

By substituting the parameter values in (0-1),

$$L_f = \frac{280}{8 * 0.1 * 48.11 * 8 * 10^3} = 0.9\ mH \qquad (0\text{-}3)$$

The capacitance C_f is calculated using (2.28), such that the reactive power consumed capacitor C_f is less than 0.05 pu of the inverter rated power.

$$C_f = \frac{x * S_n}{\omega * V_{LL}^2} = \frac{0.05 * 10 * 10^3}{377 * 120^2} = 92\ \mu F \qquad (0\text{-}4)$$

The coupling transformer is rated for 120/208V, 10 kVA and 0.05 pu impedance. The inductance of the trasnformer L_t is calculated using (0-5).

$$L_t = \frac{x * V_{LL}^2}{\omega * S_n} = \frac{0.05 * 120^2}{377 * 10 * 10^3} = 0.2 \ mH \qquad (0\text{-}5)$$

The resonant frequency f_r is calculated using (0-6).

$$f_r = \frac{1}{2\pi} \sqrt{\frac{L_t + L_f}{L_f C_f L_t}} = 1297 \ Hz \qquad (0\text{-}6)$$

The resonant frequency $\boldsymbol{f_r}$ satisfies the condition required by (2.28) and (0-7)

$$10 f_0 \ (600 \ Hz) < \ f_r = (1297 \ Hz) < 0.5 \ f_s = (4 * 10^3) \qquad (0\text{-}7)$$

The damping resistance $\boldsymbol{R_{f2}}$ for the designed filter is

$$R_{f2} = \frac{1}{3 * 2 * \pi * f_r * C_f} = \frac{1}{3 * 2 * \pi * 1297 * 92 \ \mu F} = 0.45 \ \Omega \qquad (0\text{-}8)$$

The filter parameters used for study system 1 are $\boldsymbol{L_f = 0.9 \ mH}$, $\boldsymbol{C_f = 92 \ \mu F}$ and $\boldsymbol{R_{f2} = 0.45 \ \Omega}$.

Design of PLL

The PLL design strategy is discussed in Sec. 2.4.3.1. The compensator $H(s)$ is designed for a gain cross over frequency of 100 Hz and 60° phase margin. The designed compensator for the PLL is given in (0-9).

$$H(s) = \frac{3.8 * 10^3 (s + 271.3 * 10^3)}{s(s + 373.2)} \qquad (0\text{-}9)$$

The Bode plot of the compensated system is shown in Figure B.1. It demonstrates the controller parameters are designed correctly to achieve the target gain cross over frequency and phase margin.
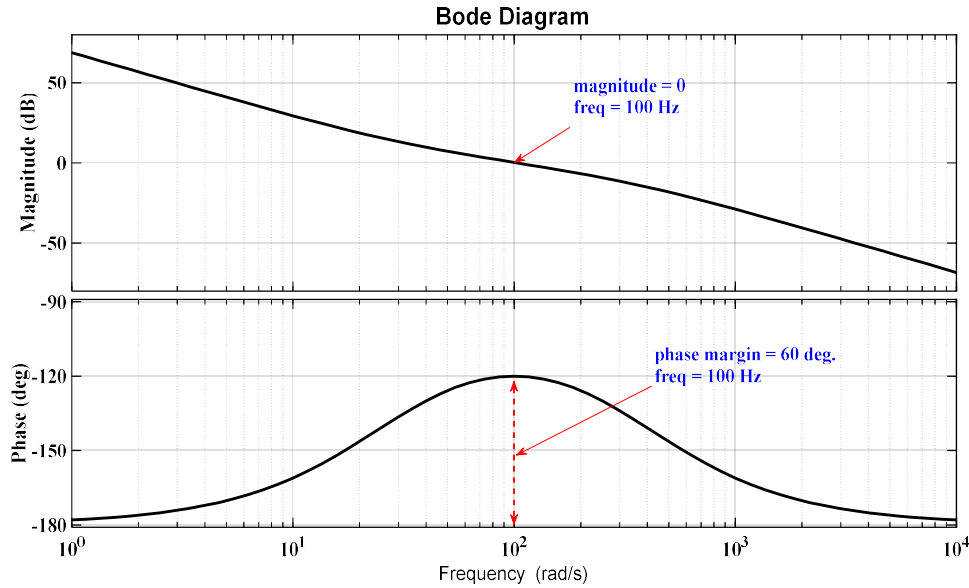
Figure B.1: Bode plot of the compensated PLL control loop

Design of Current Controller

The model and design strategy of the current controller for a three phase inverter is discussed in Sec. 2.4.4. The current controller is designed with a bandwidth of 750 Hz, so that the bandwidth of the controller is at least 10 times smaller than the switching frequency (8 kHz). The controller is designed with a bandwidth of 60° to ensure stable operation.

The designed compensator for current controller is given in (0-10),

$$K_d(s) = K_q(s) = \frac{(0.778s + 338.15)}{s} \qquad (0\text{-}10)$$

The Bode plot of the compensated current controller loop is depicted in Figure B.2. It shows that the controller is designed correctly according to the design objectives.
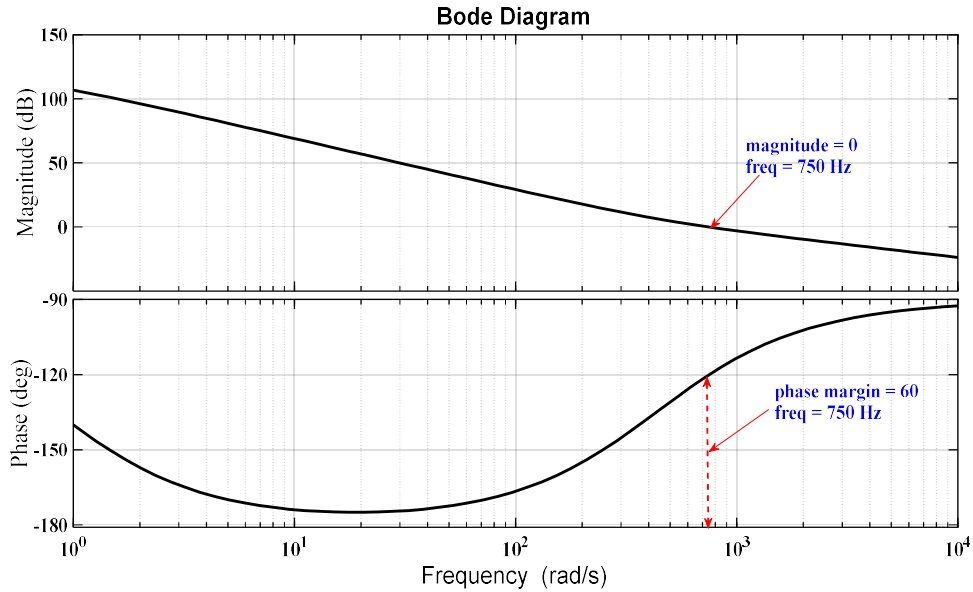
Figure B.2: Bode diagram of the compensated current controller loop.

Design of DC Voltage Controller

The DC link voltage controller bandwidth should be at least three times lower than the current controller bandwidth. Thus, the DC link controller is modelled with a bandwidth of 150 Hz. The model and design strategy of the DC link controller is explained in Sec. 2.4.5.

The designed compensator for DC link voltage controller is given in (0-11),

$$K_{dc}(s) = \frac{(0.77s + 64.28)}{s} \tag{0-11}$$

The Bode plot of the compensated current controller loop is depicted in Figure B.3. It shows that the controller is designed correctly according to the design objectives.
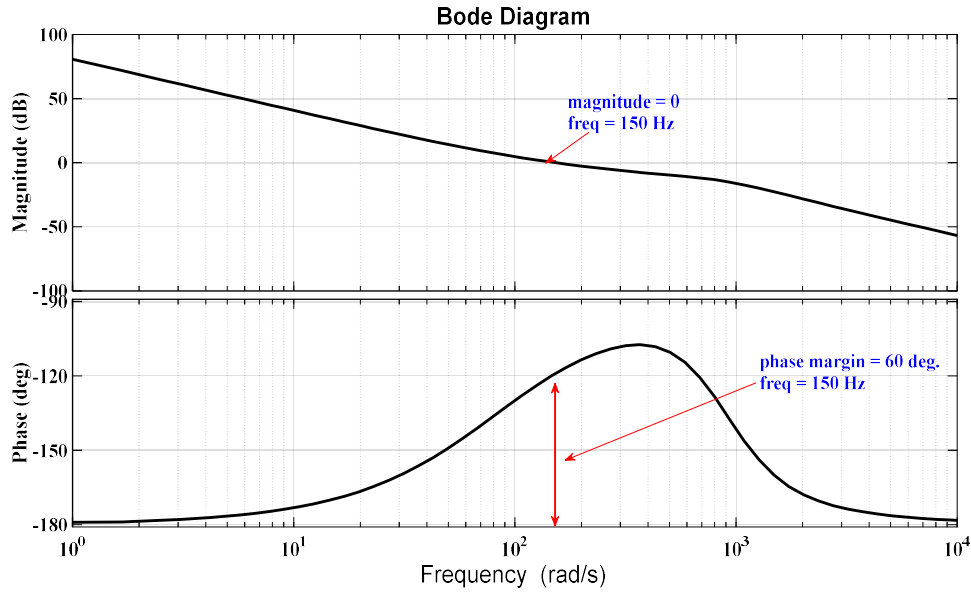
Figure B.3: Bode diagram of the compensated DC voltage controller loop.

Design of PCC Voltage Controller

The PCC voltage controller bandwidth should be at least three times lower than the current controller bandwidth. Thus, the PCC controller is modelled with a bandwidth of 150 Hz. The model and design strategy of the PCC voltage controller is explained in Sec. 2.4.6.

The designed compensator for DC link voltage controller is given in (0-12),

$$K_{vc}(s) = \frac{33909}{s} \tag{0-12}$$

The Bode plot of the compensated current controller loop is depicted in Figure B.4. It shows that the controller is designed correctly according to the design objectives.
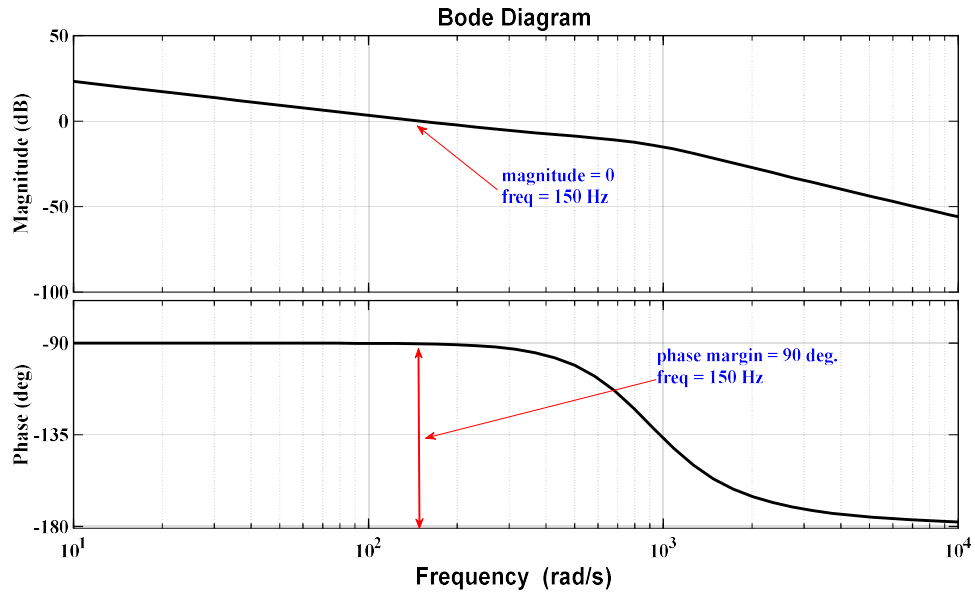
Figure B.4: Bode diagram of the PCC voltage control loop.

Curriculum Vitae

Name: Sibin Mohan

Post-secondary Education and Degrees:
Rajiv Gandhi Institute of Technology
Kottayam, Kerala, India
2007-2011 B.Tech. in Electrical and Electronics Engineering.

Indian Institute of Technology, Bombay,
Mumbai, India
2012-2014, M.Tech in Power System and Power Electronics.

The University of Western Ontario
London, Ontario, Canada
2014-2019 Ph.D. in Electrical Engineering (In progress)

Honours and Awards:
Outstanding Presentation, Graduate Symposium
Electrical and Computer Engineering Dept
2018

NSERC Industrial Postgraduate Scholarship
2015 - 2017

Western Graduate Research Scholarship
2014-2019

Related Work Experience
Teaching Assistant
The University of Western Ontario
2015-2019

Teaching Assistant
The University of Waterloo
2016

Research Associate
Bluewater Power Distribution Corp, Sarnia
2015-2019

Publications:

Journal papers:

1. R. K. Varma, E. M. Siavashi, **S. Mohan** and T. Vanderheide, "First in Canada, Night and Day Field Demonstration of a New Photovoltaic Solar Based Flexible AC Transmission System (FACTS) Device PV-STATCOM for Stabilizing Critical Induction Motor," in *IEEE Access,* vol. 7, pp. 149479-149492, 2019.

2. R. K. Varma, S. A. Rahman, V. Atodaria, **S. Mohan** and T. Vanderheide, "Technique for Fast Detection of Short Circuit Current in PV Distributed Generator," in *IEEE Power and Energy Technology Systems Journal*, vol. 3, no. 4, pp. 155-165, Dec. 2016.

3. R. K. Varma, and **S. Mohan**, " Mitigation of Fault Induced Delayed Voltage Recovery (FIDVR) by PV-STATCOM," in *IEEE Trans. on Power System (under review)*.

4. R. K. Varma, **S. Mohan** and T. Vanderheide, " Solar Farm control as PV-STATCOM for stabilization of Remote Critical Induction Motor," Paper ready to be submitted to *IEEE Journal on Photovoltaics*.

5. R. K. Varma, **S. Mohan** and T. Vanderheide, " Coordinated Active and Reactive Power control of PV-STATCOM for stabilization of Remote Critical Induction Motor," Paper ready to be submitted to *IEEE Access*.

Conference Papers:

1. **S. Mohan**, and R. K. Varma, " Stability Analysis of Two PV power plants while providing Plant Level Voltage Control," Submitted for *2020 PES General Meeting*, Montreal, Canada.

2. **S. Mohan**, S. Hasan, Y. Gebremariam and R. K. Varma, "Increasing Hosting Capacity of PV Solar Systems using Smart Inverter Volt-Var Control," *2018 20th National Power Systems Conference (NPSC)*, Tiruchirappalli, India, 2018, pp. 1-6.

3. Sridhar S, **S Mohan**, M Akbari, R Salehi, R K Varma, Wayne H. Litzenberger "Control of STATCOMs – A Review," 2018 IEEE Power & Energy Society General Meeting (PESGM), Portland, OR, 2018, pp. 1-5.

4. Rajiv K. Varma, Ehsan Siavashi, **S. Mohan**, Hesamaldin Malek, Sridhar Balasubramiam, and Tim Vanderhide, "First in Canada Field demonstration of Night time motor stabilization by PV solar farm as PV-STATCOM", Proc. 2018 Solar Power International Conference, Anaheim, USA, Sep. 2018

5. Rajiv K. Varma, Ehsan Siavashi, Hesamaldin Maleki, Reza Salehi, **S. Mohan**, Mahendra A.C., S. Arifur Rahman and T. Vanderheide, "PV-STATCOM: A Novel Smart Inverter for Transmission and Distribution System Applications", 7th International Conference on Integration of Renewable and Distributed Energy Resources", Niagara Falls, Canada, Oct. 24-28, 2016

6. R. K. Varma, A. A. Hameed, S. Al Hmaidi, S. Mir and **S. Mohan**, "Adverse harmonic impact of network resonances on smart meters," *2015 IEEE Electrical Power and Energy Conference (EPEC)*, London, ON, 2015, pp. 146-151.

7. Rajiv K. Varma and **S. Mohan**, "New PV Solar Farm Control as STATCOM (PV-STATCOM) for Stabilization of a Critical Motor Load", Proc. 2015 Solar Power International Conference, Anaheim, USA, Sep. 2015